REPORT NO.
UCD/CGM-98/04

CENTER FOR GEOTECHNICAL MODELING

SOIL-PILE-SUPERSTRUCTURE INTERACTION IN LIQUEFYING SAND AND SOFT CLAY

Ph.D. DISSERTATION

BY

D. W. WILSON

Research supported by the California Department of Transportation under Contract Number 65V495. The contents of this report reflect the views of the author who is responsible for the facts and the accuracy of the data presented herein. The contents do not necessarily reflect the official views or policies of the STATE OF CALIFORNIA or the FEDERAL HIGHWAY ADMINISTRATION. This report does not constitute a standard, specification, or regulation.

DEPARTMENT OF CIVIL & ENVIRONMENTAL ENGINEERING
COLLEGE OF ENGINEERING
UNIVERSITY OF CALIFORNIA AT DAVIS

SEPTEMBER 1998

Soil-Pile-Superstructure Interaction in Liquefying Sand and Soft Clay

By

DANIEL WAYNE WILSON
B.S. (University of California at Davis) 1992
M.S. (University of California at Davis) 1994

DISSERTATION

Submitted in partial satisfaction of the requirements for the degree of

DOCTOR OF PHILOSOPHY

in

Engineering

in the

OFFICE OF GRADUATE STUDIES

of the

UNIVERSITY OF CALIFORNIA
DAVIS

Approved:

Ross W. Boulanger

I.M. Idriss

Bruce L. Kutter

Committee in Charge

1998

Daniel Wayne Wilson
September 1998
Civil Engineering

Soil-Pile-Superstructure Interaction in Liquefying Sand and Soft Clay

Abstract

The behavior of pile foundations under earthquake loading is an important factor affecting the performance of many essential structures. Analysis and design procedures have been developed for evaluating pile behavior under earthquake loading. The application of these procedures to cases involving soft or liquefied ground is uncertain, however, due to both a lack of physical data against which they can be evaluated, and the continued lack of understanding of the mechanisms involved in soil-pile-structure interaction. Resolving these uncertainties is an important step in current earthquake hazard remediation.

This dissertation describes the results of a study on the dynamic response of pile foundations in liquefying sand and soft clay during strong shaking. The research consisted of: (1) a series of dynamic centrifuge tests of pile supported structures; (2) a critical study of modeling techniques and limitations; (3) back-calculation of p-y behavior; and (4) comparison of pseudo-static analyses to the dynamic centrifuge model tests.

These dynamic model tests were among the first performed using the new shaking table on the 9 m radius centrifuge at UC Davis. The results of the modeling study presented herein will benefit other current and future projects utilizing the large centrifuge.

Back-calculation of dynamic p-y curves for liquefying sand was needed because the dynamic interaction cannot necessarily be extrapolated from static tests. This dissertation presents the first experimentally determined dynamic p-y curves in liquefying sand of which the author is aware. The p-y resistances showed characteristics that are consistent with the undrained behavior of liquefying sand, including the effects of relative density, dilation, cyclic degradation, and displacement history.

It is expected that dynamic numerical models will need at a minimum to account for undrained loading conditions to capture behaviors such as those observed in these tests. Alternatively, simplified pseudo-static analyses using reduction factors on p-y resistance can also yield reasonable design criteria provided the factors are applied with an appreciation for the time varying properties of soils during seismic loading, and special care is taken where the soil may dilate. Sensitivity studies should be performed to help determine the critical loading conditions when using simplified methods.

ACKNOWLEDGMENTS

This dissertation represents the hard work of many individuals to whom I could never express the extent of my gratitude. My wife, Cristin, and son, Justin, have shown remarkable patience during my preparation of this document. My wife in particular has had to carry more than her fair share of the duties in raising our son and our new daughter Ashley, and we have two wonderful children as a result of her efforts. I would also like to thank my parents, who supported me through my undergraduate years and encouraged me to push my education as far as I could.

The UC Davis faculty have without exception been supportive and helpful during my studies. Professor Kutter gave me my first job in research, building centrifuge models as an undergraduate. My thesis advisor, Professor Boulanger, has sat with me for hours at a time going over the details of our work. Professors Kutter, Boulanger, and Idriss have always had open doors to discuss whatever I had on my mind, and each was willing to help when I had a problem, even when it meant loaning me a car so that I could go home for vacation when mine broke down. They have spent many hours discussing this research project and reviewing papers associated with the project, and have also provided much appreciated opportunities to me outside of this research.

Other faculty members have provided guidance and encouragement when needed. In particular, I would like to thank Professor Rashid for his suggestion of the Weighted Residual method for calculating derivatives of moment distribution and for his review comments on Chapter 5.

I would like to thank the various members of the centrifuge support staff, including Bill Sluis for his work instrumenting the model piles; Dr. Doug Stewart, John Lakeland, and Dennis O'Brien for their work supporting my tests; and Tim Evans for relieving me of much of my duties as facility manager so that I could focus on completing this dissertation. And finally, I'd like to thank Tom Kohnke. Tom and I started in the department together and through the years we have become friends as well as co-workers. His work at the centrifuge facility has helped build the Center, and I'd like to thank him for all of his hard work, on my project and others.

I would also like to thank the department staff for always being patient when I forgot a deadline, or helping out when a paycheck was lost.

Many student colleagues also contributed to this project. Philip Robins, Cristina Curras, and Jason DeJong in particular helped with the sometimes-tedious work of model preparation.

The California Department of Transportation (CALTRANS) supported this research under research contract number 65V495. Abbas Abghari was the contract monitor for Caltrans, and provided valuable collaboration throughout this project. The contents of this report reflect the views of the author, who is responsible for the facts and the accuracy of the data presented herein.

TABLE OF CONTENTS

LIST OF FIGURES

LIST OF TABLES

CHAPTER ONE

Dynamic Soil-Structure Interaction

1.1 PILE PERFORMANCE

The behavior of pile foundations under earthquake loading is an important factor affecting the performance of many essential structures. The potential significance of liquefaction-related damage to piles was clearly demonstrated during the 1964 Alaskan earthquake (e.g., Youd and Bartlett 1989) and again more recently during the 1995 Kobe earthquake. Observations of modern pile foundations during past earthquakes have shown that piles in firm soils generally perform well, while the performance of piles in soft or liquefied ground can range from excellent to poor (i.e., structural damage or excessive deformations). Analysis and design procedures have been developed for evaluating pile behavior under earthquake loading. The application of these procedures to cases involving soft or liquefied ground is uncertain, however, due to both a lack of physical data against which they can be evaluated, and the continued lack of understanding of the mechanisms involved in soil-pile-structure interaction in soft or liquefied soils. Resolving these uncertainties is an important step in current earthquake hazard remediation.

Predicting the behavior of pile foundations in soft clay or liquefied ground under earthquake loading is a complex problem involving consideration of design motions, free-field site response, superstructure response, and soil-pile-superstructure interaction.

Evaluating pile foundation behavior requires consideration of the loads imposed on the piles and their pile-cap connections, transient or permanent deformations of the foundation, and the influence of the pile foundation on the dynamic response of the superstructure. Centrifuge or 1 g shaking table studies of the seismic behavior of pile foundations in soft clay or liquefied ground are needed as a means for understanding the fundamental mechanisms of soil-pile-superstructure interaction, for evaluating the reliability of current design procedures, and for the development of improved design procedures. The obvious advantage of centrifuge or 1 g shaking table studies is the ability to obtain detailed measurements of response in a series of tests designed to physically evaluate the importance of varying the earthquake characteristics (e.g. level of shaking, frequency content, waveforms), soil profile characteristics, and/or pile-superstructure characteristics. Used in conjunction with lessons from case histories and numerical analyses, results from centrifuge or 1 g shaking table studies are an essential tool in ongoing studies of this complex problem.

A separate and important issue is the question of what constitutes satisfactory performance of a pile foundation. The most common design approach in the US today is to avoid inelastic behavior of piles and their connections below the ground surface, where damage would be difficult to detect or to repair. Maintaining elastic behavior in the structural components of a pile foundation often governs the design. Thus, the possibility of allowing for inelastic behavior of the piles and their connections may provide significant economy in certain cases, but will require broader discussions of what constitutes satisfactory pile performance and a greater understanding of soil-pile interaction mechanisms.

1.2 REPRESENTATION OF SOIL-PILE INTERACTION

Various approaches have been developed for the dynamic response analysis of single piles. One such method which will be used throughout this dissertation is the Beam on Nonlinear Winkler Foundation (BNWF) model, where the soil-pile interaction is approximated using parallel nonlinear soil-pile (p-y) springs (e.g. Matlock 1978). Currently available p-y curve recommendations (e.g. API 1993) are based on static and cyclic lateral load tests, and are not necessarily applicable to seismic loading conditions as the tests didn't necessarily excite the mechanisms involved in seismic loading (e.g. loads from the soil profile, local and global pore pressure generation).

Others have attempted to extend the recommended p-y curves by incorporating the effects of liquefaction on soil-pile interaction. The Architectural Institute of Japan (AIJ 1988) and Japan Road Association (JRA 1980) codes include the scaling of p-y curves to account for liquefaction. Liu and Dobry (1995) also derived scaling factors from centrifuge model tests with liquefied sand. While some of these recommendations are based on dynamic tests, or at least tests involving liquefied soil, the resulting p-y curves are based on adjusting curves derived from static and cyclic loading tests. In this dissertation an attempt has been made to look at soil-pile interaction from a BNWF perspective under seismic loading directly. The resulting behavior is compared to the current recommended p-y curves, and some simplified analyses are performed using simple multipliers on the API (1993) recommended p-y curves to account for liquefied soil.

1.3 SCOPE OF RESEARCH

This dissertation describes the results of a study on the dynamic response of pile foundations in soft clay and liquefying sand during strong shaking. The research consisted of four components: (1) a series of dynamic centrifuge tests of pile supported structures in soft and liquefying soils performed using the recently completed shaking table on the large centrifuge at UC Davis; (2) a critical study of physical modeling techniques and limitations; (3) back-calculation of p-y behavior from recordings of pile bending moment, pilehead and superstructure accelerations, and soil profile accelerations; and (4) comparison of pseudo-static BNWF analyses to the results of the dynamic centrifuge model tests.

Dynamic centrifuge experiments were performed using several different structural models, different earthquake input motions (varying level of shaking, frequency content, and waveforms), and different soil profiles. Experiments were performed with the upper soil layer being either loose to medium dense saturated sand or normally consolidated clay. The results of these experiments have been documented in detail with individual hard-copy data reports and diskettes with raw time histories [Wilson et al. 1997 (a-e)].

The dynamic centrifuge tests performed in this study were among the first performed using the recently completed shaking table on the large centrifuge, and thus it was necessary to evaluate the centrifuge modeling system before analyzing the recorded physical data. The importance of characterizing the centrifuge modeling system was demonstrated by the recent VELACS cooperative study (e.g., Arulanandan et al. 1994) and further discussed by Scott (1994).

The soil-pile interaction was quantified by back-calculating dynamic p-y time histories. The observed p-y behavior was examined to understand the mechanisms of soil-pile-structure interaction under large strain conditions. The results of the back-calculation procedures are expected to provide a better basis for developing p-y elements for use in dynamic BNWF analysis methods.

The dynamic centrifuge experiments were then analyzed using simplified pseudo-static nonlinear BNWF methods. The analyses were consistent with certain current design methods, and demonstrate the capability of simplified analyses to adequately capture these complex phenomena in design problems.

Continuing research efforts that are based on the experimental findings of this project, and recommendations for future research, are also described. It is hoped that the results of this research will contribute to ongoing efforts to mitigate earthquake hazards.

1.4 ORGANIZATION OF DISSERTATION

A tremendous about of data was collected in the course of this research. Data from a total of 87 shaking events on seven single-pile-, four 2x2 pile-group-, and three 3x3 pile-group-supported structures was obtained. All of the data from these tests are reported by Wilson et al. (1997a-e). This dissertation focuses on the data from single pile supported structures during selected shaking events. This dissertation consists of seven chapters:

Chapter 1. Dynamic Soil-Structure Interaction - includes a brief discussion on the importance of understanding soil-structure interaction and an organizational summary of the dissertation.

Chapter 2. Background - numerical and physical modeling of soil-pile-superstructure interaction and the derivation and application of the BNWF model is discussed. The relevance of pseudo-static analyses in design is discussed. Chapter 2 also includes a brief overview of published knowledge on soil-pile interaction that (1) revealed general features of behavior for lateral loading of piles; (2) specifically discussed large strain seismic loading of piles; or (c) discussed experimental procedures of direct relevance to this present study.

Chapter 3. Centrifuge Testing of Piles under Seismic Loading - the centrifuge testing and results are discussed in general and the modeling equipment and techniques are critically evaluated.

Chapter 4. Centrifuge Results - select data and general behavior from the different centrifuge tests are discussed.

Chapter 5. Experimental Observations of p-y Behavior - soil-structure interaction is examined by back-calculating p-y behavior. The observed behavior is found to be consistent with the expected behaviors of the different soil types used.

Chapter 6. Pseudo-Static Analyses of Single Pile System - snapshots in time of the pile response are analyzed as pseudo-static problems using the program PAR (PMB 1988).

Chapter 7. Conclusions - includes a summary of the dissertation and its findings, their relevance to design procedures, and recommendations for future work.

CHAPTER TWO

Background

2.1 DYNAMIC RESPONSE ANALYSIS METHODS FOR PILES

Evaluating the interaction of soil-pile-structure systems to earthquake ground motions is an important step in the seismic design of both the structure and piles. In the case of relatively flexible piles in stiff soils it may be reasonable to model seismic excitation of a structure using only free field ground surface motion applied to a set of springs at the pilehead representing the stiffness of the foundation. In the case of stiff piers that penetrate through soft surface deposits and into a deep stiff soil layer, the free-field ground motions of the stiff layer may be a more appropriate input excitation to the structure. For other cases, it is important to have a procedure to account for the dynamic interaction between the various layers of soil, the pile, and the superstructure.

Various approaches have been developed for the dynamic response analysis of single piles, including the finite element method (Kuhlemeyer 1979; Angelides and Roesset 1980; Randolph 1981; Faruque and Desai 1982) and the boundary element method (Sanchez 1982; Sen et al. 1985), both of which treat the soil media as a continuum. The discretization of a three-dimensional continuum generates a multitude of degrees of freedom, rendering the method impractical for the design of anything but extremely expensive structures (e.g., large toll bridges or major port facilities). The Beam on Nonlinear Winkler Foundation (BNWF) model, illustrated in Figure 2.1, is a

simplified approach using nonlinear soil pile (p-y) springs that can account for nonlinear soil-pile-structure interaction, and has proven useful in engineering practice (e.g. Abghari and Chai 1995). Trochanis et al. (1991) showed that the response of laterally loaded piles predicted using a BNWF formulation agreed well with static load test data and nonlinear 3-D finite element analyses. Trochanis et al. (1991) used a degrading constitutive model developed by Wen (1976) to represent the p-y springs.

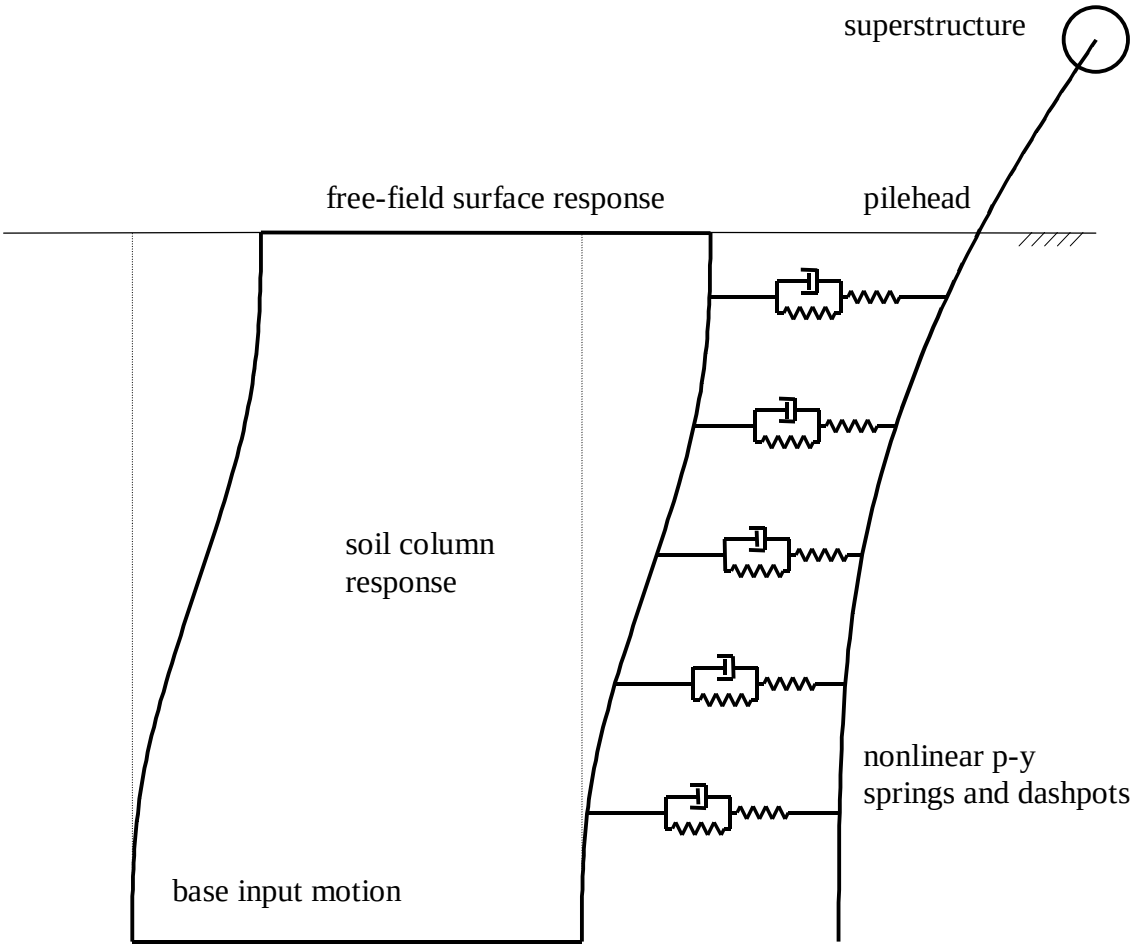

Figure 2.1. Schematic of dynamic Beam on Nonlinear Winkler Foundation (BNWF) analysis model

The Winkler assumption is that the soil-pile interaction resistance at any depth is related to the pile shaft displacement at that depth only, independent of the interaction

resistances above and below. In the BNWF method, the pile itself is modeled as a series of beam-column elements, each with discrete springs connecting the pile to the soil, as shown in Figure 2.1. In a program called SPASM (‘Seismic Pile Analysis with Support Motion’), Matlock et al. (1978) extended the BNWF concept to seismic problems by calculating the ground motion time histories along the depth of the soil profile and then applying the ground motion time histories to the p-y springs as excitation to the system. Kagawa (1980) further extended the BNWF analysis in seismic problems by including viscous dashpots with the nonlinear p-y springs to model the effects of radiation damping. The dynamic BNWF model as applied by Wang et al. (1998) is shown in Figure 2.1, including a linear "far-field" spring in parallel with the radiation damping dashpot, and that combination in series with a non-linear "near-field" spring.

There are several existing computer programs that can be used for analyzing the dynamic response of pile-supported structures using the BNWF method. The computer codes PAR (PMB Engineering 1988), NONSPS (Kagawa 1983) and DRAIN-2D (Prakash and Powell 1993) were evaluated by Wang et al. (1998). Boulanger et al. (1998) extended the work of Wang implementing a new p-y element in the Finite Element program GeoFEAP (Bray et al. 1995). These programs all gave consistent results for several cases studied, provided that the model parameters and radiation damping mechanisms were represented consistently. Two main problems in the analyses were the ongoing difficulty in reliably estimating ground motions during strong shaking events (e.g., the free-field response problem) and the uncertainty in representing soil-pile interaction during strong shaking events. The consequence of these uncertainties can only be evaluated by

comparing analysis results against physical data, and thus is further incentive for the physical modeling efforts undertaken by this study.

2.2 PSEUDO-STATIC ANALYSIS METHODS FOR PILES

2.2.1 A Current Design Methodology

One current design methodology as implemented in practice involves breaking down the soil-pile-structure system into two uncoupled problems, the superstructure and the foundation, and then finding solutions to each that are compatible with the expected response of both parts (e.g. Lam and Kapuskar 1998-under review). In the first step of the analysis, the linear dynamic response of the superstructure is calculated by replacing the foundation with a set of springs that represent the effective foundation stiffness. The result of the linear dynamic response analysis is the displacement demand for the superstructure. Note that load demands will be reduced from those calculated in the linear dynamic analysis due to nonlinear behavior of the superstructure system.

The structure and foundation system is then analyzed using a nonlinear push-over analysis, where the superstructure is statically pushed to the displacement level established in the linear dynamic analysis step. Nonlinear behavior of both the structure and foundation are included. The pseudo-static response of the foundation may be modeled using a BNWF method as previously described with the soil parameters appropriately modified to account for the effects of seismic loading. The displacement associated with the onset of structural yielding is compared to the displacement demand to find the ductility demand on the structure. The load at the displacement demand is the

design load for the foundation. Note also that the design load may be limited by the formation of plastic hinges, or load fuses, in the superstructure. Finally, the foundation displacements found in this step must be consistent with the effective foundation stiffness used in the linear dynamic analysis of the superstructure.

This pseudo-static analysis methodology implicitly assumes that the foundation is being loaded primarily by the superstructure through inertial forces. It is recognized that the pile foundation may also experience significant "kinematic" loads that are imposed by the surrounding soil mass as it deforms relative to the pile during earthquake shaking. Kinematic loads may not be significant in competent soil profiles that experience relatively small strains and deformations during shaking. Large kinematic loads can develop, however, due to lateral spreading of liquefied soils or due to high strain gradients in soft clays, and may be particularly damaging under certain stratigraphies (e.g. strong crusts overlying soft clay or liquefied soils).

A pseudo-static method incorporating kinematic loads directly into the BNWF method was introduced by Byrne et al. (1984). Byrne suggested combining the shear and moment load at the pilehead with a deformed soil profile in a static BNWF analysis. In such an analysis the pilehead shear and moment and the soil profile free-field displacements are known inputs into the BNWF model. Abghari and Chai (1995) applied this method using a site response program to predict maximum kinematic displacements of the soil profile, and response spectra of surface accelerations to predict maximum pile loads due to superstructure inertial forces. When they combined the two sources of load in a static BNWF analysis they found they tended to overestimate maximum moments in the pile as predicted by dynamic BNWF analyses, and suggested some simple

adjustments to arrive at reasonable values for design. Tabesh (1997) did a parametric study on this pseudo-static method and found the method gave reasonable answers in many cases, but could over predict maximum moment and shear in the pile if the period of the structure and the site were similar. The authors of both papers attributed the overestimations to applying both the maximum kinematic and maximum inertial loads simultaneously.

2.2.2 Application to Liquefied Soils

Three different pseudo-static approaches have been proposed to account for the effects of liquefaction on soil-pile interaction. In the first method the lateral resistance of liquefied soil is represented as a scalar multiple of its static drained lateral resistance, even though the loading conditions may in fact be undrained. Scaling of static p-y curves is used in the Architectural Institute of Japan (AIJ 1988) and Japan Road Association (JRA 1980) codes. Liu and Dobry (1995) derived scaling factors from centrifuge model tests, and suggested that the scaling factor would vary linearly with excess pore pressure ratio (r_u) and have a minimum value of about 0.10 when r_u=100%. This approach will be examined in Chapter 6.

It should be noted that in Liu and Dobry's work, a single pile embedded in liquefied sand was subjected to slow, cyclic lateral displacements at the pilehead (Δ_{head}) while the sand was re-consolidating. The magnitude of displacements was held constant at Δ_{head}/Diameter = 2 in./15 in. In applying their results to seismic design, it is necessary to consider the effects of strain history, strain rate, and drainage conditions on p-y behavior. The importance of strain history will be investigated in Chapter 6 of this dissertation. The importance of strain rate was discussed by Tokida et al. (1992).

A second approach for representing the lateral resistance of liquefied sand is to treat it as a material with an undrained residual shear strength (ϕ_u=0). This aspect seemed to be a reasonable representation of the physical model data presented for piles in laterally spreading ground by Abdoun and Dobry (Abdoun et al. 1997).

The third approach is to represent the effect of laterally spreading liquefied soil as a lateral pressure against the pile. This lateral pressure is commonly assumed to increase linearly with depth. Within the liquefied zone, the pile is no longer connected to any p-y spring supports. Thus, this approach is intended to represent the effects of lateral spreading on piles, and cannot be realistically used for modeling dynamic response.

The preceding three approaches for representing the lateral resistance of liquefied soil have been evaluated against several cases from Kobe, such as described in the presentations by Koseki, Fujii, and Tokimatsu at a 1997 US-Japan Workshop (proceedings in press, Idriss and Ishihara 1998). They found that none of the three approaches had proven entirely satisfactory in distinguishing between cases of damage versus no damage for those sites that provided such a contrast in performance. However, these cases have many complicating factors, such as differences in superstructures, basements, and ground displacement levels. In addition, it was recognized that the reliability of these approaches for representing lateral resistance of liquefied soil may simply be limited by the fact that they are approximations of a rather complex phenomena that is poorly understood. For example, these three approaches give different distributions of lateral pressure versus depth, and hence predict different variations in bending moment versus depth. Additional studies are continuing to evaluate these approaches by comparisons with the growing database of documented cases from the Kobe earthquake.

Participants of the 1997 US-Japan Workshop (Idriss and Ishihara 1998) reported that the codes by the Japan Road Association (JRA 1980) and Architectural Institute of Japan (AIJ 1988) were currently being revised in accordance with the findings.

2.3 PHYSICAL MODELING STUDIES OF PILES

A review of the literature identified an abundance of research on soil-pile interaction, including behavior under axial, lateral, and uplift loading. Experimental data are available for monotonic, cyclic, free vibration, and dynamic tests. Experiments have been performed at full scale, reduced scale, on shaking tables, or on centrifuges using a range of soil types. The review presented herein is therefore limited to research that: (1) revealed general features of behavior for lateral loading of piles; (2) specifically discuss large strain seismic loading of piles; or (c) discuss experimental procedures of direct relevance to the present study.

Many researchers (e.g. Brown et al. 1988, Crouse et al. 1993, Dunnavant and O'Niell 1989, and Ochaoa and O'Neill 1989) have performed tests with cyclic loads applied at the pilehead. Degradation of the static p-y curves with increasing number of loading cycles would then be investigated. Procedures have been developed for coupling monotonic p-y curves with p-y degradation factors to derive an equivalent pile foundation stiffness for use in dynamic superstructure finite element models (e.g. Matlock 1978).

The extension of cyclic pilehead loading tests to seismic loading conditions has several limitations. With pilehead loading the soil remains a passive resistor, while in seismic events the soil is applying load to the pile. This "kinematic" loading (i.e. pile

loading due to soil displacements) can be important at soft soil sites, particularly when the site is stratified with soft soil and stiffer soil layers. Radiation damping effects are potentially different for the pilehead and kinematic loading conditions. Excess pore pressures generated by pilehead loading can dissipate to the surrounding soil, while in seismic events there will be global as well as local pore pressure generation. Some cyclic load tests have been done with cyclic base motion (Kobayashi et al. 1991; Yan et al. 1991, Dou and Byrne 1996), which may be a more appropriate model of seismic loading conditions. Free vibration tests in the field (e.g., Crouse et al. 1993; El Sharnouby and Novak 1984) have also been performed, but the small strain levels imposed on the soil make it difficult to extend the results to strong seismic shaking levels.

The only well-defined case history involving strong motion records of soil-pile interaction is the recorded response of the pile foundation for the Ohba-Ohashi Bridge (Gazetas et al. 1993).

A list of physical modeling studies involving seismic response of pile foundations is given in Table 2.1. The amount of detailed physical data (field or model) on the seismic performance of pile foundations in soft or liquefying soil is very limited. Many of these physical modeling studies are very recent, and represent the increased capabilities of modern testing facilities. A review of each of the references is included in Boulanger et al. (1998).

Table 2.1: Physical Modeling Studies Related to the Seismic Behavior of Pile Foundations

Reference	Soil type	Super-structure	Base motion	Shaking level (prototype)	Method
Finn & Gohl (1987)	dry sand	simple mass	seismic	0.15 g	centrifuge
Chang & Kutter (1989)	dry sand	2-story structure	seismic	0.24 g	centrifuge
Café (1991)	peat	bridge deck	seismic	0.05-0.48 g	centrifuge
Kobayashi et al. (1991)	liquefied sand	2-story structure	uniform cyclic	variable	shaking table
Rashidi (1994)	clay	2-story bent	seismic	0.18-0.30 g	centrifuge
Honda et al. (1994)	dry sand	none	seismic	0.02-0.20 g	centrifuge
Tokida et al. (1992)	liquefied sand	none	none	single impact load to induce liquefaction	1-g tank
Liu & Dobry (1995)	liquefied sand	none	uniform cyclic	0.06-0.40 g; pile loaded monotonically after shaking ends	centrifuge
Dou & Byrne (1996)	saturated sand	simple mass	uniform cyclic	0.19-0.49 g	hydraulic gradient
Abdoun et al. (1997)	liquefied sand	none	uniform cyclic	0.25 g	centrifuge
Horihoshi et al. (1997)	liquefied sand	none	uniform cyclic	0.15 g	centrifuge
Wang et al. (1998)	soft clay	simple mass	seismic	0.25 g	centrifuge

These physical modeling studies demonstrate that the lateral resistance of liquefied sand depends on several factors. Variables that have been shown to, or are expected to, significantly affect the lateral resistance of liquefied sand include:

- soil type,
- soil density (this study, as described in Chapter 5),
- loading rate (Tokida et al. 1992),
- excess pore pressure ratio (Liu and Dobry 1995, Tokida et al. 1992),

- installation method (Abdoun et al. 1997),
- displacement level and history (this study, as described in Chapter 5),

The performance of piles in deposits that contain liquefying sand or soft soils will also be strongly affected by

- a non-liquefied crust overlying the liquefied layer (Abdoun et al. 1997),
- group and cap effects (Tokida et al. 1992, Abdoun et al. 1997),
- shaking characteristics, stratigraphy, and other factors.

The results of the studies involving liquefying soils illustrate the complexity of soil-pile interaction phenomena in liquefied soils, and provide data for evaluating the analysis and design methods used to represent the soil-pile interaction phenomena. Most of the published studies on liquefied soils, however, did not include superstructures and thus do not provide data on the effect of soil-pile interaction on the dynamic response characteristics of pile-supported structures in soft or liquefied soils. None of the studies have looked at dynamic time histories of p-y curves in liquefied sand.

Thus, there remains a strong need for physical data on the effect of soil-pile interaction on the dynamic response characteristics of pile-supported structures in soft clay or liquefied soils. In such soft-ground conditions, the fundamental period of the structure may be significantly affected by the compliance of the pile foundation. In addition, the reliability of assuming that the pilehead motion is the same as the anticipated "free-field" ground surface motion may be questioned. These and other concerns regarding the design of pile foundations in soft clay or liquefied ground are not addressed by the data available in the open literature.

CHAPTER THREE

Centrifuge Testing of Piles Under Seismic Loading

3.1 DESCRIPTION OF THE CENTRIFUGE AND MODEL LAYOUTS

The National Geotechnical Centrifuge at UC Davis has a radius of 9 m and is equipped with a large shaking table driven by servo-hydraulic actuators (Kutter et al. 1994). The earthquake simulator was recently completed with funding from the National Science Foundation, Obayashi Corporation, Caltrans, and the University of California. The centrifuge has a maximum model mass (container and sample) of about 2500 kg, an available bucket area of 4.0 m^2, and a maximum centrifugal acceleration of 50 g. The new earthquake simulator was designed to accommodate 1.7 m long models and provide 15 g input shaking accelerations. Earthquake motions are produced by two pair of servo-hydraulic actuators acting in parallel, one pair mounted on either side of the model container. Kutter et al. (1991) and Kutter et al. (1994) give details of the centrifuge and the new earthquake simulator, respectively.

A new Flexible Shear Beam (FSB1) container was designed and constructed for this project. The new FSB1 container has inside dimensions of 1.72 m long, 0.685 m wide, by 0.70 m deep. FSB1 consists of six hollow aluminum rings separated by 12 mm thick layers of 20 durometer neoprene. The mass of each of the upper three rings is about one-half the mass of each of the lower three rings. The combined mass of the six rings

and rubber is about 25% of the soil profile mass (assuming the container is full of soil). The amount of neoprene separating the rings is varied such that the shear stiffness of the container increases with depth. The fixed base natural frequency of the empty container is about 15-20 Hz (0.5 to 0.67 Hz prototype) for the larger shaking events presented herein. Vertical shear rods in the soil near the container ends provide complementary shear stresses (Divis et al. 1996). A section of a portion of the rings, neoprene layers, and shear rods at the end of the container is shown in Figure 3.1.

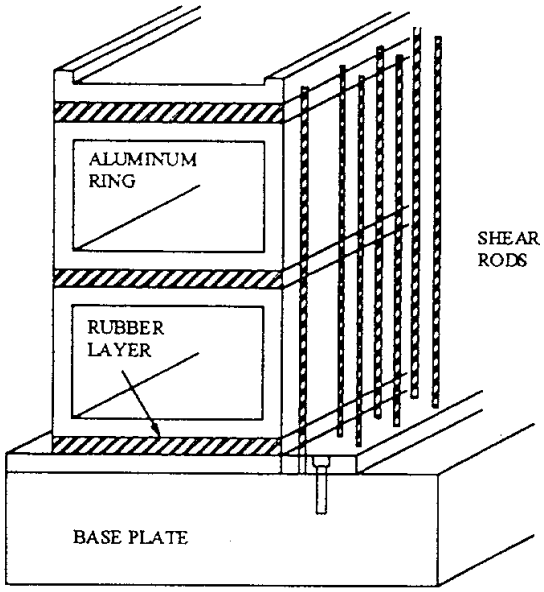

Figure 3.1: Schematic of rings and shear rods (from Divis et al. 1997)

Five containers of soil-structure systems were tested on the large centrifuge. Full details for each centrifuge test can be found in Wilson et at. [1997 (a-e)]. All tests were performed at a centrifugal acceleration of 30 g. Note that the centrifugal acceleration varies with radial position, and thus varied from 29.2 g at the soil surface to 31.5 g at the container base. All results are presented in prototype units unless otherwise noted. For details of the applicable scaling laws, see Kutter (1992).

The soil profiles used in the five containers are summarized in Table 3.1. In all cases, the soil profile consisted of two horizontal soil layers. The lower layer for all tests was dense Nevada sand, a fine, uniform sand (C_u=1.5, D_{50}=0.15 mm). The upper layer

Table 3.1: Summary of Soil Profiles

Container	Soil profile		Pore fluid
	Upper layer (≈ 9 m thick)*	Lower layer (11.4 m thick)	
Csp1	Sand ($D_r \approx 55\%$)	Sand ($D_r \approx 80\%$)	Water
Csp2	Sand ($D_r \approx 35$-40%)	Sand ($D_r \approx 80\%$)	HPMC-water
Csp3	Sand ($D_r \approx 55\%$)	Sand ($D_r \approx 80\%$)	HPMC-water
Csp4 & 5	Reconstituted Bay Mud (NC)	Sand ($D_r \approx 80\%$)	Water

*Upper layer was only 6.1 m thick (prototype - before testing) in Csp4 & Csp5.

was medium-dense Nevada sand in Csp1 and Csp3, loose Nevada sand in Csp2, and normally consolidated (NC) reconstituted Bay Mud (LL ≈ 90, PI ≈ 40) in Csp4 and Csp5. In all tests the sand was air pluviated, subjected to a vacuum (typically achieving ≈ 90 kPa vacuum), flushed with carbon dioxide, and then saturated under vacuum. The pore fluid was water in tests Csp1, Csp4, and Csp5, and was a viscous fluid in tests Csp2 and Csp3. The viscous fluid consisted of a mixture of water and hydroxy-propyl methyl-cellulose (HPMC) (Stewart et al. 1998). The viscosity of the pore fluid was increased to improve the simultaneous scaling of consolidation and dynamic processes. Note that dynamic time on the centrifuge is scaled as 1/n and consolidation time is scaled as $1/n^2$, resulting in a prototype that consolidates n-times faster than desired. By increasing the pore fluid viscosity in the model the consolidation rate can be decreased. In these tests, the 10-fold increase in pore fluid viscosity and the 1/30th scale modeling can be viewed as having the net result of consolidation occurring three times faster than would occur in the prototype, assuming pure water as the prototype pore fluid.

P-wave velocities were measured from top to bottom of the soil profile near the container center. Values were high enough (on the order of 1000 m/s) to indicate the sample was very close to saturated. Note it is difficult to determine the p-wave velocity in

the sample with certainty, as the sampling rate required for accurate measurement is beyond the capability of the data acquisition system. Fortunately the relationship between p-wave velocity and degree of saturation is very steep as complete saturation is approached (e.g. see Gazetas 1991), so simply showing that the p-wave velocity is close to 1000 m/s was considered sufficient to ensure a high degree of saturation (i.e. >99.5%).

The structural systems in each of the five containers are illustrated in Figures 3.2 to 3.6. Detailed drawings of each structure are given in Wilson et al. [1997 (a-e)], while detailed drawings of the highly instrumented single pile system used in tests Csp2-5 are given in Figure 3.7. Foundation models included single pile foundations, four-pile groups, and nine-pile groups. The superstructure mass was typically about 500 kN (prototype) per each supporting pile; i.e., 500 kN for a single-pile-supported structure, and 2000 kN for a four-pile-group supported structure. All piles were models of a prototype steel pipe pile 0.67 m in diameter, 16.8 m long, with a 19 mm wall thickness. Pile material properties are listed in Table 3.2. To represent typical bridge fundamental periods, column heights were selected to give fundamental periods for the structural systems ranging from 0.5 to 1.0 seconds. For all structural models, the pile tips were about 3.7 m above the container base (about 5.5 pile diameters); thus the end bearing of the piles should not have been significantly influenced by the container base.

Table 3.2: Pile Properties (tests performed at 30 g)

	model units	prototype units
material	6061-T6 Aluminum	
yield stress (MPa)	290	
Young's modulus (MPa)	70	
outside diameter (m)	0.0222	0.667
wall thickness (mm)	2.4	72.4
moment of inertia (m^4)	7.5×10^{-9}	6.1×10^{-3}
yield moment, M_y (MN-m)	0.195×10^{-3}	5.3

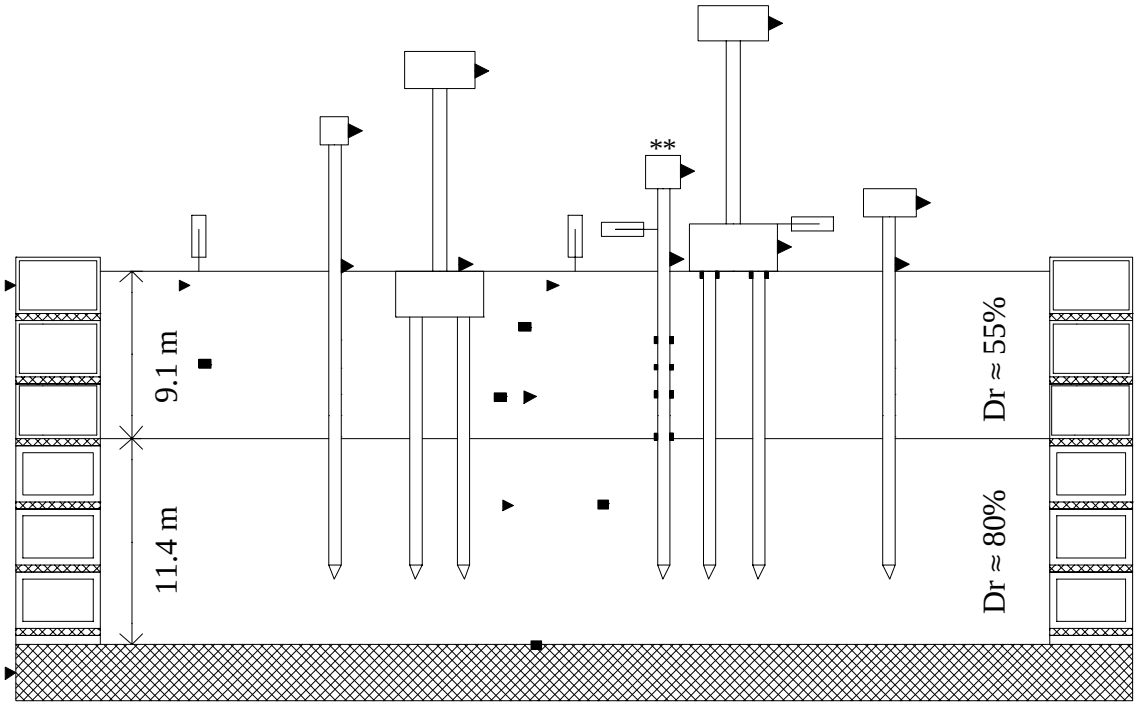

** - lightly instrumented single pile

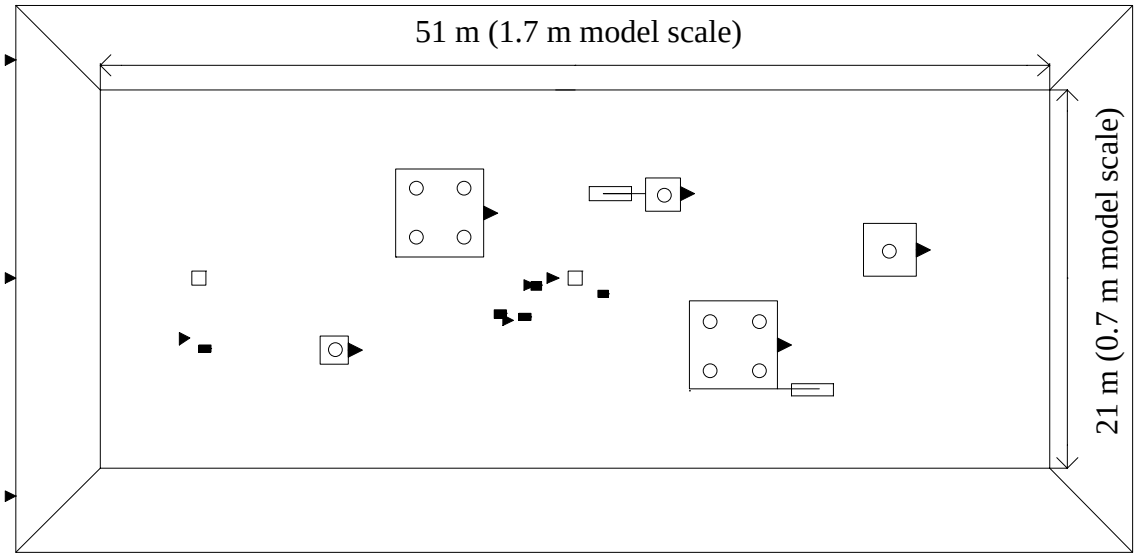

pore pressure
bending moment
displacement
acceleration

Figure 3.2: Model layout in Csp1

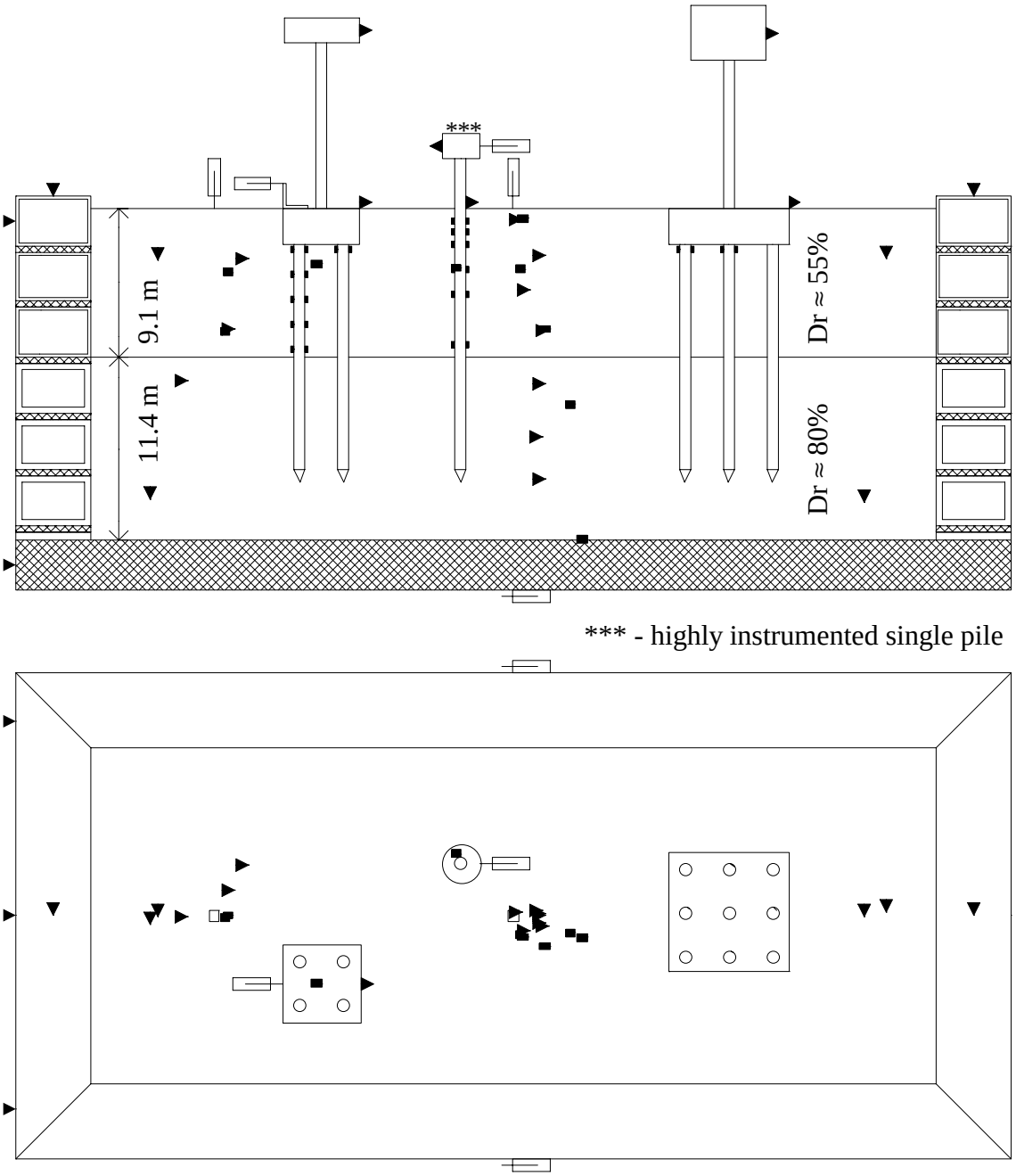

Figure 3.3: Model layout in Csp2

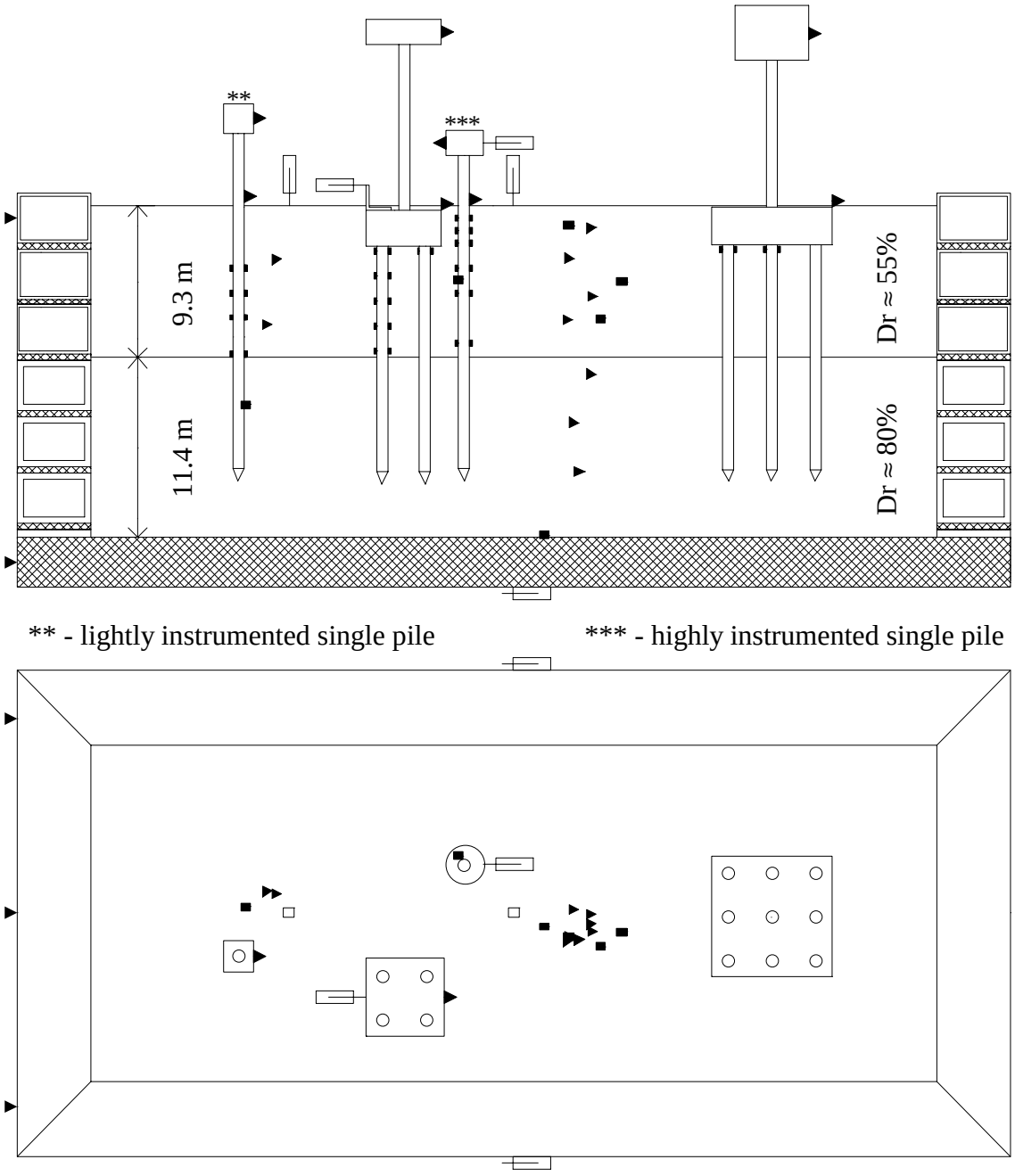

Figure 3.4: Model layout in Csp3

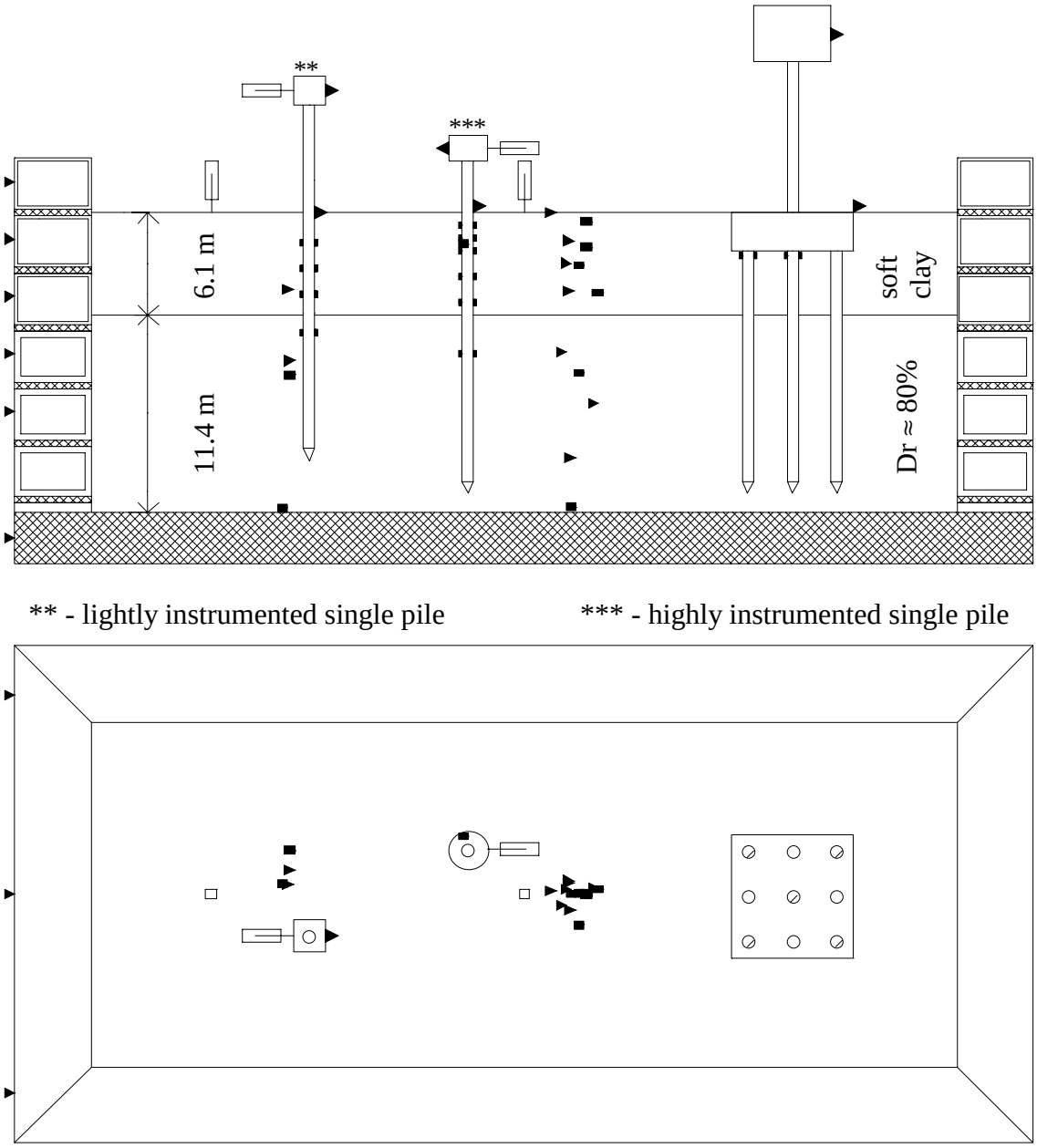

Figure 3.5: Model layout in Csp4 (dimensions prior to spinning)

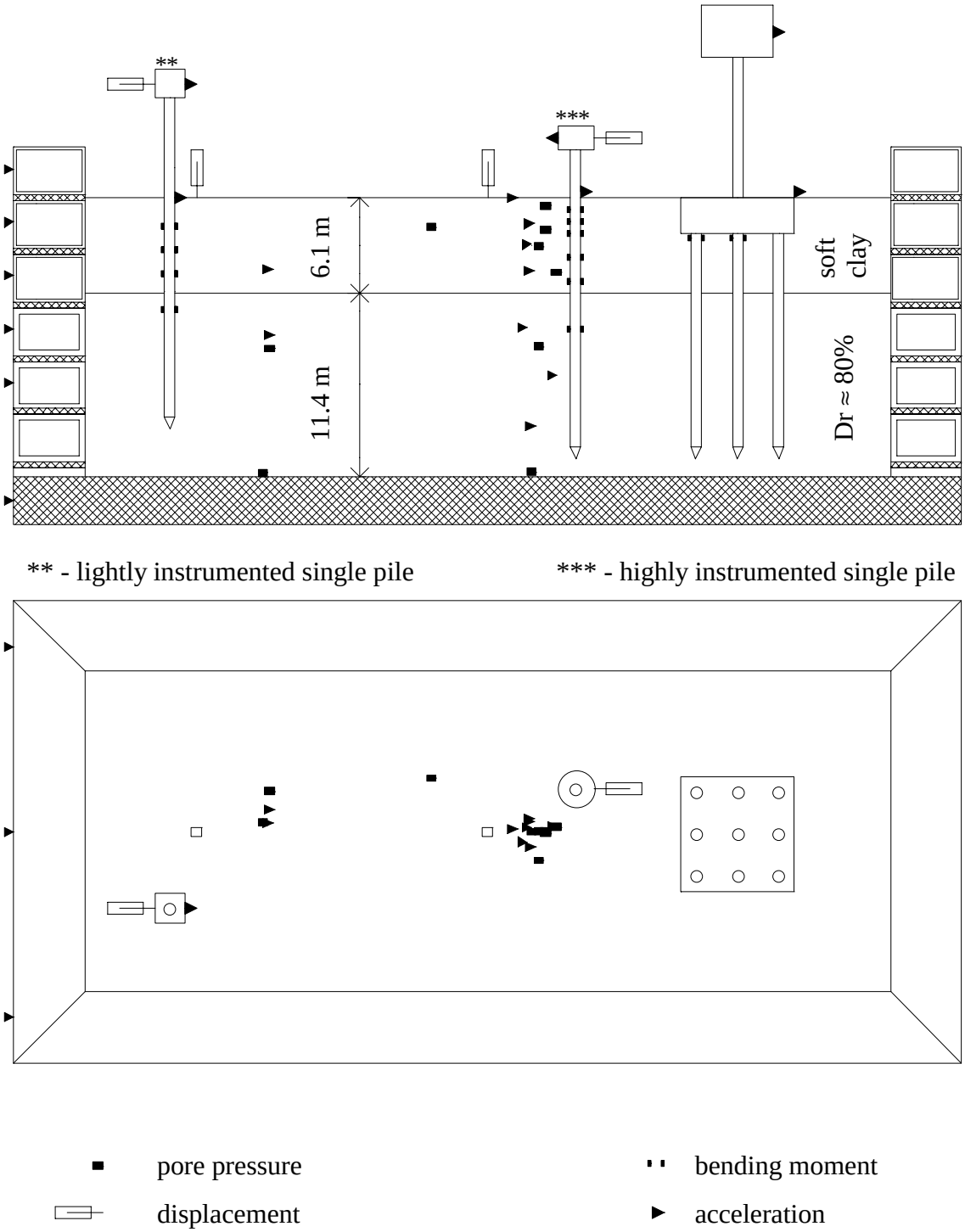

Figure 3.6: Model layout in Csp5 (dimensions prior to spinning Csp4)

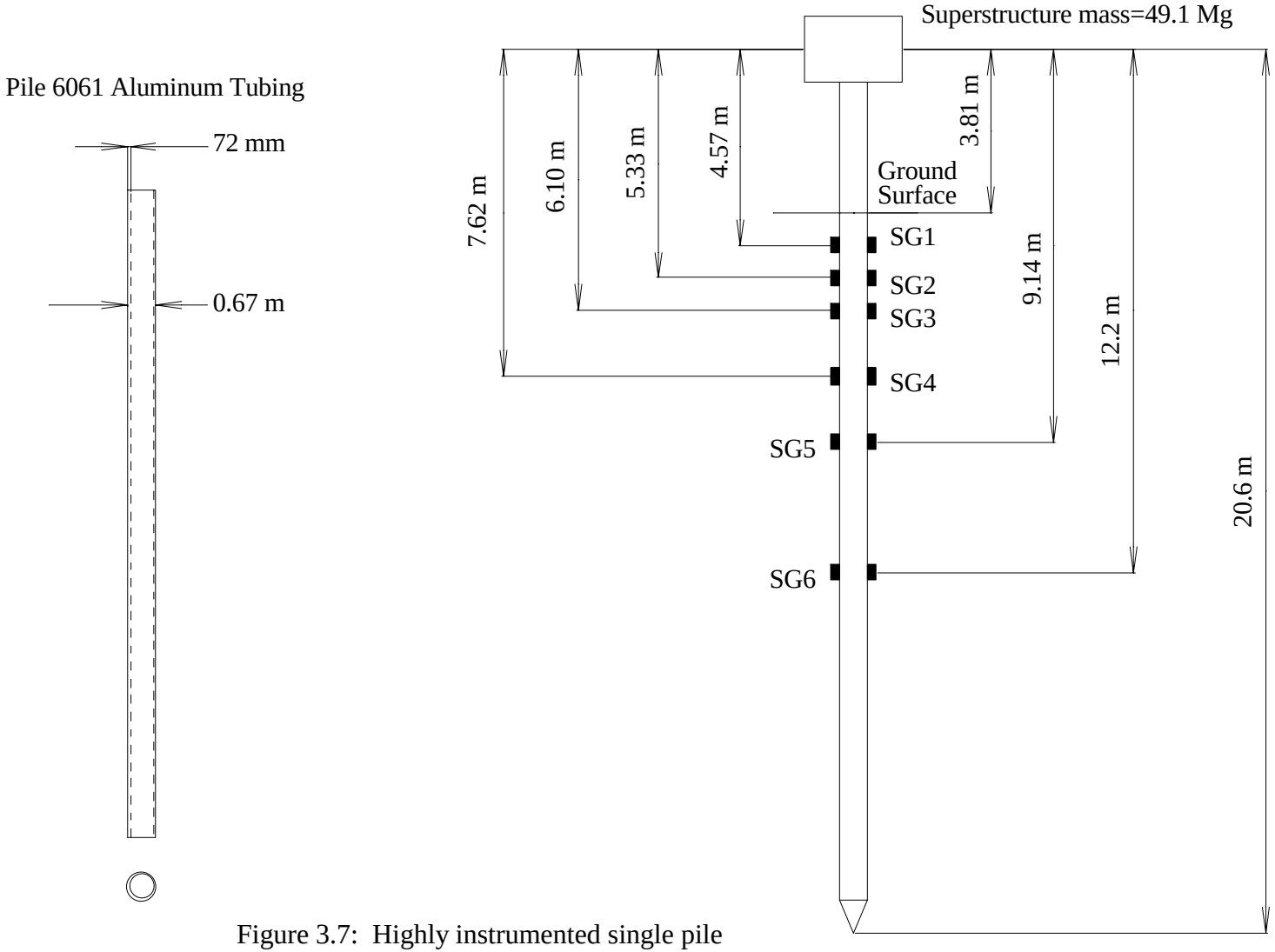

Figure 3.7: Highly instrumented single pile

Piles were driven into the sand at 1 g. Driving was done by dropping hammers from constant drop-heights onto the superstructure masses. A guide rod kept the hammer impact centered on the superstructure mass and a guide bar kept the piles aligned horizontally and vertically. Hammer blows per 2.54 cm (1 inch) of penetration were recorded. In all tests the single pile structures were driven after saturation. In tests Csp1 and Csp3, the pile groups were driven through both soil layers before saturation. In Csp2 the pile groups were impact driven into the dense sand layer and the loose sand was pluviated around the piles. In Csp4 and Csp5 the pile group was driven after saturation.

Each container was subjected to a series of shaking events, beginning with very low-level shaking events to characterize the low-strain response of the soil and soil-structure systems. Successive events progressed through very strong motions with peak base accelerations of up to 0.6 g. Earthquake events generally were sequenced in order of increasing amplitude, with periodic repeats of smaller events. Input base motions included step displacement waves and scalar multiples of recorded earthquake motions. The earthquake motions used are summarized in Table 3.3 and shown in Figure 3.8. Each shaking event was separated by an amount of time that exceeded the time required for full dissipation of any excess pore pressures. All in all, the first three containers (all sand profiles) were subjected to 16 to 17 shaking events each, while the fourth and fifth containers (upper layer of clay) were subjected to five shaking events each. The entire shaking schedule is shown in Table 3.4.

Table 3.3: Earthquake Motions Used

Motion	Recording
Kobe	1995 Kobe earthquake - Port Island 83 m depth, NS direction
Santa Cruz	1989 Loma Prieta earthquake - UCSC/Lick Lab, Ch. 1 - 90 degrees
Santa Cruz*	Same as above, but the original time step was doubled

Table 3.4: Suite of Centrifuge Shaking Events

Test	Event	Input	$a_{max,base}$ (g)
Csp1	A	step	
	B	Kobe	0.01
	C	Kobe	0.04
	D	Kobe	0.08
	E	Kobe	0.12
	F	Kobe	0.15
	G	Kobe	0.26
	H	Kobe	0.34
	I	step	
	J	Kobe	0.08
	K	Kobe	0.16
	L	Kobe	0.24
	M	Kobe	0.32
	N	step	
	O	Kobe	0.47
	P	Kobe	0.55
	Q	Kobe	0.17
Csp2	A	step	0.05
	B	Santa Cruz	0.01
	C	Santa Cruz	0.04
	D	Kobe	0.04
	E	Santa Cruz	0.49
	F	Kobe	0.22
	G	Santa Cruz	0.10
	H	Kobe	0.10
	J	Santa Cruz*	0.45
	K	Santa Cruz*	0.12
	L	Kobe	0.62
	M	Kobe	0.24
	N	Kobe	0.44
	O	Santa Cruz	0.53
	P	Kobe	0.60
	Q	Santa Cruz*	0.56
Csp3	A	step	0.06
	B	Santa Cruz	0.01
	C	Santa Cruz	0.01
	D	Santa Cruz	0.04
	E	Kobe	0.04
	F	step	0.06
	G	Santa Cruz	0.03
	H	Kobe	0.03
	I	Santa Cruz	0.49
	J	Kobe	0.22
	K	Santa Cruz	0.11
	L	Kobe	0.11
	M	Santa Cruz*	0.41
	N	Santa Cruz*	0.10
	O	Kobe	0.60
	P	Santa Cruz	0.55
Csp4	A	Kobe	0.05
	B	Kobe	0.05
	C	Kobe	0.02
	D	Kobe	0.20
	E	Kobe	0.58
Csp5	A	Santa Cruz	0.04
	B	Santa Cruz	0.12
	C	Santa Cruz	0.30
	D	Santa Cruz	0.60

* The time step of the original recording was doubled for this motion

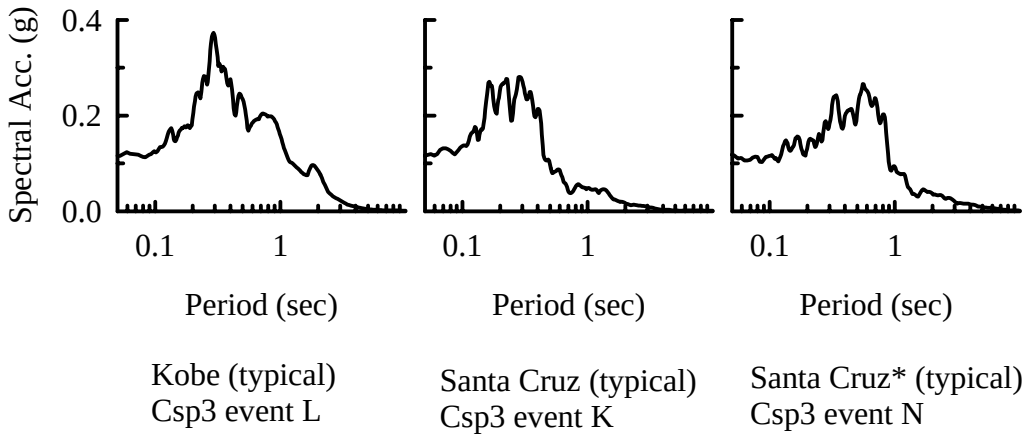

* - the time step of the original earthquake was doubled for this motion

Figure 3.8: Spectral accelerations of typical centrifuge input motions (5% damping)

3.2 CENTRIFUGE MODELING TECHNIQUES

The dynamic centrifuge tests of pile-supported structures in soft or liquefied soils performed in this study were among the first performed using the recently completed shaking table, and thus it was necessary to evaluate the centrifuge modeling system before analyzing the model structures. The importance of characterizing the centrifuge modeling system was demonstrated by the VELACS cooperative study (e.g., Arulanandan et al. 1994) and further discussed by Scott (1994). Difficulties or limitations with dynamic centrifuge modeling systems can include: (1) non-repeatability of model tests; (2) undesirable vertical motions, including rocking of the soil column; (3) inability to produce input motions with the broad frequency content of real earthquake motions; and (4) container effects. These and other aspects of the dynamic centrifuge modeling system

on the large centrifuge at UC Davis are evaluated using the results of the soil-pile-superstructure interaction experiments.

3.2.1 Uniformity of Sand Layers

The density, uniformity, and repeatability of sand layers were evaluated by measuring the force required to push a 6 mm diameter rod with a 60° conical tip at various locations while at 1 g (Divis et al. 1996). The force was divided by the tip area and presented as a penetration resistance (Q), although it is noted that Q reflects both tip and shaft resistances. Results of penetration tests on Csp2 and Csp3 (both before shaking) are shown in Figure 3.9. In both containers, tests in the free field showed nearly uniform profiles of Q, with Q being much higher in the lower dense layer than the upper loose layer. In Csp2 ($D_r \approx 35\%$) the single pile was driven and likely densified the soil near the pile. But the loose sand was placed around the pile groups and the penetration tests there showed the sand was softer (less penetration resistance) near the pile groups. Pile groups were driven in Csp3. Three tests located alongside the 2x2 and 3x3 pile groups showed substantial increases in Q due to pile driving. Two tests pushed between the piles of the 2x2 and 3x3 groups (through holes in the caps) showed even greater values of Q, particularly in the 3x3 group. Interpretation of these penetration tests is complicated by the low confining pressures (at 1 g), the mix of shaft and tip resistances, the relatively large zone of influence of the tip [e.g., 10-20 probe diameters is 9-18% of the total soil thickness (Vesic 1970)], and the influence of the boundaries. Nonetheless, these data are a valuable indicator of specimen density and uniformity, and were useful for evaluating the pile installation effects.

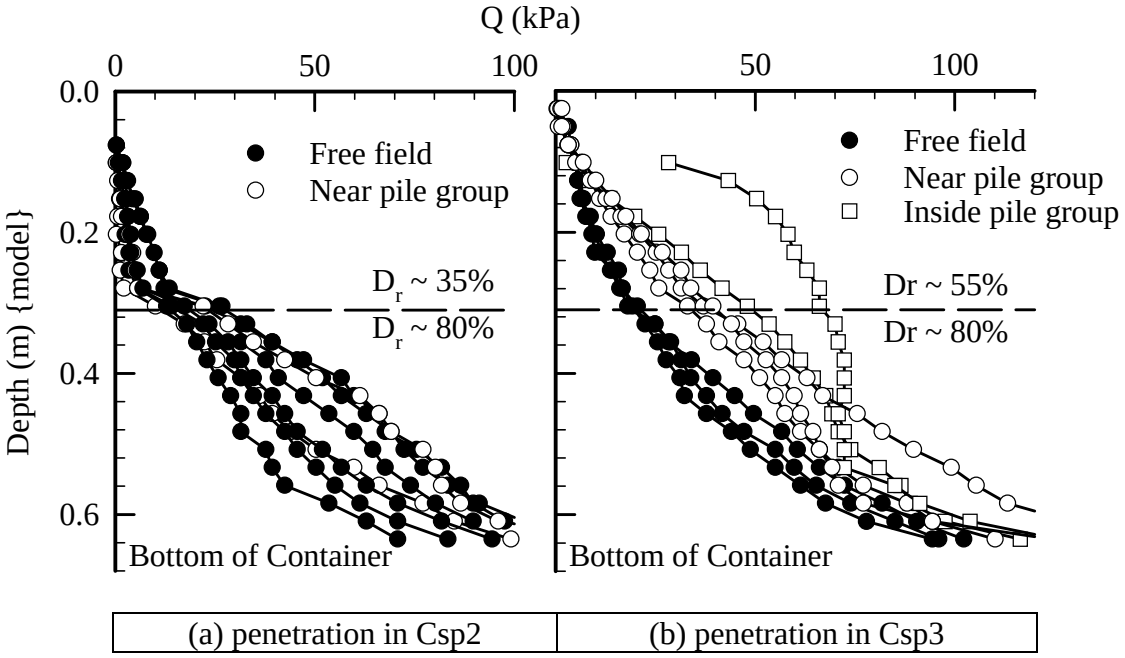

Figure 3.9: Penetration resistances in tests (a) Csp2 and (b) Csp3. Penetration tests performed at 1 g before spinning

3.2.2 Input Motions

For realistic seismic modeling of pile-supported structures, the simulated motion should reasonably reproduce the full range of frequencies present in recorded earthquake motions. The input motion should also be repeatable and reasonably unchanged when scaling the acceleration amplitude to minimize difficulties with evaluating nonlinear behavior between scaled shaking events. Travel limitations of the shaker limit the low frequency content of the simulated motion, and the dynamic performance of the shaker system will affect the overall spectrum of the simulated motion. The dynamic performance of centrifuge shaker systems has sometimes resulted in less than desirable simulations of earthquake motions (Scott 1994). The shaker on the large centrifuge at UC Davis is relatively new, so the system performance was evaluated during this project.

The performance of the shaking table is shown in Figure 3.10. Acceleration response spectra (ARS, 5% damping) of the recorded east and west base motions during three scaled Kobe events ($a_{max} \approx 0.04$, 0.23, and 0.6 g prototype) on each of three containers (total of nine events) are shown, with the ARS normalized to a zero period value of one on the east actuator. The ARS are very similar at each level of shaking, and show only small spectral variations across the full operational range of the shaker (i.e., $a_{max} \approx 0.04$ to 0.6 g prototype corresponds to $a_{max} \approx 1.2$ to 18 g model for a centrifugal acceleration of 30 g). East and west base motions are also seen to be closely in-phase and parallel, as shown at the bottom of Figure 3.10 by the nearly identical acceleration time histories during a typical Kobe event. The ARS of the original recording from Port Island is shown in Figure 3.10 for comparison to the achieved spectra. The base motions retain the full spectrum of the original recording in the range of interest, about 0.5-5 Hz prototype in this study.

3.2.3 Effect of Pore Fluid Viscosity

The effect of changing pore fluid viscosity was evaluated by comparing results from Csp1 and Csp3 for four comparable shaking events. Note that results from these tests are described in detail in later sections of this report, while select results are used here to address issues related to the centrifuge modeling techniques. Containers Csp1 and Csp3 had identical soil profiles and one identical single-pile-supported structure [model details in Wilson et al. 1995, Boulanger et al. 1997, Wilson et al. 1997 (a) and (c)], but the viscosity of the pore fluid differed by a factor of 10 (Table 3.1).

The responses of the soil profiles and single-pile-supported structures were similar for comparable shaking events except the rate of pore pressure dissipation was always

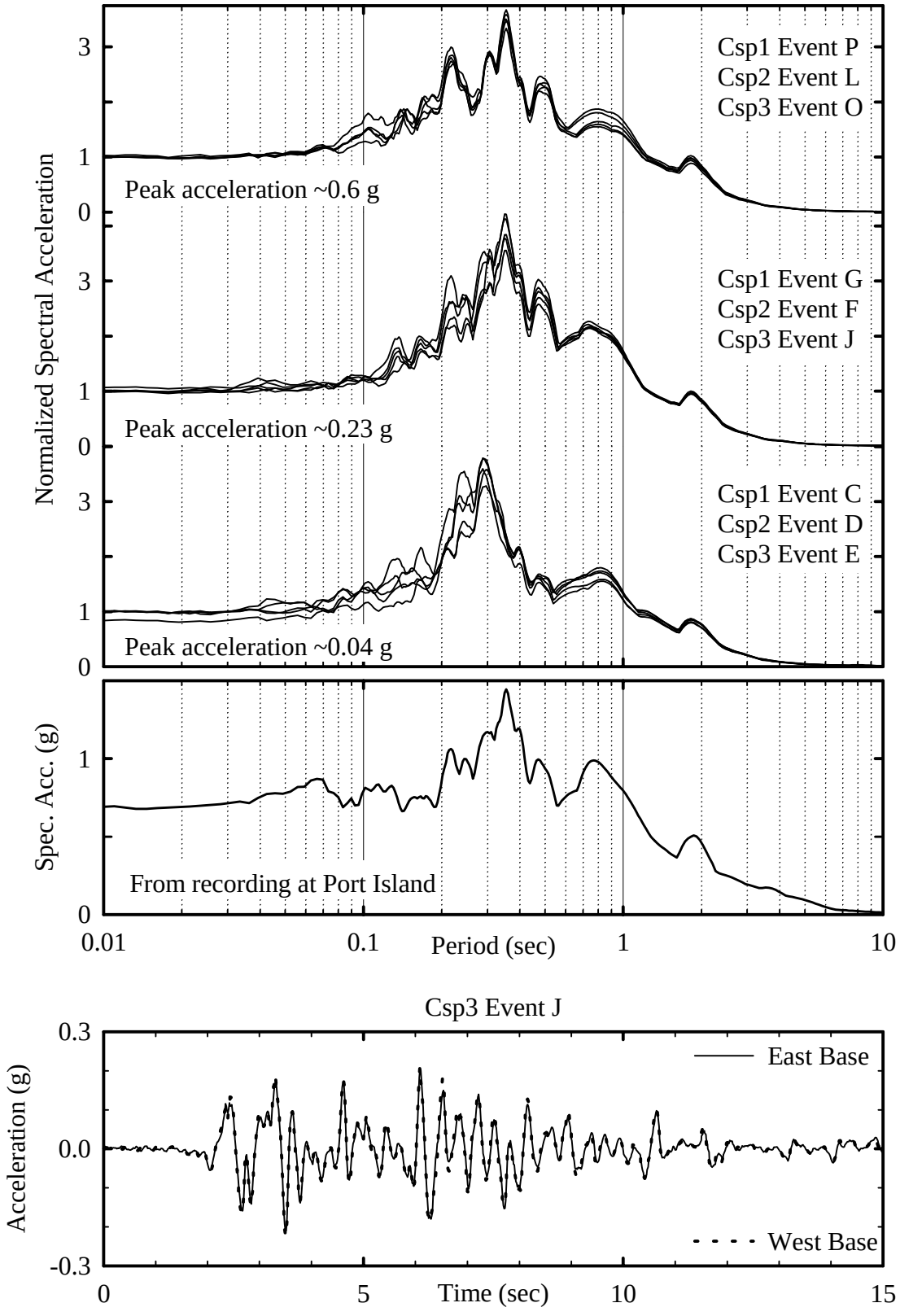

Figure 3.10: Repeatability of input motion (all spectra at 5% damping)

faster in Csp1 than in Csp3. This is exemplified in Figure 3.11 by time histories of excess pore pressure ratios at similar locations during Kobe events with $a_{max,base} \approx 0.23$ g. During shaking, however, the difference in pore pressure ratios was typically less than about 10%, and the cyclic pore pressures were similar. ARS for various locations in the upper sand layer in Csp1 and Csp3 also had similar normalized shapes, although Csp1 typically had slightly greater spectral accelerations near a period of one second (e.g. see Figure 3.12). The difference in pore pressure dissipation rates between Csp1 and Csp3 is expected due to the change in pore fluid viscosity. Other slight differences in the soil profile response were likely due to a combination of factors, including slight variations in soil densities, model preparation techniques, input motions, and the different pore fluids used.

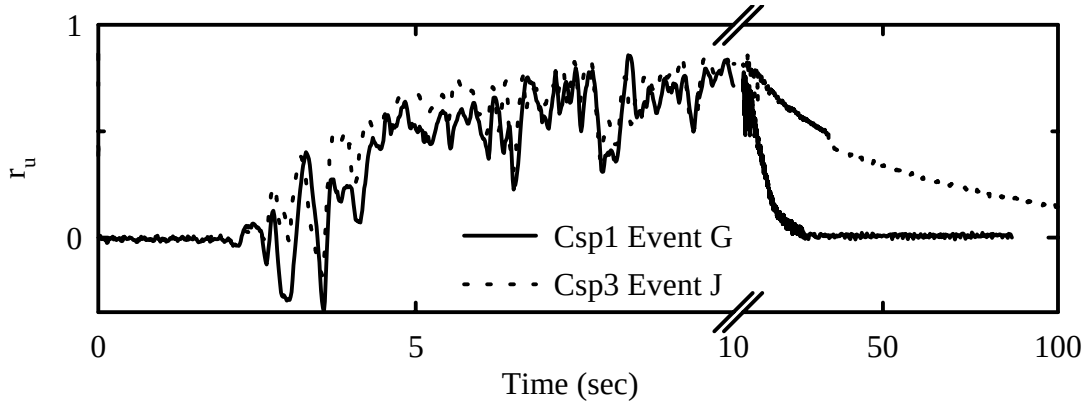

Figure 3.11: Generation and dissipation of pore pressure in 55% D_r soil with water (Csp1) or viscous mixture (Csp3)

The response of the lightly instrumented single pile system during these same events is illustrated by bending moment time histories at depths of 3.8 and 5.3 m in Figure 3.13. Bending moments were normalized by the peak superstructure acceleration because the peak superstructure acceleration in Csp1 was about 50% greater than in Csp3.

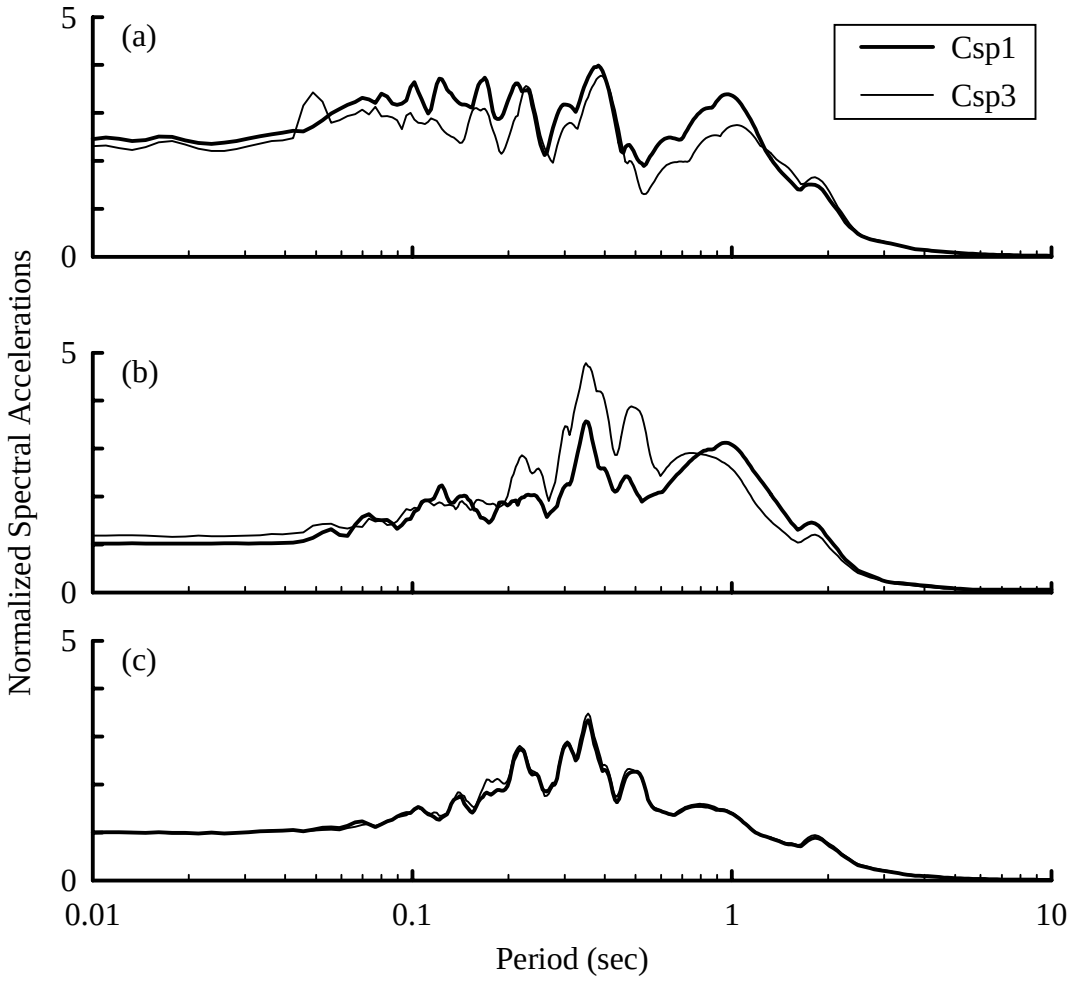

(a) near surface	(b) near bottom of loose layer	(c) base motion

Figure 3.12: Response spectra (5% damping) for Csp1 event G and Csp3 event J normalized by the peak base accelerations of each event. Peak base acceleration in Csp1 event G = 0.26 g. Peak base acceleration in Csp3 event J = 0.22 g.

The difference in superstructure accelerations is due to both a 20% difference in the peak base input motion and the previously described differences in the soil profile ARS at the natural period of the structure, at about one second. Normalized bending moments for the lightly instrumented single pile system in Csp1 and Csp3 show very little difference during shaking, but do show interesting, although inconsequential for design, differences

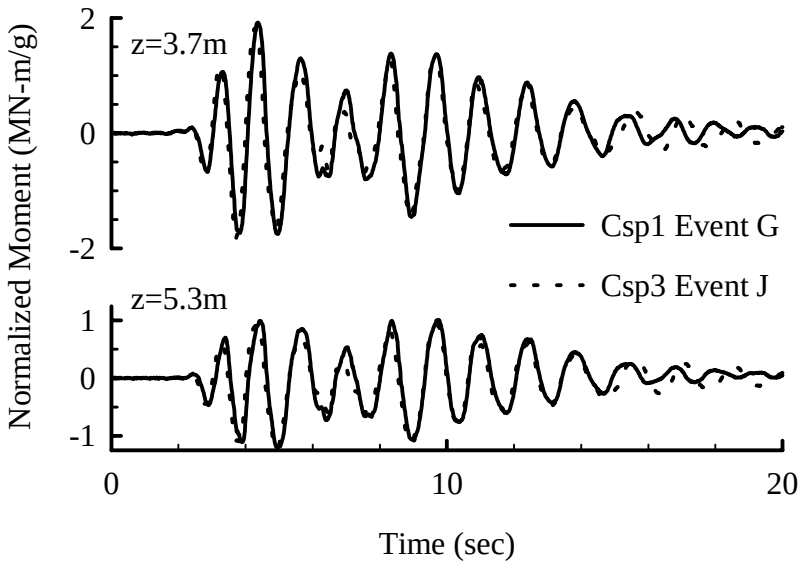

Figure 3.13: Bending moment distribution when $D_r \approx 55\%$

developing after strong shaking. Comparing bending moment time histories at other depths and other levels of shaking also gave very similar results, and thus the bending moment distributions at any time were essentially the same in Csp1 and Csp3. These results and the behavior of the soil profile response suggest that changing pore fluid viscosity by a factor of 10 had only minor effects on the transient soil-pile interaction.

The relatively minor effect of changing pore fluid viscosity seems to imply that the dynamic soil-structure interaction was essentially undrained in all cases presented herein. Note this is not expected to be true in general. Changing pore fluid viscosity may have a more noticeable effect on other model configurations where partial drainage during dynamic loading may be significant, such as if a more permeable soil or a smaller diameter pile was used.

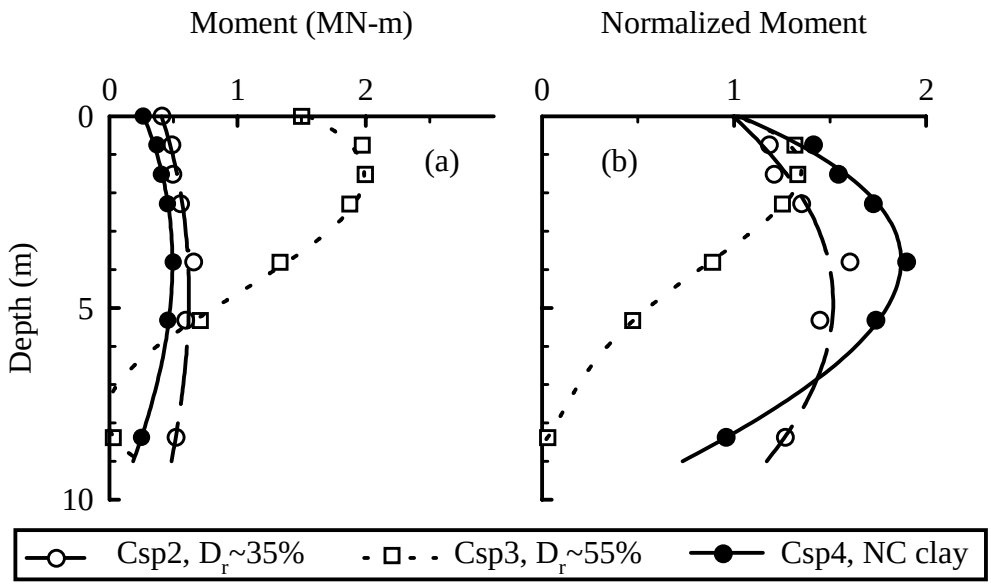

Figure 3.14: Bending moment distribution with varying soil types

3.2.4 Effect of Soil Type and Density

The effect of the upper soil layer on structural response and bending moment distribution is illustrated by a comparison of results from Csp2, Csp3, and Csp4 (see Table 3.1). Results from these tests are described in detail in later sections of this report, while select results are used here to illustrate issues related to the centrifuge modeling techniques. In Figure 3.14(a), the bending moment distributions versus depth are shown for the highly instrumented single pile system in Csp2, Csp3, and Csp4 during a Kobe event with $a_{max,base} \approx 0.23$ g. In Figure 3.14(b), these bending moments are normalized to a ground surface moment of unity. Note that liquefaction was more extensive in Csp2 than in Csp3 during these events, as evidenced by pore pressure time histories showing that pore pressures increased much quicker, and dissipated slower, in the $D_r \approx 35\%$ sand layer of Csp2 than in the $D_r \approx 55\%$ sand layer of Csp3 (Figure 3.15). The looser condition of the upper layer in Csp2, relative to Csp3, resulted in generally lower ground surface

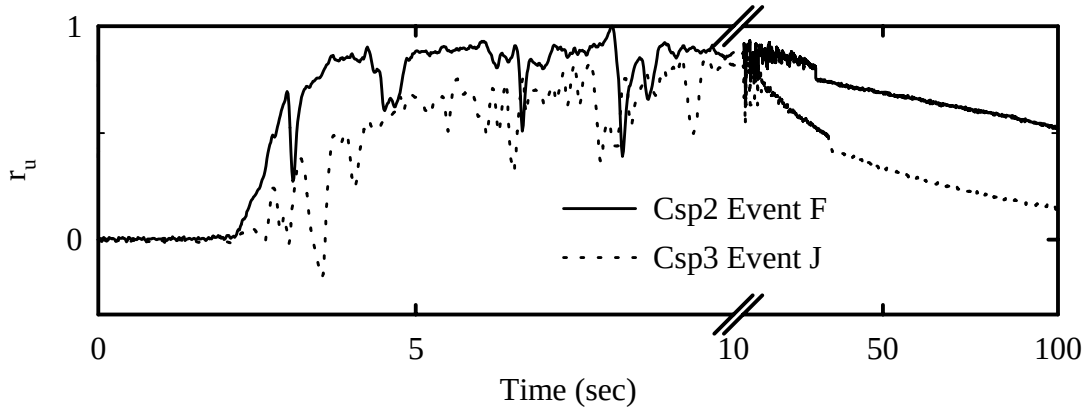

Figure 3.15: Generation and dissipation of pore pressure when $D_r \approx 35\%$ (Csp2) and $D_r \approx 55\%$ (Csp3)

accelerations, lower peak superstructure accelerations, and a greater apparent softening of the liquefied soil's p-y resistance (Boulanger et al. 1997). These aspects of behavior are shown by the smaller bending moment at the ground surface [Figure 3.14(a)], but a greater depth to peak bending moment [Figure 3.14(b)]. In Csp4 (upper layer of soft clay), the peak superstructure acceleration was lower than that of Csp2 and Csp3, and the depth to peak bending moment was comparable to that of Csp2. These results are consistent with expected soil behaviors for the soil conditions and input motions used in these tests.

3.2.5 Behavior of the Container and Soil Column System

The dynamic characteristics of a model container and its interaction with the soil column must be clearly understood if reliable interpretations of test results are to be made. Container effects on the soil column response have been studied using several different measurements of response (e.g., Fiegel et al. 1994, Van Laak et al. 1994, Whitman and Lambe 1986). In this study, the interaction is evaluated in terms of the

uniformity of horizontal motions and differential vertical displacements in the soil near the container ends.

The uniformity of horizontal motions across the soil column and container rings indicates whether the container and soil are moving in unison during shaking. To measure uniformity, accelerometers were attached to the individual rings of the FSB1 container and at corresponding depths near the center and corners of the soil profile. Accelerometer records were high-pass filtered and double integrated to get displacements following the procedures outlined later in this chapter. Results for several shaking events on each container show that horizontal acceleration and displacement time histories are nearly identical (i.e., highly coherent) at any given elevation in the soil column and on the corresponding container ring for tests involving non-liquefied sand or low shaking levels with soft clay.

Horizontal motions at shallow depths in Csp1 during a Kobe event ($a_{max,base} \approx 0.23$ g) causing liquefaction of the $D_r \approx 55\%$ layer late in shaking are shown in Figure 3.16. Accelerations at the soil surface near the center and one end of the model, and on the top ring, are seen to have similar waveforms but with differing high frequency contents later in shaking. In particular, several large high-frequency acceleration spikes were recorded near the end of the container. However, horizontal displacements relative to the container base at these three points were relatively uniform (bottom of Figure 3.16).

Several investigators have observed acceleration spikes in centrifuge tests with liquefied soils, while spikes have been less obvious in field data. Note a good example where acceleration spikes were present in field data was recorded at the Wildlife site during the 1987 Superstition Hills earthquake (Zeghal and Elgamal 1994). In the

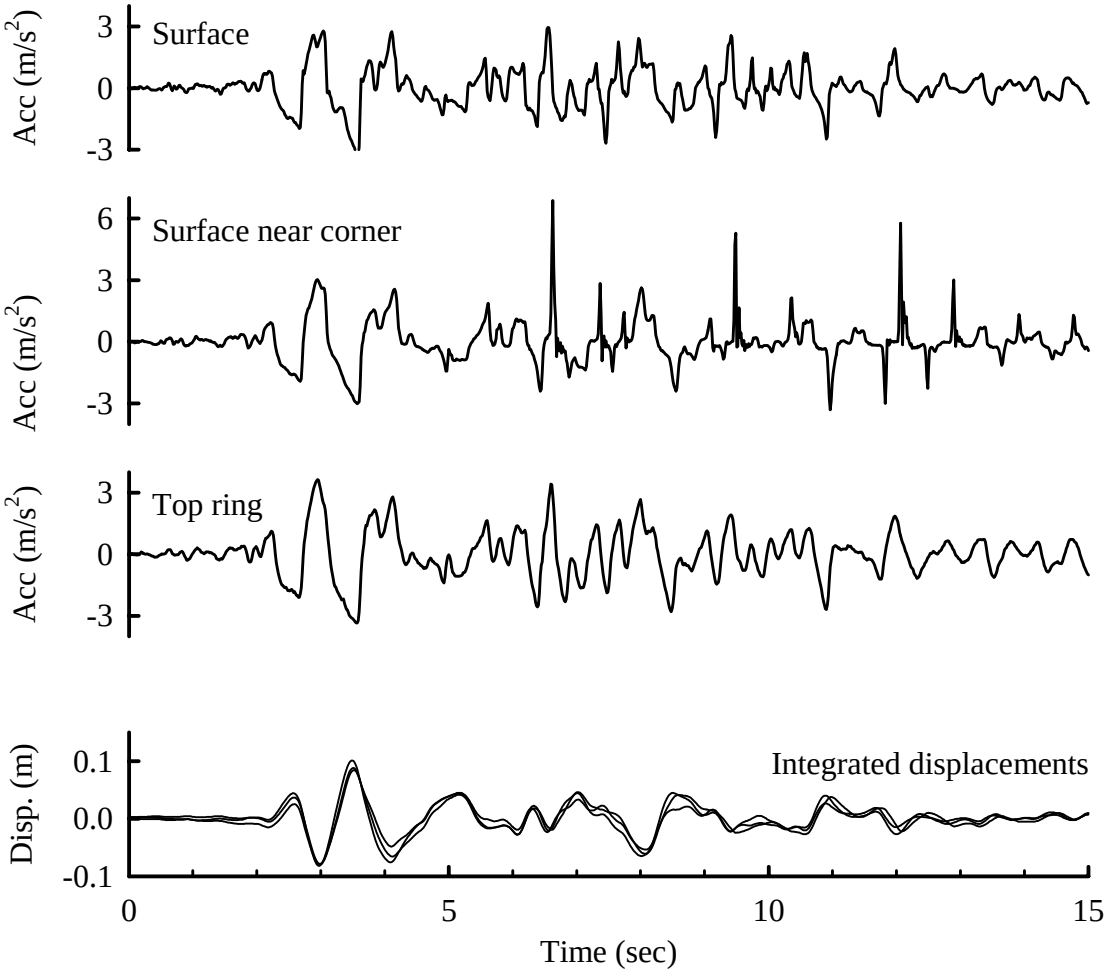

Figure 3.16: Uniformity of motion near top of container - Csp1 event G

centrifuge tests presented herein, acceleration spikes have been observed throughout liquefied layers, near the middle and ends of the container, and in horizontal and vertical directions. Acceleration spikes have not been observed when the excess pore pressure ratio is less than about 70%. Acceleration spikes coincide with rapid pore pressure drops, and thus are likely due to the uniform soil profile "locking" up all at once as the sand goes through a phase transformation (i.e., the transition from contractant to dilatant behavior at large enough shear strains).

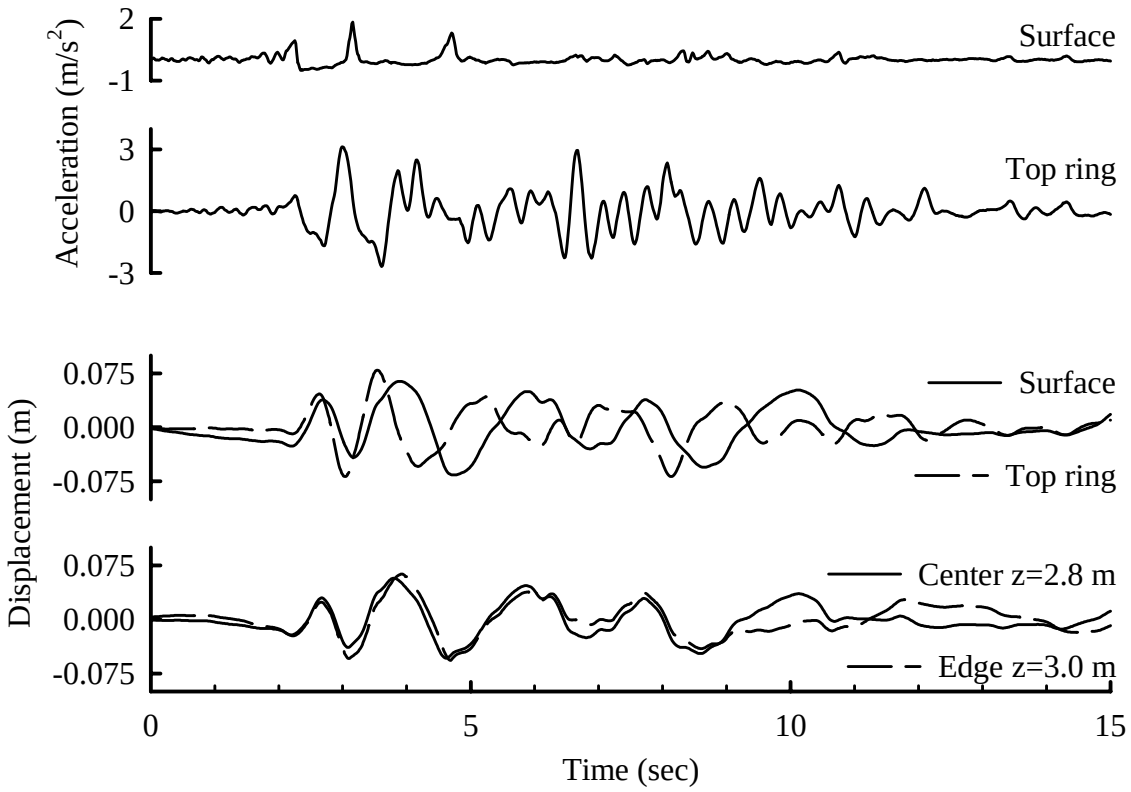

Figure 3.17: Uniformity of motion in liquefying sand - Csp2 event F

Horizontal motions at shallow depths in Csp2 during a Kobe event ($a_{max,base} \approx 0.23$ g) causing liquefaction of the $D_r \approx 35\%$ layer are shown in Figure 3.17. Accelerations at the surface of the soil near the center of the container were very different from the acceleration of the top ring. Furthermore, the displacements of the top ring and the soil relative to the container base were very different, at times nearly 180° out of phase. In this case, when r_u was high and D_r was low, the soil column became much softer than the container, as shown by the predominant frequency content of recorded motions in the profile and on the container. As a result, the container restricted lateral movements near its edge. While this is not ideal, it is physically difficult to avoid. It is expected that this effect may be incorporated into numerical analyses using two-

dimensional site response models if necessary. Uniformity of horizontal motions, however, improved with depth in the liquefied soil layer. This is illustrated at the bottom of Figure 3.17 by the horizontal displacements relative to the container base for two locations at the same elevation deeper in the liquefied layer.

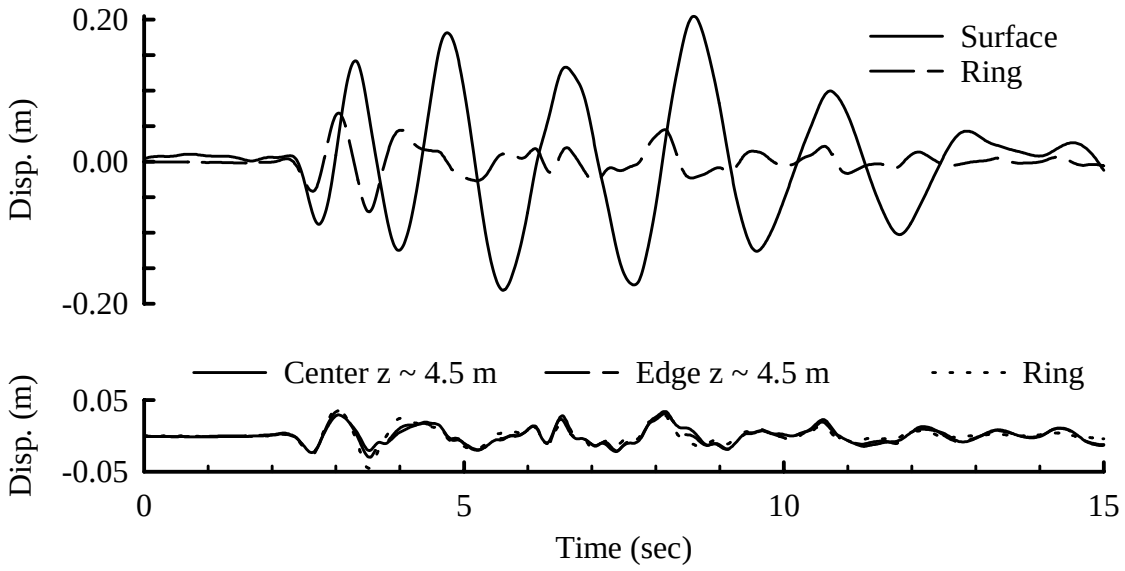

Figure 3.18: Uniformity of motion in clay - Csp4 event D

A similar set of plots from Csp4 for a Kobe event ($a_{max,base} \approx 0.23$ g), where the upper soil was normally consolidated clay, are shown in Figure 3.18. In this case, however, the top ring was empty and the soil surface was level with the second ring. The upper plot shows the difference between displacements at the surface center of the soil profile and the second ring relative to the container base. The lower plot, however, shows that by the third ring, the container and the soil are moving mostly together. It should be noted that the uppermost accelerometer in this container was very near the soil surface and may not accurately reflect the motions of the soil due to a lack of confinement.

Records from this transducer uppermost in the clay layer are thus not used in the analyses presented later in this dissertation.

In addition to the container moving with the soil, the soil profile should also deform in shear as opposed to column bending. In undrained shear, there is no vertical strain when the soil profile deforms horizontally, while column bending will cause one end to compress and the other to extend. The container should help minimize column bending by providing complementary shear stresses at the end interfaces between the soil and the container. Discussions of the role of complementary shear stresses and rocking in centrifuge modeling can be found in Zeng and Schofield (1996) and Wilson et al. [1997(f)].

In Csp2 ($D_r \approx 35\%$ upper layer), vertical accelerometers were included at the north and south ends of the model container base and top ring, and near the bottom and top of the soil profile (total eight transducers), in order to quantify rocking of the container and soil column. Figure 3.19 is a summary plot of the recorded peak accelerations and integrated peak absolute displacements from these transducers. The peak vertical accelerations were typically 20 to 30% of the peak horizontal accelerations at all locations other than the upper soil profile, and the peak vertical displacements were typically less than about 10% of the peak horizontals, again other than in the upper soil profile. Note that these data are for the ends of the container, while vertical motions within the central portion of the container are expected to be much smaller (either end is moving at about the same magnitude but out of phase, thus motion near the middle will probably be near zero).

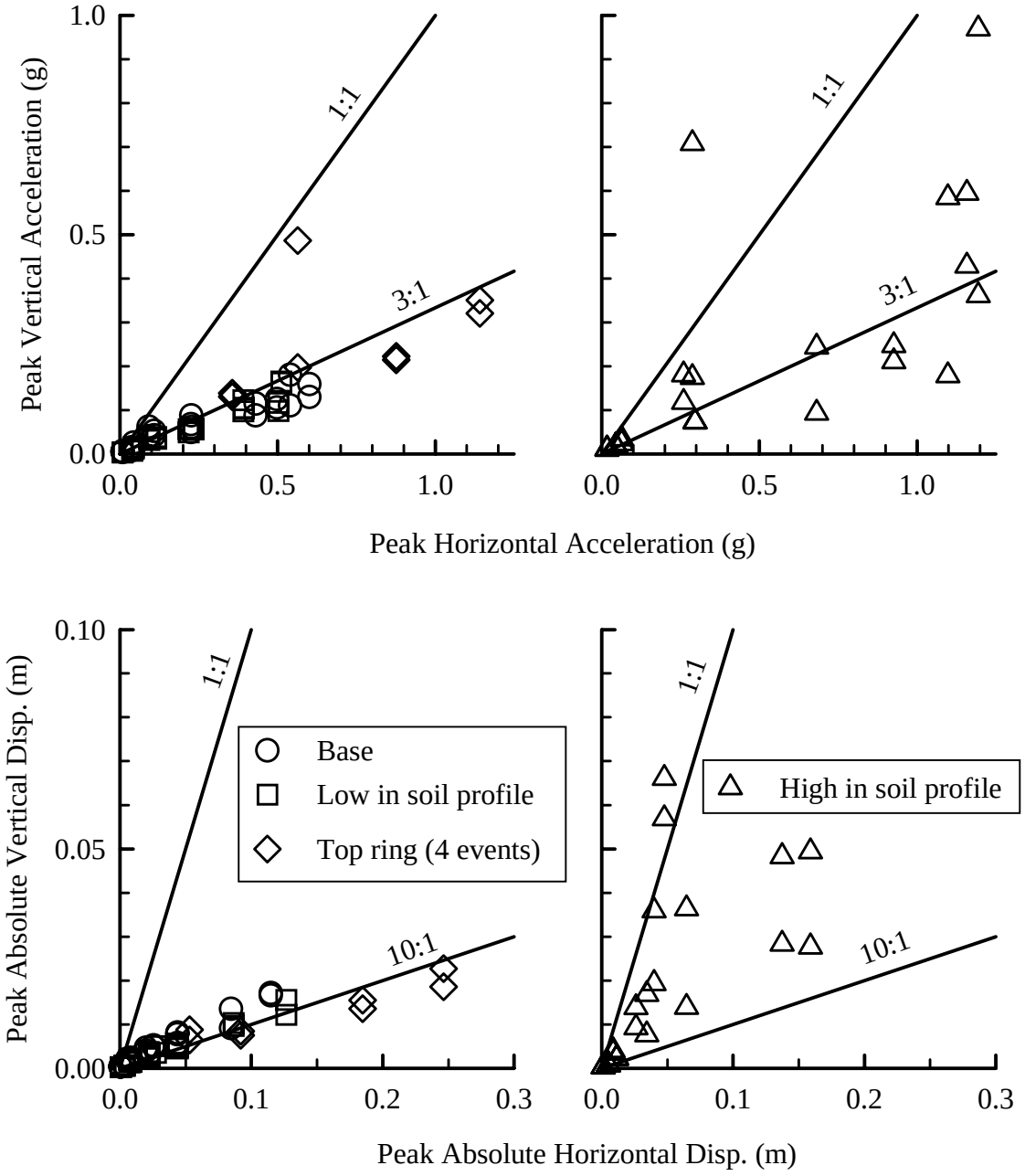

Figure 3.19: Peak vertical versus peak horizontal accelerations and displacements throughout model - Csp2 ($D_r \approx 35\%$)

The data in Figure 3.19 show that the shaking table and FSB1 container do not introduce significant rocking or pitching motions, and that the lower halves of the soil profile have similarly low levels of vertical motion. However, the vertical accelerations

and displacements in the upper soil profile near the container ends are of comparable magnitude to their horizontal counterparts, indicating that motions are not uniform within the upper soil profile. Note, however, that liquefaction occurred in all but the smallest events in Csp2. For the smallest events (see Figure 3.20), the vertical accelerations recorded in the upper soil profile appear to be consistent with the magnitude of the other vertical recordings. This indicates that the large vertical motions near the ends of the upper soil profile were due to liquefaction effects, as discussed below.

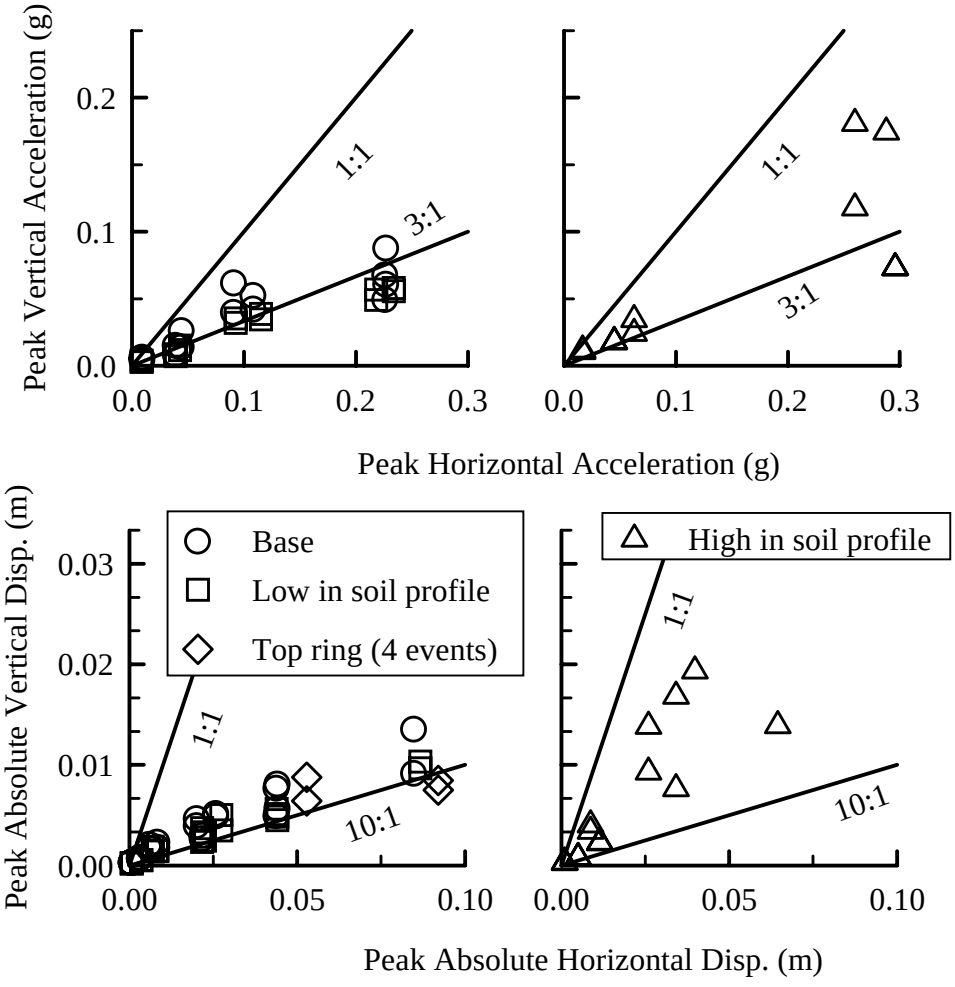

Figure 3.20: Peak vertical versus peak horizontal accelerations and displacements throughout model, small events - Csp2 ($D_r \approx 35\%$)

There are at least two simple modes of vertical displacement for the soil near the ends of the container. In the first mode, the soil profile deforms as a column bending, as shown schematically in Figure 3.21(a). As shown, when the base accelerates to the north, the relative displacement of the surface will be to the south. The vertical displacement at the south end of the container will be down, and the opposite will occur at the north end. In the second scenario, the liquefied soil "sloshes" in a relatively rigid container, as shown schematically in Figure 3.21(b). When the base accelerates to the north and the relative displacement of the surface is to the south, the soil at the south end of the container will slosh up, and the vertical displacement at the north end will be down.

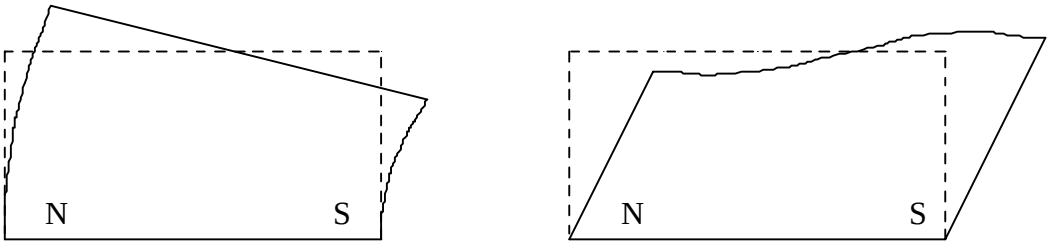

(a) column bending	(b) sloshing

Figure 3.21: Simple modes of vertical displacement

Vertical and horizontal displacements of the ground surface relative to the container base in Csp2 ($D_r \approx 35\%$ upper layer) are summarized in Figure 3.22 for both (a) a non-liquefaction and (b) a liquefaction event. The convention used in Figure 3.22 is that positive horizontal displacement is a displacement to the south, and positive vertical displacement is upward. In Figure 3.22(a), the horizontal displacement and the north vertical displacement are nearly in phase, while the south vertical is nearly 180° out of phase. This is consistent with the expected behavior for bending of the soil column, as previously described. Also, vertical displacements are on the order of 10% of the

horizontals. In Figure 3.22(b), the opposite phasing occurs, with the south vertical moving in phase with the horizontal and the north nearly 180° out. This is consistent with the sloshing mode previously described, and is consistent with Figure 3.17, where we saw the effects of the soil profile becoming softer than the container. Vertical displacements are also of the same magnitude as the horizontals in Figure 3.22(b).

Although the deformation modes shown in Figure 3.21 are greatly simplified, the results shown are consistent with the large vertical displacements not being due to a lack of complementary shear stresses, but due to the differences in stiffness between the soil and the container. While not ideal, this problem is physically difficult to avoid. An appreciation of this limitation is necessary for realistic interpretations or analyses of the centrifuge data.

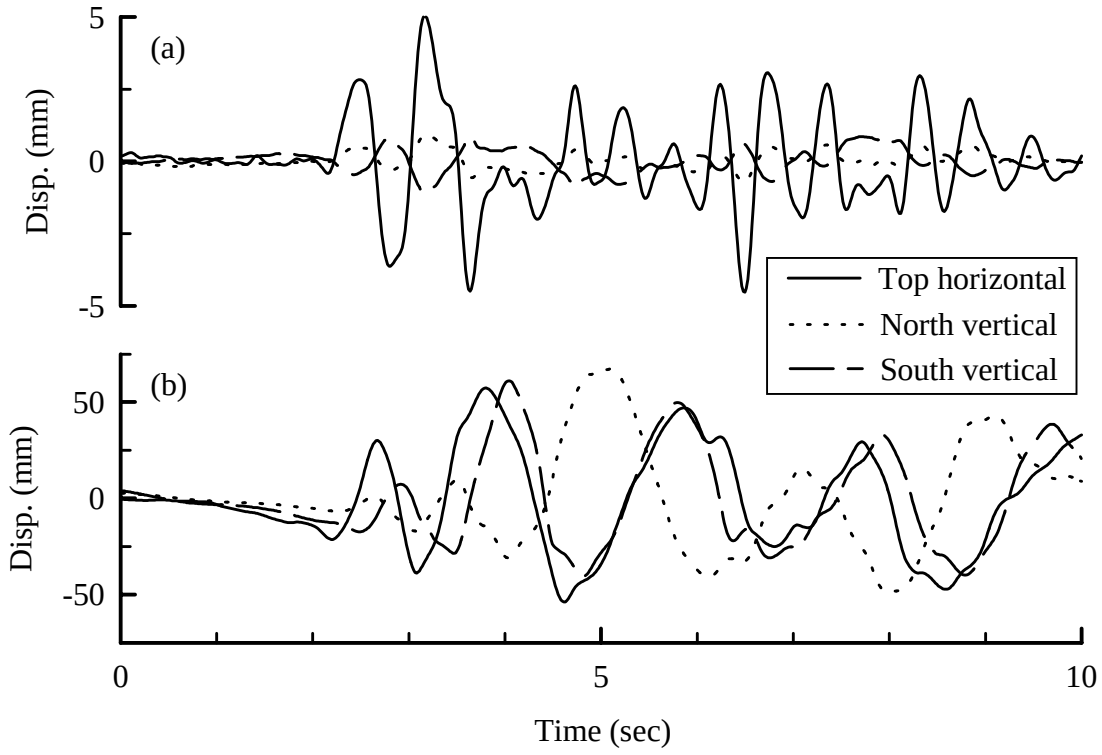

Figure 3.22: Relative displacements at the top of FSB1 showing (a) column bending, and (b) sloshing of liquefying soil

3.2.6 Pore Pressures Near Structures

The influence of the pile foundations on the excess pore pressures in the upper sand layers of Csp1, Csp2, and Csp3 were evaluated by placing pore pressure transducers both near and far from the structures. For example, Figure 3.23 shows excess pore pressure ratios (r_u) at depths of approximately 3.5 m in the $D_r \approx 35\%$ layer of Csp2: (a) at a free field location, (b) about 0.3 m prototype from the highly instrumented single pile, and (c) about 3 m prototype from a 2x2 pile group. Pore pressures near the single pile system show a cyclic component at the predominant period of the single pile system (i.e. about 1.0 sec.). Pore pressures near the 2x2 pile group also show a significant cyclic component corresponding to the horizontal motions of the pile cap. While pore pressures near foundations are not quite equal to those in the free field, these data show very similar trends in their mean values over time.

3.3 DEVELOPMENT OF SIGNAL PROCESSING PROCEDURES

Signal processing and integration methods were developed for calculating displacement time histories from acceleration time histories. The development of a reliable procedure for double-integration of accelerometers was necessary to: (1) evaluate the deformed shape of the free-field soil profile, which forms an essential input to several of the analysis methods presented later in this dissertation; and (2) evaluate aspects of the modeling system such as container effects, container rocking, and uniformity of motions.

Displacements tend to be dominated by low frequencies, but the accelerometers used in this study, like most piezoelectric accelerometers, are not capable of recording

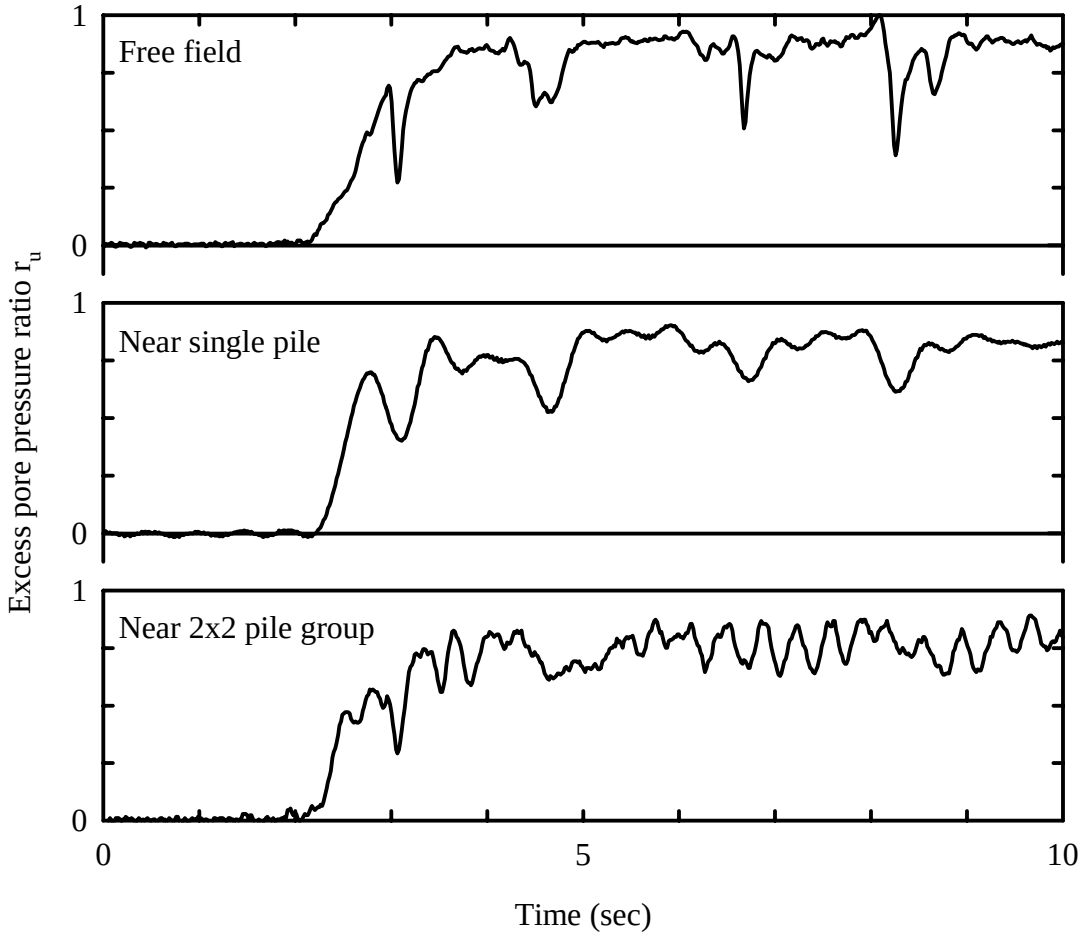

Figure 3.23: Pore pressures near a depth of 3.5 m - Csp2 event F

very low frequencies. High-pass filters are generally included in the analog circuits to prevent drift in piezoelectric accelerometer signals. Analog high-pass filters remove low frequency information, but also corrupt the amplitude and phase of the signal near the filter corner frequency. To remove the corrupted acceleration data, non-causal digital high-pass filters were applied in the frequency domain using a 10th order zero phase delay Butterworth filter.

Maximizing the useful amount of low frequency data from the acceleration records is somewhat subjective, requiring careful consideration of signal processing

techniques, the instrumentation characteristics, the signal conditioning and data acquisition systems, and the characteristics of the physical system being studied. There are over 1400 acceleration time histories in the suite of tests reported in this dissertation, so looking at each record individually was not deemed reasonable. Fortunately, the noise characteristics are generally similar in all acceleration time histories because they all (with few exceptions) come from the same accelerometer type and pass through the same electronic components before being recorded. Thus, a single high-pass corner frequency was selected for mass-processing of all the acceleration time histories. Selection of the optimum high-pass corner frequency was based on detailed analyses of representative recordings, and the following considerations.

- The input base motions had been high-pass filtered at about 0.3 Hz to reduce the peak displacements to values that the shaker could physical accommodate. Consequently, there is little input motion below this frequency from the shaker.
- Fourier spectra of acceleration time histories almost always had a sharp decay in spectral amplitude at about 0.1 Hz, and the spectral amplitude progressively increased below that frequency (a common characteristic of accelerometer noise; as illustrated in Figure 3.24). Integration of the acceleration time histories resulted in calculated displacements that were dominated by very large, low frequency drifts unless the spectral content below about 0.1 Hz was filtered out.
- High-pass filtering with a 10th order Butterworth filter applied only to the spectral magnitudes (acausal filter) was found to yield better displacements than those calculated using lower order Butterworth filters (e.g., a 4th order filter is common). This relatively steep filter appears to work best because the acceleration spectra also have steep drop-offs

with narrow windows of frequencies over which the spectral amplitudes are very small. This is evident in the accelerometer spectra presented in Figure 3.24, where the unfiltered spectra from two locations in one event are shown with various filtered spectra.

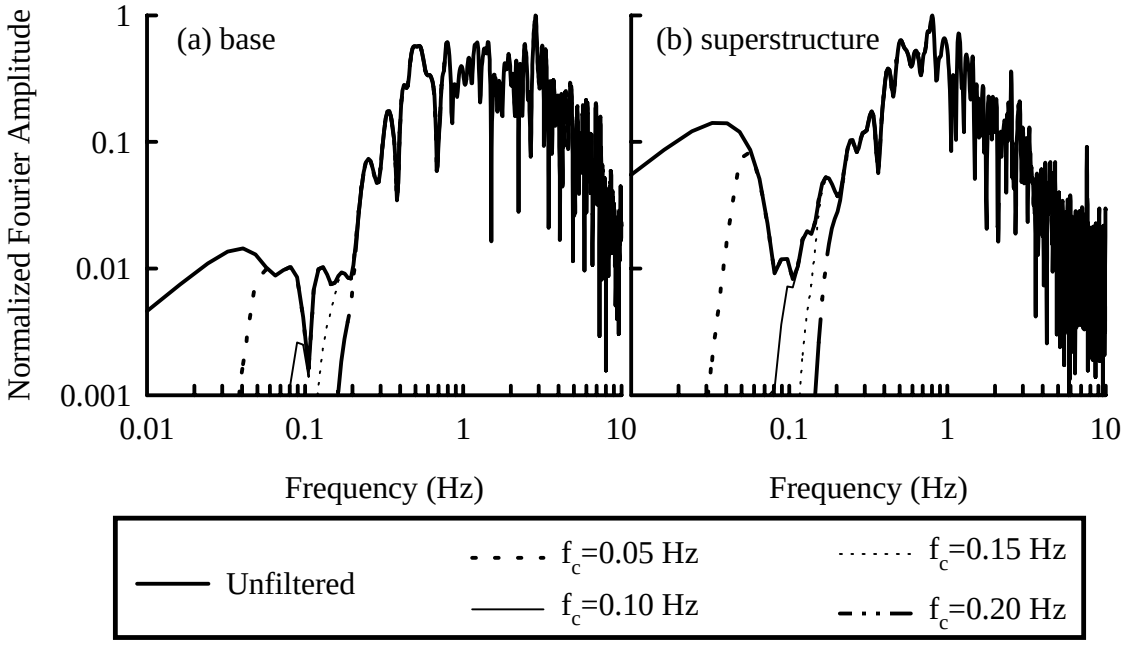

Figure 3.24: Fourier spectra of accelerations in Csp2 event F filtered with 10th order IIR Butterworth filters

Several instrumentation tests were performed where pairs of accelerometers were placed on opposite ends of a linear potentiometer that was measuring the relative displacement between two objects on the centrifuge. Integration of the accelerometers gives absolute displacements, and thus the relative displacement could be obtained by subtracting the two integrated time histories. The relative displacement time histories recorded by the linear potentiometers were compared to those obtained by double-integrating the accelerometers. The best average agreement between the potentiometers and accelerometers was obtained using a corner frequency of about 0.15 Hz.

Figures 3.25 and 3.26 show comparisons of displacement time histories obtained by integrating acceleration time histories together with those recorded by linear potentiometers. Both figures show results for the range of corner frequencies shown in Figure 3.24. Figure 3.25 is for a case where no permanent deformations occurred, and illustrates the very good agreement obtained in such cases. The displacements change very little as the filter corner is changed, as there is very little low frequency content in the signal [see Figure 3.24(a)]. Figure 3.26 is for a case with significant permanent deformations, and illustrates how the accelerometers captured the transient deformations but not the permanent deformations. From Figure 3.24(b), we can see there is more low frequency signal in this record, so the choice of filter corner has more effect on the calculated displacements. Note, however, that as more low frequency signal is included, the calculated displacements do not approach the recorded values.

Numerous comparisons such as shown in this figure provided an appreciation of this limitation on displacements obtained by integrating accelerometers. Attempts to calculate the relative displacements from acceleration records with too little digital high-pass filtering produce obvious drift and poor approximations to the recorded displacement. Increased filtering of the data results in a good approximation to the dynamic component of displacement, but the permanent component is lost. Any real signal related to permanent displacement is obscured by noise, and thus removed by the high-pass filtering.

Note detailed examination of individual records is needed for certain analyses, including the work assembled in this dissertation. For example, while the earlier specified corner of 0.15 Hz yielded the best results on average (i.e. best match to recorded

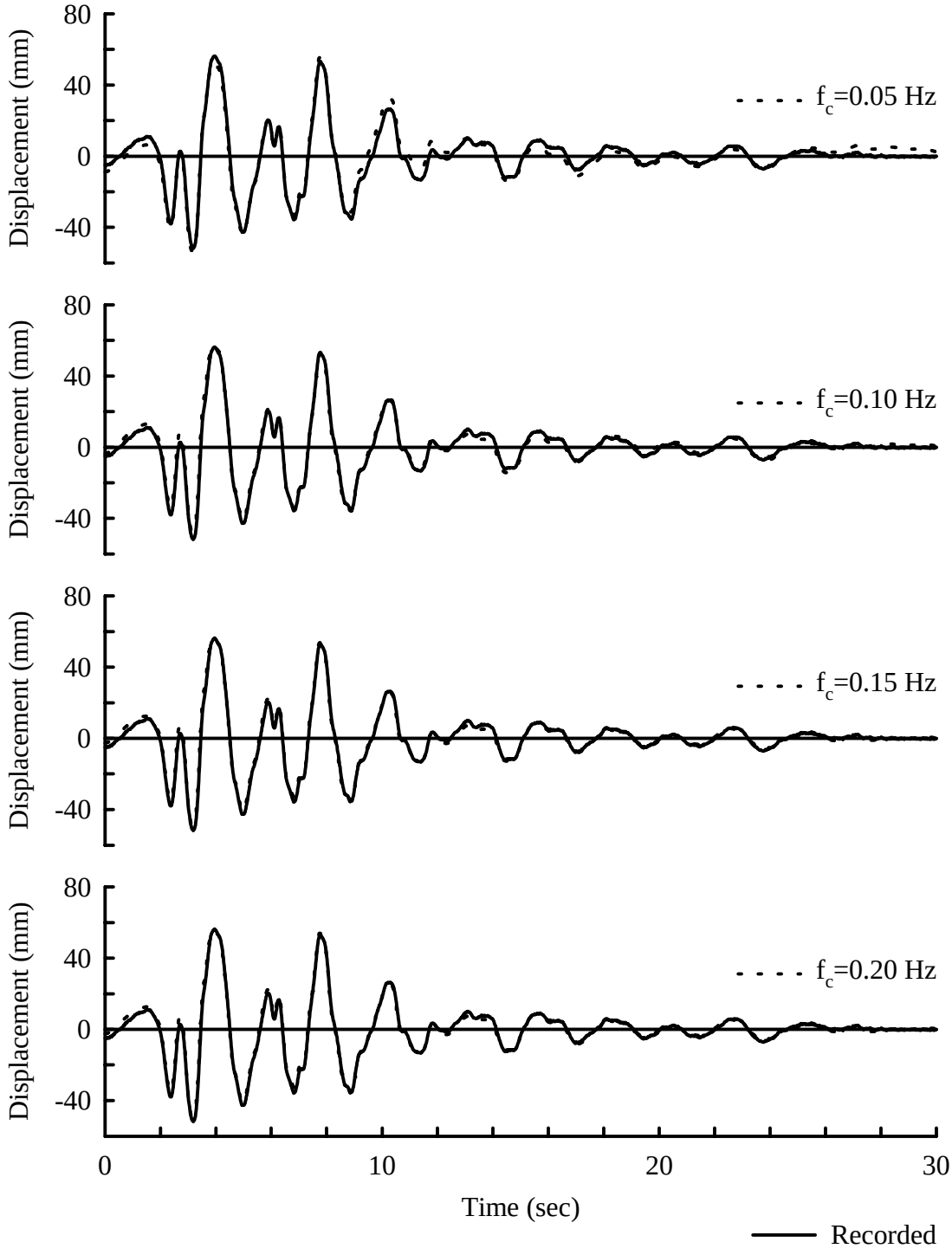

Figure 3.25: Effect of changing corner frequency on calculated displacement of the base relative to the manifold - Csp2 event F

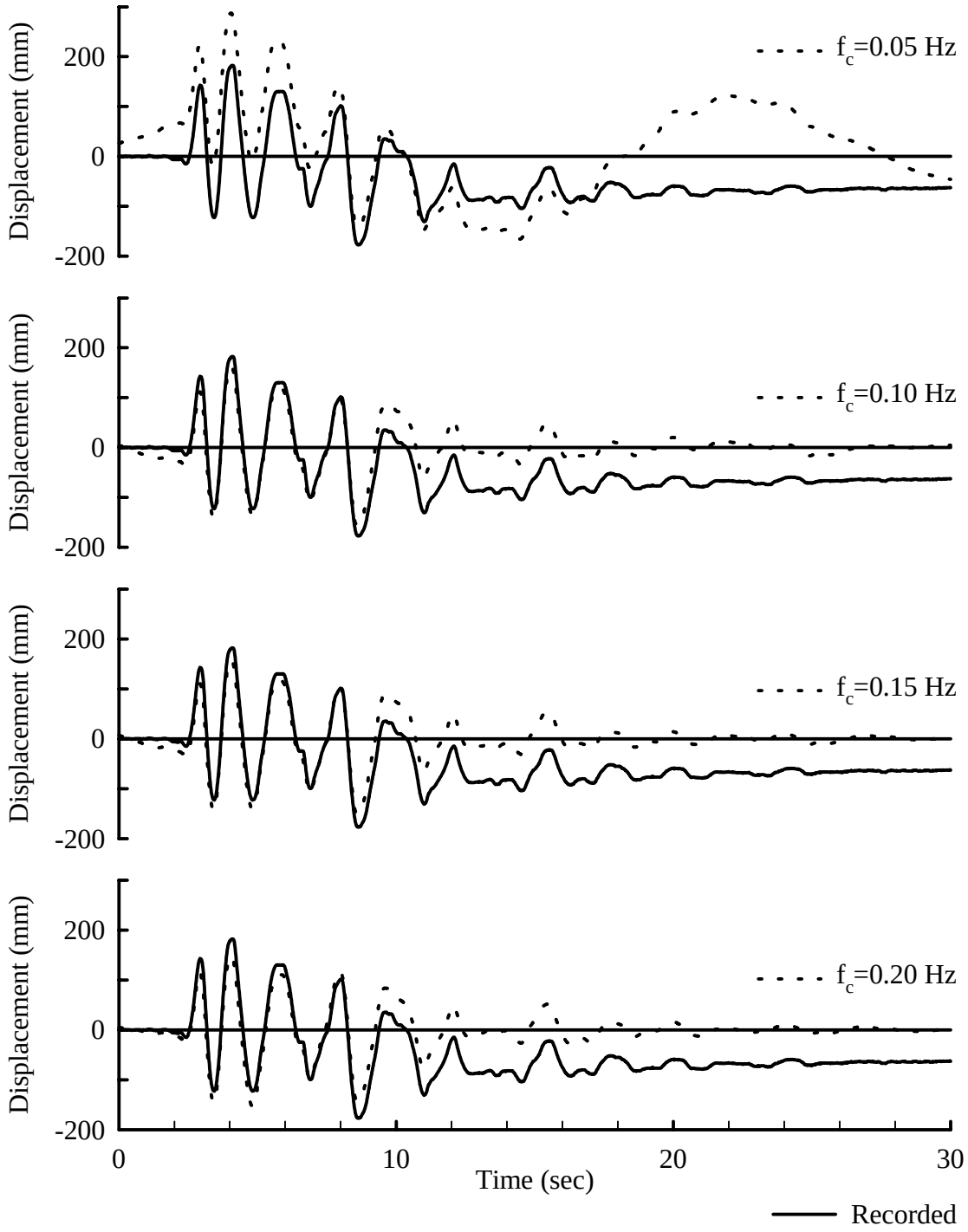

Figure 3.26: Effect of changing corner frequency on calculated displacement of the superstructure relative to the top ring - Csp2 event F

displacements when available), the back-calculation of p-y curves in Chapter 5 required all the accelerometers in a particular event to yield reasonable displacements. For these calculations the filter corner was raised to 0.25 Hz. This eliminated the corrupted low frequency data from virtually all the accelerometers. While some real data was unavoidably removed, the trends in behavior are adequately captured.

3.4 CONCLUSIONS ON MODELING TECHNIQUES AND SYSTEMS

Results from dynamic centrifuge tests of pile-supported structures in soft or liquefied soils were used to evaluate several aspects of the centrifuge modeling system that could potentially affect subsequent interpretations and analyses. Detailed examination of the centrifuge modeling system was necessary because of the newness of the shaking table, and since recent reviews have highlighted important limitations that can exist in dynamic centrifuge systems (Scott 1994, Arulanandan et al. 1994).

Performance of the shaking table on the large centrifuge at UC Davis was shown to be satisfactory. Full frequency spectra of desired input motions (including real earthquake records) were recreated, with the motions being scaleable and repeatable. Dynamic vertical displacements at the ends of the container base were limited to about 10% of the dynamic horizontal displacements, indicating that rocking of the container base was reasonably small over the full operating range of the shaker.

The FSB1 container produced satisfactorily uniform and coherent horizontal motions, with relatively little rocking of the soil column, in tests on non-liquefied sand or even liquefied $D_r \approx 55\%$ Nevada sand. Non-uniform horizontal motions and differential

vertical displacements developed at shallow depths in upper layers of liquefied $D_r \approx 35\%$ Nevada sand or strongly-shaken soft clay, indicating that the soil column had become effectively "softer" than the FSB1 container in these tests. While not ideal, this problem is physically difficult to avoid. An appreciation of this limitation is necessary for realistic interpretations or analyses of the centrifuge data.

Changing pore fluid viscosity by a factor of ten between two containers appeared to have a negligible effect on the soil-pile interaction, with or without liquefaction of the upper soil layer. Furthermore, the nearly identical dynamic pore pressures and bending moment distributions obtained in these two tests showed that reasonably repeatable test results could be obtained nearly a year apart.

Signal processing procedures and methods for calculating displacement time histories from accelerometer records were evaluated. Test results showed that the transient displacement time histories could be calculated reliably using the established procedures, but that permanent displacements could not (as expected). It was also noted that a default corner frequency used to mass-process all acceleration time histories may not be the best choice for an individual recording (either passing too much noise or removing too much real signal). The best results from high-pass filtering of accelerometer records are obtained by individually evaluating the noise on each accelerometer record.

CHAPTER FOUR

Centrifuge Results

4.1 PRESENTATION OF DATA

The complete set of centrifuge test data is presented in five data reports published by the Center for Geotechnical Modeling at UC Davis [Wilson et. al. 1997 (a-e)]. This chapter looks at typical results from several events in select containers that typify the measured soil and structure responses. The purpose of this chapter is to give some background information for the analyses presented in Chapters 5 and 6. An entire dissertation could be written based on the site response results; this dissertation presents a sampling of these results.

Acceleration and pore pressure time histories are presented for various depths throughout the soil profile for tests Csp2 (upper layer sand $D_r \approx 35\%$), Csp3 (upper layer sand $D_r \approx 55\%$), and Csp4 (upper layer soft NC clay). Note the buoyant unit weight of the sand in these tests is very closely equal to the unit weight of water whether its state is loose, medium dense, or dense (see Table 4.1). Also note the water table was approximately at the surface of the soil. The depth of any pore pressure transducer in Csp2 and Csp3 can thus be very closely approximated by dividing the initial pore pressure (u_o) by the unit weight of water. The excess pore pressure ratio can be very closely approximated by dividing the change in pore pressure by the initial pore pressure

(i.e. $r_u = \Delta u/\sigma_{vo}' \approx \Delta u/u_o$). Note that in Csp4 the saturated unit weight of the clay was approximately 15 kN/m^3.

Table 4.1: Buoyant Unit Weights

Density of Nevada sand	γ_{dry} (kN/m^3)	void ratio	G_s*	γ' (kN/m^3)
loose	14.9	0.743	2.65	9.3
medium dense	15.5	0.677	2.65	9.7
dense	16.2	0.606	2.65	10.1

* assumed specific gravity

The locations of all the acceleration and pore pressure transducers presented in this chapter are summarized in Table 4.2.

Table 4.2: Instrument Location Key

Csp2		Csp3		Csp4	
Instrument	depth (m)	Instrument	depth (m)	Instrument	depth (m)***
accel	0.75	accel	1.4	accel	1.5
accel	2.9	accel	3.2	accel	3.0
accel	5	accel	5.6	accel	4.5
layer*	9.1	layer*	9.3	layer*	5.8
accel	10.7	accel	10.3	accel	8.0
accel	20.5	accel	20.4	accel	17.5
ppt	0.7	ppt	1.2	ppt	0.7
ppt **	3.7	ppt **	4.8	ppt **	1.9
ppt	3.8	ppt	4.6	ppt	2.1
ppt	7.4	ppt	6.8	ppt	4.5
layer*	9.1	layer*	9.3	layer*	5.8
ppt	20.3	ppt	20.1	ppt	9.1

accel = accelerometer ppt = pore pressure transducer

* interface between upper and lower soil layers (after shaking in Csp4)

** pore pressure transducer located very near the single pile

*** depths in Csp4 are referenced to the after shaking profile and pressures include 1 m of water above the soil surface.

The accelerations at the superstructure and pilehead of the highly instrumented single pile (see Figure 3.7), bending moments along this pile, and superstructure displacements are also presented for each event. Note superstructure displacements are relative to the top container ring and thus only approximate the displacement relative to

the free field soil surface. A complete listing of the centrifuge events was presented in Table 3.4, including container, input motion, and peak base accelerations. All results presented in this chapter are for scaled Kobe input motions, with the exception of Csp2 event E, which was a very large ($a_{max,base}$ = 0.49 g) Santa Cruz event.

4.2 RESULTS IN LOOSE SAND - CSP2

The soil profile and structure responses in Csp2 are presented in Figures 4.1 through 4.12. The response of the soil profile during three events with Kobe input motions (events D, H, and F) is presented in Figures 4.1 - 4.4, 4.7 and 4.9. The base accelerations in events H and F (Figures 4.2 and 4.7, respectively) appear to be nearly scalar multiples of the base acceleration in event D (Figure 4.1). Accelerations at the bottom, middle, and top of the loose sand layer show progressive amplification in event D, compared to progressive and dramatic overall de-amplification in events H and F. Note, however, the presence of large (but short duration) spikes of acceleration in some of these records. Excess pore pressure ratios ($r_u = \Delta u/\sigma_{vo}' \approx \Delta u/u_o$) were negligible throughout the soil profile in event D (Figure 4.3), but approached 100% throughout the loose sand layer early in events H and F (Figures 4.4 and 4.9, respectively). Excess pore pressures in the dense sand layer in events H and F slowly increased toward values approximately equal to the excess pore pressure at the base of the liquefied loose sand layer. This suggests that little, if any, excess pore pressure were generated in the dense sand layer in events H and F. The pore pressure increase in the dense sand was primarily due to excess pore pressures in the loose sand layer.

The response of the single pile system during events D, H, and F is shown by the time histories of superstructure acceleration, pilehead acceleration, superstructure displacement, and bending moment time histories at various depths in Figures 4.5, 4.6, and 4.11. All recordings show that the system's "fundamental" period lengthened considerably due to liquefaction (events H and F) relative to its initial value (event D). The bending moments and lateral displacements were strongly correlated to the superstructure acceleration. The depth to the largest bending moment increased as a result of liquefaction, as would be expected for a pile foundation loaded primarily by the inertia of the superstructure. The largest recorded bending moment was at a depth of 0.75 m in event D and a depth of 3.8 m in event H. This is highlighted in Figure 4.13, where the peak bending moments versus depth are plotted for events D, H, F, and E. Note event E experienced permanent displacements, as discussed further below.

The response of the soil profile in Csp2 during a Santa Cruz motion event (event E) is presented in Figures 4.8 and 4.10, while the response of the structure is presented in Figure 4.12. Recordings in the soil profile show similar characteristics to those recorded in the Kobe events with liquefaction, i.e., progressive and dramatic de-amplification of larger accelerations and complete liquefaction of the upper soil layer. The response of the superstructure in this event is notable, however, because of the significant permanent displacement of approximately 0.20 m. The effect of this permanent displacement is clearly evident in the time history of the lowest bending gauge (Figure 4.12, z = 8.4 m) and in the plot of peak bending moments in Figure 4.13. Note the depth to the interface between the loose and dense soil layers was approximately 9 m in this test. This recording

represents the largest permanent deformation of the highly instrumented single pile system observed in the tests with an upper layer of sand (Csp2 and Csp3).

It should be noted here that while the soil profile is assumed to be horizontal, during these tests the bucket of the centrifuge was actually tilted 1-2° relative to the g-field. This was due to a combination of factors, but the net result was that the soil profile was actually inclined slightly. The permanent displacements observed in this container were thus due to permanent displacements of the soil profile (due to both the bucket inclination and to unsymmetrical base motions), rather than yielding of the pile or structure.

4.3 RESULTS IN MEDIUM DENSE SAND - CSP3

The soil profile and structure responses in Csp3 are presented in Figures 4.14 through 4.19. The response of the soil profile during Kobe input motions is presented in Figures 4.14 - 4.17. The base acceleration in event J (Figure 4.15) appears to be a nearly scalar multiple of the base acceleration in event E (Figure 4.14). Accelerations at the bottom, middle, and top of the loose sand layer show progressive amplification in event E, while the accelerations in event J show less amplification than in event E, but also include several large sharp peaks in acceleration. The lack of overall de-amplification is in contrast to the general de-amplification of motions observed in Csp2 (loose sand - e.g. compare to Figures 4.1 and 4.2), though the large spikes of acceleration are similar. Excess pore pressure ratios were negligible throughout the soil profile in event E, but ranged from about 50 to 90% throughout the looser sand layer in event J (Figures 4.16

and 4.17, respectively). The increases in pore pressure were less sudden than the increases observed in Csp2. The differences between Csp2 and Csp3 are consistent with what might be expected when comparing behaviors of very loose and medium dense sands under seismic loading.

The response of the single pile system during events E and J is shown by the time histories of superstructure acceleration, pilehead acceleration, superstructure displacement, and bending moment time histories at various depths in Figures 4.18 and 4.19. All recordings show that the system's "fundamental" period lengthened somewhat due to liquefaction (event J) relative to its initial value (event E). The bending moments and lateral displacements were strongly correlated to the superstructure acceleration. The depth to the largest bending moment increased as a result of liquefaction, as would be expected for a pile foundation loaded primarily by the inertia of the superstructure. As summarized in Figure 4.20, the largest recorded bending moment was at a depth of 0.75 m in event E and a depth of 1.5 m in event J, though the change was less pronounced than that observed in Csp2.

4.4 RESULTS IN SOFT NC CLAY - CSP4

The soil profile and structure responses in Csp4 are presented in Figures 4.21 through 4.26. The response of the soil profile during Kobe input motions is presented in Figures 4.21 - 4.24. The base acceleration in event E (Figure 4.22) appears to be a nearly scalar multiple of the base acceleration in event D (Figure 4.21). The motions are seen to be strongly affected as they propagate through the clay layer. The higher frequency

components are removed by the time they reach the soil surface, especially in event E. Excess pore pressure ratios after shaking were negligible throughout the soil profile in both events D and E (Figures 4.23 and 4.24). Note the response time and arching around a transducer in clay (see Kutter et al. 1990) complicate the interpretation of dynamic pore pressures in clay. The records thus are most reliable before and after shaking.

The response of the single pile system during events D and E is shown by the time histories of superstructure acceleration, pilehead acceleration, superstructure displacement, and bending moment time histories at various depths in Figures 4.25 and 4.26. All recordings show that the system's "fundamental" period was significantly longer than observed in the tests with sand (Csp2 and Csp3). The bending moments and lateral displacements were strongly correlated to the superstructure acceleration. The depth to the largest bending moment was larger than in the tests with sand, as would be expected for a pile foundation loaded primarily by the inertia of the superstructure. The largest recorded bending moment was at a depth of 5.3 m in event D and a depth of 8.4 m in event E. This is highlighted in Figure 4.27, where the peak bending moments versus depth are plotted for events D and E.

4.5 SUMMARY

From the time histories of acceleration and pore pressure throughout the soil profiles we saw that the soil conditions had a dramatic affect on the site response (as expected). Recordings made in the upper sand layers were markedly different in amplitude and frequency content depending on whether or not there was extensive

liquefaction. In the test where the upper soil layer was soft clay the ground motions were also strongly affected in both magnitude and frequency content.

The effects of relative density and input motions on superstructure response for the tests in sand are summarized in Figure 4.28. The peak superstructure acceleration is plotted versus the peak base acceleration for all of the events in Csp2 ($D_r \approx 35\%$) and Csp3 ($D_r \approx 55\%$). Upon careful inspection two important trends are evident. First, for a given level of peak base acceleration, the Kobe events produced higher peak superstructure accelerations. This is due to the high energy content of this motion near the one second natural period of the structure (see Figure 3.8). The Santa Cruz and modified Santa Cruz motions did not contain as much energy near the fundamental period of the structure. Second, for a given earthquake, superstructure accelerations in the medium dense sand were usually greater than in the loose sand. This is consistent with both the de-amplification of ground motions in the loose, liquefied sand and with the soil softening, therefore imparting less load to the structure.

There is one notable exception to this trend, however. The 0.6 g Kobe event in Csp2 (event L) produced superstructure accelerations of 1.5 g. This acceleration is as great as those observed in Csp3 with the same base input motion and is much greater than any other superstructure accelerations observed for Csp2. It is thought that the motions of this event were severe enough and the strains large enough that the soil became dilatant. The dilative tendency of the soil in Csp2 ($D_r \approx 35\%$) can be observed in the free field accelerations and pore pressures in Figure 4.29 for event L, and also in Figures 4.7 and 4.9 for event F (a smaller Kobe event than event L). Here sharp peaks in the free field accelerations correspond to sharp decreases in the free field excess pore pressures. It

appears that in Csp2 event L the soil dilated long enough to cause negative pore pressures, and had sufficient strength to transmit very large accelerations through the ground to the superstructure.

Unfortunately, the free field motions in event L often exceeded the capacity of the accelerometers used, i.e. accelerations exceeded 50 g's of real motion (≈1.7 g's prototype), as was observed in Figure 4.29. Clearly there is useful information in the acceleration record, but every time the capacity of an instrument was reached, there was a long-term offset in the accelerometer reading. The interpretation of the data will require careful consideration of the effects of exceeding the capacity of the transducers on the transducers' signals. Obtaining more detailed information from event L will require more testing of the instrumentation used.

The relationship between superstructure acceleration and peak bending moments is investigated in Figure 4.30. We saw in previous figures that the bending moment time histories closely followed the superstructure accelerations. In Figure 4.30, we see that the peak bending moment is approximately linearly proportional to the peak superstructure acceleration in both containers where the upper soil layer was sand. This implies that the foundation loading is dominated by inertial loads from the superstructure for these model configurations. The one point that least fits this linear trend is from Csp2 event E, where we saw significant permanent displacement of the superstructure.

Note the domination of inertial loading may not hold true in a general sense, as other soil-structure combinations could have significant pile loads due to kinematic loading. Cases where kinematic loads may be important are expected to include lateral spreading and certain soil stratigraphies with highly contrasting layer strengths.

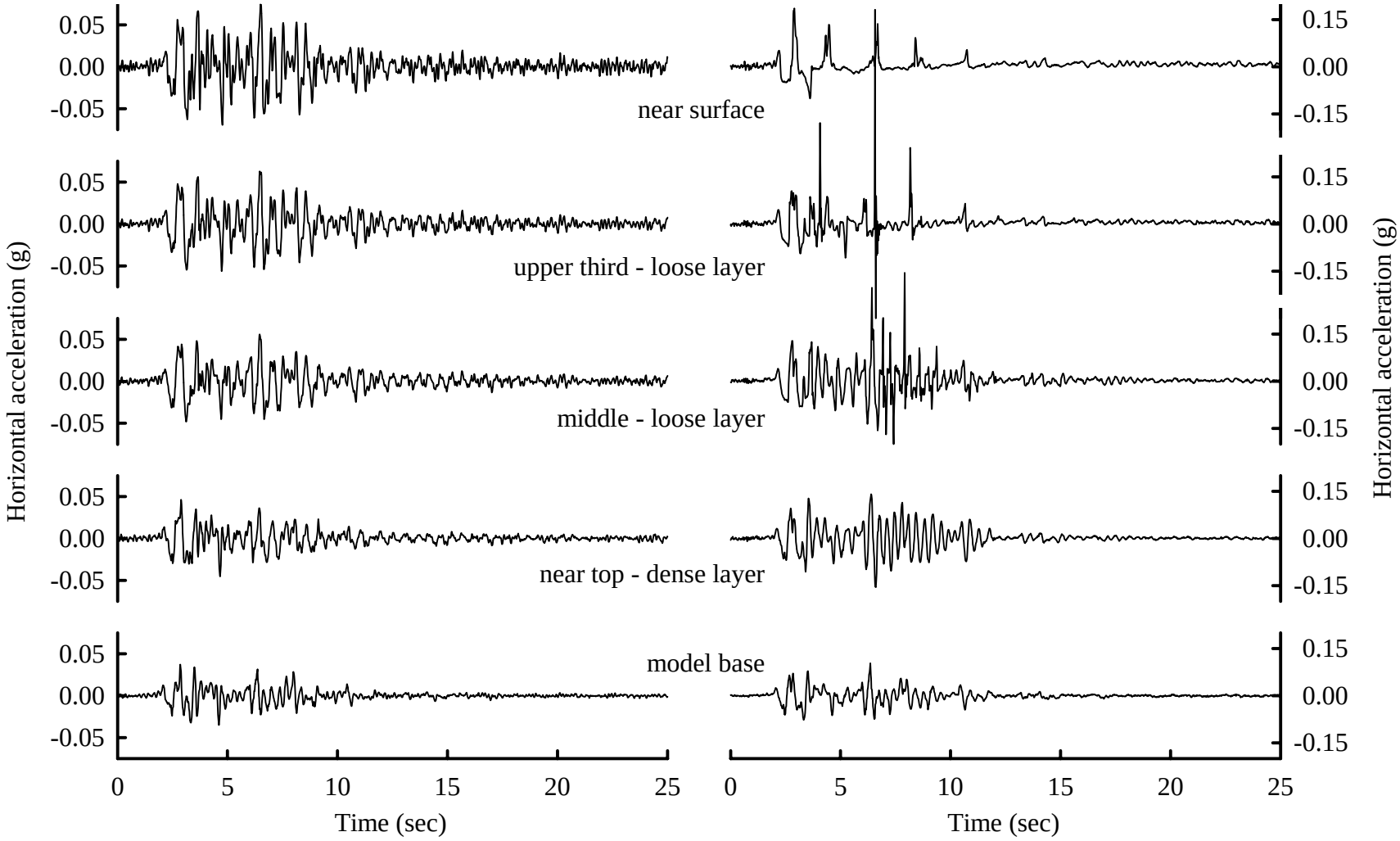

Figure 4.1: Acceleration time histories from the central vertical array in Csp2 event D

Figure 4.2: Acceleration time histories from the central vertical array in Csp2 event H

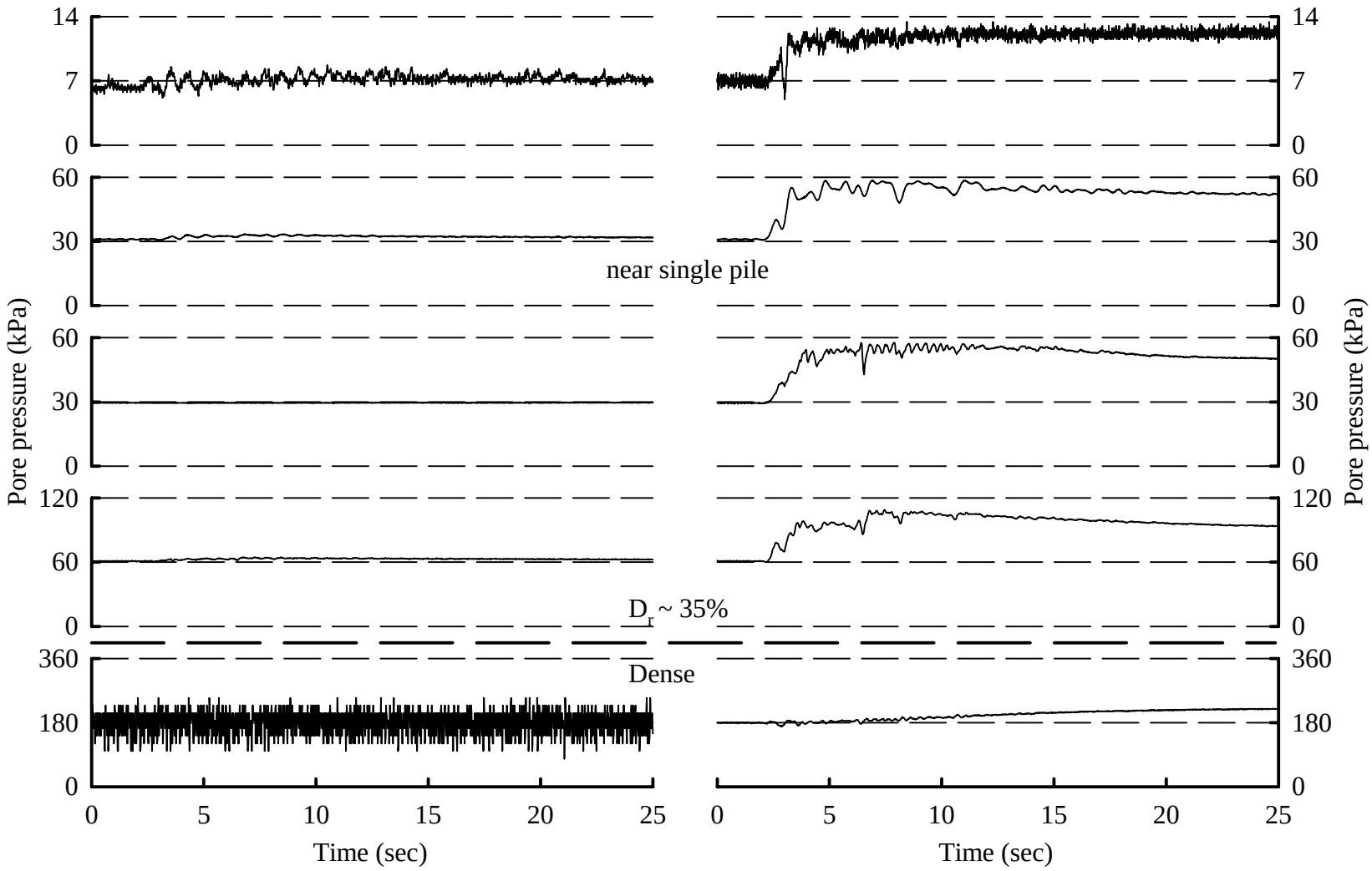

Figure 4.3: Pore pressure time histories from the central vertical array in Csp2 event D

Figure 4.4: Pore pressure time histories from the central vertical array in Csp2 event H

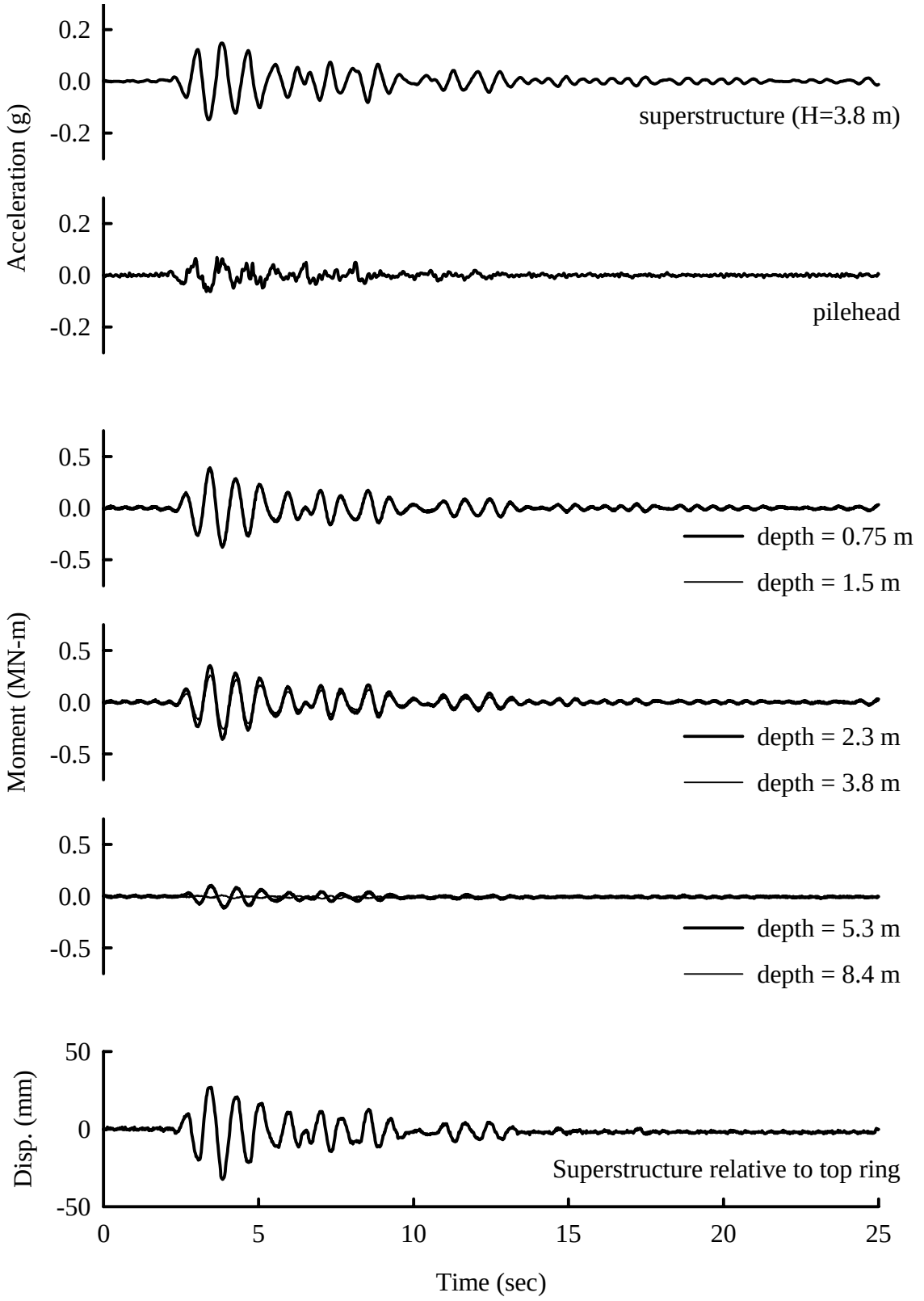

Figure 4.5: Response of highly instrumented single pile in Csp2 event D

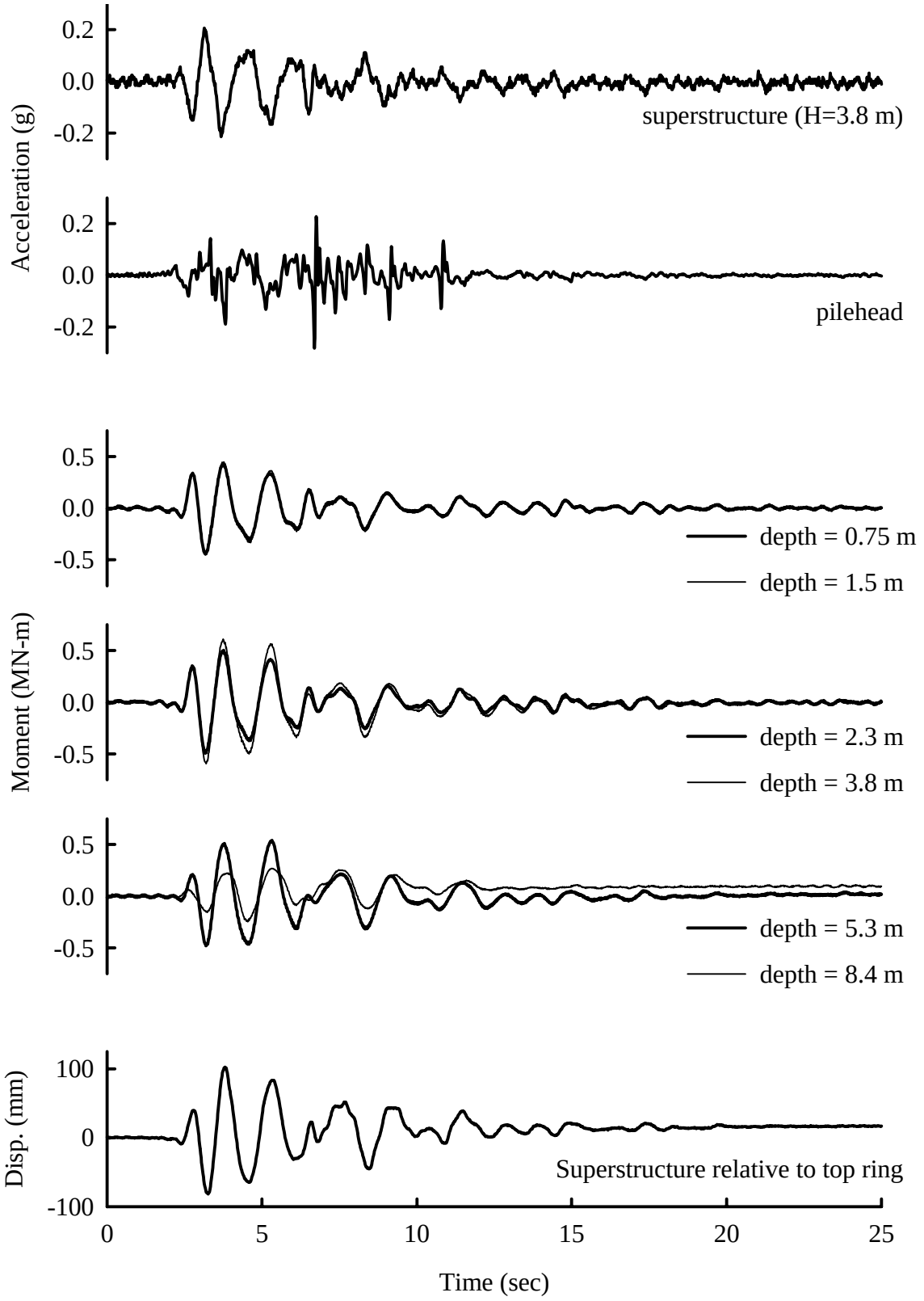

Figure 4.6: Response of highly instrumented single pile in Csp2 event H

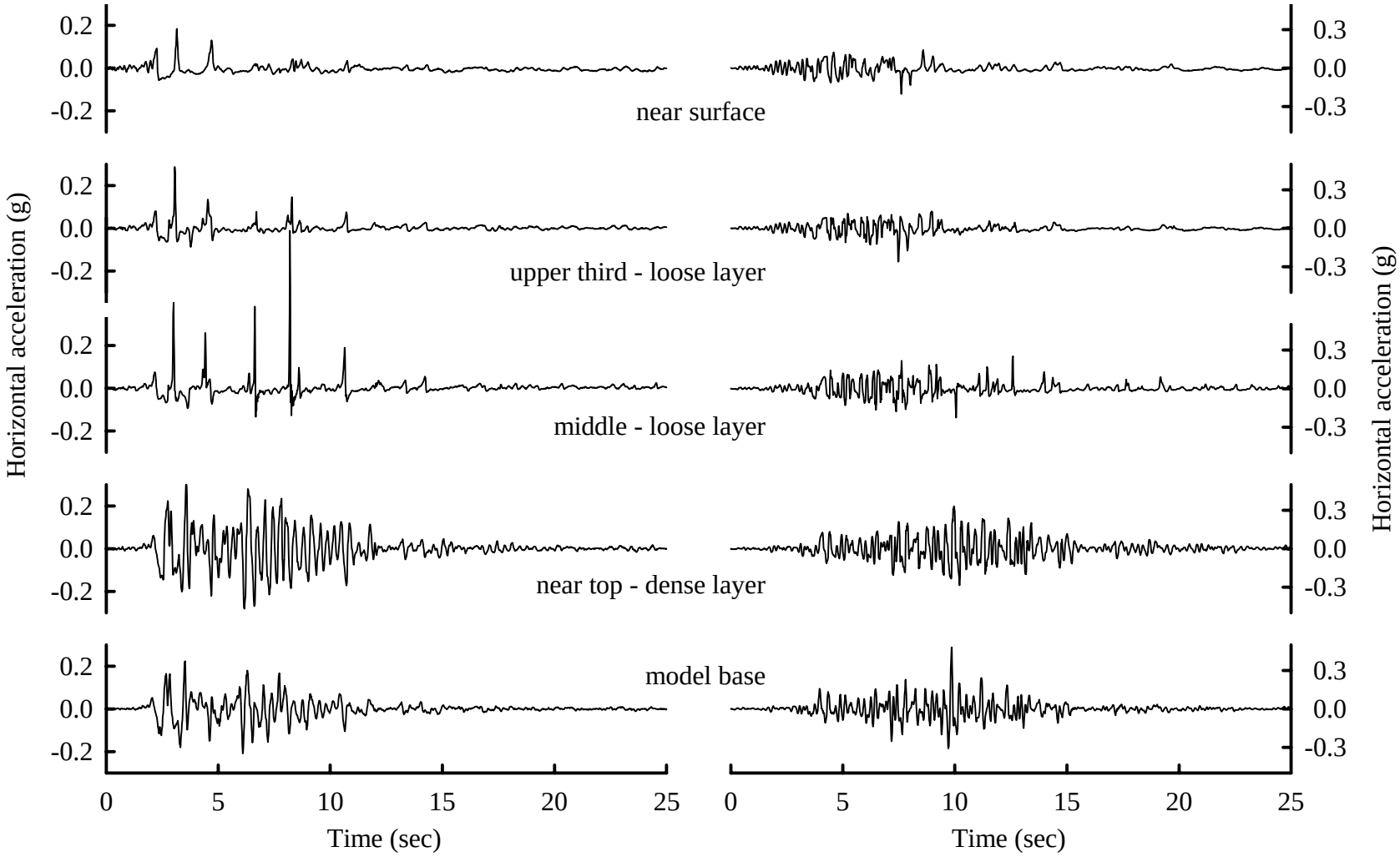

Figure 4.7: Acceleration time histories from the central vertical array in Csp2 event F

Figure 4.8: Acceleration time histories from the central vertical array in Csp2 event E

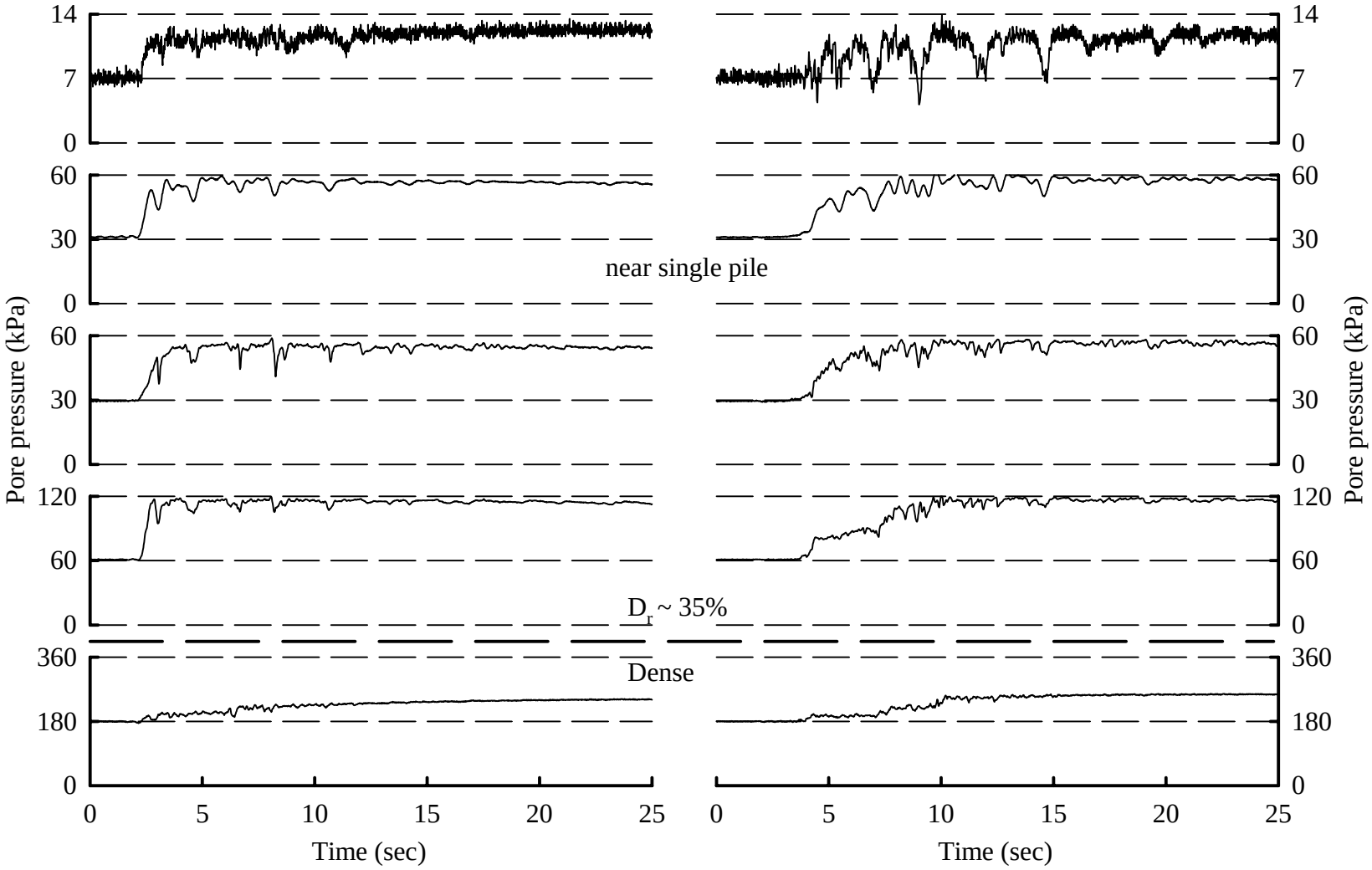

Figure 4.9: Pore pressure time histories from the central vertical array in Csp2 event F

Figure 4.10: Pore pressure time histories from the central vertical array in Csp2 event E

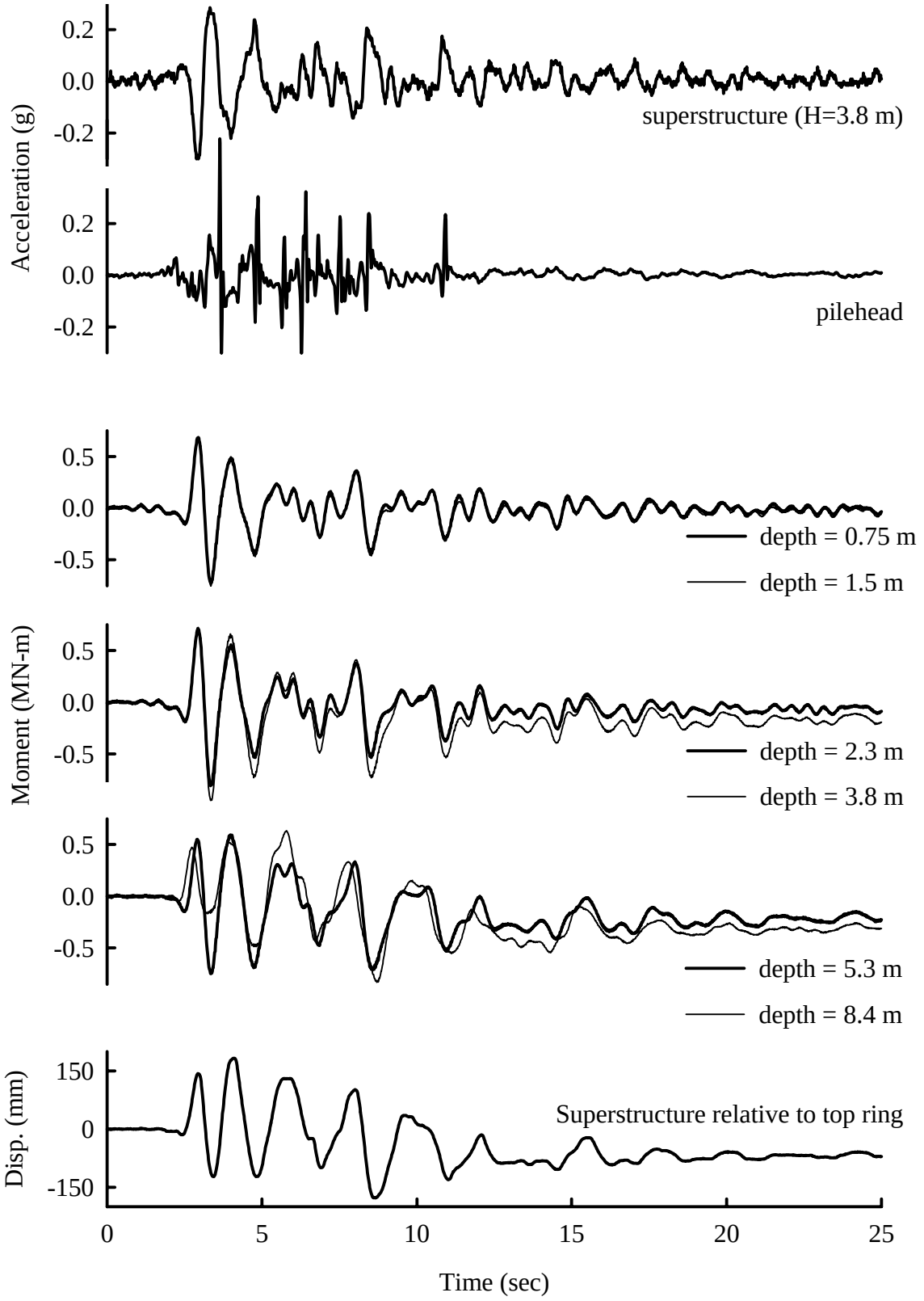

Figure 4.11: Response of highly instrumented single pile in Csp2 event F

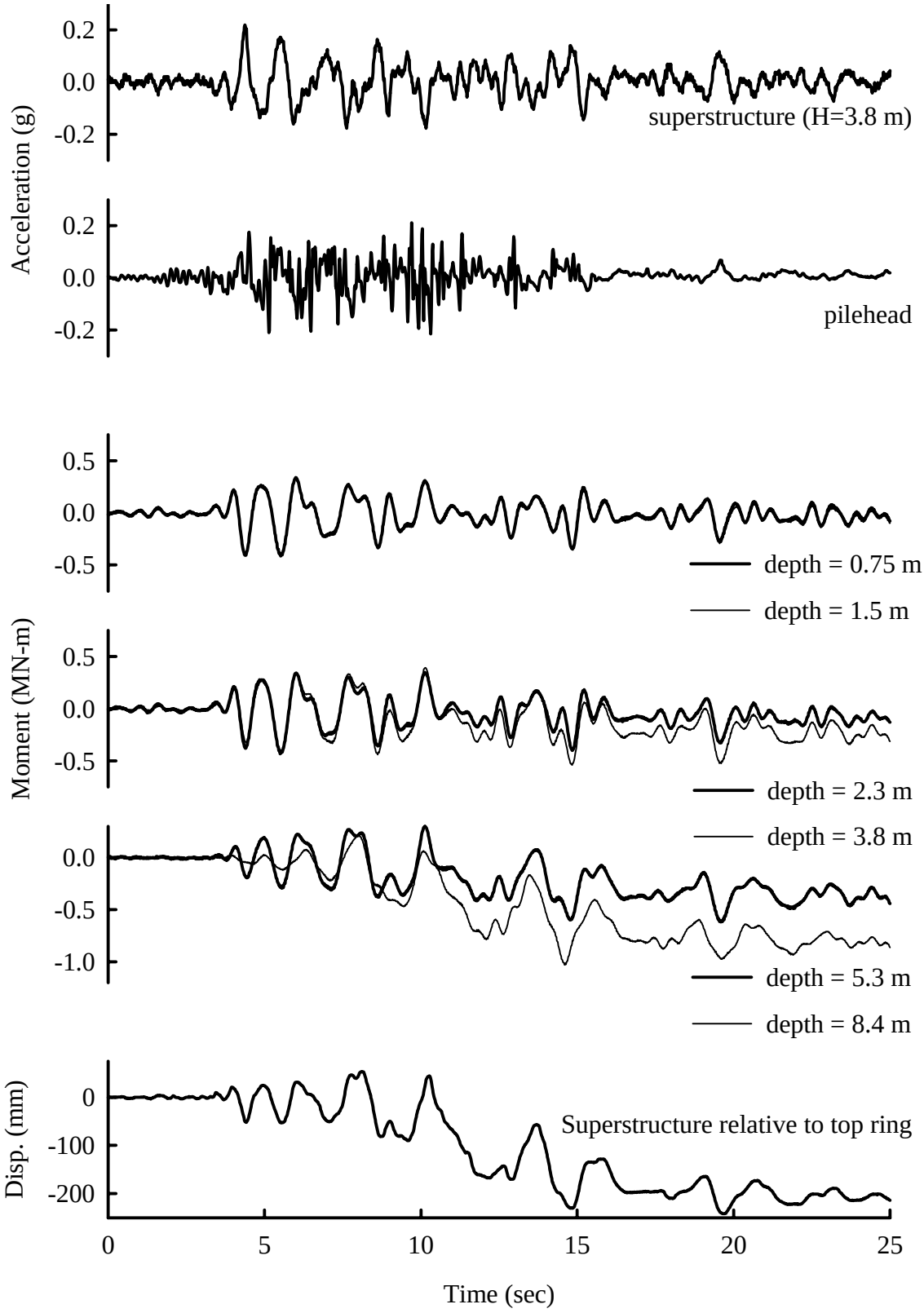

Figure 4.12: Response of highly instrumented single pile in Csp2 event E

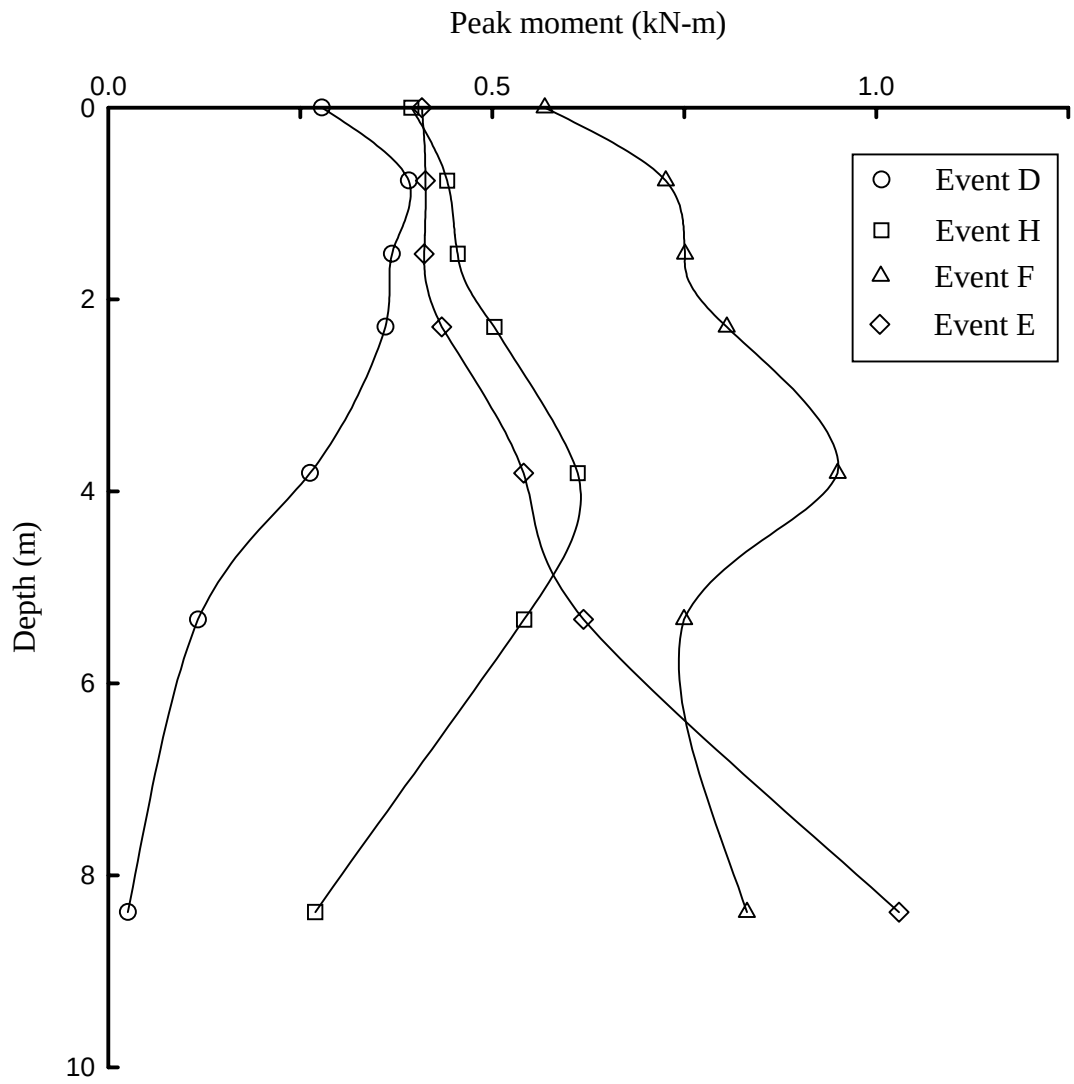

4.13: Distribution of peak bending moment in Csp2 events D, H, F, and E

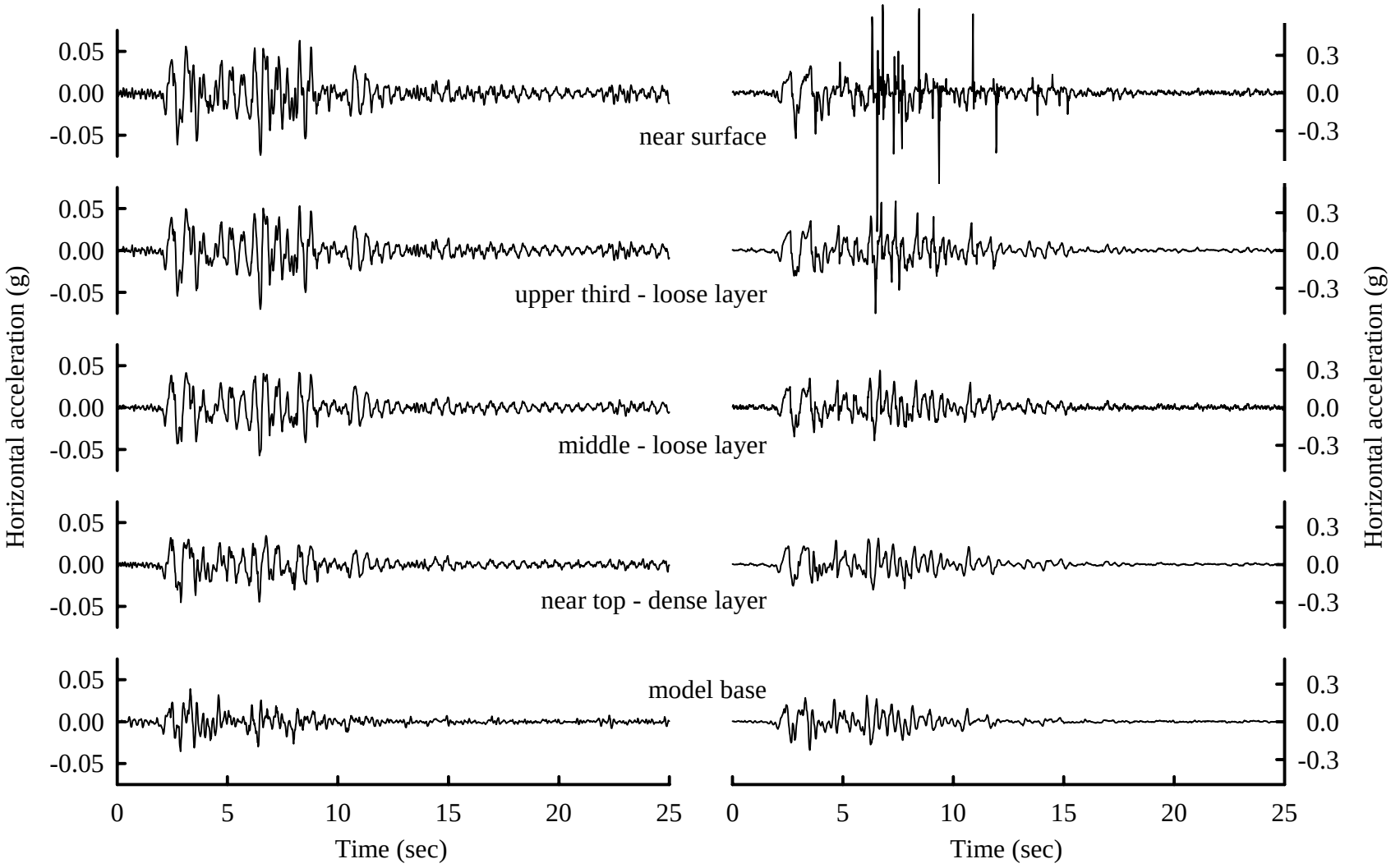

Figure 4.14: Acceleration time histories from the central vertical array in Csp3 event E

Figure 4.15: Acceleration time histories from the central vertical array in Csp3 event J

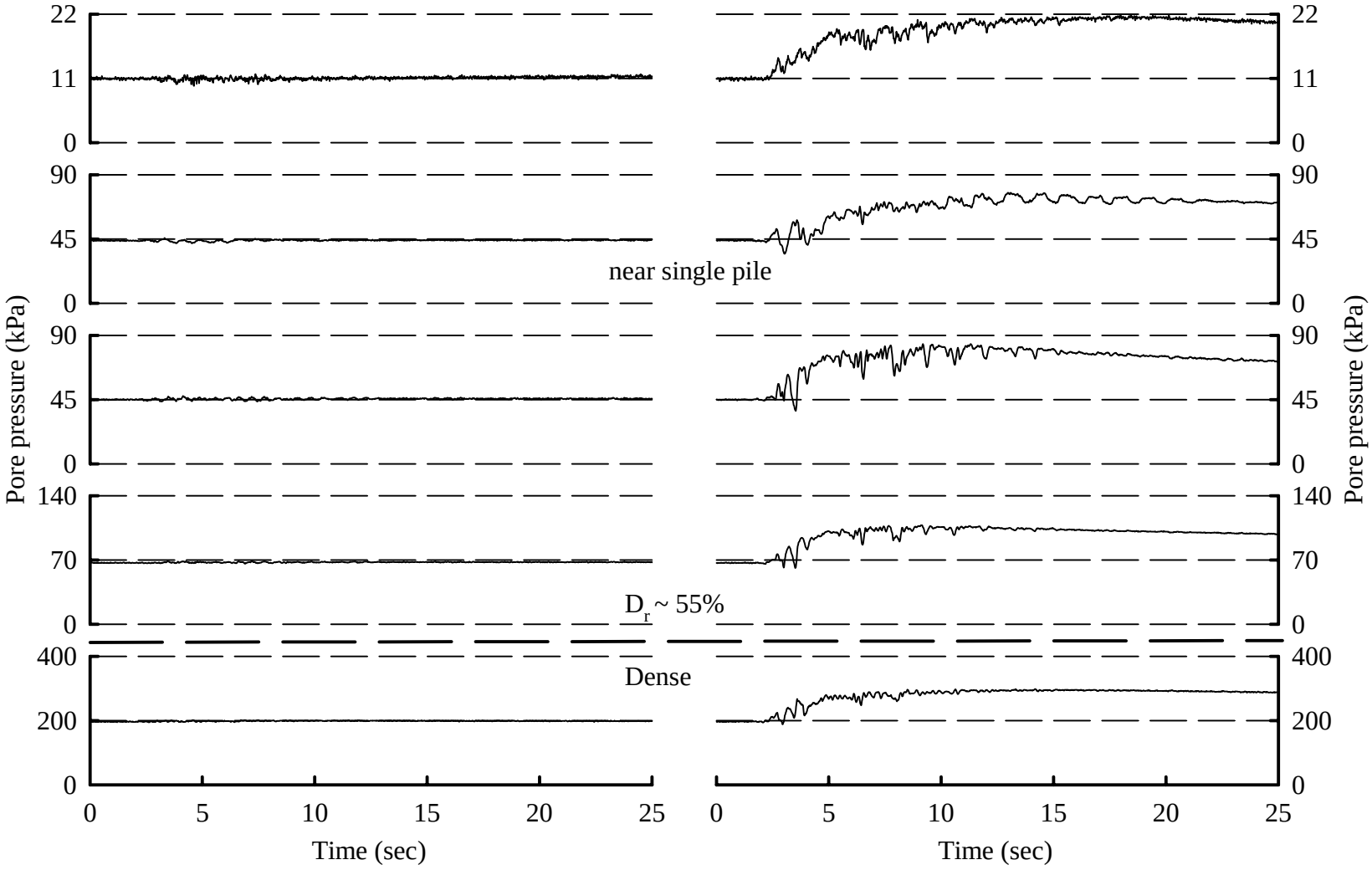

Figure 4.16: Pore pressure time histories from the central vertical array in Csp3 event E

Figure 4.17: Pore pressure time histories from the central vertical array in Csp3 event J

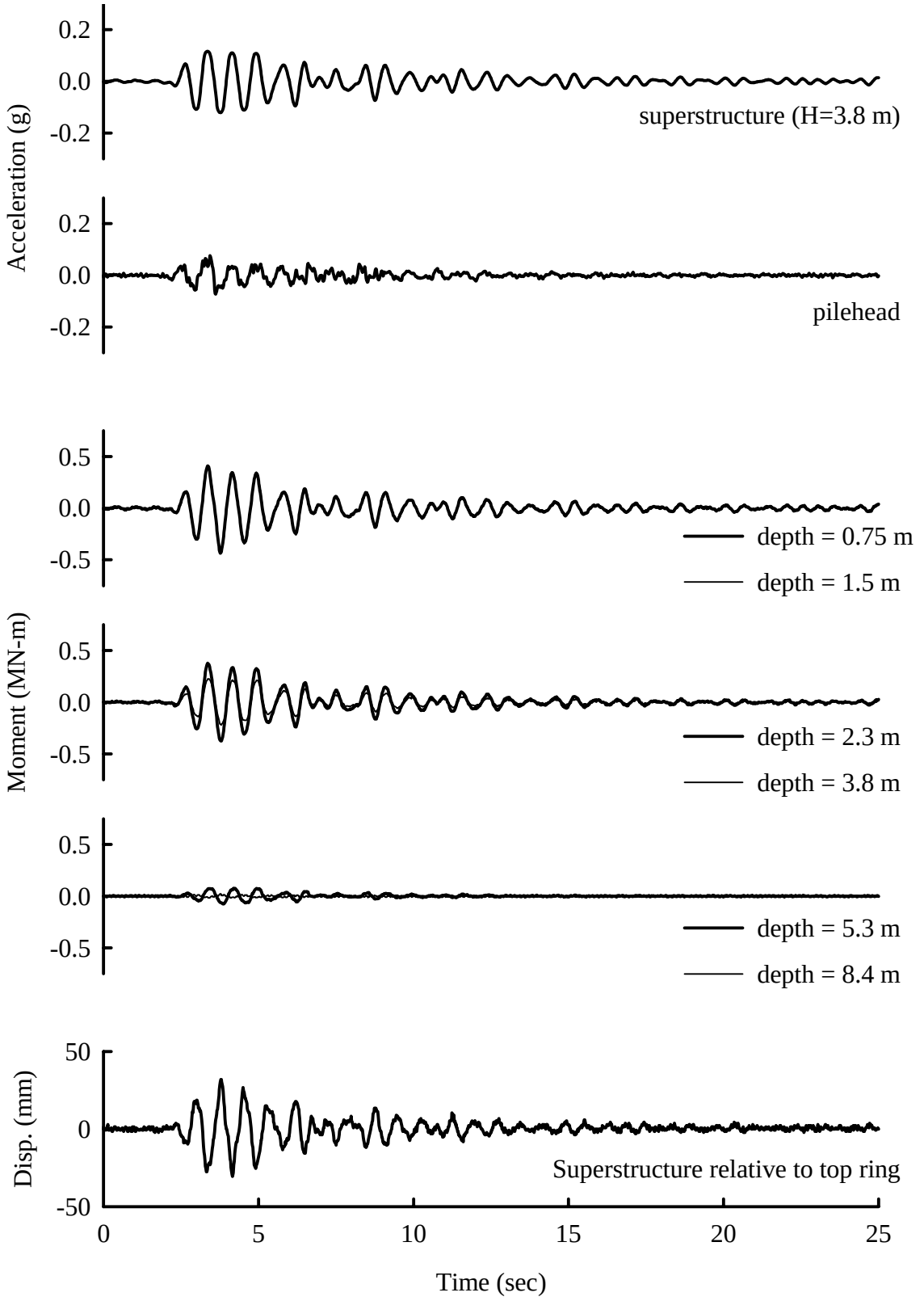

Figure 4.18: Response of highly instrumented single pile in Csp3 event E

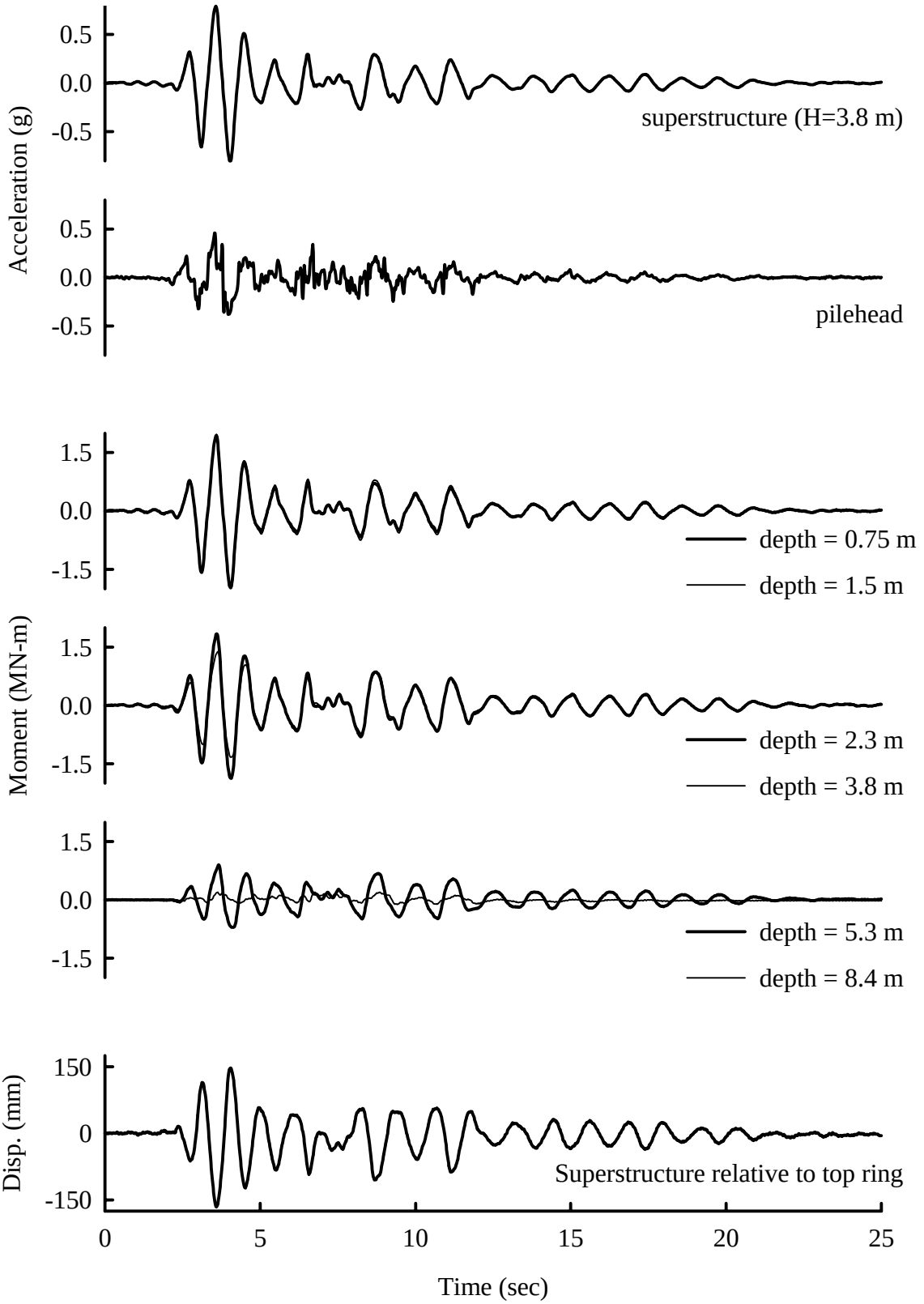

Figure 4.19: Response of highly instrumented single pile in Csp3 event J

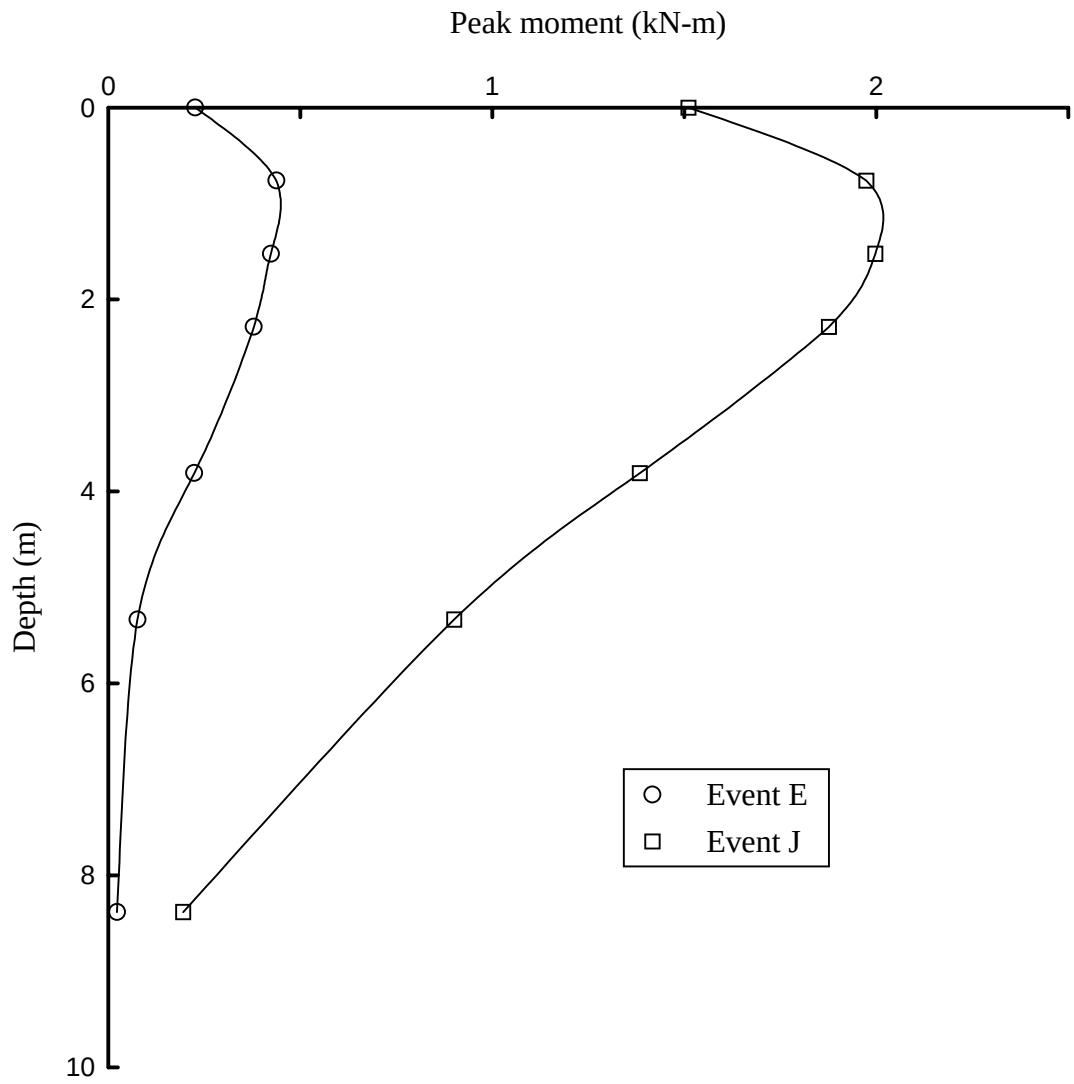

4.20: Distribution of peak bending moment in Csp3 events E and J

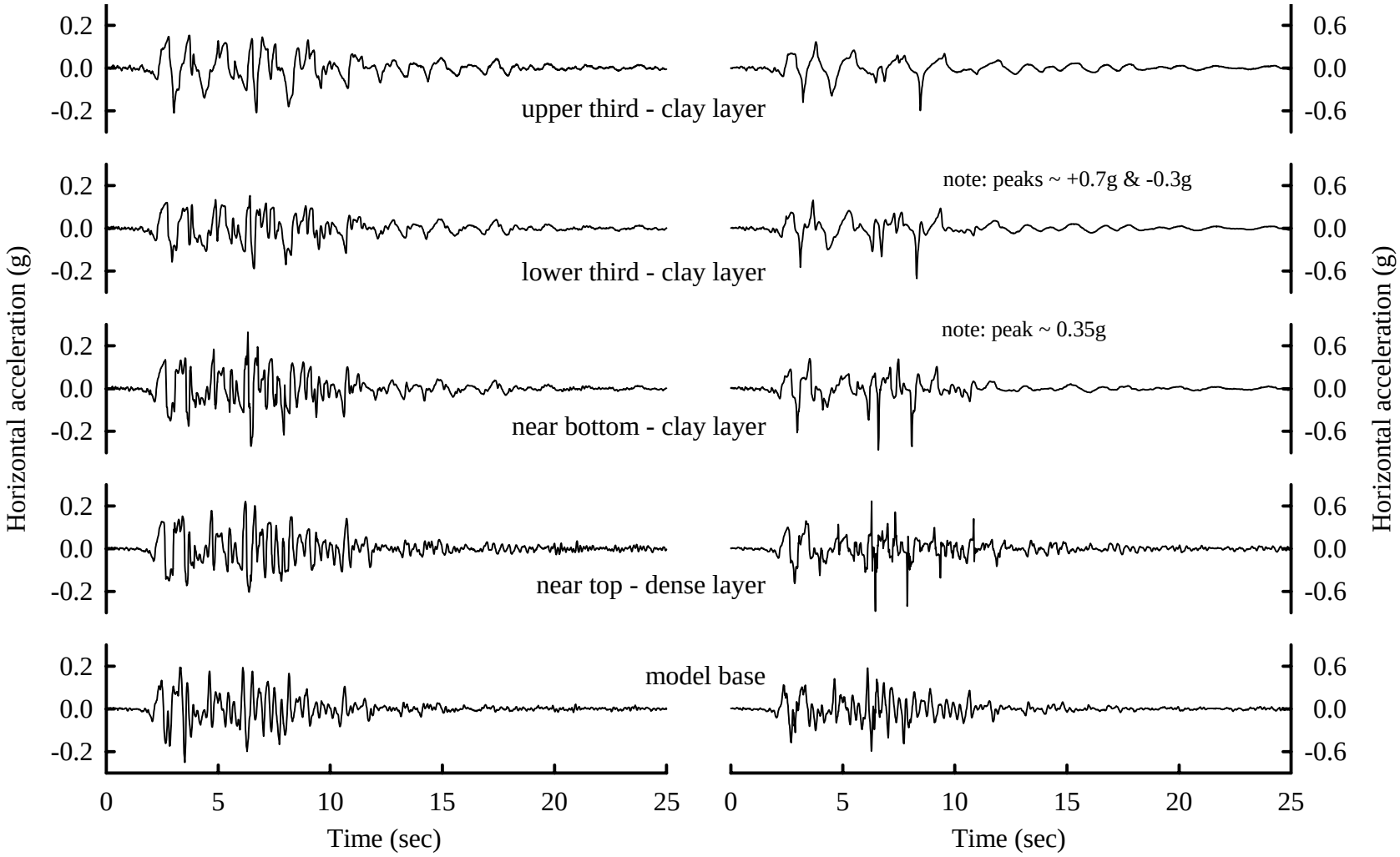

Figure 4.21: Acceleration time histories from the central vertical array in Csp4 event D

Figure 4.22: Acceleration time histories from the central vertical array in Csp4 event E

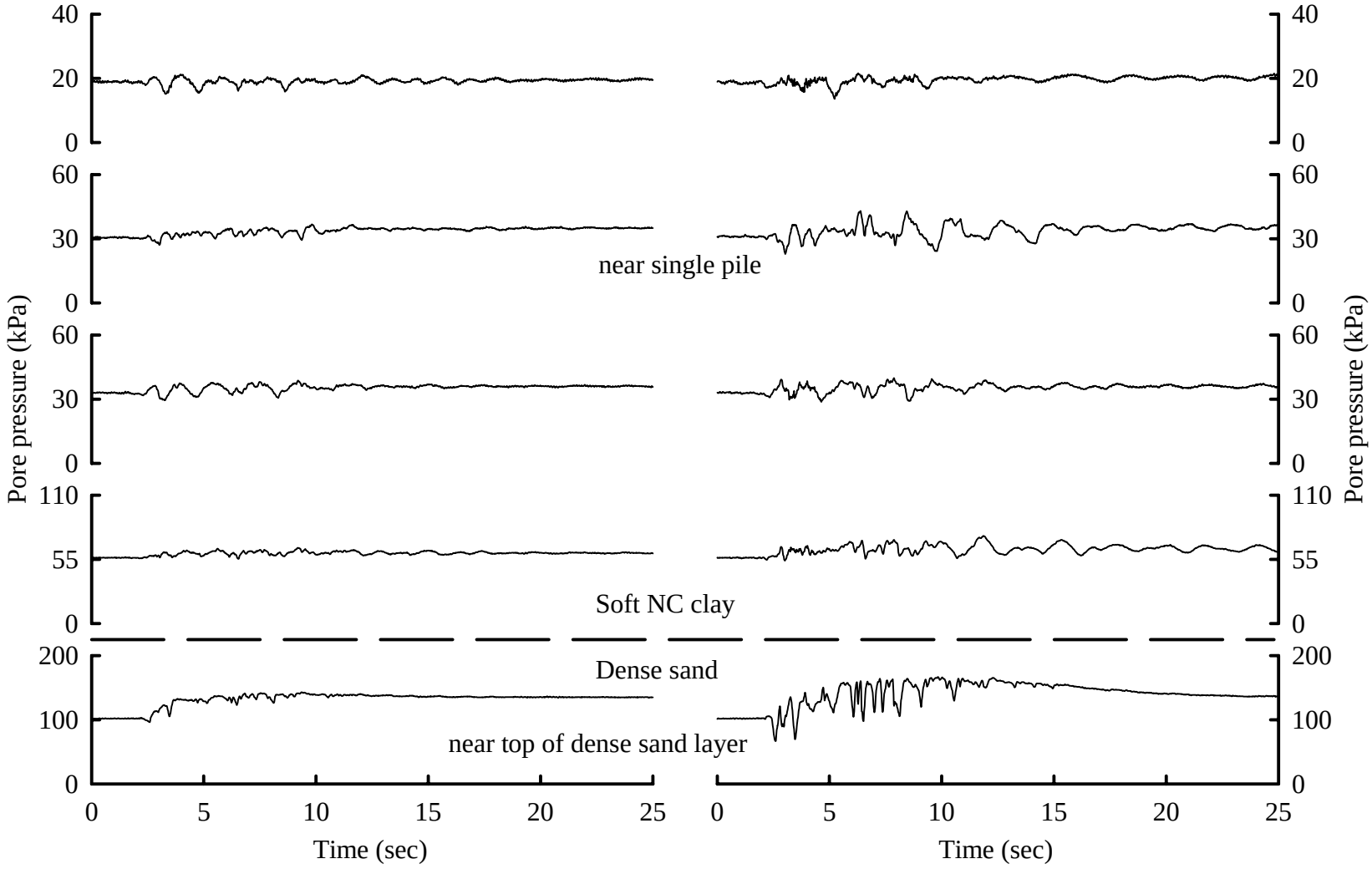

Figure 4.23: Pore pressure time histories from the central vertical array in Csp4 event D

Figure 4.24: Pore pressure time histories from the central vertical array in Csp4 event E

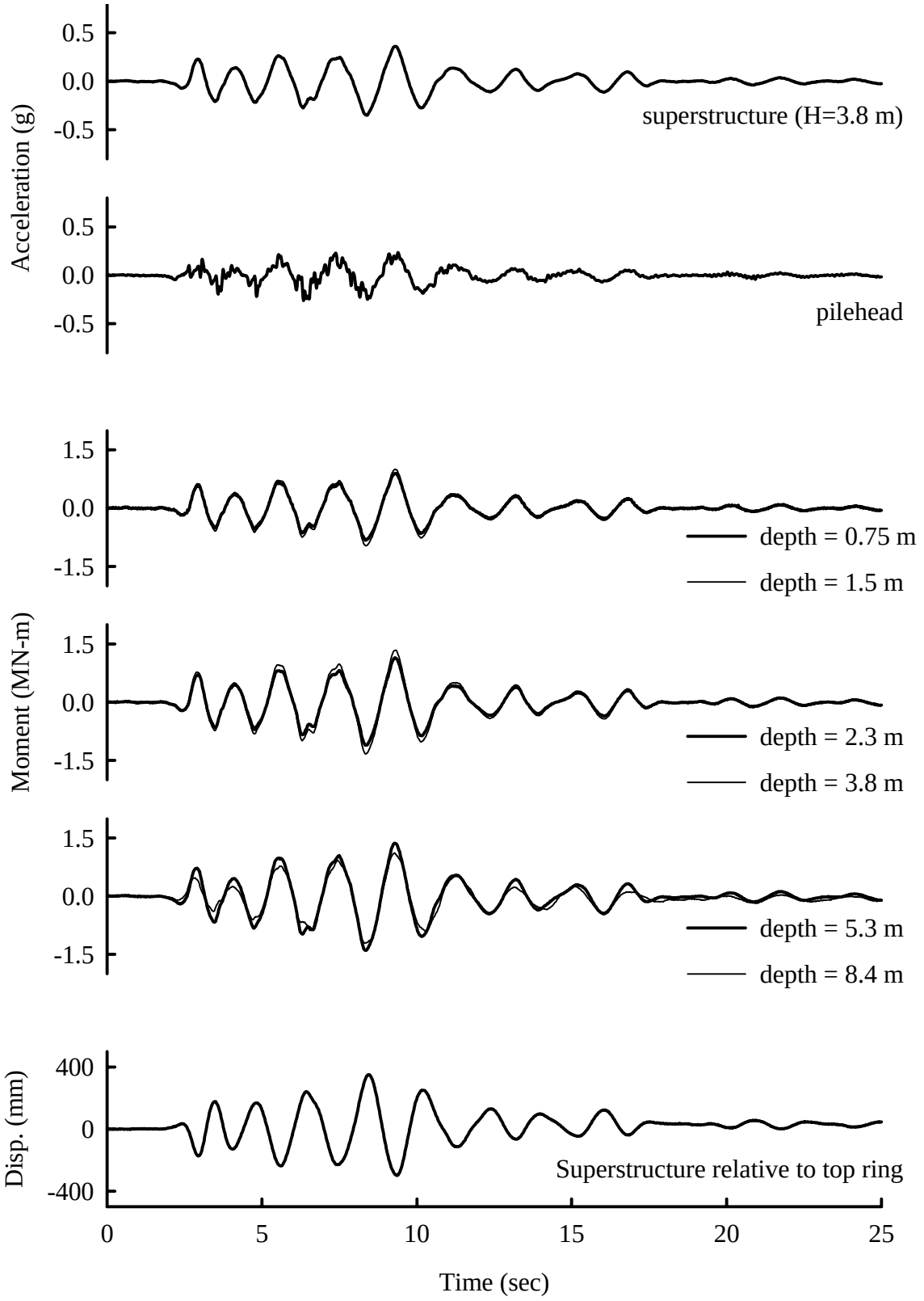

Figure 4.25: Response of highly instrumented single pile in Csp4 event D

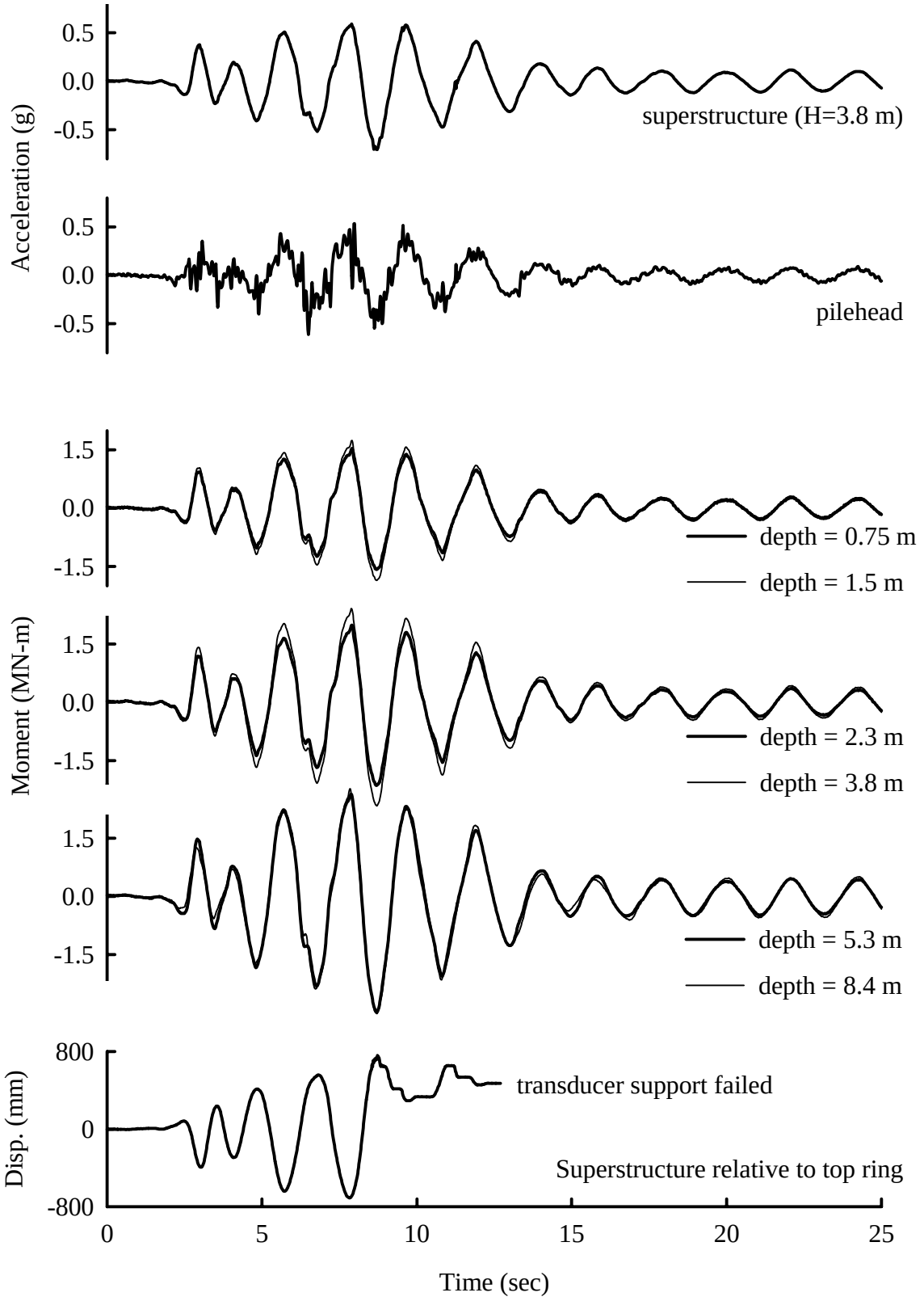

Figure 4.26: Response of highly instrumented single pile in Csp4 event E

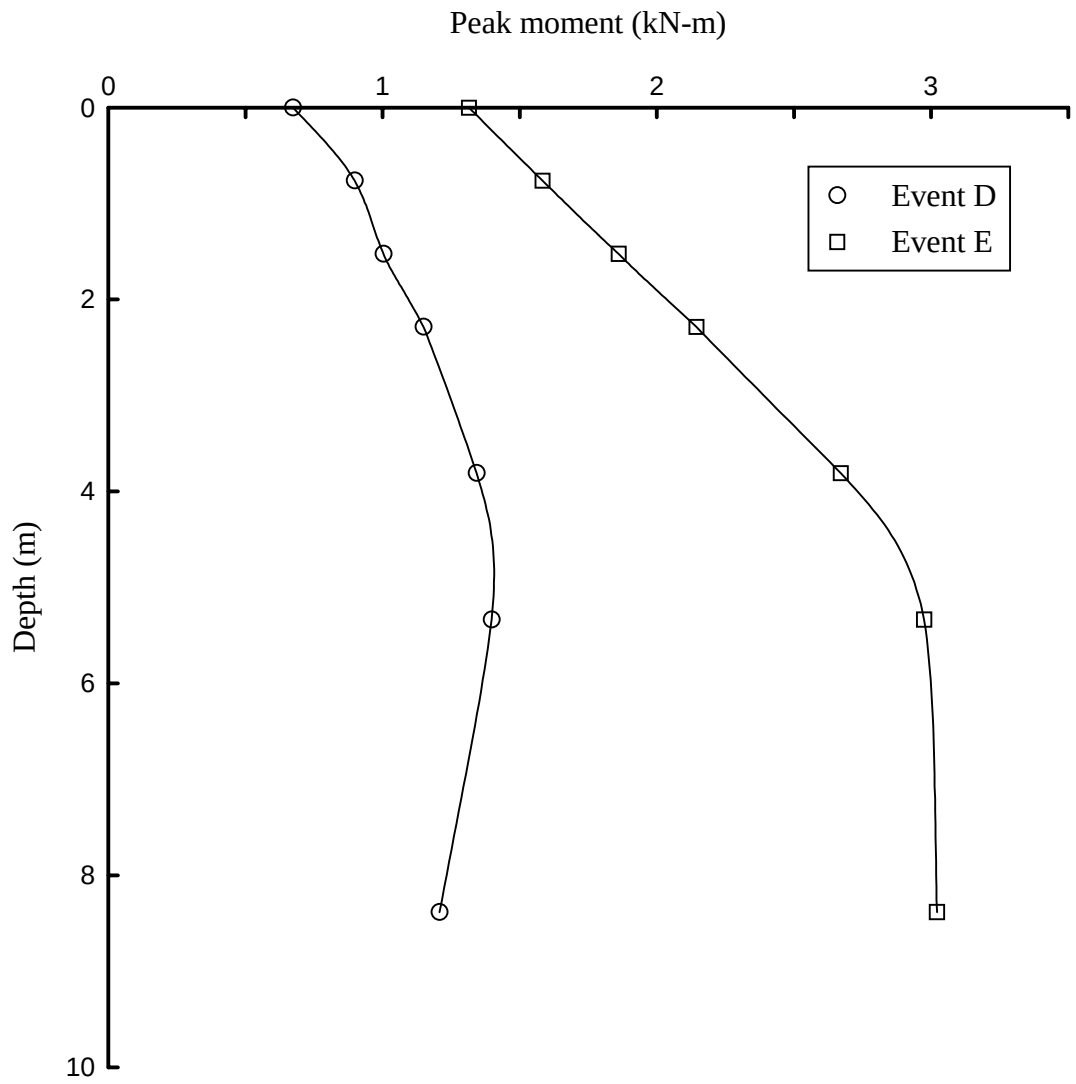

4.27: Distribution of peak bending moment in Csp4 events D and E

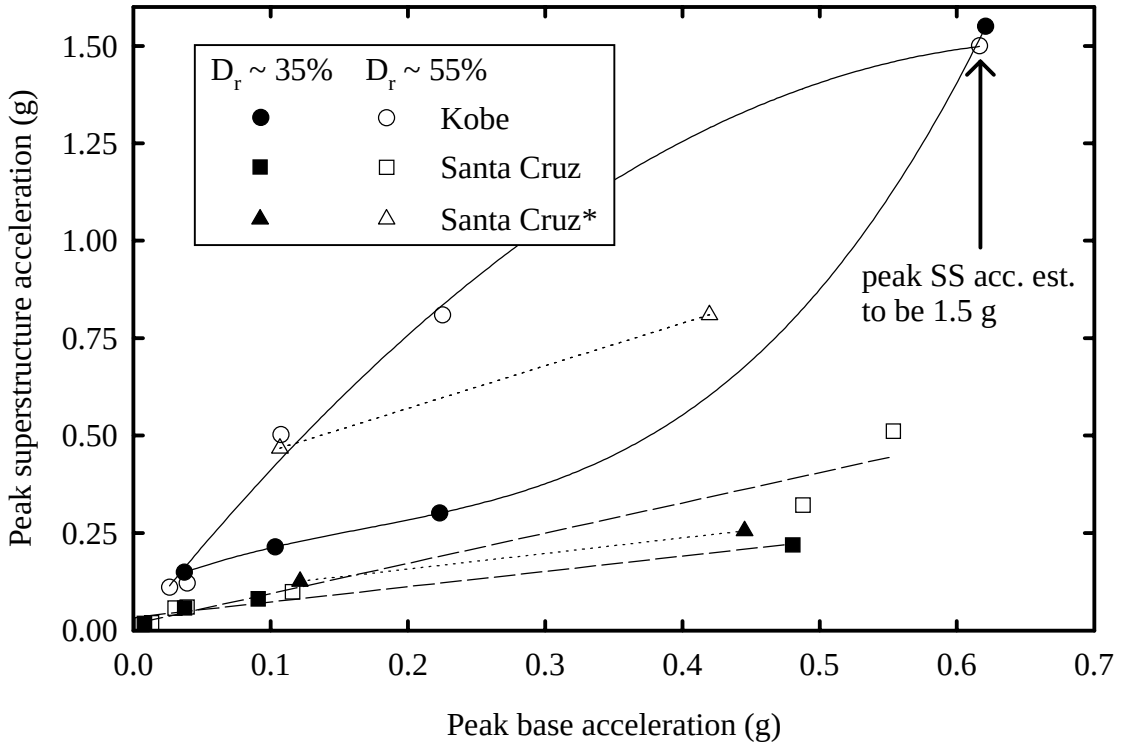

Figure 4.28: Peak superstructure accelerations versus peak base accelerations in sand

* The time step of the original recording was doubled for this motion

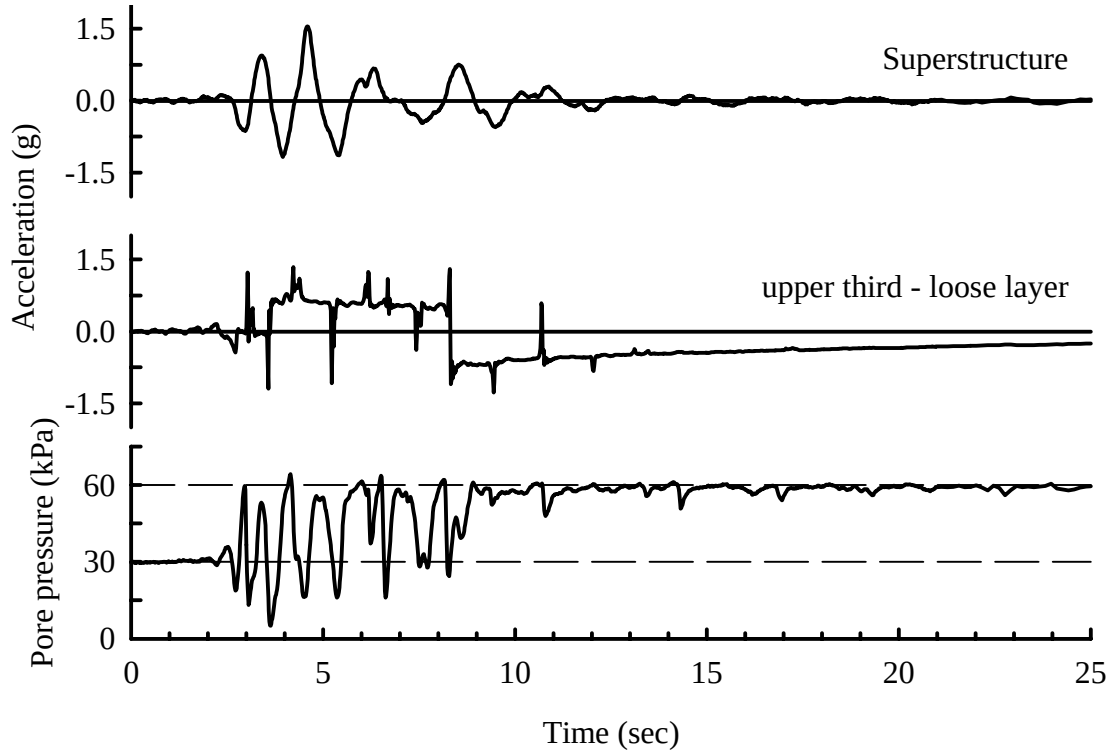

Figure 4.29: Effect of exceeding capacity of soil profile accelerometer in Csp2 event L

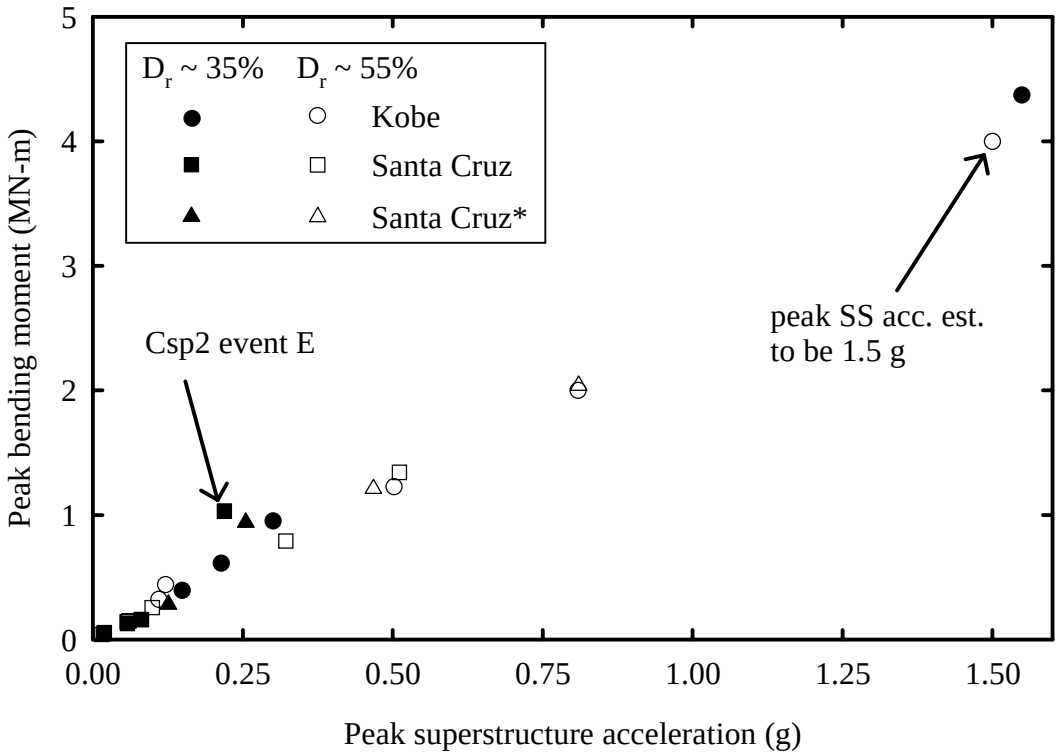

Figure 4.30: Peak bending moments versus peak superstructure accelerations in sand

* The time step of the original recording was doubled for this motion

CHAPTER FIVE

Experimental observations of p-y behavior

5.1 INTRODUCTION

In this chapter, soil-pile interaction observed in the centrifuge experiments is used to back-calculate seismic p-y behavior consistent with the assumptions of the Beam on Nonlinear Winkler Foundation (BNWF) method. The BNWF, as described in Chapter 2, is a simplified numerical modeling approach that can account for nonlinear soil-structure interaction in large seismic events, and has proven useful in engineering practice (Abghari and Chai 1995). The Winkler assumption is that the soil-pile interaction resistance (p) at any depth depends on the relative displacement between the pile shaft and soil (y) at that depth only, independent of the interaction forces above and below. In the BNWF method, the pile is modeled as a series of beam-column elements, each with discrete springs connecting the pile to the soil (see Figure 2.1). Lateral soil-structure interaction is represented through nonlinear p-y springs. Longitudinal support (t-z) springs may also be included, but are not addressed in this study.

5.2 BACKGROUND TO CALCULATING p-y CURVES

The seismic p-y behavior can be back-calculated from the recorded bending moment distribution M(z) on a pile using simple beam theory according to the equations

$$p = \frac{d^2}{dz^2} M(z) \text{ and}$$

$$\frac{d^2}{dz^2} y_{pile} = \frac{M}{EI},$$

where p is the lateral resistance on the pile, y_{pile} is the absolute lateral displacement of the pile, EI is the flexural rigidity of the model pile, and z is the vertical distance along the pile. Note that to get the relative displacement between the soil and pile, y, the displacement of the soil must be calculated separately. For this dissertation the soil displacements were calculated from accelerometer readings, as will be described in section 5.4. All back-analyses presented herein are for the highly instrumented single pile supported structure described previously in section 3.1 and shown in Figure 3.7.

5.3 DERIVATION OF LATERAL RESISTANCE FROM RECORDED DATA

The distribution of lateral resistance (p) was obtained by double differentiating the bending moment distribution with respect to depth. Many researchers have interpolated discrete measurements of moment (or curvature) of a pile and double differentiated their interpolation functions to calculate the lateral resistances along the pile (e.g. Matlock and Ripperger 1956, Dou and Byrne 1996). Two of the most common interpolation

techniques involve fitting cubic splines or polynomial functions to the data. These two methods were applied to the data in this test series along with a third method derived from finite element techniques. But just as integration is subject to low frequency noise (see section 3.3), differentiation is subject to high frequency noise. Note the transform of differentiation in the time (or linear space, as applied here) domain is multiplication by $j\omega$ in the frequency domain. The three interpolation methods and the influence of differentiation-induced noise are discussed and compared below.

5.3.1 Calculating Lateral Resistance Using Weighted Residuals

A differentiation scheme based on minimizing weighted residuals, as is often used in finite element approximations, was applied to the data in this study in the following way. Imagine we want to approximate a function u(x) over some interval from x = 0 to x = L using an approximation function a(x). Note that $u(x) \neq a(x)$ in general, and we can define the difference a(x) - u(x) = R(x) as the residual. While R(x) may not be zero anywhere in our range of x, we can chose a(x) such that R(x) is zero in an average sense by requiring that $\int_0^L R(x)\cdot\psi(x)\,dx = 0$, where $\psi(x)$ is selected from a set of weighting functions. This is commonly referred to as saying a(x) = u(x) "weakly". The method of weighted residuals can be found in any introductory finite element analysis textbook (e.g. Cook et al. 1989).

The pile can be thought of as being discretized into finite elements with nodes at each bending moment gauge location. Let f(z) represent the actual bending moment distribution of the pile as a function of depth z; f(z) is known at the nodes. Let

$g(z) = \frac{d}{dz} f(z) = f'(z)$ "weakly", i.e. g(z) represents the first derivative of the bending moment distribution, or the shear force distribution, as a function of depth. This is written as

$$\int \{g(z) - f'(z)\} \cdot \psi(z) dz = 0, \qquad 5.3\text{-}1$$

where ψ(z) can be any arbitrary weighting function. Both f(z) and g(z) are written as linear combinations of basis functions of "finite element type" (e.g. linear "hat" functions shown in Figure 5.1) and ψ(z) is taken to be each basis function in turn to generate a system of linear equations for the coefficients of g(z). In other words,

$$f(z) = \sum_{i=0}^{n} f_i \cdot \psi_i(z) \ , \ g(z) = \sum_{i=0}^{n} g_i \cdot \psi_i(z) \ ,$$

and ψ_i = basis function corresponding to node i. Equation 5.3-1 is rewritten below for the three cases of linear basis functions shown:

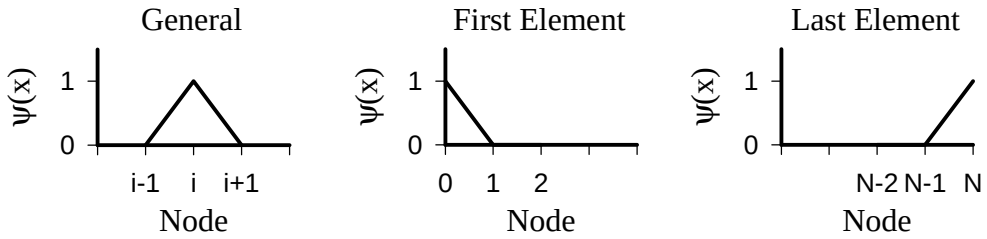

Figure 5.1: The linear basis functions of "finite element type" ("hat" functions)

Case 1: First element

$$\int_{z_0}^{z_1} \frac{\left[\left(f_1 - f_0\right) - \left[\left[\left(z_1 - z_0\right) - \left(z - z_0\right)\right]\cdot g_0 + \left(z - z_0\right)\cdot g_1\right]\right]\cdot\left(z_1 - z\right)}{\left(z_1 - z_0\right)^2} dz = 0$$

Case 2: General element

$$\int_{z_{i-1}}^{z_i} \frac{\left[\left(f_i - f_{i-1}\right) - \left[\left[\left(z_i - z_{i-1}\right) - \left(z - z_{i-1}\right)\right]\cdot g_{i-1} + \left(z - z_{i-1}\right)\cdot g_i\right]\right]\cdot\left(z - z_{i-1}\right)}{\left(z_i - z_{i-1}\right)^2} dz +$$

$$\int_{z_i}^{z_{i+1}} \frac{\left[\left(f_{i+1} - f_i\right) - \left[\left[\left(z_{i+1} - z_i\right) - \left(z - z_i\right)\right]\cdot g_i + \left(z - z_i\right)\cdot g_{i+1}\right]\right]\cdot\left(z_{i+1} - z\right)}{\left(z_{i+1} - z_i\right)^2} dz = 0$$

Case 3: Last element

$$\int_{z_{n-1}}^{z_n} \frac{\left[\left(f_n - f_{n-1}\right) - \left[\left[\left(z_n - z_{n-1}\right) - \left(z - z_{n-1}\right)\right]\cdot g_{n-1} + \left(z - z_{n-1}\right)\cdot g_n\right]\right]\cdot\left(z - z_{n-1}\right)}{\left(z_n - z_{n-1}\right)^2} dz = 0.$$

In the above equations, i is the node number and ranges from 0 to n, f_i is the recorded moment, and z is the vertical location along the pile. These equations are solved simultaneously for the values of g(z) at each node. Boundary conditions such as zero lateral resistance and known shear force at the soil surface can easily be incorporated into the solution of simultaneous equations, though none were used in this study.

The piecewise linear approximation g(z) is then differentiated by repeating the procedure to obtain an approximation of lateral resistance as a function of depth, z. I.e., let h(z) = g'(z) weakly, and solve for h(z) using the WR derivative as previously

described. Finally, since h(z) is piecewise linear, the approximation to the distribution of lateral resistance p(z) is obtained by sampling h(z) at element midpoints.

Note the bending moment distribution f(z) was approximated as piecewise linear using the basis functions $\psi(z)$. The derivative of a piecewise linear function is discontinuous piecewise constant, and the second derivative consists of Dirac-delta singularities at the nodes and is zero elsewhere. The WR approximation to the derivative of f(z), however, is piecewise linear, and can be applied a second time to obtain a piecewise linear approximation to the second derivative. Thus, this method of differentiation provides a means of obtaining, from discrete data, a derivative that has the same smoothness properties as the original WR interpolation of the data.

5.3.2 Calculating Lateral Resistance Using Cubic Spline Interpolation

A cubic spline is perhaps the simplest interpolation of discrete test data that can be double differentiated. The natural cubic spline is simple to implement, has continuous piecewise linear second derivatives, and assumes the second derivative is zero at the ends of the data. But since the spline fits every point exactly, it is prone to high frequency noise upon differentiation. Note that since the second derivative is approximated as piecewise linear, the approximation should be sampled at midpoints as was done with the WR derivative. This will eliminate the high frequency oscillations often presented when cubic splines are used to double differentiate moment data. Dou and Byrne (1996) used cubic splines to derive p-y relationships from dynamic hydraulic gradient model tests with a similar pile instrumentation setup to this test program with good results.

5.3.3 Calculating Lateral Resistance Using Polynomial Interpolation

Another common interpolation method is to fit the data with polynomials to effectively filter some of the high frequency noise. Matlock and Ripperger (1956) suggested using a series of low order polynomials over subsets of several contiguous data points, and this method has been applied successfully by Dunnavant and O'Neill (1989) and Brown, Morrison, and Reese (1988). However, this method works best with many data points, and was thus not applicable to this research. Many others have fit a single polynomial to the data set (e.g. Ting 1987), incorporating such constraints as zero lateral resistance at the surface for cohesionless soil; zero displacement, shear, and lateral resistance at some depth; and known shear at the pilehead. This method has the advantage of resulting in a continuous function for the lateral resistance.

For this study, several interpolating polynomials were fit to the moment data and the resulting lateral resistance distributions were compared. The first polynomial, $M = a+bz+cz^2+dz^3+ez^4+fz^5$, represents the five lowest order integer terms to fit seven recorded moment points. The polynomial $M = a+bz+dz^3+ez^4+fz^5+gz^6$ also includes five fitting terms but assumes the lateral resistance is zero at the surface of the soil by leaving out the quadratic term. Finally, the polynomial $M = a+bz+cz^{2.5}+dz^3+ez^4+fz^5$ includes the assumption of zero lateral resistance at the surface but contains non-integer fitting terms. In all cases, the polynomials were fit to the data using a least-squared fit. These three interpolation functions are compared at a snapshot in time from Csp3 (medium dense sand in the upper layer) event J (t = 3.589 seconds) in Figure 5.2. The three polynomials fit the recorded moments nearly equally over the range of recorded data.

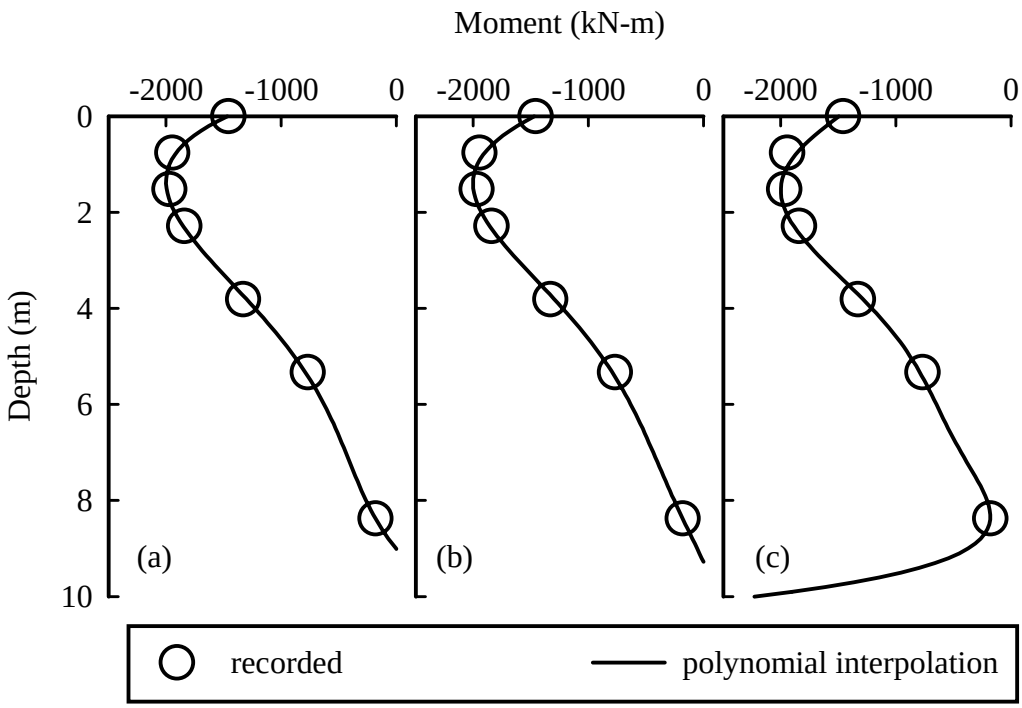

(a) $M=a+bz+cz^2+dz^3+ez^4+fz^5$

(b) $M=a+bz+cz^{2.5}+dz^3+ez^4+fz^5$

(c) $M=a+bz+dz^3+ez^4+fz^5+gz^6$

Figure 5.2: Interpolating polynomials for recorded moments in Csp3 event J at time t = 3.589 seconds

In Figure 5.3, the distribution of lateral resistance calculated from WR derivatives, cubic spline interpolation, and the interpolation polynomials shown in Figure 5.2 are shown for the same snapshot in time. For this case, leaving the quadratic term out of the polynomial completely is clearly inconsistent with the other methods (see Figure 5.3c). Dou and Byrne (1996) also reported less than optimal results using a 7^{th} order polynomial in cohesionless soil with the zero lateral resistance at the surface boundary condition imposed (following the procedure suggested by Ting 1987) when the moment gradient was high. As expected, including the quadratic term in the polynomial (Figure 5.3a)

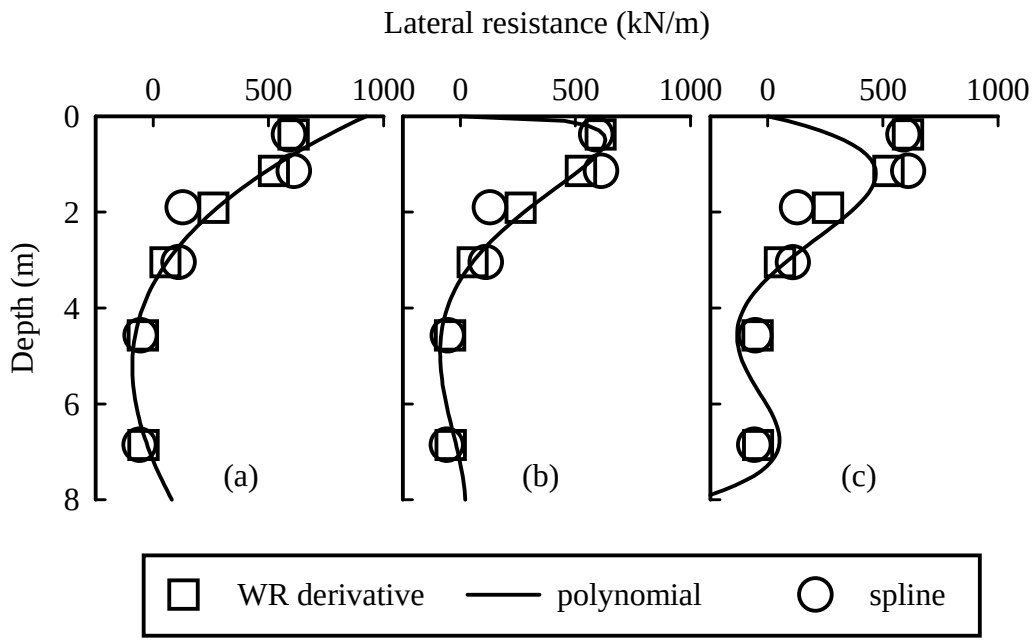

(a) $M=a+bz+cz^2+dz^3+ez^4+fz^5$

(b) $M=a+bz+cz^{2.5}+dz^3+ez^4+fz^5$

(c) $M=a+bz+dz^3+ez^4+fz^5+gz^6$

Figure 5.3: Calculated lateral resistances using three methods and three interpolating polynomials in Csp3 event J at time t = 3.589 seconds

results in a large lateral resistance (p) at the ground surface. Although the lateral resistance may not be zero at the surface for undrained seismic loading of saturated cohesionless soils, the magnitude of the lateral resistance at the ground surface calculated with the quadratic term appears unreasonably large. The non-integer polynomial form appears to provide the most reasonable approximation, as shown in Figure 5.3(b), although there is little difference from the results shown in Figure 5.3(a) below a depth of about 1.3 m (2 pile diameters). Hereafter, all results shown for a polynomial interpolation method will be based on this non-integer form.

5.3.4 Consistency of Lateral Resistance Back-Calculations

Lateral resistances calculated using WR derivatives, cubic spline interpolation, and the interpolating polynomial $M = a+bz+cz^{2.5}+dz^3+ez^4+fz^5$, were checked for consistency for all events shown in this study. The degree of agreement varied depending on the model container, event, and depth at which the lateral resistance was calculated. In general, results were consistent for depths ranging from one pile diameter (D = 0.67 m) to 3-D for Csp2, 1- to 4-D for Csp3, and 3- to 8-D for Csp4. These depth intervals are within the most heavily strain-gauged portions of the piles, which is a necessary (but not sufficient) condition for the back-calculation to be insensitive to the interpolation method.

Figure 5.4 shows an example of very good agreement between the different methods of approximating lateral resistance at a depth of 2-D. Figure 5.5 shows an example of poor agreement. Poor agreement indicated the data did not uniquely define the bending moment distribution, due to either an insufficient sampling of the bending moment distribution or an instrumentation error. Thus, comparisons of results from the different methods served as a check as to how well the sampled data represented the bending moment distribution. For this reason, all analyses in this study included a comparison of results for all three interpolation methods. For brevity, the p-y behaviors presented hereafter were derived using the WR derivative unless otherwise noted. The results are also largely limited to those cases where the different interpolation methods were in reasonable agreement to help ensure the lateral resistance was captured uniquely.

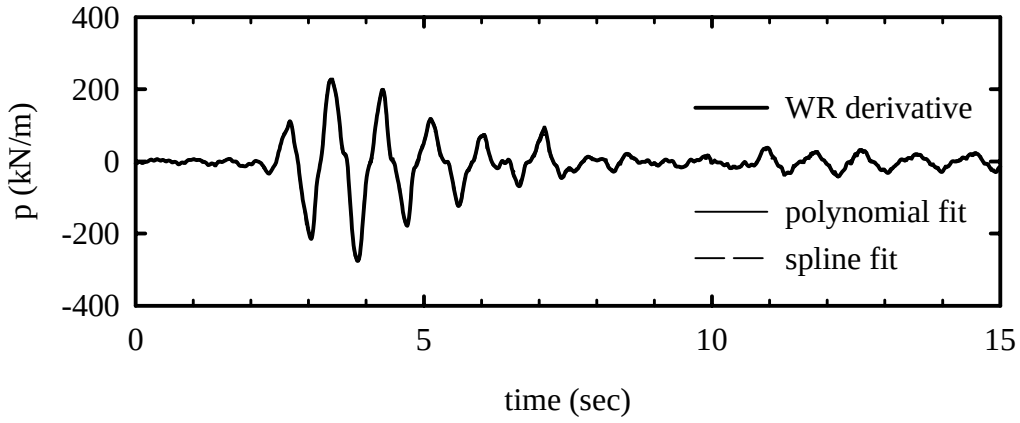

Figure 5.4: Lateral resistances in Csp3 event J, depth = 2-D (z=1.3 m)

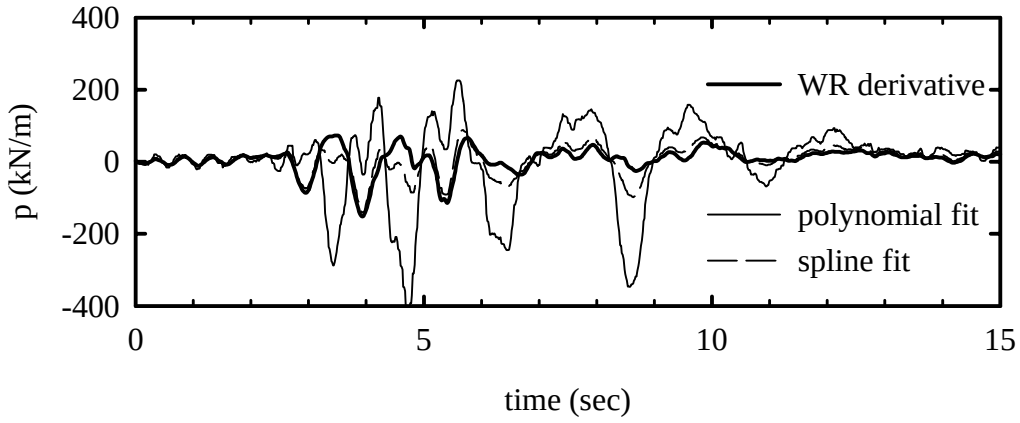

Figure 5.5: Lateral resistances in Csp2 event L, depth = 4-D (z=2.7 m)

5.4 DERIVATION OF LATERAL DISPLACEMENTS

Displacement time histories were calculated for each accelerometer of the vertical array in the soil profile near the middle of the container using the integration scheme outlined in section 3.3. Only transient soil displacements are obtained from the accelerometer records, but permanent horizontal displacements should be small for the approximately level soil profiles. The deformed soil profile at any time step (y_{soil}) was

defined by fitting an interpolation function to the displacements at different depths. For most events, a fourth order polynomial was fit to the displacement data. Other functions were used when the strains in the upper layer were dramatically larger than those in the lower layer (e.g. large seismic events in Csp2 and Csp4).

Pile displacements (y_{pile}) were calculated by double integrating the bending moment distribution interpolation polynomial ($M = a+bz+cz^{2.5}+dz^3+ez^4+fz^5$) with respect to distance along the pile. Note that integration was found to be insensitive to the interpolation function (as was expected), and thus the polynomial interpolation function was used for computational ease. Global movements were defined by two boundary conditions. Pilehead displacements (calculated from accelerations) were used as one boundary condition and the net displacement between the pile and soil was assumed to be zero at 9 m depth - just below the lowest strain gauge bridge. The independently calculated superstructure displacements were then used as a check on the calculated shape, and were found to be in good agreement most of the time.

For example, Figure 5.6 shows the deformed soil and deformed pile shapes at two snapshots in time from test Csp3 event M. Time histories of the base acceleration, excess pore pressure ratio at 4.6 m depth, and the bending moment near the top of the pile are shown for comparison. Note again the good agreement between the pile position and the superstructure position provides an independent check on the calculations.

Lastly, time histories of p and y were low-pass filtered to remove high frequency noise introduced during the numerical processing steps.

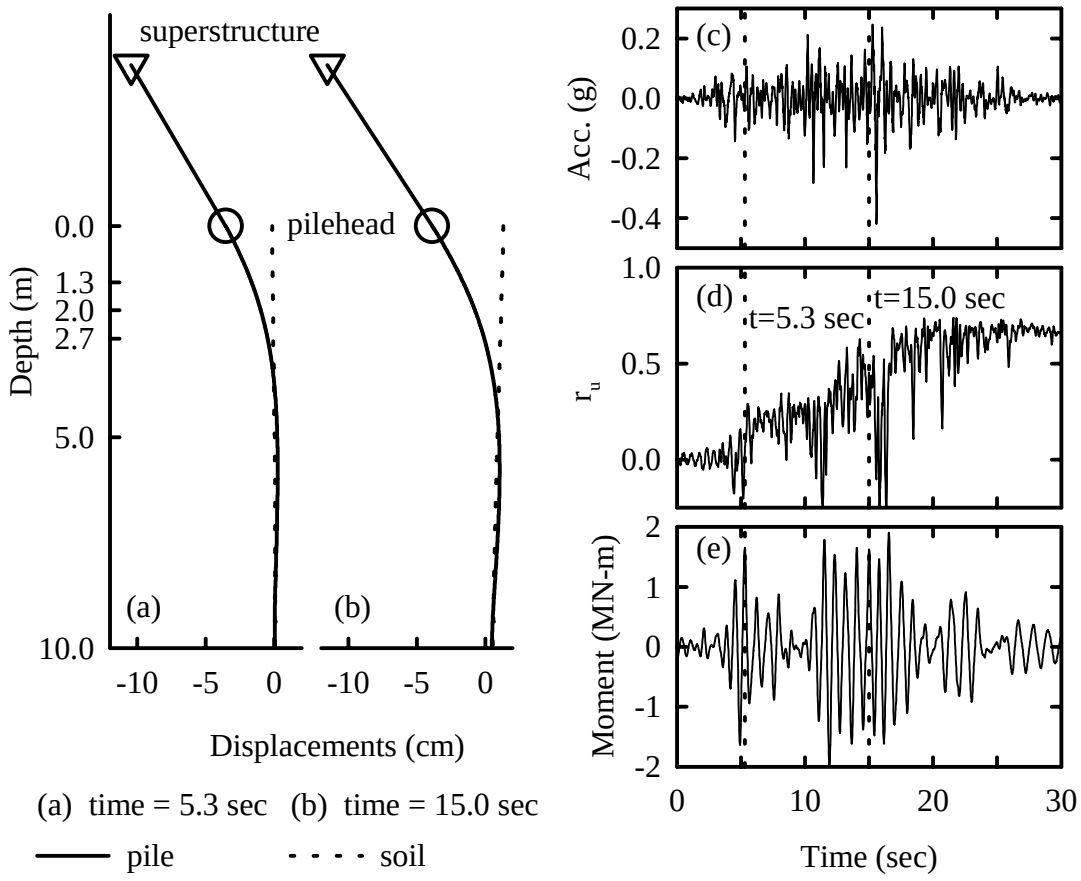

Figure 5.6: Soil and pile deformed shape at two snapshots in time from test Csp3 event M (Dr ≈ 55%), with time histories of (c) base acceleration, (d) excess pore pressure ratio at 4.6 m depth, and (e) bending moment near the top of the pile

5.5 OBSERVED p-y BEHAVIOR

An effort has been made to keep the numerical processing as consistent as possible across the suite of centrifuge tests. Minor tuning of such things as the interpolation function for fitting soil profile displacements, or corner frequencies when filtering accelerometers, can sometimes slightly improve the visual quality of the results for individual shaking events. However, presentation of the results for an established set

of numerical processing procedures allows a baseline look at the quality and consistency of the data across the suite of centrifuge tests.

5.5.1 Presentation of Results

The back-calculated p-y behavior is presented in Figures 5.7 through 5.24. Results for Csp2 are presented in Figures 5.7-5.14, Csp3 in Figures 5.15-5.22, and Csp4 in Figures 5.23-5.25. P is plotted versus y at depths of 2-D, 3-D, and 4-D for tests in sand (Csp2 and Csp3). For the test with an upper clay layer (Csp4), results are presented at depths of 3.4-D, 5.5-D, and 7.7-D. Also included on each of these figures are p and y time histories at the intermediate depth (3-D for Csp2 and Csp3, 5.5-D in Csp4) and a pore pressure time history near the single pile. Events presented are summarized in Table 5.1; the motions are described in detail in Section 3.1. Monotonic p-y curves based on American Petroleum Institute (API 1993) recommendations are shown on the p-y plots for reference. The parameters used to develop the API based p-y curves are summarized in Table 5.2. It should be noted that the API curves for sand are based upon drained loading and are not rigorously applicable to dynamic undrained loading conditions.

Several features of the back calculated p-y behaviors, as often noted upon first viewing them, result from certain limitations in the experimental data and numerical processing schemes. Some important features are discussed briefly here prior to evaluating the physical meaning of the results.

1) Why are p-y curves presented at different depths in Csp4 vs. Csp2 and Csp3?

There were two effects that controlled the choice of depths for presenting p-y results. First, in test Csp3 (medium dense sand), the net displacement between the soil and pile approaches zero at a shallower depth than in Csp4 (soft clay). This made the

Table 5.1: Events Presented in Figures 5.7-5.25

Csp2									
Motion	Kobe				Santa Cruz			Santa Cruz*	
Event	D	H	F	**	C	G	E	K	J
a_{peak} (g)	0.04	0.10	0.22	**	0.04	0.10	0.49	0.12	0.45
Csp3									
Motion	Kobe				Santa Cruz			Santa Cruz*	
Event	E	L	J	O	D	***	I	N	M
a_{peak} (g)	0.04	0.11	0.22	0.6	0.04	***	0.49	0.10	0.41
Csp4									
Motion	Kobe								
Event	B	****	D	E					
a_{peak} (g)	0.055	****	0.20	0.58					

* The time step of the original recording was doubled for this motion

** Accelerations were unreliable during the 0.6 g Kobe event in Csp2 (see discussion in Section 5.5.2)

*** The pilehead displacement boundary condition appeared inconsistent with the superstructure displacements during the 0.1 g Santa Cruz event in Csp3

**** A 0.1 g Kobe motion was not performed in Csp4

Table 5.2: Properties Used for Monotonic API Curves in Upper Soil Layer

Test	γ' (kN/m^3)	ϕ'	k (kN/m^3)
Csp2 ($D_r \approx 35\%$)	9.8	30	8100
Csp3 ($D_r \approx 55\%$)	9.8	35	21700
	γ' (kN/m^3)	C_u/σ_v'	ε_c
Csp4 (soft NC clay)	5.2	0.45	0.01

calculation of y at depth more sensitive in the tests with sand than in the tests with clay. Secondly, the response of the uppermost accelerometer in the clay profile of Csp4 may not have captured the motion of the soil as it was intended. This transducer was too close to the soil surface and may have moved relative to the soil during shaking. As a consequence, displacements calculated in the uppermost layer of clay in Csp4 were inconsistent with those calculated for the rest of the soil profile. This was also noted in Section 3.2.5. Thus, y values at shallow depth in Csp4 were less reliable than those calculated in the sand tests (Csp2 and Csp3).

2) Difficulties with the p-y curves for Csp2

Several things combined in test Csp2 to make the calculation of p and y difficult. Three factors complicated the calculation of y. First, the soil was loose ($D_r \approx 35\%$) and had a relatively high strain potential upon liquefying. The liquefied soil tended to slosh in the container and motions were not completely uniform across the profile (see section 3.2.5). Second, low shear wave velocities associated with liquefied loose soils imply a short wavelength across the profile. There may not have been an adequate number of accelerometers in the vertical array to satisfactorily sample these short wavelengths. And finally, very high peak accelerations in the soil profile exceeded the capacity of certain transducers. This resulted in electronic saturation of the accelerometer, which introduced a low frequency drift that is difficult to remove when calculating displacements. This clearly affected most of the recordings in event L, and possibly affected certain recordings in other large events.

There was also a hardware problem with the data acquisition system in this test. Specifically, the anti-aliasing filters used with the bending moment transducers were set too low due to a hardware malfunction in the data acquisition system. This corrupted the high frequency content of the data. The data was corrected to remove the effects of the filter, but some high frequency information was unavoidably lost. Note the lateral resistances calculated using the three methods for events in Csp2 varied more than those calculated from Csp3 and Csp4.

Regardless of these limitations, the analysis is useful because it does show that, in Csp2, lateral resistances were relatively small and the displacements were very large.

3) Difficulties with low-frequency components of motion

Some of the y time histories show displacement occurring before shaking. This is due to the soil profile displacements calculated from the accelerometer array (see section 3.3).Typically in processing strong ground motions, the corner and or the order of the high pass filter is changed until this effect is removed. However, for this data it was found that the calculated displacements compared more favorably with the recorded displacements overall if this early drift was left in. As mentioned previously, these low frequency components can be removed with additional processing, but this was not done in the interest of keeping the processing consistent across the suite of all tests.

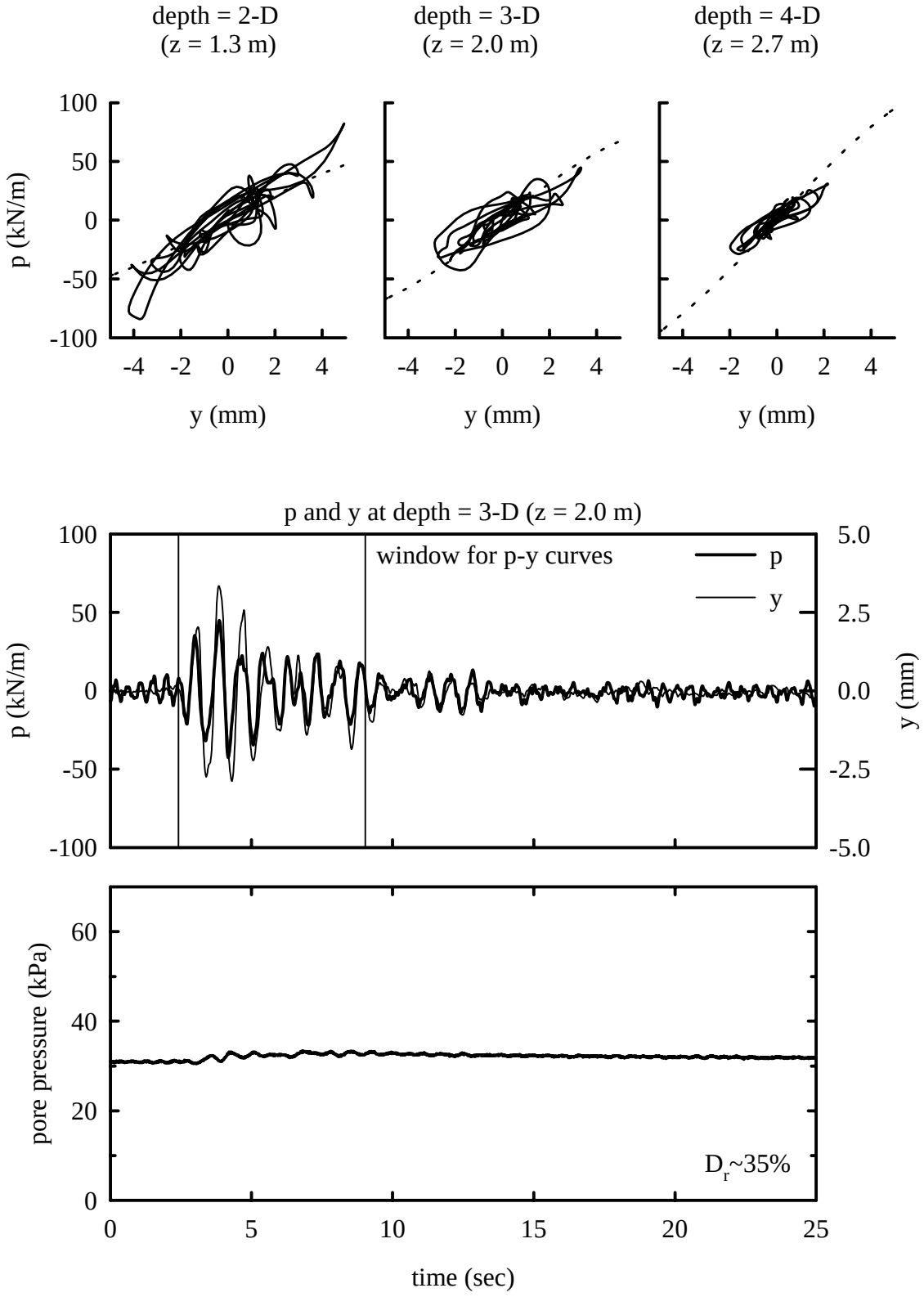

Figure 5.7: p-y behavior in test Csp2 event D
Kobe input with $a_{max,base}$=0.04 g

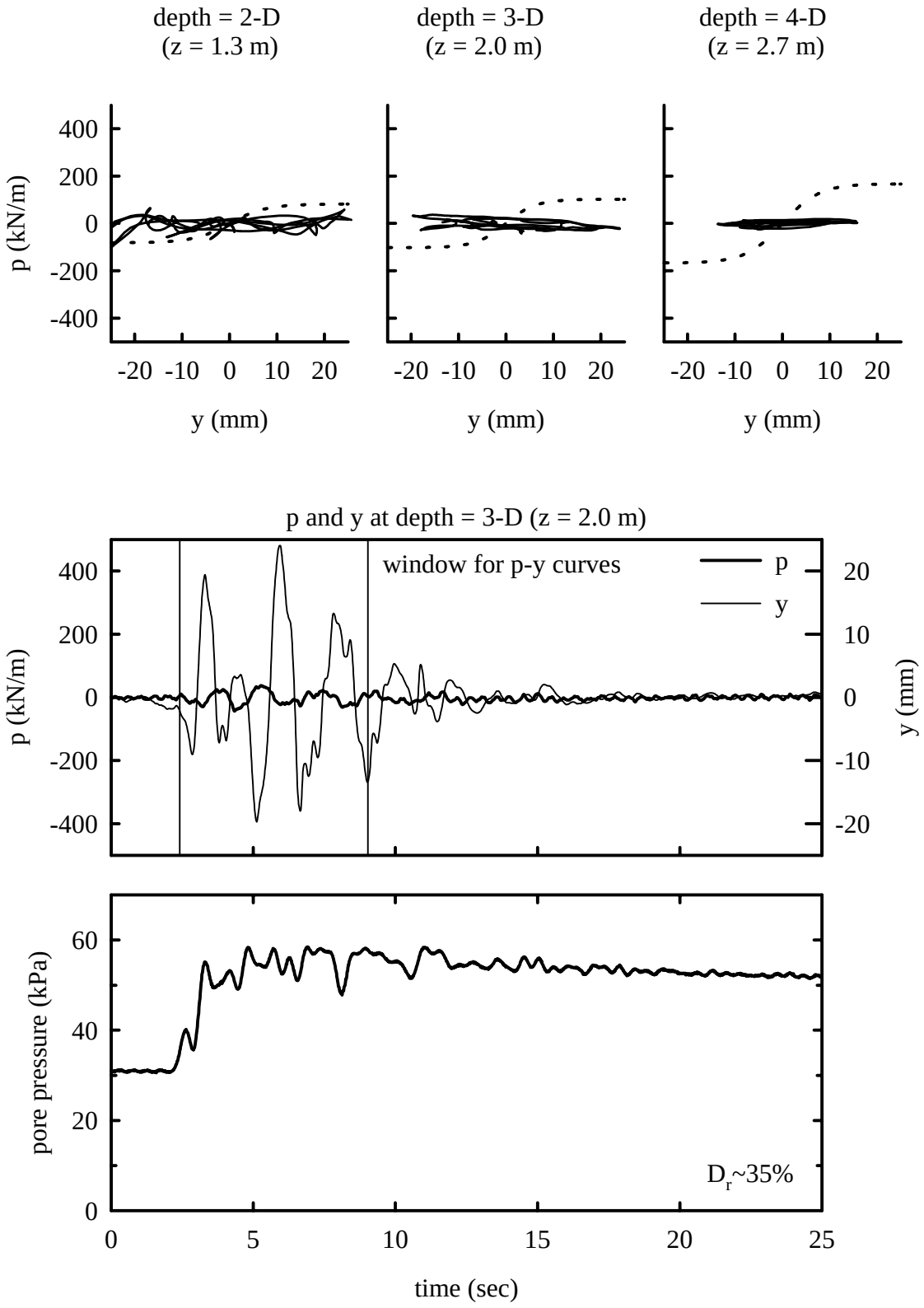

Figure 5.8: p-y behavior in test Csp2 event H
Kobe input with $a_{max,base}$=0.10 g

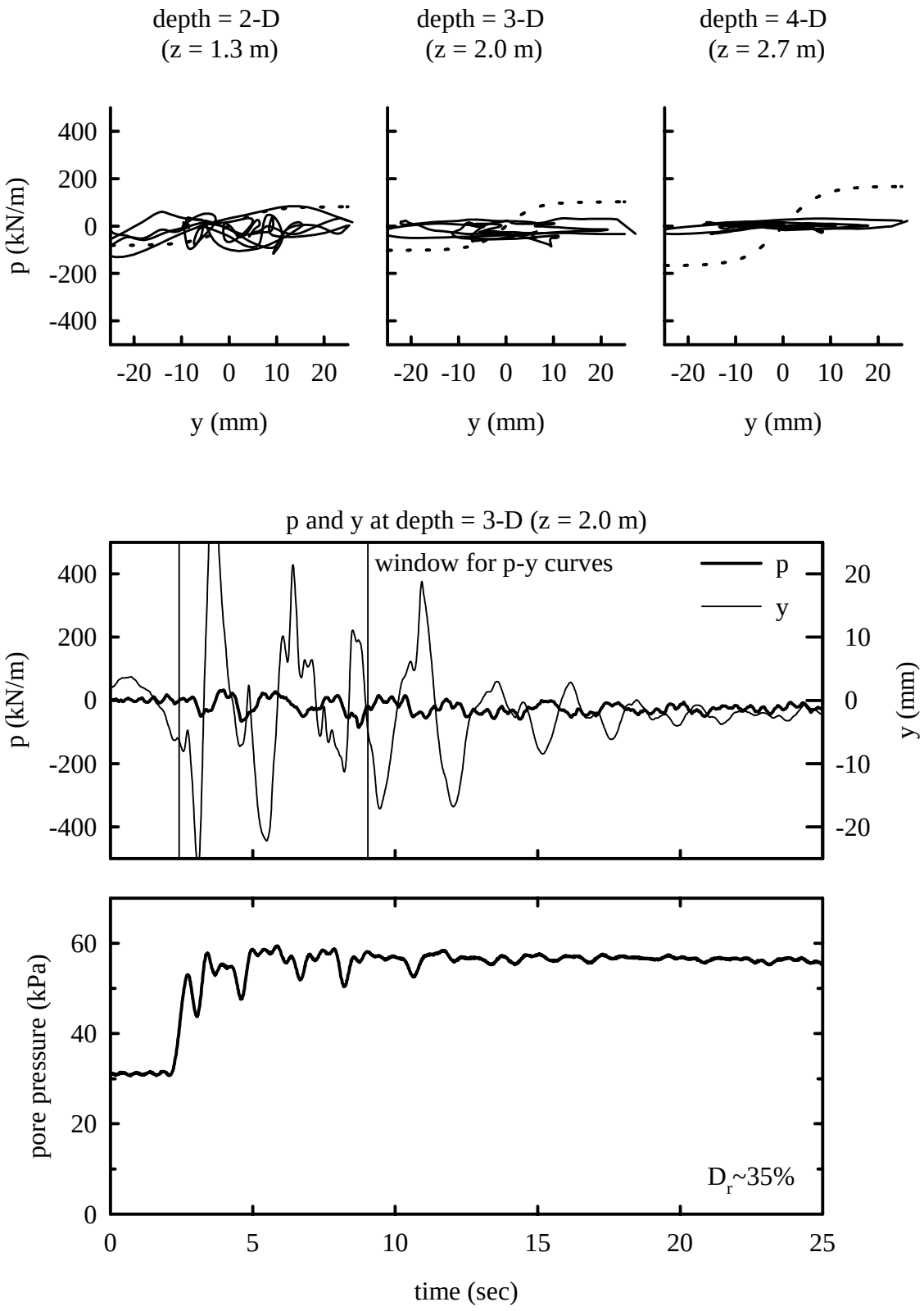

Figure 5.9: p-y behavior in test Csp2 event F
Kobe input with $a_{max,base}$=0.22 g

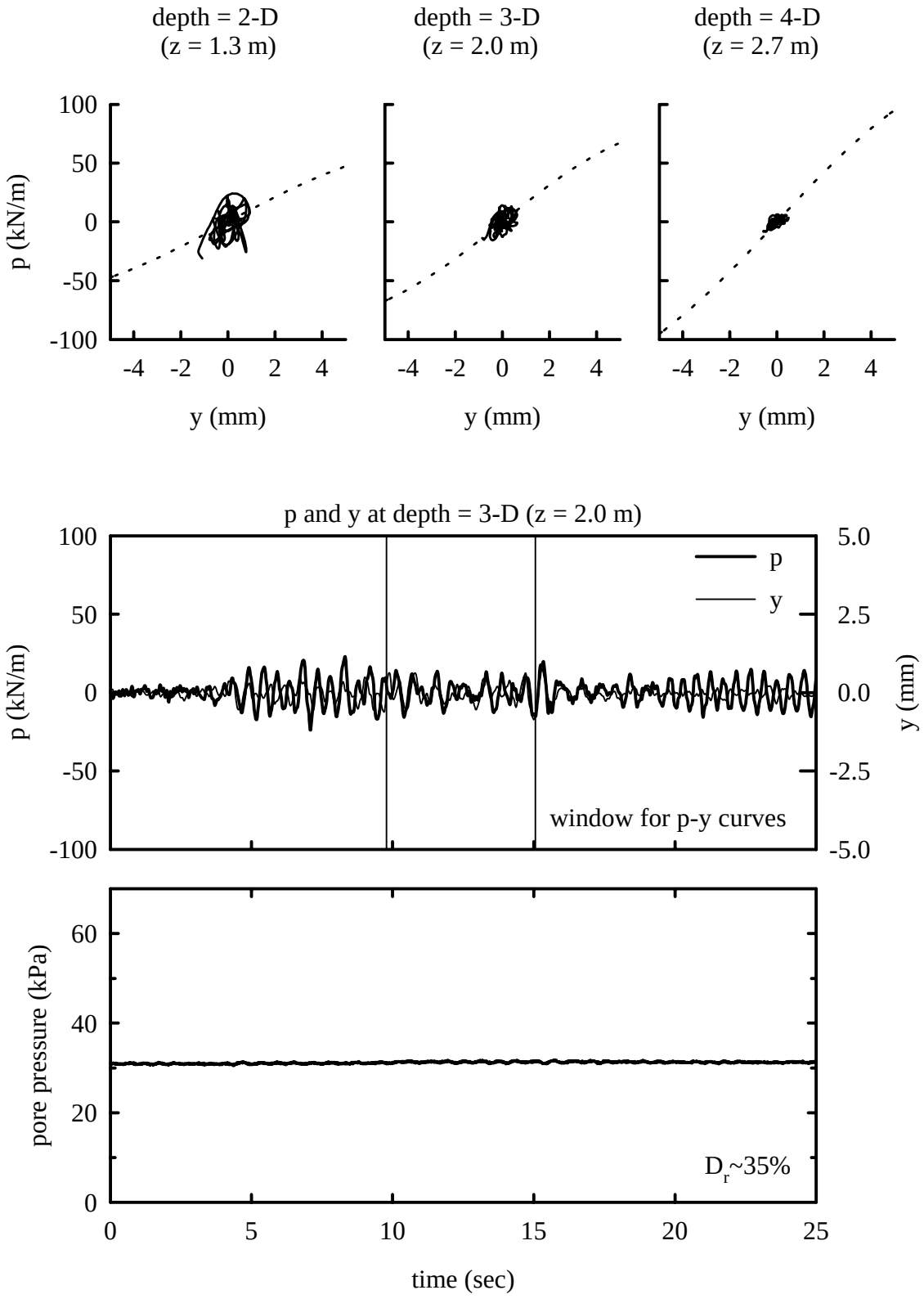

Figure 5.10: p-y behavior in test Csp2 event C
Santa Cruz input with $a_{max,base}$=0.04 g

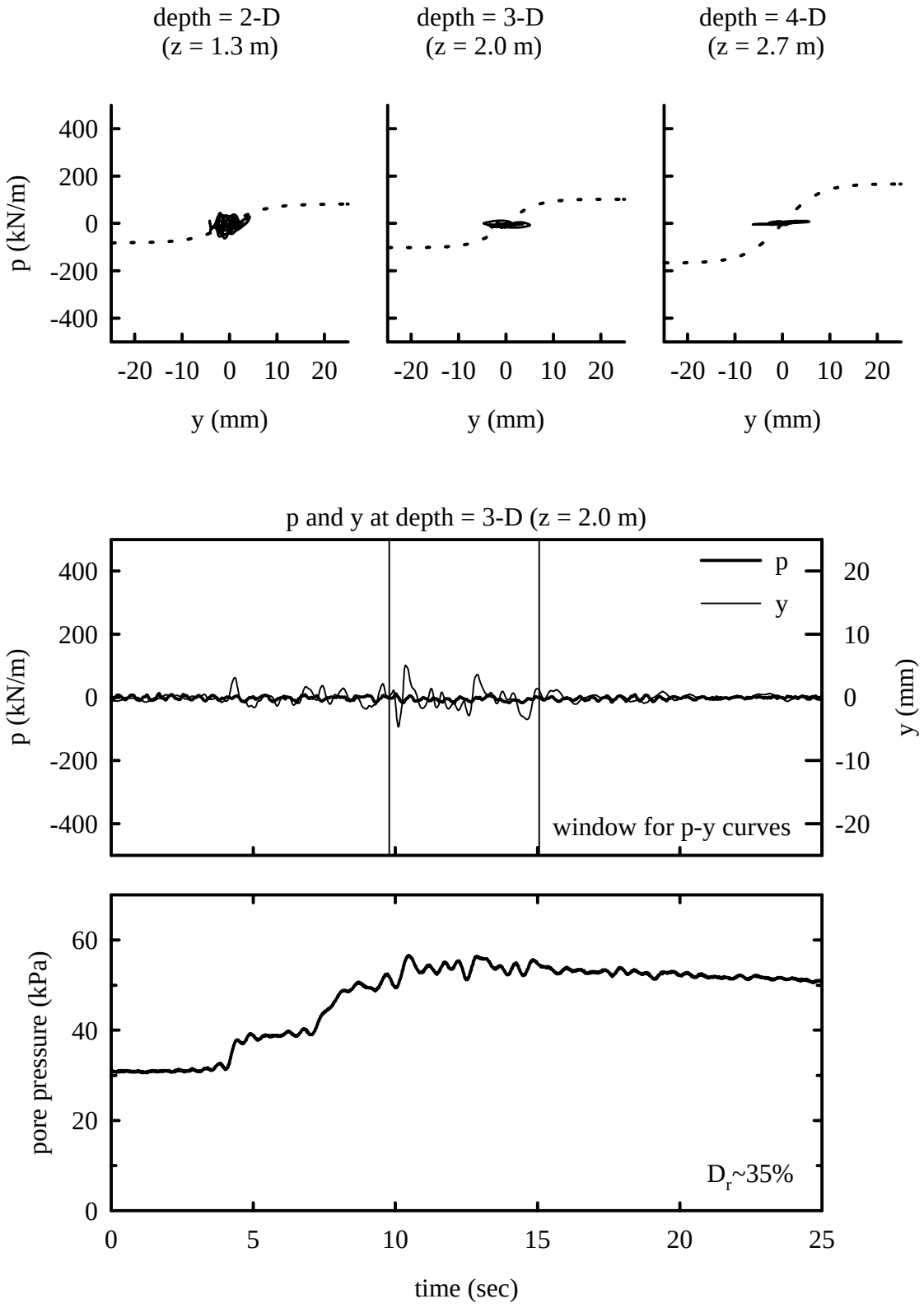

Figure 5.11: p-y behavior in test Csp2 event G
Santa Cruz input with $a_{max,base}$=0.10 g

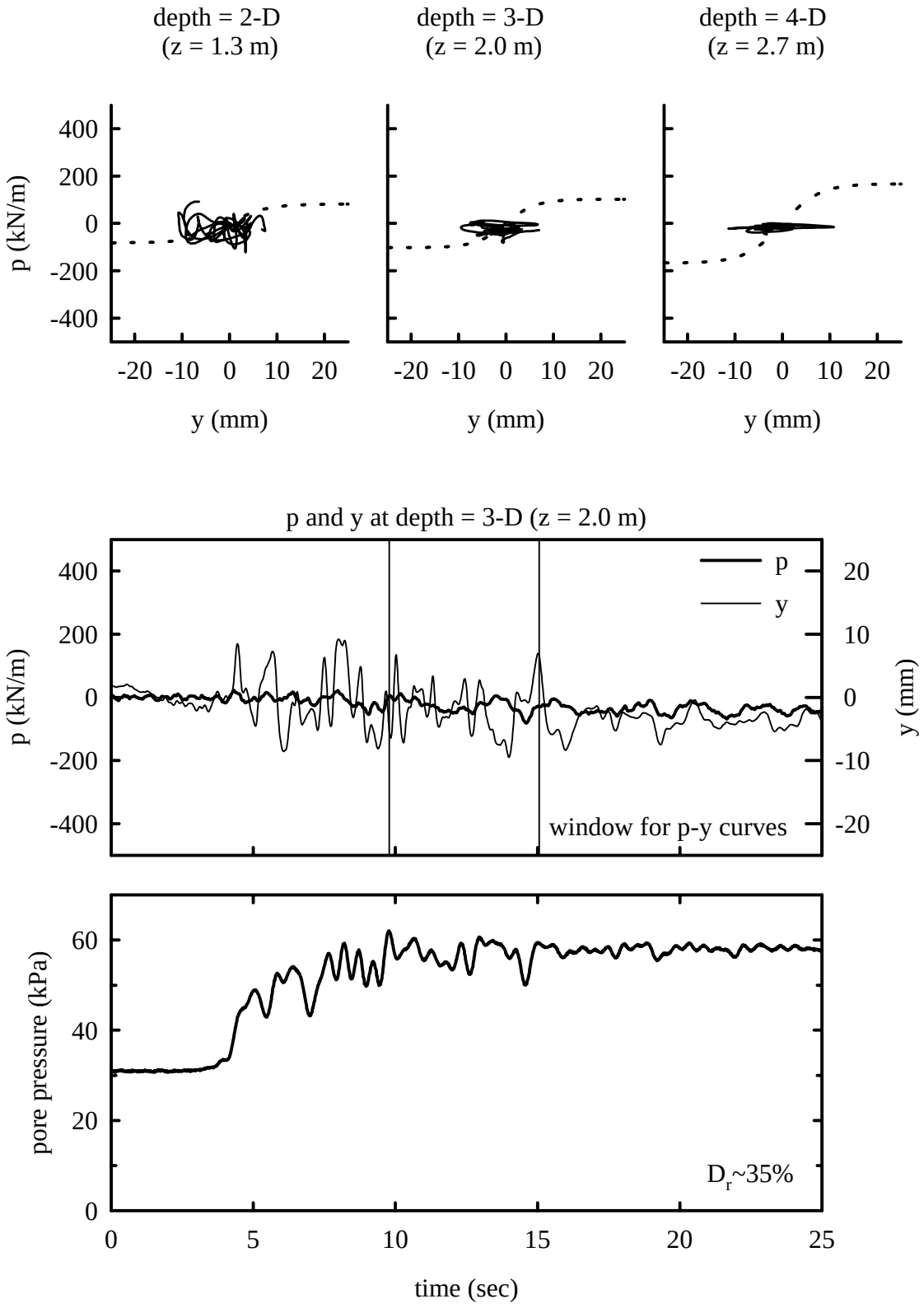

Figure 5.12: p-y behavior in test Csp2 event E
Santa Cruz input with $a_{max,base}$=0.49 g

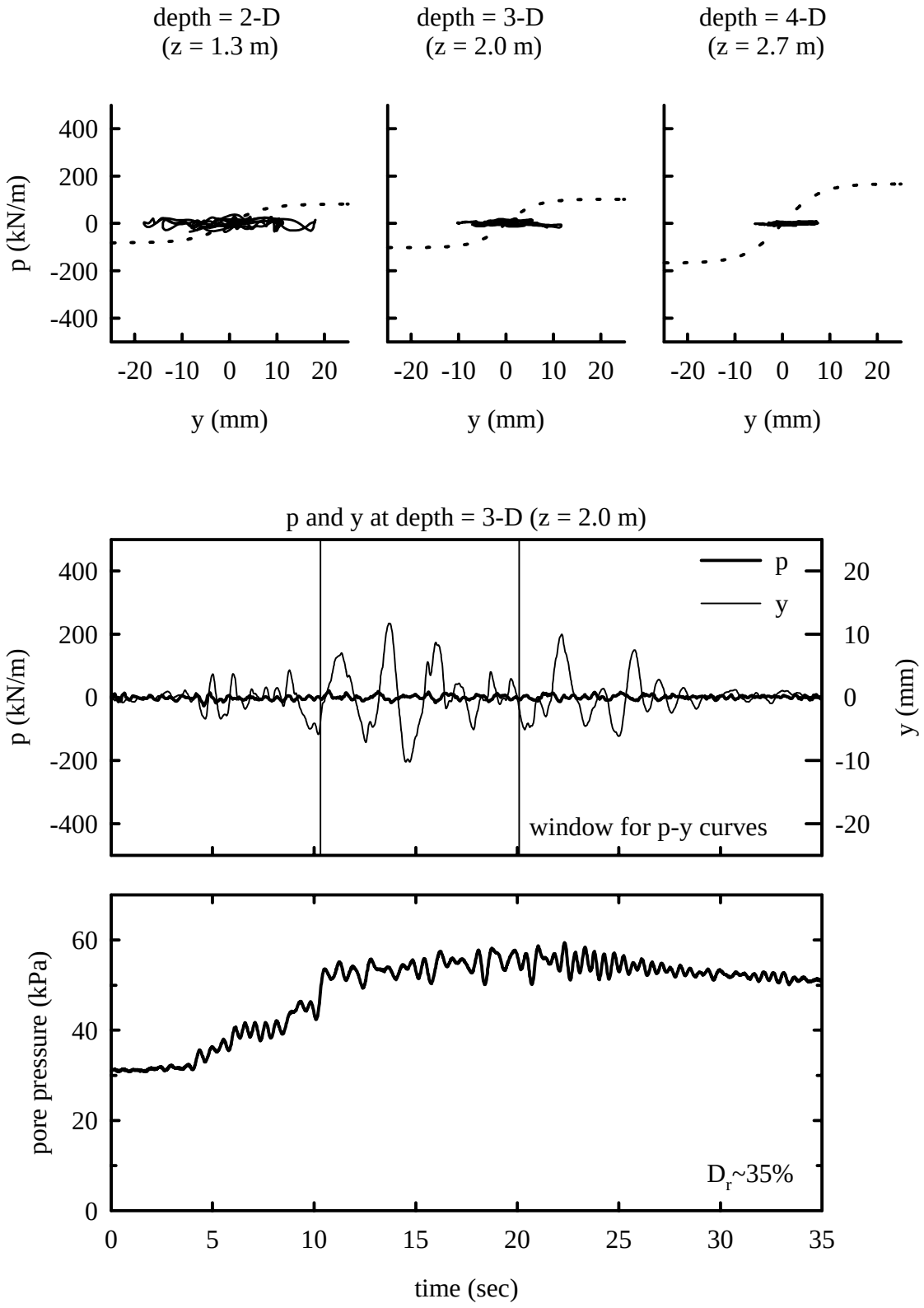

Figure 5.13: p-y behavior in test Csp2 event K
Santa Cruz* input with $a_{max,base}$=0.12 g

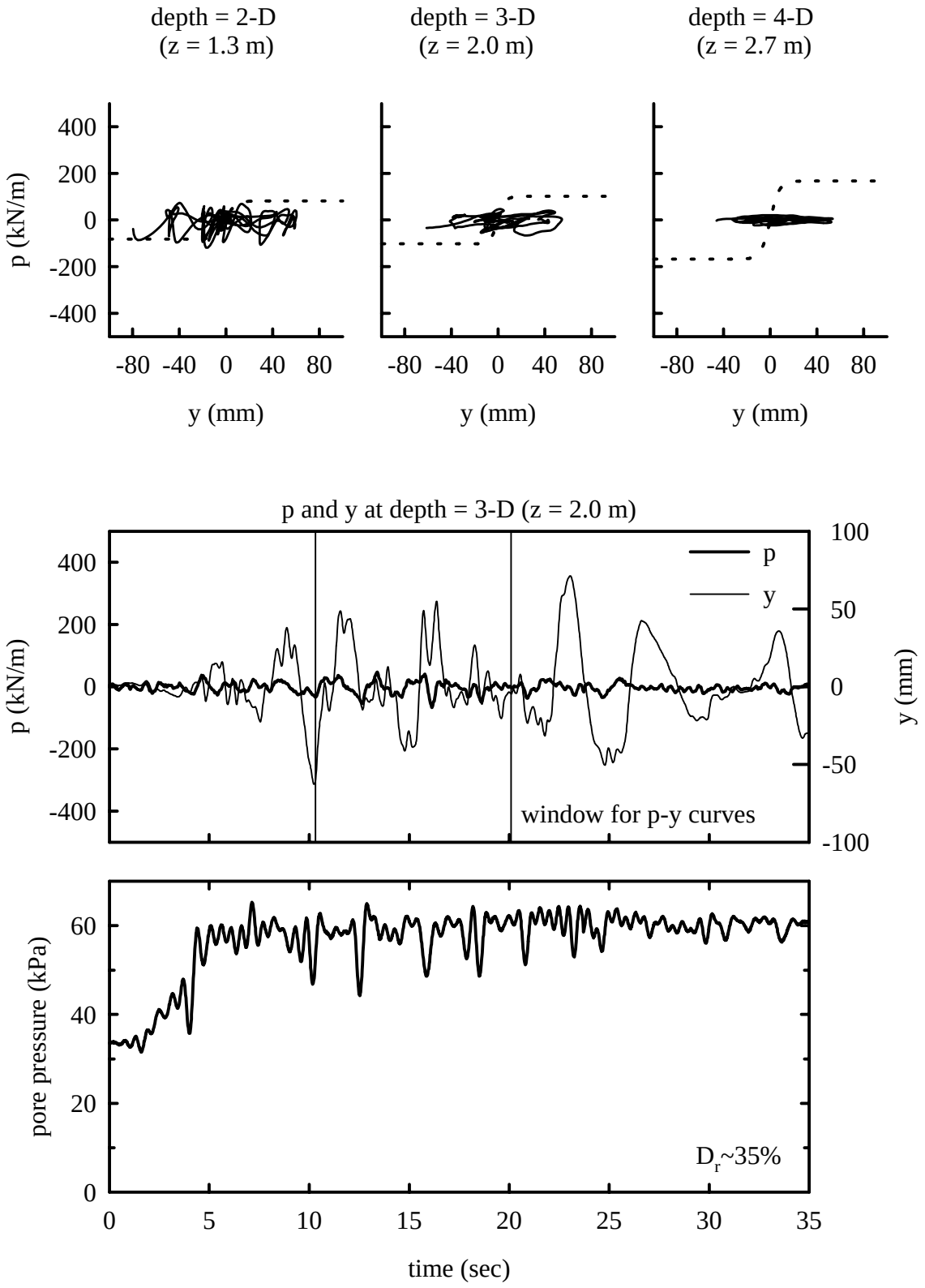

Figure 5.14: p-y behavior in test Csp2 event J
Santa Cruz* input with $a_{max,base}$=0.45 g

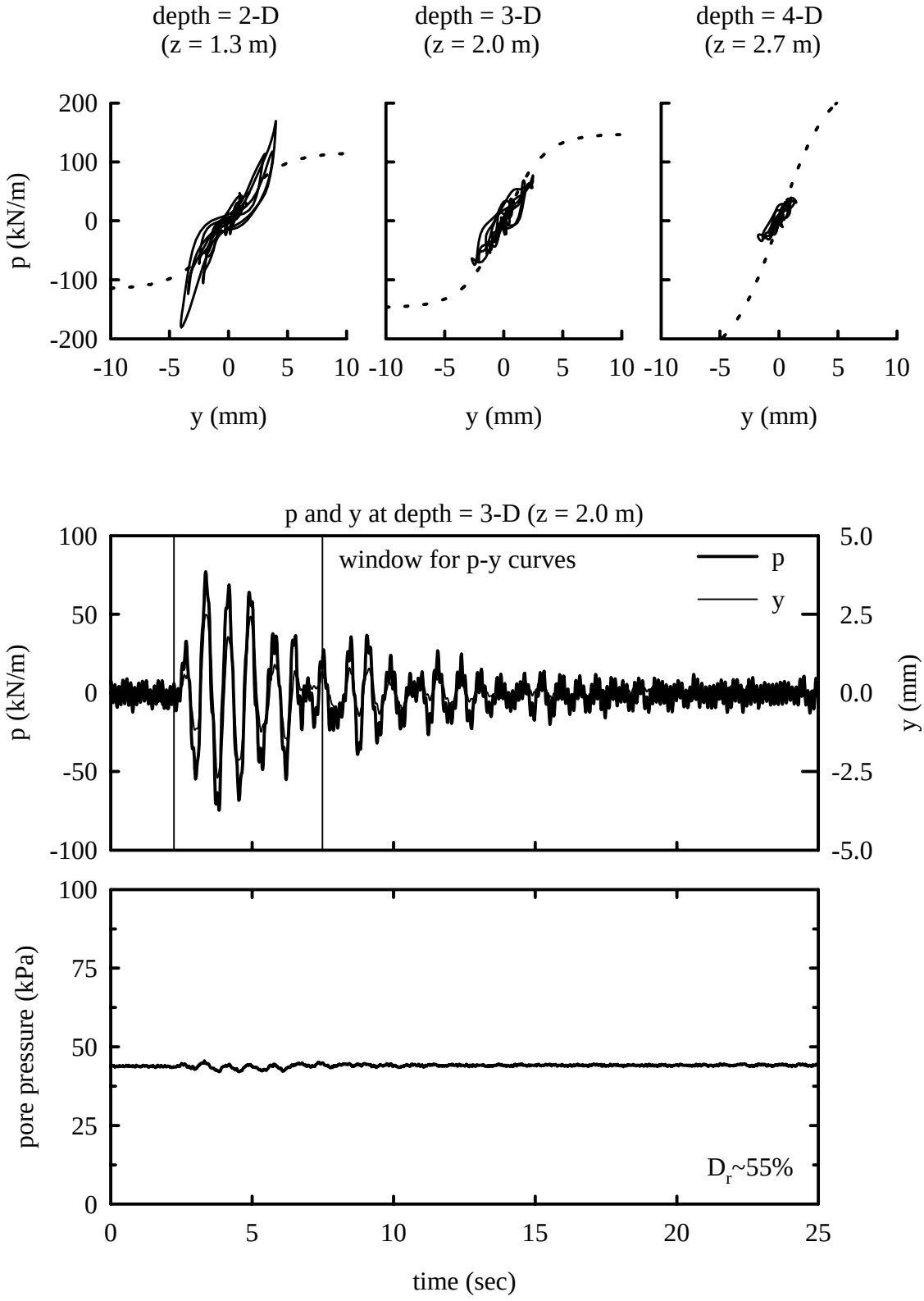

Figure 5.15: p-y behavior in test Csp3 event E
Kobe input with $a_{max,base}$=0.04 g

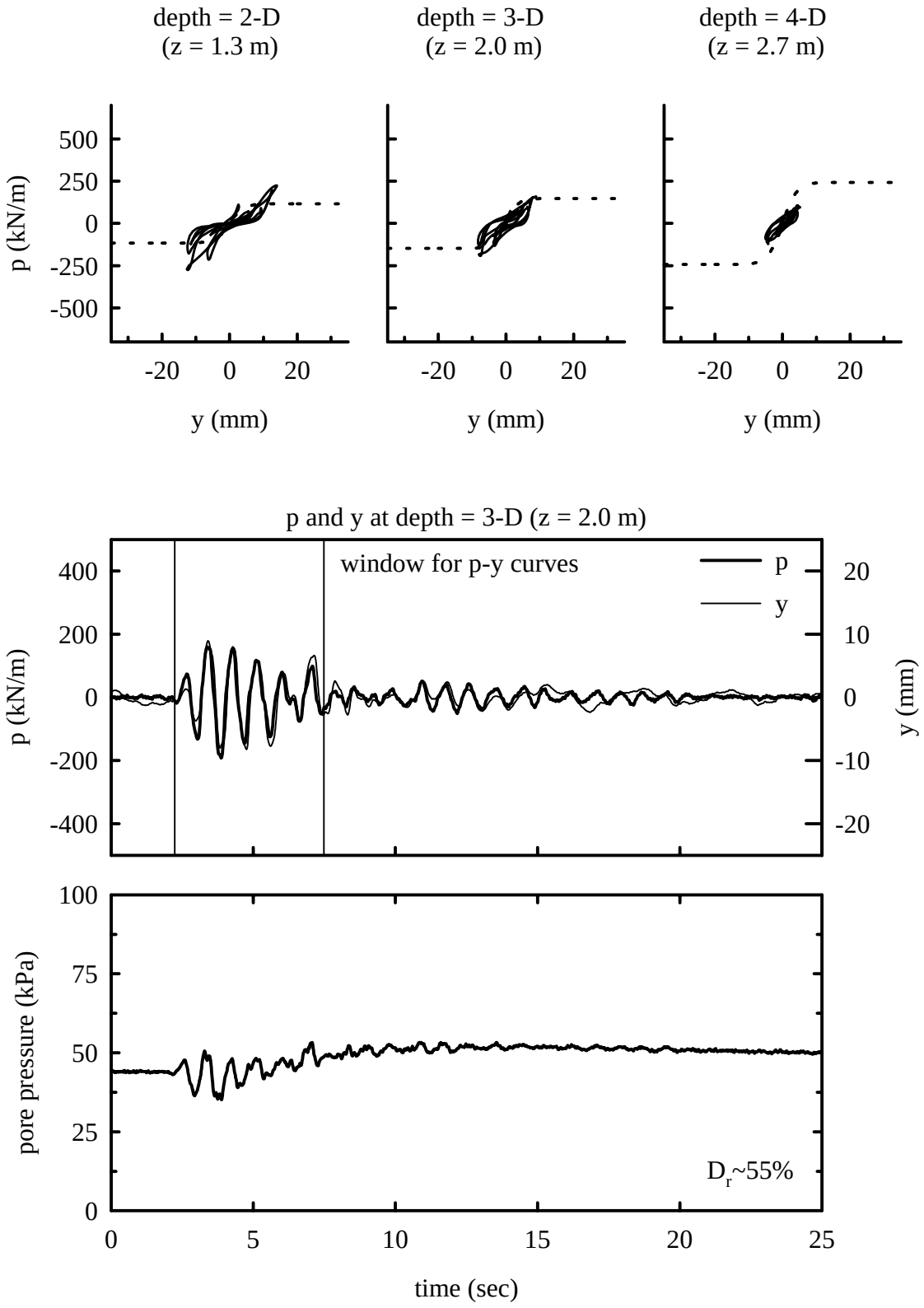

Figure 5.16: p-y behavior in test Csp3 event L
Kobe input with $a_{max,base}$=0.11 g

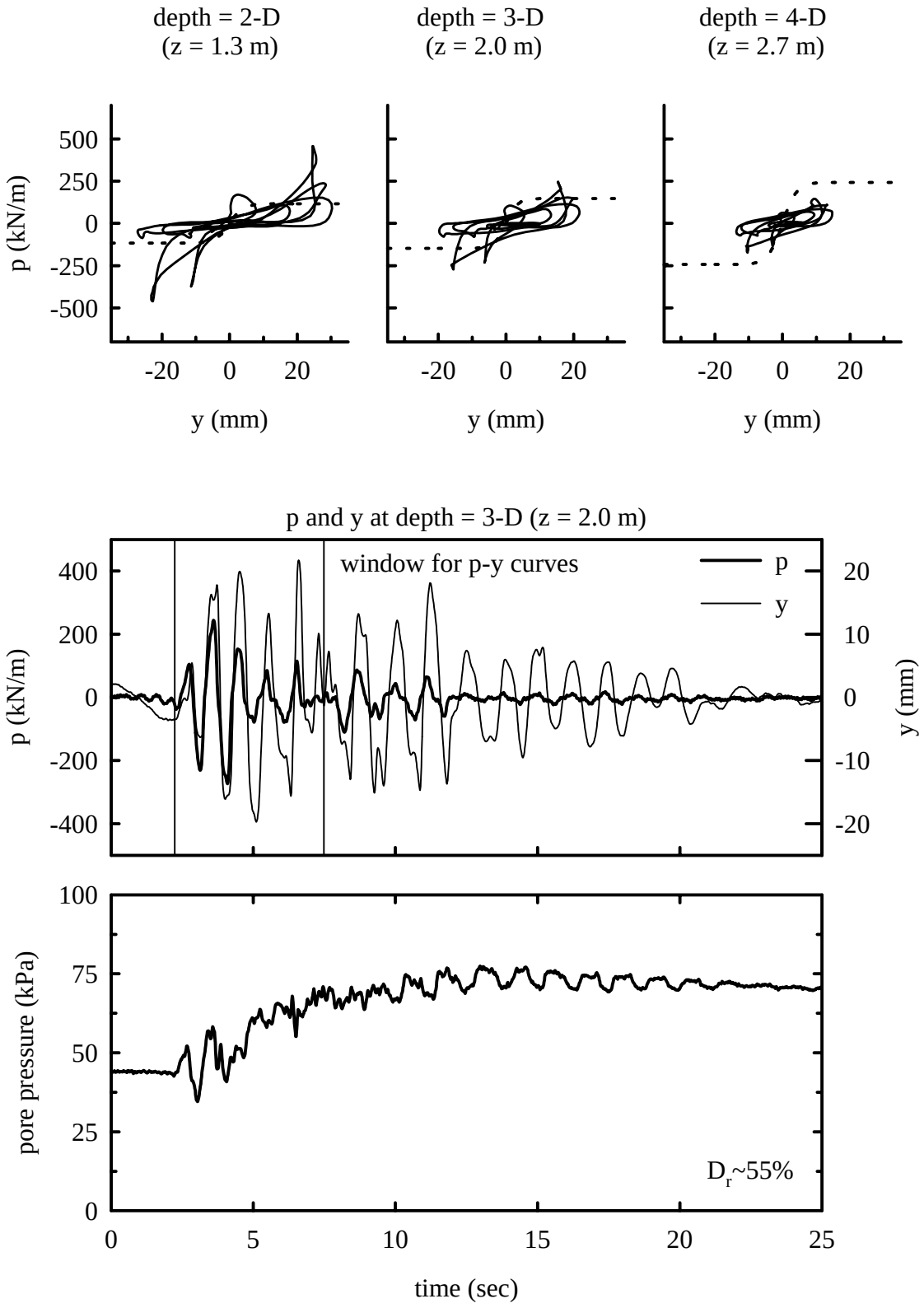

Figure 5.17: p-y behavior in test Csp3 event J
Kobe input with $a_{max,base}$=0.22 g

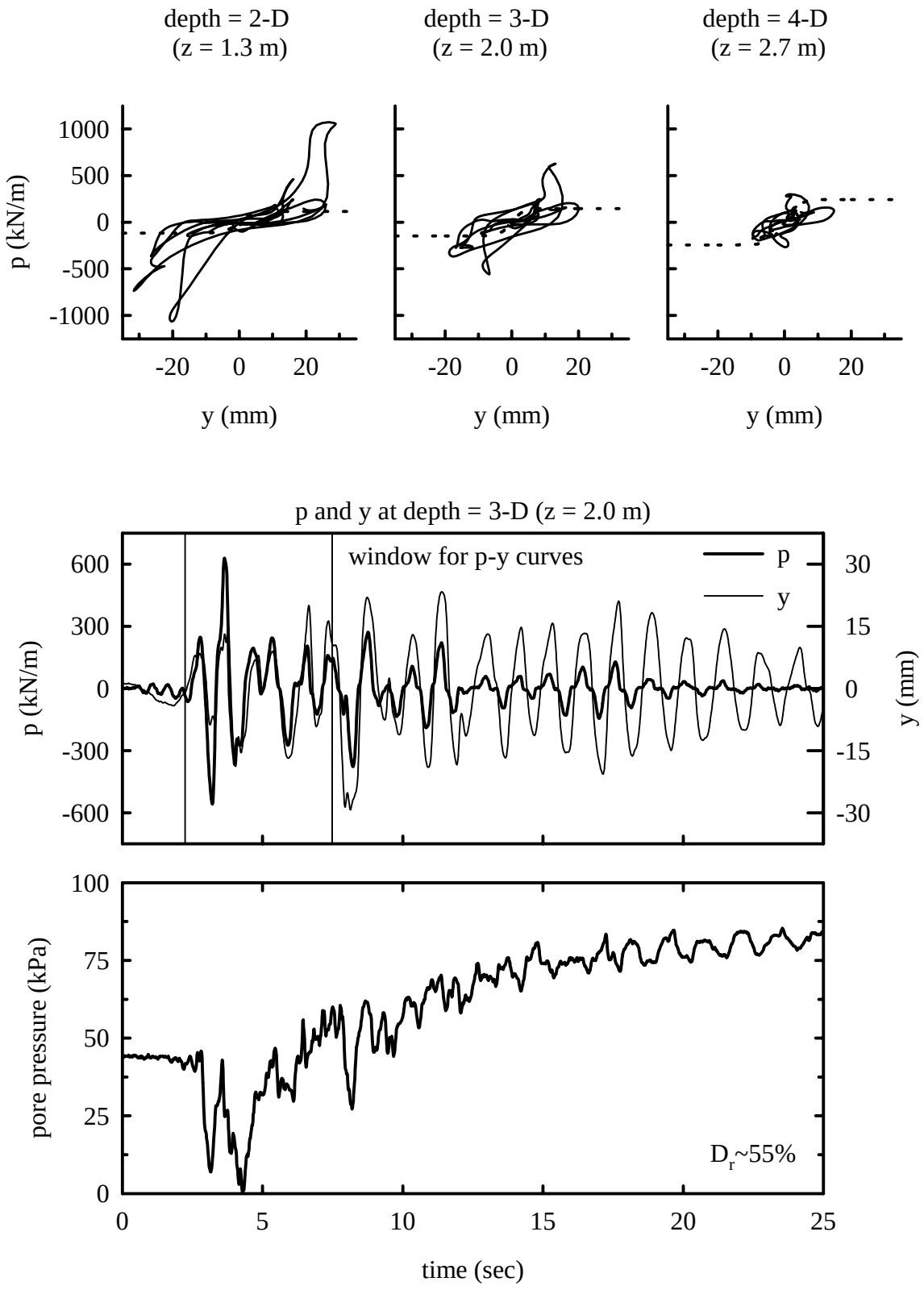

Figure 5.18: p-y behavior in test Csp3 event O
Kobe input with $a_{max,base}$=0.60 g

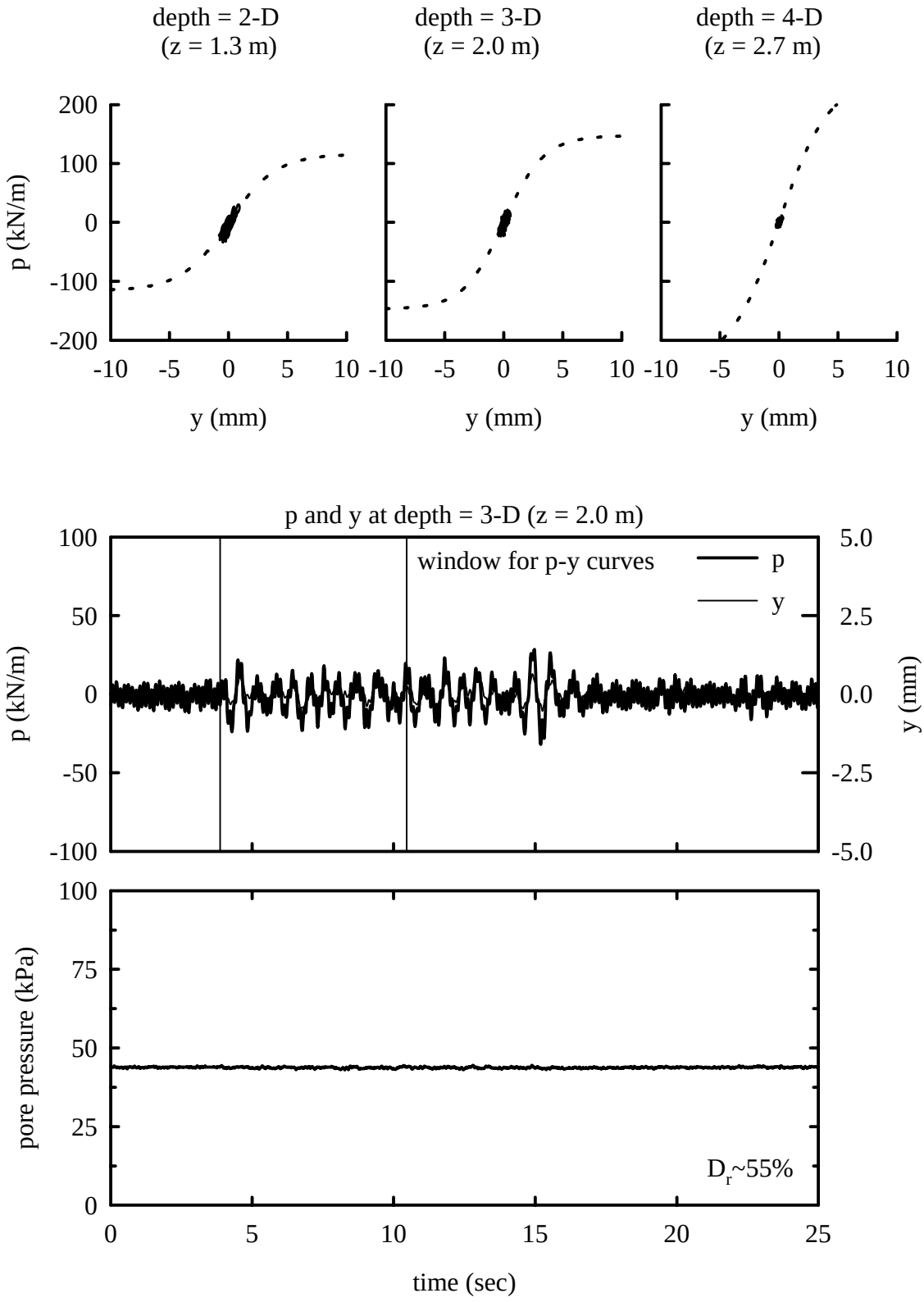

Figure 5.19: p-y behavior in test Csp3 event D
Santa Cruz input with $a_{max,base}$=0.04 g

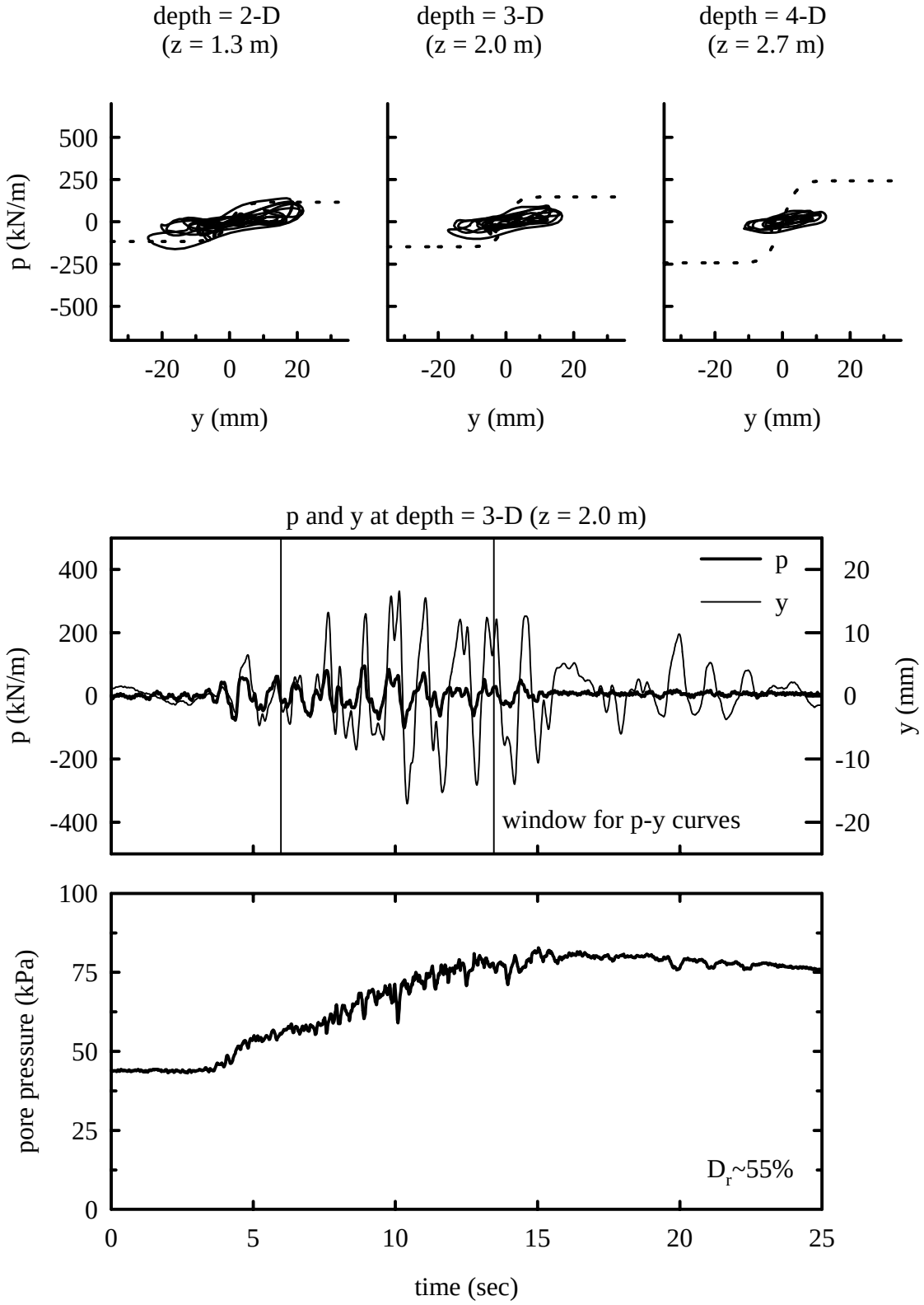

Figure 5.20: p-y behavior in test Csp3 event I
Santa Cruz input with $a_{max,base}$=0.49 g

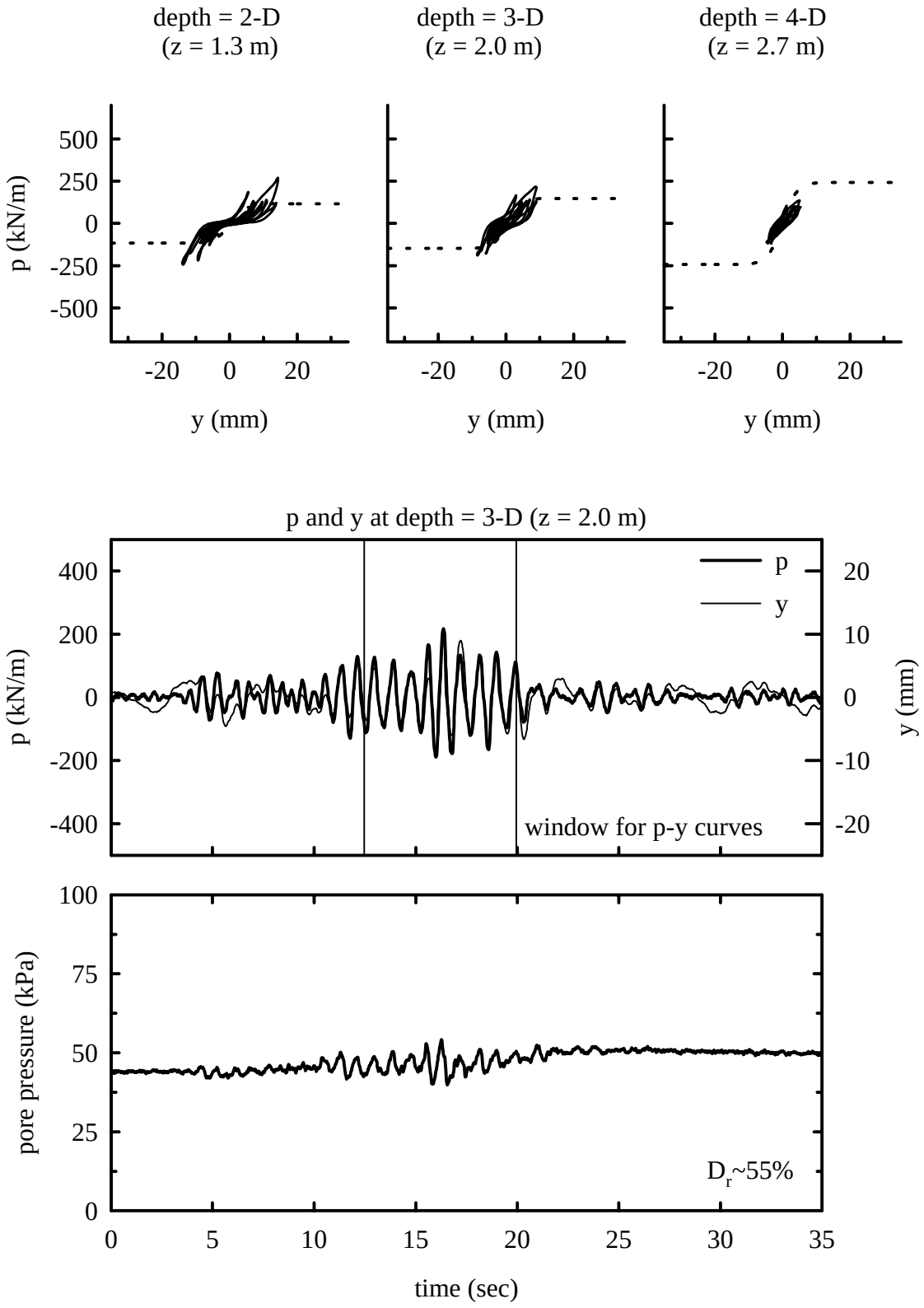

Figure 5.21: p-y behavior in test Csp3 event N
Santa Cruz* input with $a_{max,base}$=0.10 g

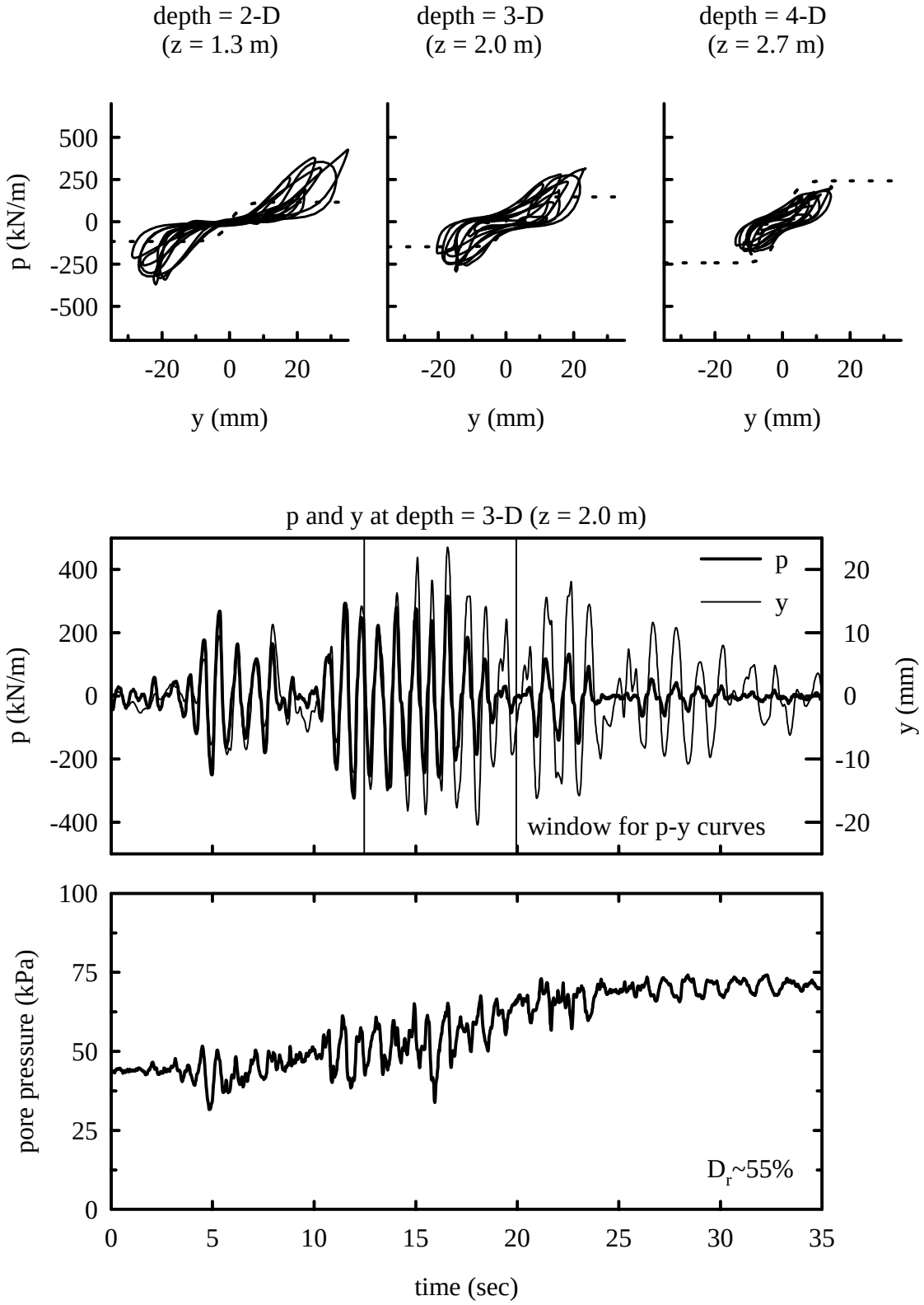

Figure 5.22: p-y behavior in test Csp3 event M
Santa Cruz* input with $a_{max,base}$=0.41 g

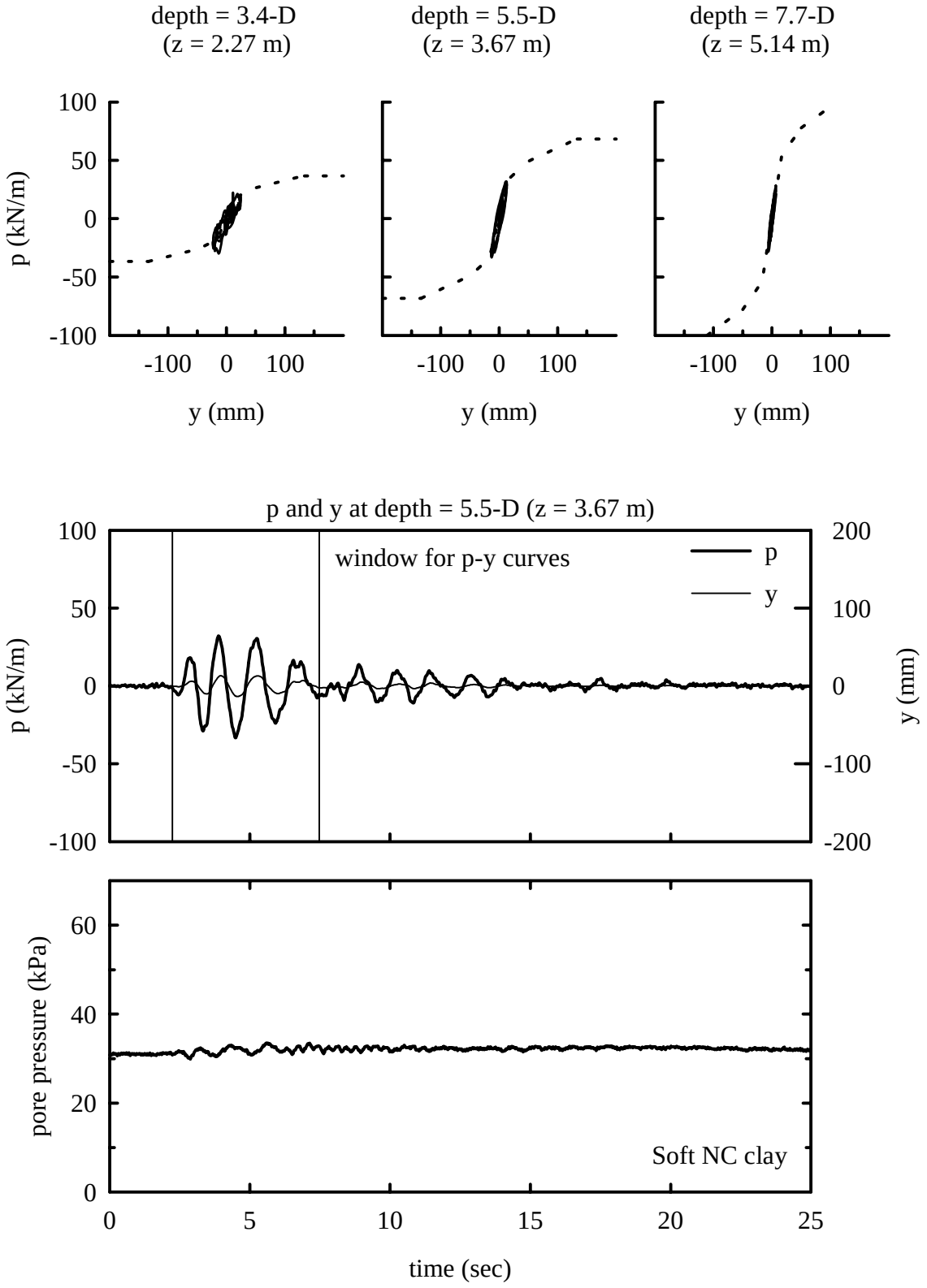

Figure 5.23: p-y behavior in test Csp4 event B
Kobe input with $a_{max,base}$=0.055 g

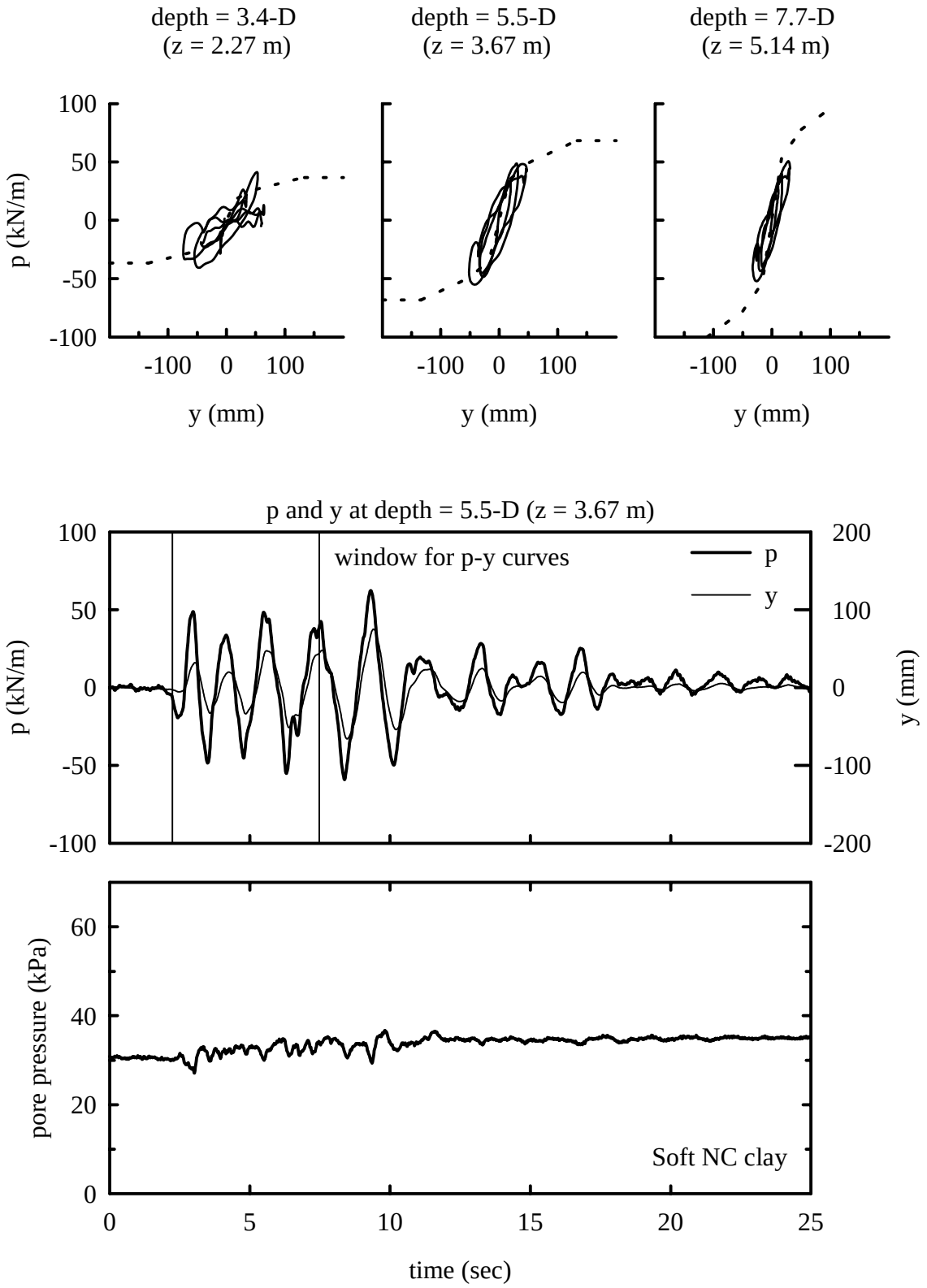

Figure 5.24: p-y behavior in test Csp4 event D
Kobe input with $a_{max,base}$=0.20 g

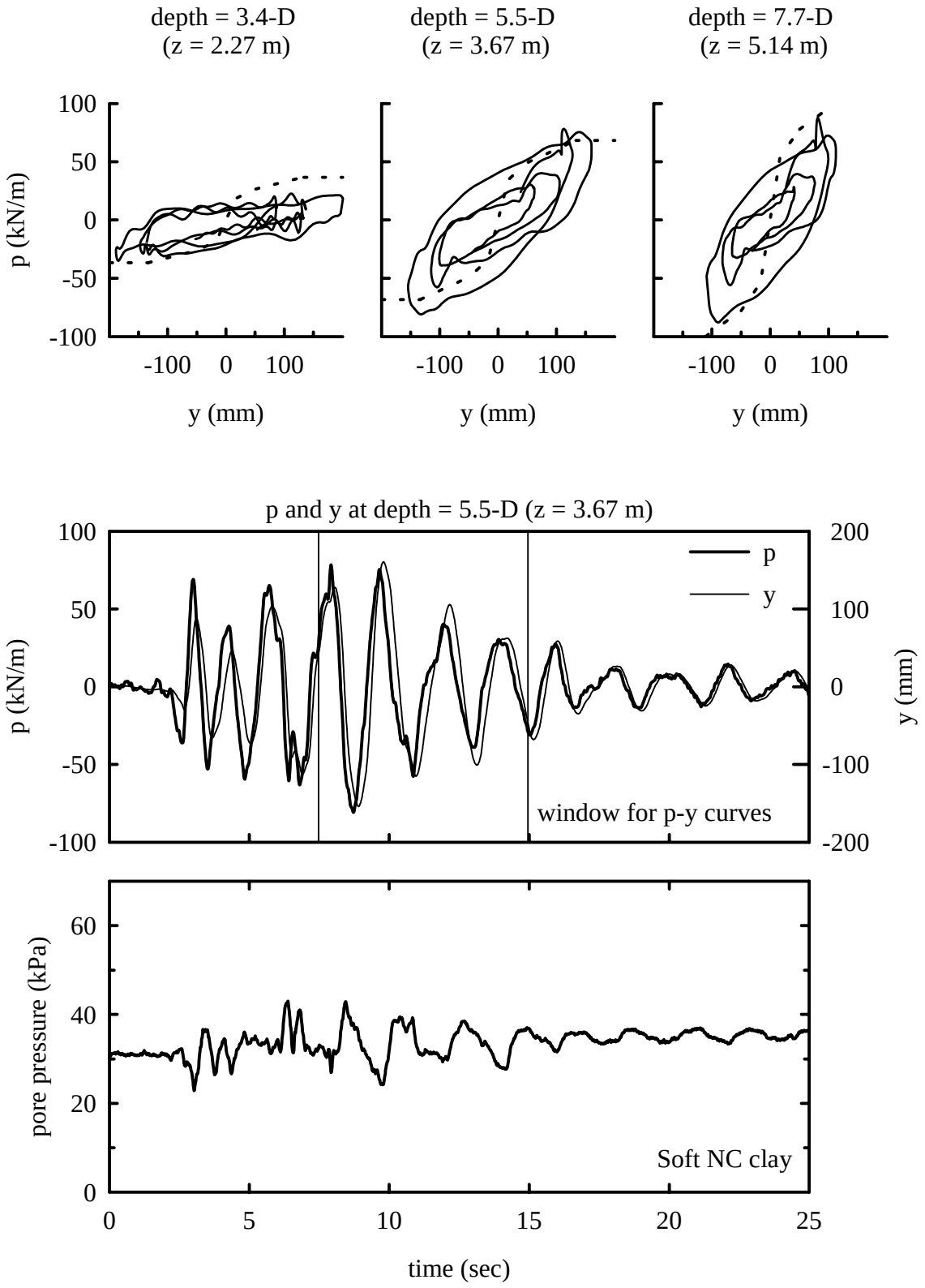

Figure 5.25: p-y behavior in test Csp4 event E
Kobe input with $a_{max,base}$=0.58 g

5.5.2 Observations in Loose Sand (Csp2)

The upper soil layer in Csp2 was loose ($D_r \approx 35\%$) and liquefied early in shaking for most events. Liquefaction did not occur under the low shaking levels of events D (Figure 5.7) and C (Figure 5.10). For event D (no liquefaction, stronger shaking than C), the p-y curves in Figure 5.7 are well below the expected p_{ult} values and show no signs of cyclic degradation or softening in time. P and y remain relatively proportional throughout shaking. After liquefaction in Csp2 (events H, F, G, E, K, and J), the back-calculated p-y results show there is very little lateral resistance on the pile (<150 kN/m) even under large relative displacements (>25 mm).

Note that the largest lateral resistances in Csp2 were calculated for event L (Kobe, $a_{max,base}$ = 0.6 g, not shown), where the strains and relative displacements were also large. The peak lateral resistances in this event reached 350 kN/m at a depth of 2.0 m. This is at least four times the maximum lateral resistance recorded at this depth in other events of Csp2. This finding is consistent with Figure 4.28, where we saw larger than expected superstructure accelerations during this event. In Chapter 4 this behavior was attributed to possible dilation of the sand layer at very high strain levels.

The importance of this event (largest superstructure acceleration, largest bending moment, and largest lateral resistance) makes it worthy of detailed investigation. Unfortunately, the accelerations in the soil profile for this event exceeded the capacity of most of the accelerometers in the vertical accelerometer array (i.e. accelerations were greater than 50 g – see Figure 4.29). For this dissertation, the data from this event could not be realistically interpreted using the baseline procedures outlined above and so they are not presented further. For example, compare the soil profile displacements calculated

for event H to those for event L, plotted in Figures 5.26 and 5.27, respectively. Displacements calculated from the three uppermost accelerometers in event L (after the obvious offsets in acceleration were removed) are large before shaking even begins. Interpretation of event L will require careful consideration of the dynamic effects of exceeding the capacity of the transducers during shaking. Future investigations could even include repeating this event with accelerometers of higher capacity (i.e. 500 g accelerometers).

5.5.3 Observations in Medium Dense Sand (Csp3)

The upper sand layer in Csp3 was medium density ($D_r \approx 55\%$) and had a greater resistance to liquefaction than in Csp2. Consequently there is more information on how the p-y behavior changed as pore pressure increased than in Csp2. The observed p-y behavior in these events is hardening; it stiffens as the relative displacement approaches or exceeds maximum past values, especially near the surface, and degrades with cyclic loading and high pore pressures.

The softening of the p-y relationship with increasing pore pressure is examined first by comparing events L (Figure 5.16, $a_{max,base}$=0.11 g) and J (Figure 5.17, $a_{max,base}$=0.22 g). Several loading cycles at similar levels of lateral resistance from each event are combined in Figure 5.28. The p-y loops from event J are significantly softer than those from event L. The average pore pressure ratio during these time frames was negligible in event L, and was approximately 40% at 4.5 m depth in event J (see Figures 5.17 and 4.16). Recall that the saturated unit weight of the sand used in these tests was very close to two times the unit weight of water, and that the water level was nearly coincident with the soil surface, so that the excess pore pressure ratio can be

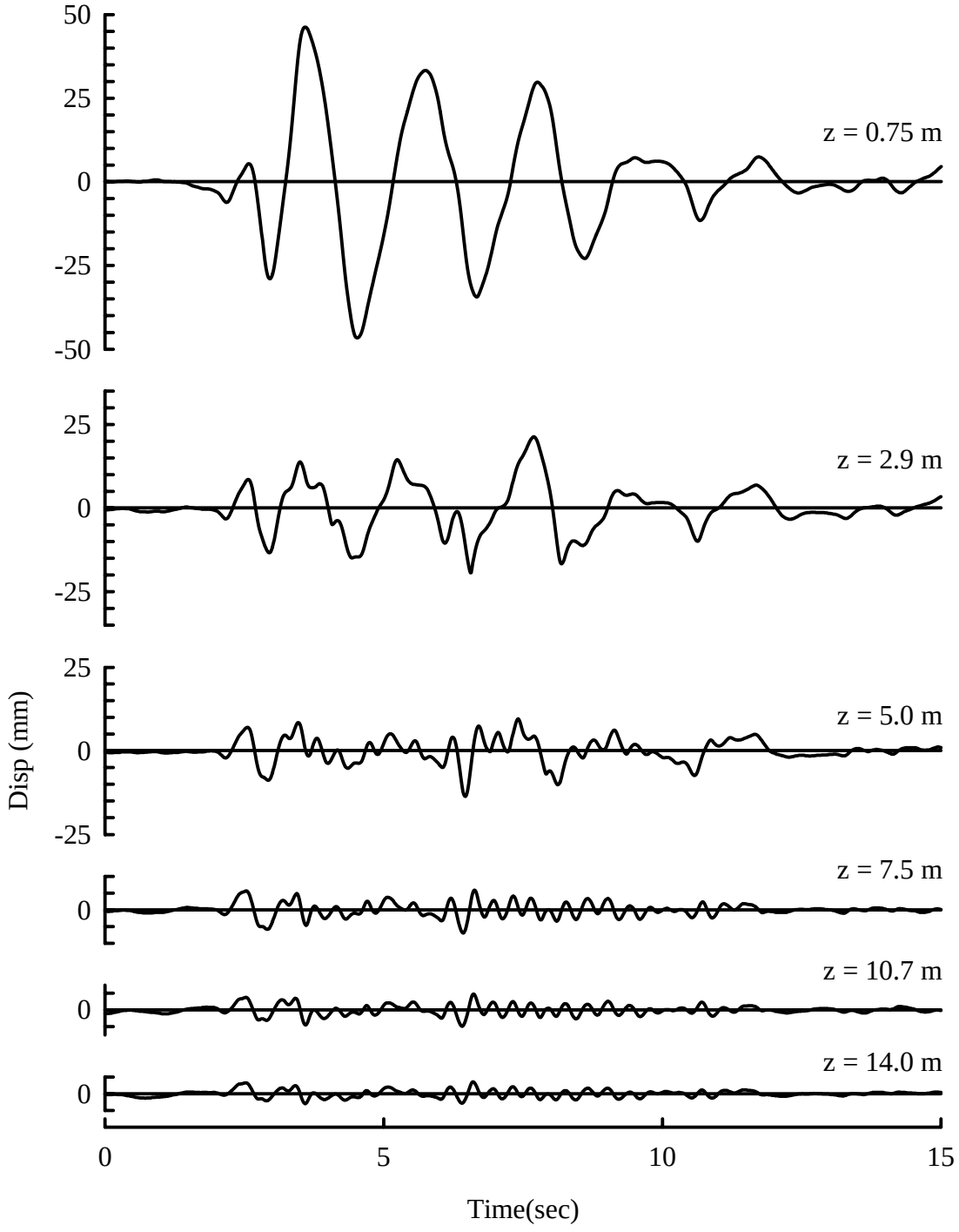

Figure 5.26: Displacements, calculated from accelerometer recordings, within the soil profile in Csp2 event H (interface between loose and dense sand at z=9.3 m)

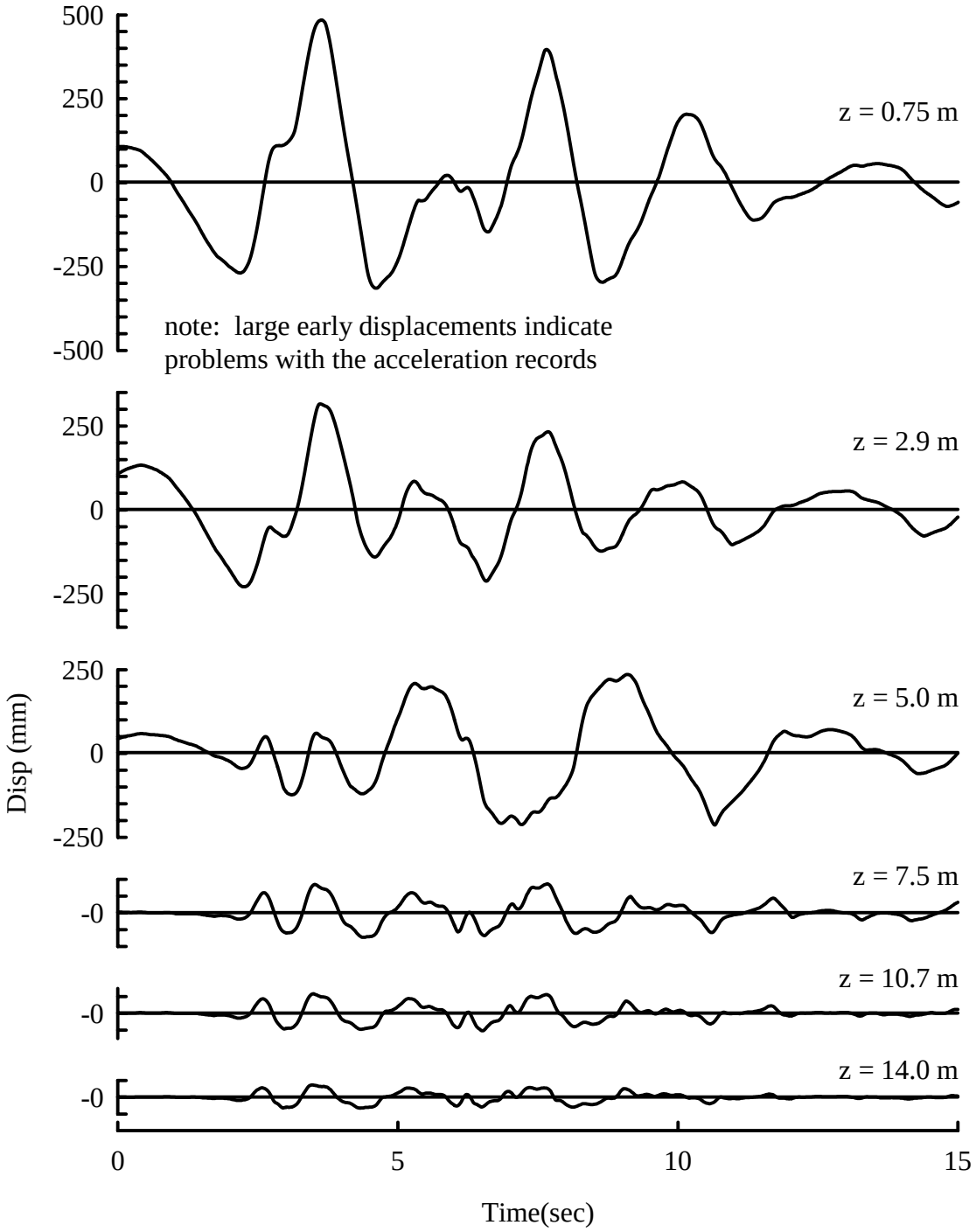

Figure 5.27: Displacements, calculated from accelerometer recordings, within the soil profile in Csp2 event L (interface between loose and dense sand at z=9.3 m)

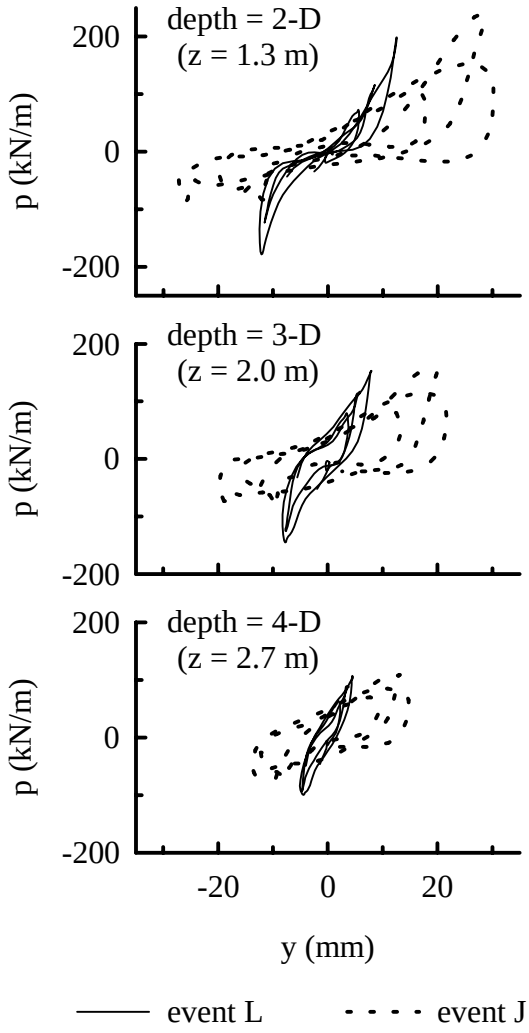

Figure 5.28: Softening of p-y during Csp3 from t ≈ 4 to t ≈ 6 seconds in events L and J

approximated as $(u-u_o)/u_o$. The effect of r_u on p-y behavior is also evident in the time histories of p and y in Figure 5.17 for event J. The peak p value occurs at about 4 seconds and only lower p values develop afterward. In contrast, several peaks of similar magnitude in the y values occur between 4 and 11 seconds. For event L, the p and y time histories in Figure 5.16 remain almost scalar multiples throughout shaking.

Similar observations are illustrated in event M (Figure 5.22, $a_{max,base}$=0.41 g), where there are four distinct time intervals with nearly constant lateral loading; (1) t=4.3

to t=7.3 where $r_u \approx 0$ at about 4.5 m depth, (2) t=11.3 to t=17.3 where $r_u \approx 20\%$, (3) t=20.7 to t=23.7 where $r_u \approx 50\%$, and (4) t=26.2 to t=29.2 where $r_u \approx 60\%$. The progressive effects of increasing r_u are seen in the time histories of p and y in Figure 5.22. Early in shaking (0-12 sec.), p and y stay almost constant scalar multiples of each other, even between 8-12 seconds when the peak y values are smaller than those earlier in shaking. Then, after 15 seconds and at higher r_u values, the y values stay large while the p values decrease. The p-y loops for the first and last time interval are plotted together in Figure 5.29. Again, the softening of lateral resistance with increasing pore pressure and number of cycles is clearly evident. Note that the softer p-y behavior exhibited late in shaking is due to both the increased pore pressure ratio, the memory of larger prior relative displacements, and possibly the number of cycles.

The p-y curves shown are consistent with the expected behavior of saturated, medium dense sand under undrained seismic loading. The observed p-y curves show a stiffening effect as relative displacement (y) increases beyond a certain limit, and the maximum lateral resistances (p) are significantly greater than expected for drained conditions at depths less than about three diameters (as per API recommendations). This behavior is consistent with the expectation that a medium dense sand, under the range of confining stresses involved, would be dilatant at large enough shear strains (i.e., large enough to move the sand through a phase transformation). The p-y curves soften as pore pressures increase, and also show a memory of past maximum relative displacement (y). The p-y curves are softest (smallest p-y slope) for deflections less than the maximum past values.

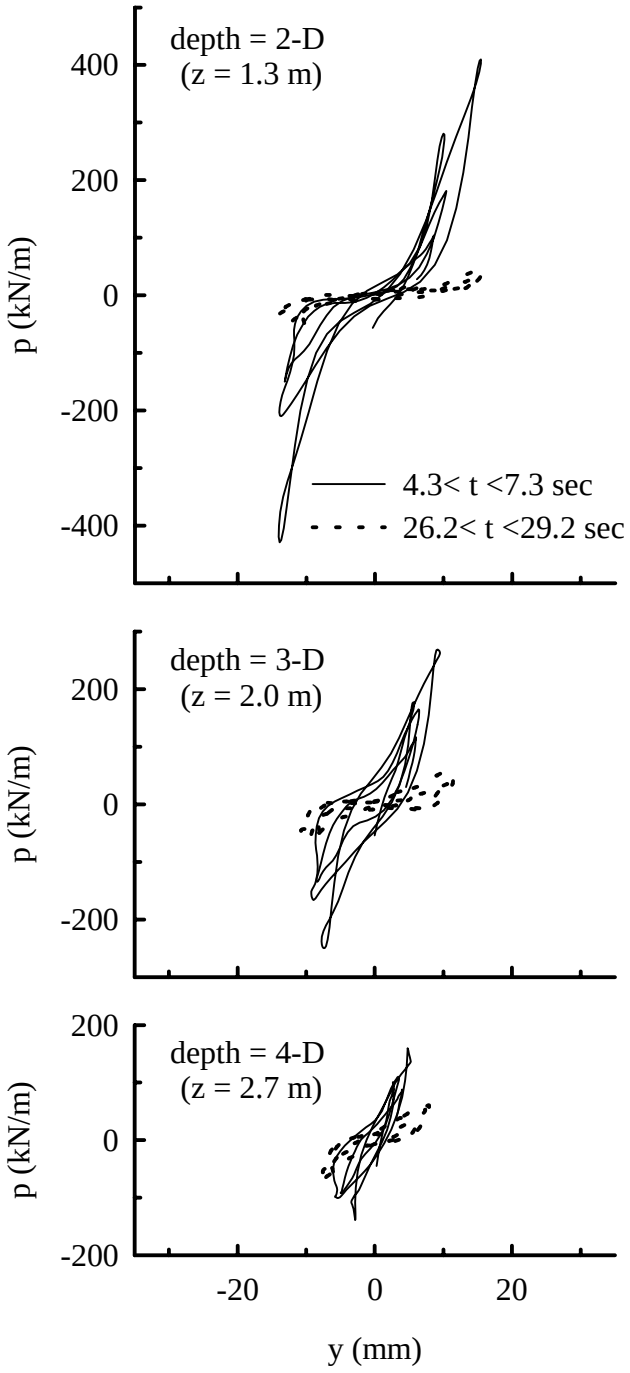

Figure 5.29: Softening of p-y during Csp3 event M

Note that the largest lateral resistances in Csp3 were calculated for event O (Kobe, $a_{max,base}$ = 0.6 g,), shown in Figure 5.18. The peak lateral resistances in this event reached 1000 kN/m at a depth of 1.3 m. This is about two times the maximum lateral resistance

recorded at this depth in other events. The pore pressure time history near the single pile in this event shows the extent of dilation that occurred early in shaking, when the lateral resistances were at their maximum. The behavior shown, while more extreme, is consistent with the behavior shown in Figure 5.17 for Csp3 event J, a smaller Kobe event (0.22 g peak base acceleration versus 0.6 g in event O).

Unfortunately, the recorded accelerations on the pilehead and superstructure were questionable (see Figure 5.30) in this event and thus provided poor boundary conditions for calculations of y_{pile}. The data could not be realistically interpreted using the baseline procedures outlined above. To generate p-y curves for this event the two truncated peaks in superstructure acceleration were augmented in proportion to the shallowest moment gauge. Superstructure displacements (calculated from the adjusted accelerations) were then used as a boundary condition on y_{pile}. In the baseline procedure the pilehead displacements (as calculated from accelerations) were used as a boundary condition. Interpretation of this event is complicated by this manipulation of the data.

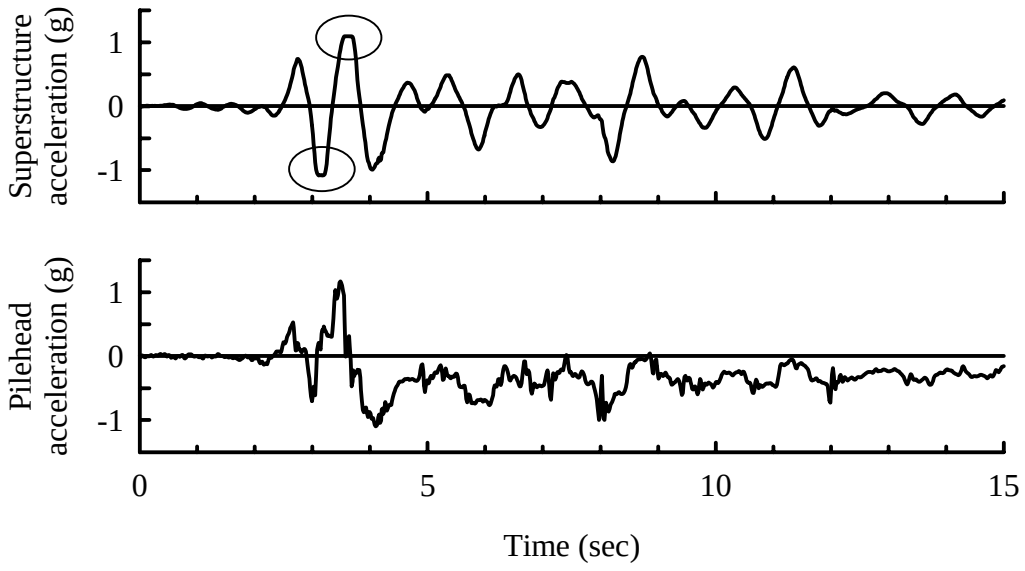

Figure 5.30: Data errors in Csp3 event O

5.5.4 Observations in Normally Consolidated Clay (Csp4)

The observed p-y behavior during the first load cycle from each event in the soft clay test was in good agreement with the curves recommended by API (1993) for static short term loading. The p-y relationship was seen to soften as the number of large strain load cycles increased. In the relatively low acceleration levels of event B (Figure 5.23) the p-y loops remain fairly closed and uniform throughout shaking. Under the stronger shaking levels of event D (Figure 5.24), the loops begin to open at a depth of 3.4-D (2.27 m). Under the very strong shaking of event E (Figure 5.25) the reduction in lateral stiffness with prior cyclic loading is evident at all depths. This is highlighted in Figure 5.31, where p-y loading cycles near the beginning and the end of this event are plotted.

5.6 CONCLUSIONS

Dynamic p-y behavior was observed by back analysis of soil accelerations, pile and superstructure accelerations, and pile bending moments. The lateral resistances were found to be relatively independent of the method used to double differentiate the pile bending moment distribution within the depth range of interest, indicating the sampled data uniquely represented the bending moment distribution.

The back-calculated p-y curves show characteristics that are consistent with the stress-strain response of liquefied sand. The p-y resistance of the $D_r \approx 35\%$ upper sand layer in Container 2 is much smaller and softer than for the $D_r \approx 55\%$ upper sand layer in Container 3. This observation is consistent with effects of D_r on the undrained shear

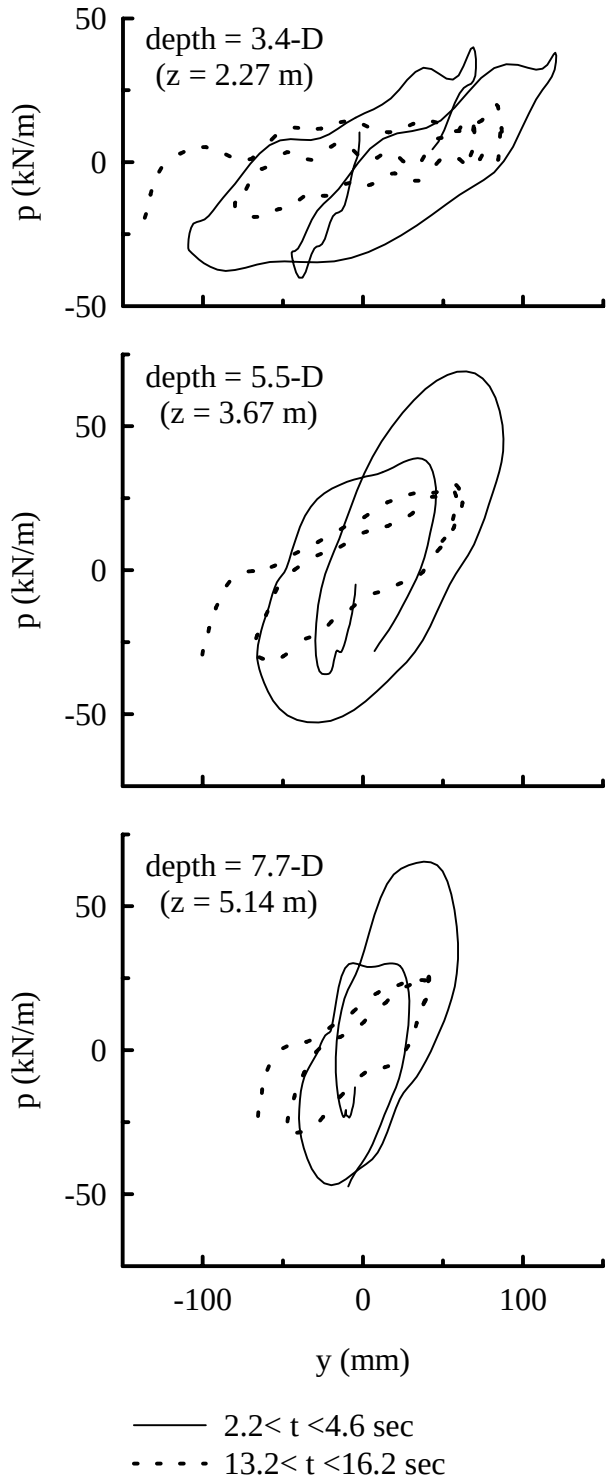

Figure 5.31: Softening of p-y during Csp4 event E

resistance (or cyclic mobility) of saturated sand, as shown for example in undrained cyclic triaxial tests.

The p-y curves for the $D_r \approx 55\%$ sand show: (1) a stiffening effect as relative displacement (y) increases beyond a certain limit, and (2) maximum lateral resistances that can be significantly greater than expected for drained conditions (as calculated using API recommendations) at depths less than about 3 diameters. This behavior for the $D_r \approx 55\%$ sand is consistent with the expectation that a medium dense sand, under the range of confining stresses involved, would be dilatant at large enough shear strains (i.e., large enough to move the sand through a phase transformation). The observed behavior is consistent with results reported by Dou and Byrne (1996) and by Kagawa et at. (1994). For example, see Figure 5.32, from Dou and Byrne (1996).

The back-calculated p-y curves show a memory of past maximum relative displacements (y), and are softest (smallest p-y slope) for deflections less than the maximum past values. The p-y curves are shown to progressively soften with time during the earthquake event (as shown by loops for early in the earthquake shaking versus late in the earthquake shaking). Clearly, the shape and magnitude of the p-y curves for these liquefied sands are not well represented by any scalar multiple of the API p-y curves for drained loading in sand, commonly used in practice.

Back-calculated p-y curves in clay were compared to monotonic p-y curves calculated by Matlock's (1970) procedure (API recommended design curves). The back-calculated p-y curves showed maximum lateral pressures (p_{ult}) that were reasonably consistent with values calculated by Matlock's procedure. As expected, the hysteresis loops showed progressive softening with increasing displacement and number of loading

cycles (as shown by the loops for early in the earthquake shaking versus late in the earthquake shaking). The reasonableness of the results for soft clay provides a measure of confidence in the application of these back-calculation procedures to centrifuge test data.

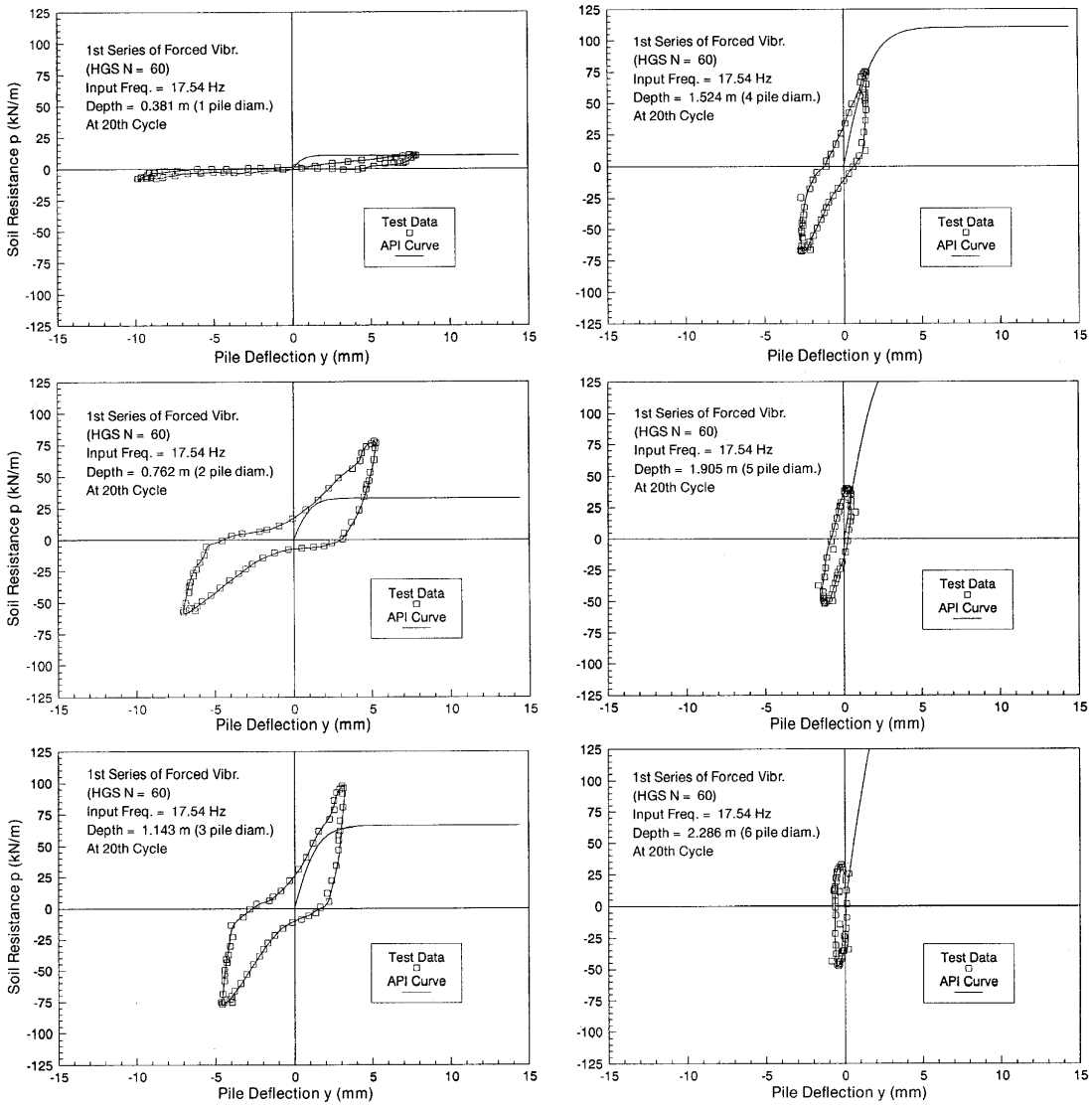

Figure 5.32: Experimental p-y curves reported by Dou and Byrne (1996)

CHAPTER SIX

Pseudo-Static Analyses of Single Pile Systems

6.1 INTRODUCTION

Pseudo-static p-y analyses of the highly instrumented single pile system (see Figure 3.7) were performed in select events using the program PAR (PMB 1988). The program is one of several programs that were used in the study by Wang et al. (1998) to perform dynamic soil-pile-superstructure interaction analyses based on the "Beam on Nonlinear Winkler Foundation (BNWF)" model (Figure 2-1). In the BNWF model, the soil-pile interaction is modeled using nonlinear p-y springs and dashpots. In a dynamic analysis, the free-field ground motions are input to the numeric model at the ends of the p-y springs. In a pseudo-static analysis, such as presented here, a lateral force is applied to the structure (representing the inertial load) and soil deformations at the snapshot are applied to the ends of the p-y springs. The use of pseudo-static p-y analyses for pile foundations was reviewed in Section 2.3.

6.2 PROCEDURE

The pseudo-static p-y analyses presented herein were performed at a snapshot in time, with the time closely corresponding to a peak inertial load (peak superstructure

acceleration). Baseline sets of p-y springs were established for each test using recommended API curves (American Petroleum Institute 1993) for static loading - see Table 5.2 for property values used in these analyses. The baseline curves provide a fixed reference and are not implied to be necessarily correct for dynamic loading due to rate effects, undrained loading, effects of dynamic pore pressures, etc. A comparison of the recommended curves versus the measured p-y curves presented in Chapter 5 shows that differences might be expected (e.g. Figure 5.22).

In an analysis, the inertial loads and free-field displacements were applied to the numerical model (dashpot forces were zero), and the calculated bending moment distribution and pile deformed shapes were compared to recorded values. The analysis was repeated with different scalar multiples of the baseline p-y springs (scalar multiplier applied to the p values) in the upper soil layer until a reasonable match between calculated and measured responses was obtained. Free-field displacements relative to the model base were calculated by double-integrating the acceleration time-histories in the soil profile as described in Section 3.3. Inertial loads were calculated directly from the recorded superstructure accelerations.

The highly instrumented single pile was analyzed for select events in tests Csp2 and Csp3 (tests involving liquefying sand), where a direct comparison between the recommended and measured p-y curves could be made. Note the highly instrumented pile was not tested in Csp1. Also, as was noted in Chapter 5, the back-calculated dynamic p-y curves were consistent with the recommended p-y curves in the test with clay (Csp4), so it is expected that analyses using the recommended curves would be consistent with the measured results and thus are not presented here.

Finally, it should be noted that measured inertial loads and soil profile deformations (both based on accelerometer records) were available as known inputs for these analyses. In a design situation, the estimation of inertial loads would require that the effects of liquefaction on the dynamic response of the soil-pile-structure system be accounted for, and the estimation of soil deformations would require a site response analysis and an accurate accounting of possible lateral spreading. These are challenging tasks given continuing questions regarding the reliability in quantifying lateral spreading, site response, and soil-pile-structure interaction in liquefying soils.

6.3 PRESENTATION OF ANALYSES

The analyses presented in this chapter are summarized in Table 6.1. In the table, the sample and event, time of snapshot, input motion type and magnitude, superstructure inertial load, and pore pressure at the snapshot are listed. Note the pore pressure listed is a snapshot value taken from the free-field pore pressure transducer at depths of 3.8 m in Csp2 and 4.6 m in Csp3. The pore pressure distribution was not uniform with depth, nor was it constant in time. For example, in Csp3 event J at 11.17 seconds (snapshot 3 J-c), the pore pressure ranged from 58% at 6.8 m to 86% at 1.2 m depth, while in Csp3 event M at 19.44 seconds (snapshot 3 M-c) the pore pressure ranged from 37% at 6.8 m to 74% at 1.2 m depth. Also in Csp3 event M, but at 19.32 seconds, the pore pressure ratios ranged from 50% at 6.8 m, 73% at 4.6 m, to 64% at 1.2 m depths.

For each shaking event analyzed, back-calculated p-y curves (using procedures outlined in Chapter 5) for individual loading cycles are presented with a bullet indicating

the time of the snapshot analysis. The recommended baseline API curve is also included for reference. See for example Figure 6.1. One to three snapshot analyses are presented for each event. Following the loading cycles, the results of the snapshot analyses are presented as pile deformed shape and pile bending moment distribution. See for example Figure 6.2. Recall that typical time histories of the various recorded responses (e.g. accelerations, bending moments, pore pressures) were shown for some of these events in Chapter 4. Time histories of all recorded responses are included in Wilson et al. [1997 (a-e)], and are not presented herein for purposes of brevity.

Table 6.1: Events Presented in Figures 6.1 - 6.20

Snapshot (event - #)	Snapshot (seconds)	Motion	$a_{max,base}$ (g)	Inertial Load (kN)	r_u** (%)
Csp2 D	3.02	Kobe	0.04	37	0
Csp2 H-a	5.99	Kobe	0.10	38	85
Csp2 H-b	8.35			57	85
Csp3 E	8.47	Kobe	0.04	30	2
Csp3 L-a	3.84	Kobe	0.11	243	20
Csp3 L-b	5.61			120	24
Csp3 J-a	3.59	Kobe	0.22	383	11
Csp3 J-b	6.56			140	64
Csp3 J-c	11.17			113	82
Csp3 M-a	5.31	Santa Cruz*	0.41	333	4
Csp3 M-b	16.52			367	42
Csp3 M-c	19.44			59	44

* The time step of the original Santa Cruz motion was doubled for this event

** r_u is a snapshot value from a depth of 3.8 m in Csp2 and 4.6 m in Csp3. Compare to time histories presented in Chapter 4.

6.4 RELATIVELY LINEAR BEHAVIOR IN SAND

Analyses are presented for a small shaking event (event D) in Csp2 (loose upper sand layer, $D_r \approx 35\%$) and a small shaking event (event E) in Csp3 (medium dense upper sand layer, $D_r \approx 55\%$). These low level shaking events resulted in little excess pore water

pressure generation, and thus help form a baseline for comparison to larger, nonlinear snapshots. In Csp2 D (Figure 6.1) and Csp3 E (Figure 6.6) the back-calculated p-y resistance of the soil was nearly linear. Good agreements between the recorded and calculated moment distributions and pile displacements were achieved using one to two times the recommended API curves in each case [see Figures 6.2(b) and 6.7(b)]. Note that in Csp2 the sand was loose ($D_r \approx 35\%$), while in Csp3 the sand was medium ($D_r \approx 55\%$) so different baseline curves were called for (see Table 5.2 for parameters used). Doubling the p-y resistance (i.e., factor of two on p values) did not significantly affect maximum calculated moments, and had only a slight effect on the moment distribution and pile displacements, as shown in Figures 6.2(a) and 6.7(a). From these figures it is clear the pile was responding in its first mode, and the free field soil displacements were small relative to the pile deformations. Thus we would expect kinematic forces to be minimal.

6.5 BEHAVIOR IN LOOSE, LIQUEFYING SAND

The behavior in loose, liquefying sand ($r_u \approx 85\%$) is illustrated by the results of two snapshot analyses of Csp2 event H, shown in Figures 6.3 through 6.5. Both snapshots are taken after the upper loose sand layer ($D_r \approx 35\%$) reached $r_u \approx 85\%$. Inertial loads at the superstructure in these two snapshots were of the same magnitude, 37 kN in snapshot H-a, 57 kN in snapshot H-b. The difference in these two snapshots is that the soil profile displacements and pile displacements are out of phase in H-a and in phase in H-b [see Figure 6.4(a) and 6.5(a)]. In both cases, using a p-multiplier of about 0.10 on the static baseline p-y curves gave reasonable agreement with the recorded behavior.

But interestingly, in snapshot H-a, using the API x 1.0 curves produced a poor approximation, while in snapshot H-b API x 1.0 curves gave a similar result to the API / 10 p-y curves. Clearly, the most significant difference in these two cases is the kinematic loading, as can be seen by comparing the deformed pile shape to the deformed shape of the soil profile. Results for H-b were insensitive to the p-y multiplier because of compensating effects on the calculated responses to the kinematic and inertial loading components. It follows that snapshot H-a provides a more sensitive and hence reliable evaluation of an appropriate p-y scaling factor.

6.6 BEHAVIOR IN MEDIUM DENSE SAND

A series of results are presented for Csp3, where the upper soil layer was medium dense sand ($D_r \approx 55\%$), as summarized in Table 6.1. Two snapshots are presented for event L (L-a and L-b, Figures 6.8-6.10), which resulted in peak r_u values less than about 25% at about 4.5 m depth. Three snapshots are presented for event J (J-a, J-b, and J-c, Figures 6.11-6.15), with r_u values increasing up to 82% at about 4.5 m depth. Three snapshots are also presented for event M (M-a, M-b, and M-c, Figures 6.16-6.20), with r_u values increasing up to 44% at 4.5 m depth. The various snapshots are used to illustrate the effects of inertial loading level, r_u level, displacement history, and kinematic loading on the lateral resistance of medium dense sand.

6.6.1 Large Lateral Loads with Low Pore Pressures

Analyses for Csp3 event L-a, event J-a, event M-a, and event M-b all correspond to relatively small excess pore pressure ratios (peak values of 20%, 11%, 4%, and 42%,

respectively). In addition, these four snapshots are for relatively high inertial loads before significant pore pressure generation, and the relative soil-pile displacements are the maximum values experienced up to the snapshot (see Figures 5.16, 5.17, and 5.22). The pseudo-static results for all four snapshots reasonably match the recorded data with p-multipliers of about two (or as high as three for M-a). A p-multiplier of about two is consistent with the comparisons of baseline API curves with the back-calculated p-y behaviors in Chapter 5. The back-calculated p-y behaviors show much higher lateral resistances at shallow depth (see Figures 6.8, 6.11, and 6.16). These analyses and the back-calculated p-y curves also show that a good match of the actual shape of the p-y resistance is not required for a good match to the recorded bending moment distribution and pile deformed shapes.

6.6.2 Effect of Load/Displacement History

Analyses for Csp3 event L-b and event M-c also correspond to relatively small excess pore pressure ratios (24% and 44%, respectively), but are for load cycles that have been preceded by other larger loading cycles. By comparing points Csp3 event L-b to Csp3 event L-a, and Csp3 event M-c to Csp3 event M-b, we can see the effect of stress/strain history on p-y resistance. In these cases, the excess pore pressure ratio is about constant between the snapshots (see figures 6.8, 6.16, 5.16, and 5.22, for example).

In Csp3 event L-b, the pseudo-static analysis matches with a p-multiplier of only 0.25 to 0.33 of the baseline API curves, whereas in Csp3 event L-a the match was at two times the baseline API curves. The inertial load for L-b is about 50% of the load at L-a, but the relative displacements are comparable. Thus the soil-pile system appears to be on the order of 15-25% as stiff/strong at L-b as it was at L-a, with virtually no increase in

pore water pressure. Note that L-b and L-a are about 1.8 seconds apart, and that one other peak loading cycle of similar displacement magnitude occurred between them.

In Csp3 event M-c, the best match is obtained using a p-multiplier of about 0.10, while the p-multiplier was two for Csp3 event M-b. The excess pore pressure again is nearly constant between the points. The inertial load at M-c, however, was only 16% of the inertial load at M-b, and the entire loading cycle shown for M-b was within the maximum past values of p and y (see Figure 6.16). These results are consistent with the back-calculated shapes of the p-y curves showing that prior p-y history has a significant effect on the lateral resistance of medium dense sand, even with only moderate excess r_u.

6.6.3 Effect of Load/Displacement History and Excess Pore Water Pressure

Following the three snapshots from Csp3 event J (Figures 6.11 through 6.15), we can track the combined effect of loading history and pore pressure increase. Each point in the progression represents approximately the same level of induced displacement (y), but decreasing levels of inertial load and increasing levels of pore pressure (r_u of about 11%, 64%, and 82%, respectively - see Figure 5.17). In a system that initially was relatively stiff (match at 3 times the baseline API curves in Csp3 event J-a), as the earthquake progresses the interaction becomes softer, with the recorded behaviors matched with p-multipliers of 0.50 and 0.25 at J-b and J-c, respectively. Thus, the effective stiffness of the soil-pile resistance late in shaking (J-c) was only about 10% of the stiffness early in shaking (J-a). This decrease in stiffness is attributable to the combined effects of stress/strain history and excess r_u.

6.6.4 Effect of Kinematic Loading

Snapshots Csp3 event J-b and Csp3 event M-c were chosen to examine the relative roles of kinematic and inertial loading, as in each case the soil profile and pile displacements were approximately 180° out of phase. Excess r_u was about 64% in J-b and 44% in M-c, and both snapshots were preceded by larger loading cycles in their respective events. The results of the analyses are shown in Figures 6.14 and 6.20. In each case, the behavior calculated using the best p-multiplier is included with both loading conditions imposed, along with results when only the superstructure inertia was imposed on the model and when only the kinematic soil displacements were imposed on the model. The kinematic loading is shown to have had its greatest influence at depths greater than 6 m (9 pile diameters), while the inertial loads dominated the moment distribution at shallower depths.

In the cases studied herein the kinematic loading was typically small compared to the inertial loads. It is noted, however, that this is likely due to the geometry and site characteristics of the models tested. There is not enough information in the data presented herein to determine whether a simple p-multiplier can account for pure kinematic loads on the foundation (e.g., lateral spreading).

6.7 CONCLUSIONS

In cases where kinematic forces are low (e.g. absence of lateral spreading or certain soil stratigraphies), the calculation of moment distribution and maximum bending moment within the pile foundation based on known (or estimated) pseudo-static structural

inertia loads is not highly sensitive to the selection of p-y curves, and a reasonable factor to account for dynamic loading or for the effects of liquefaction may be applied to the static p-y curves to calculate moment demand on the foundation. Liu and Dobry (1995) found that the appropriate scaling factor decreased more or less linearly with r_u, and reached a minimum value of about 0.1 when r_u=100%. Liu and Dobry based their conclusions on centrifuge tests for a sand at $D_r \approx 60\%$ and quasi-static cyclic displacement loading of a pile after the sand was liquefied and shaking had stopped. The displacements imposed were a constant magnitude of Δ_{head}/Diameter = 2 in/15 in at a frequency of 0.025 Hz. Using the data from the tests presented herein, an appropriate p-multiplier for peak loads during an earthquake in a pseudo-static analysis in liquefying sand would be 0.25-0.35 for $D_r \approx 55\%$, and 0.10 for $D_r \approx 35\%$. This difference in results may simply reflect differences in loading conditions, displacement levels, displacement histories, loading rates, pore pressure levels, or other factors not yet understood. For example, the experiment by Tokida et al. (1992) showed the lateral resistance of liquefied sand to increase with increasing strain rate. The loading cycles of the experiments presented herein were about forty times faster than Liu and Dobry's experiment, so we could expect some variation due to strain rate effects. I.e., perhaps their tests involved more drainage during p-y loading.

The success shown using scaled static p-y curves in pseudo-static analyses does not imply that these same curves could be used to predict the superstructure dynamic response. The back-calculated p-y curves for liquefied sand (see Chapter 5) clearly demonstrate that the use of an apparent p-y scaling factor for liquefied sand is a simplistic approximation to a complex phenomenon, and that more research is needed to evaluate

whether this concept can be reliably applied in design or used in dynamic soil-pile-superstructure interaction analyses.

Finally, it is not necessarily conservative to assume an overly soft p-y resistance for liquefied soils for evaluating their performance. A comparison of responses for the single pile supported structures in Csp2 ($D_r \approx 35\%$) and Csp3 ($D_r \approx 55\%$) showed that maximum bending moments and structural displacements were larger in Csp3 than in Csp2 for similar input base motions (e.g. see Figures 4.25 and 4.26). The stronger response of Csp3 can be attributed to the upper sand layer being more resistant to liquefaction and maintaining greater lateral resistance even after liquefying. This resulted in stronger free-field soil motions, and a shorter structural period in Csp3 than in Csp2, and thus higher superstructure accelerations under the earthquake motions input to these models. These observations are consistent with theoretical expectations and illustrate that assumptions of soft lateral resistances are not necessarily conservative in seismic design.

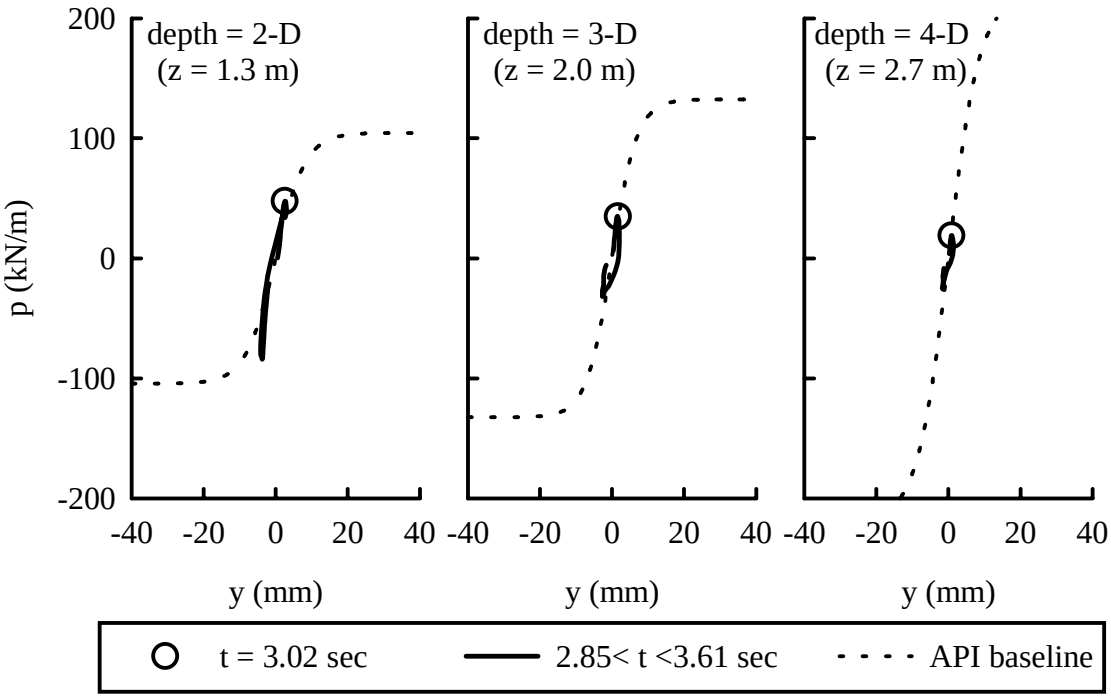

Figure 6.1: Lateral resistance in Csp2 event D
loose sand (Dr ≈ 35%), base motion Kobe, $a_{max,base}$=0.04 g

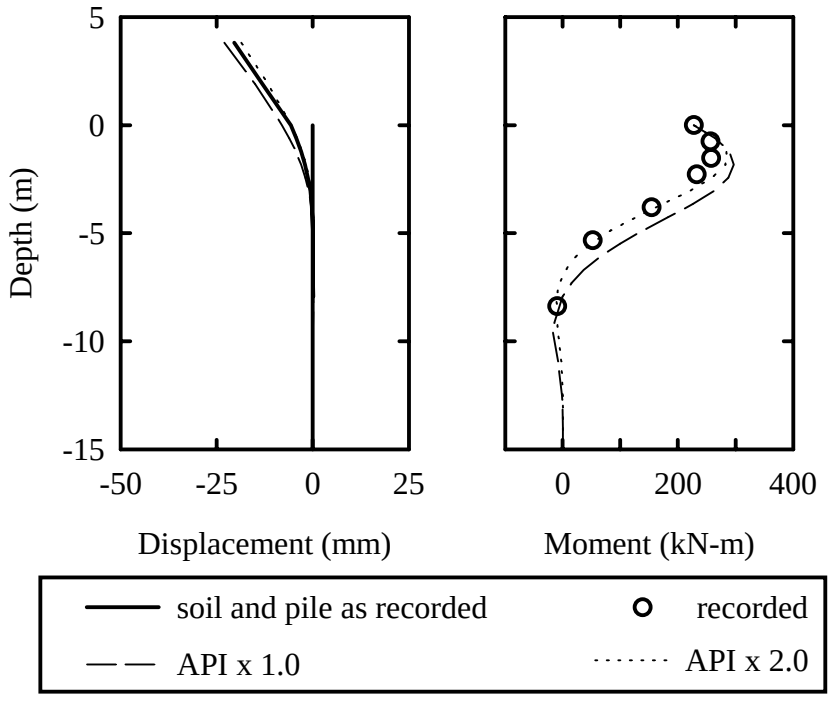

Figure 6.2: Calculated versus measured response for snapshot Csp2 D

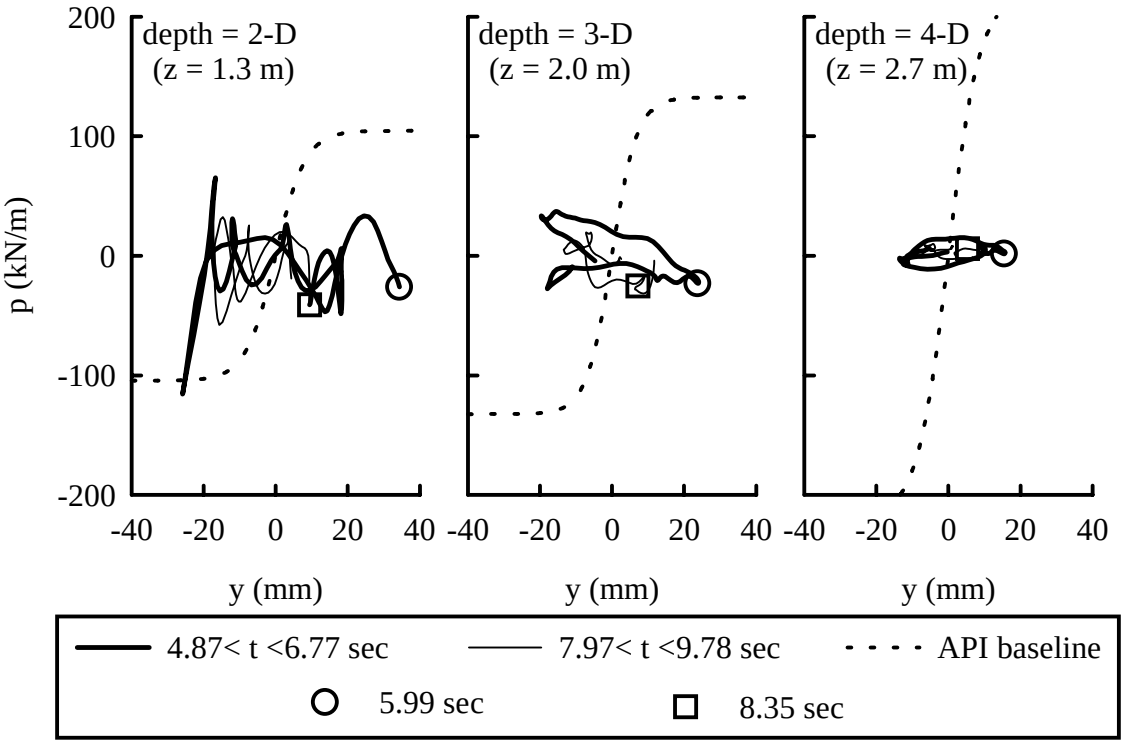

Figure 6.3: Lateral resistance in Csp2 event H
loose sand (Dr ≈ 35%), base motion Kobe, $a_{max,base}$=0.10 g

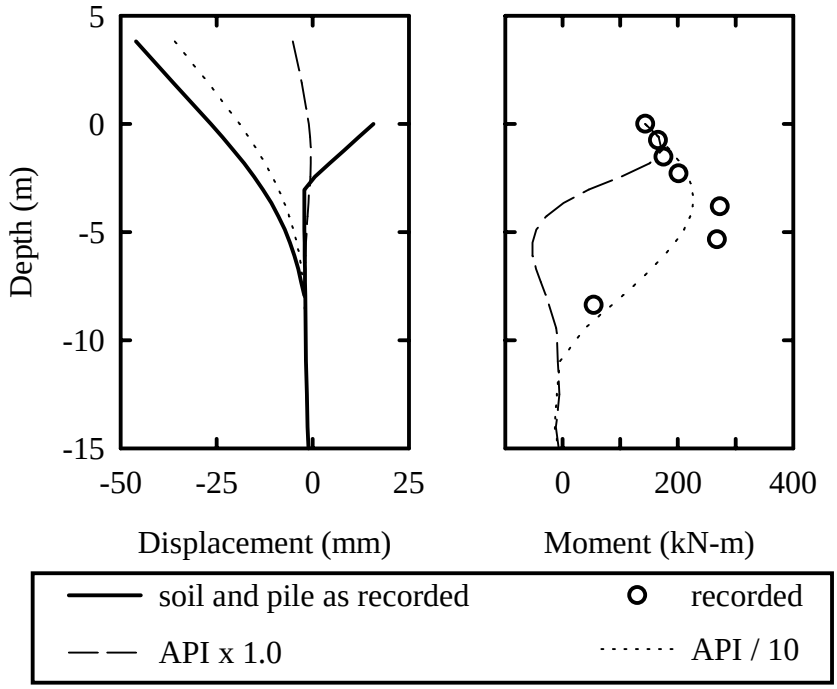

Figure 6.4: Calculated versus measured response for snapshot Csp2 H-a

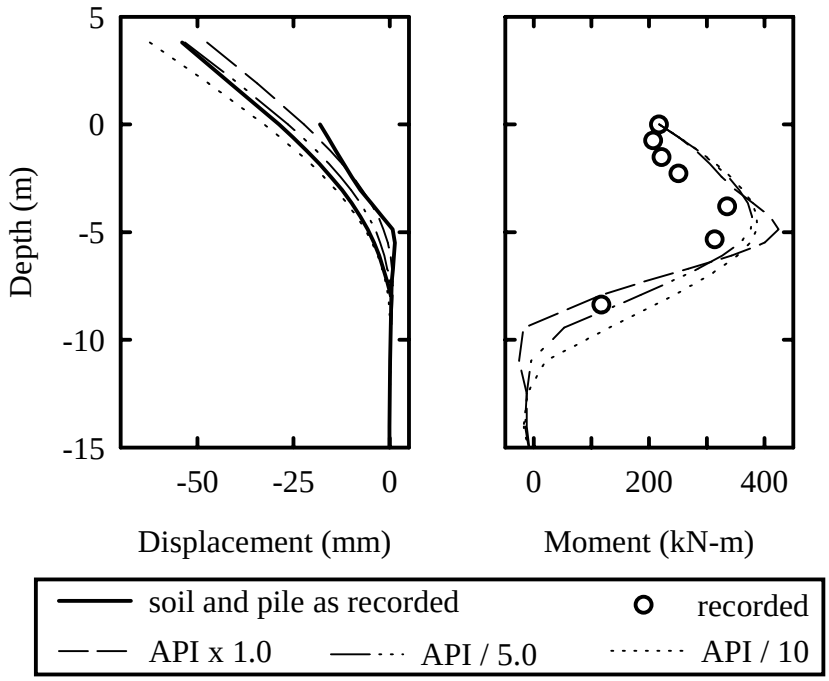

Figure 6.5: Calculated versus measured response for snapshot Csp2 H-b

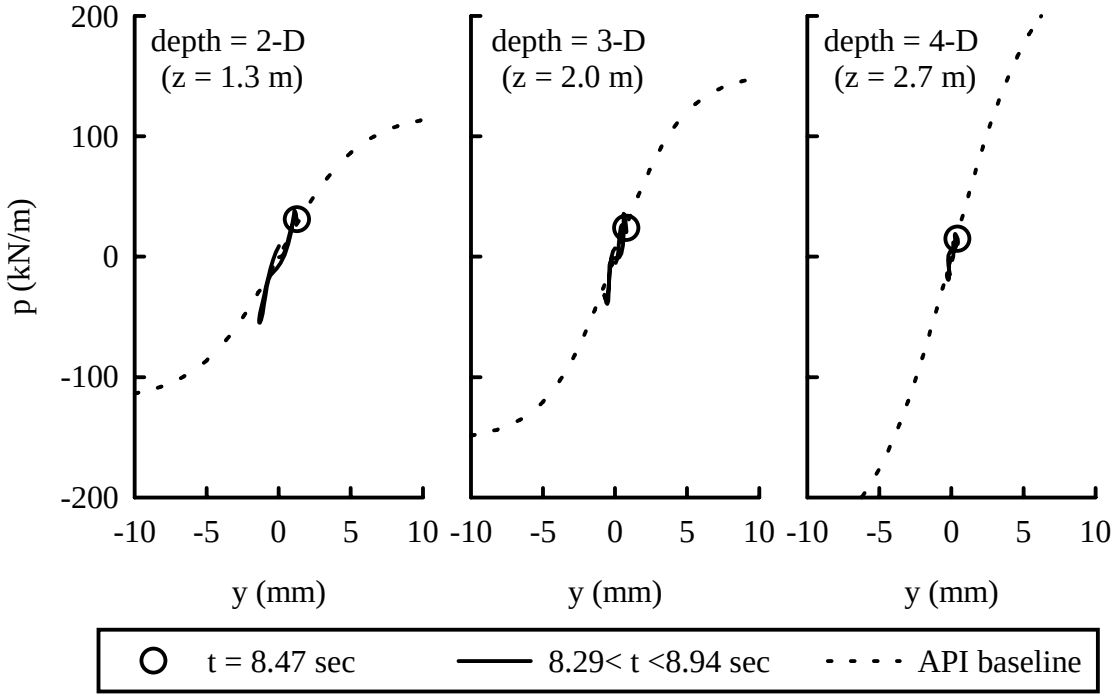

Figure 6.6: Lateral resistance in Csp3 event E
loose sand (Dr ≈ 55%), base motion Kobe, $a_{max,base}$=0.04 g

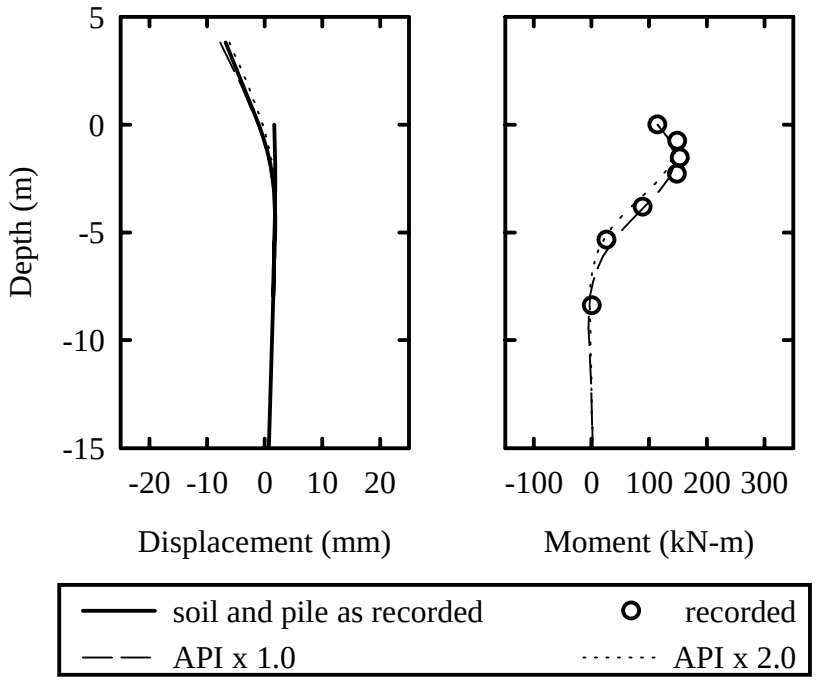

Figure 6.7: Calculated versus measured response for snapshot Csp3 E

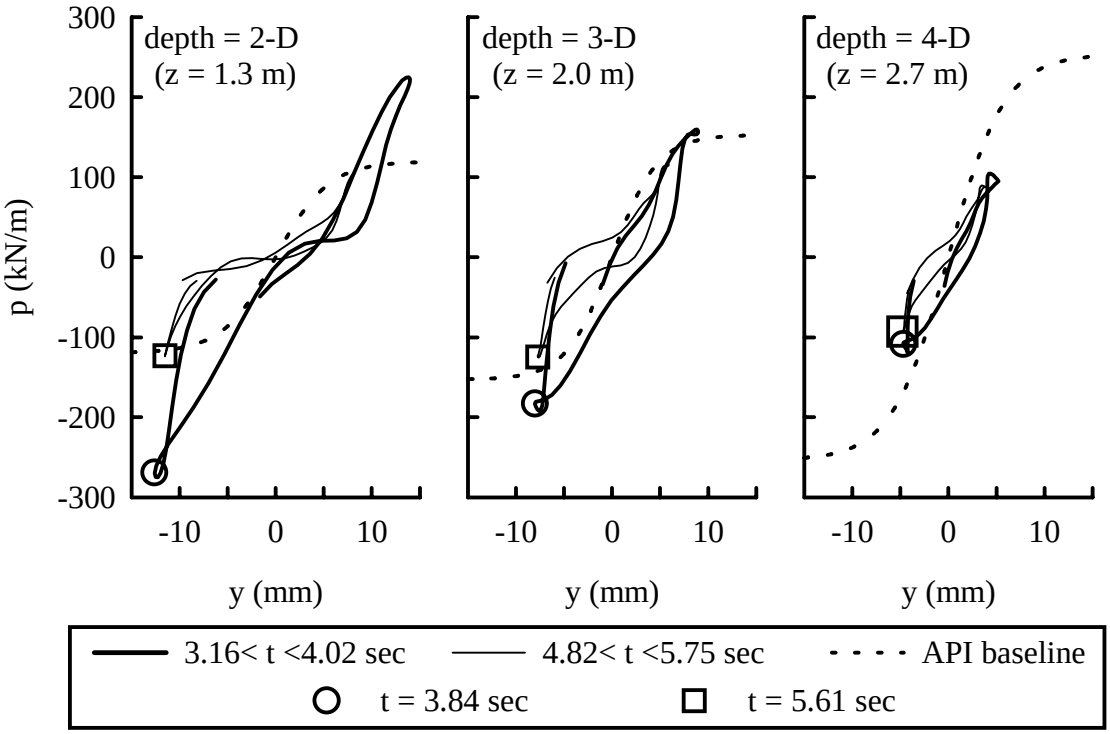

Figure 6.8: Lateral resistance in Csp3 event L
loose sand (Dr ≈ 55%), base motion Kobe, $a_{max,base}$=0.11 g

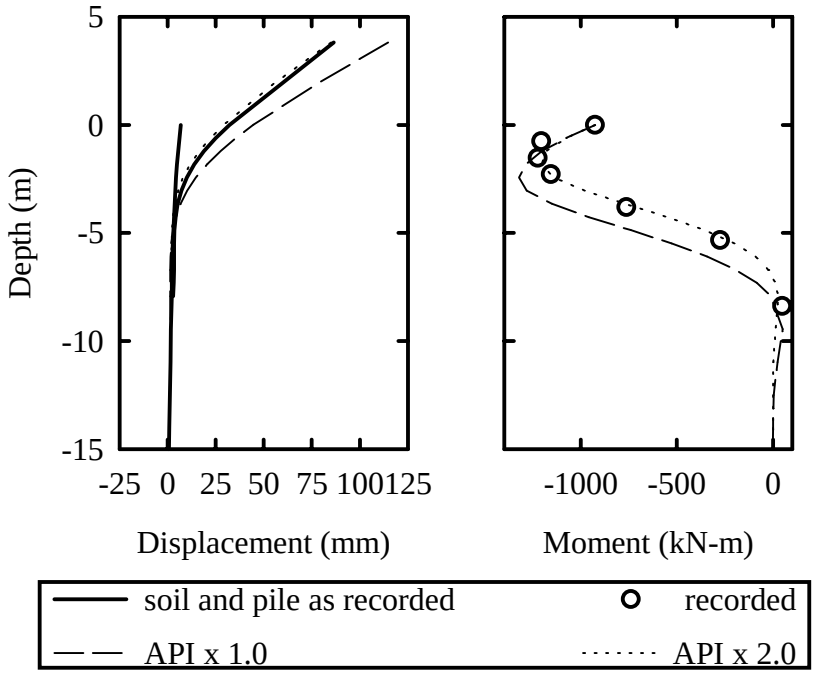

Figure 6.9: Calculated versus measured response for snapshot Csp3 L-a

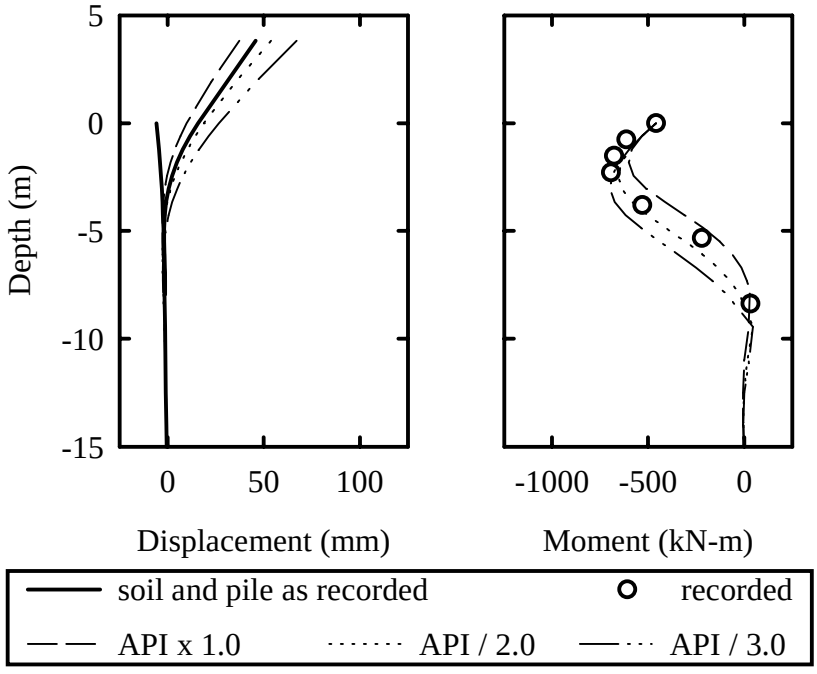

Figure 6.10: Calculated versus measured response for snapshot Csp3 L-b

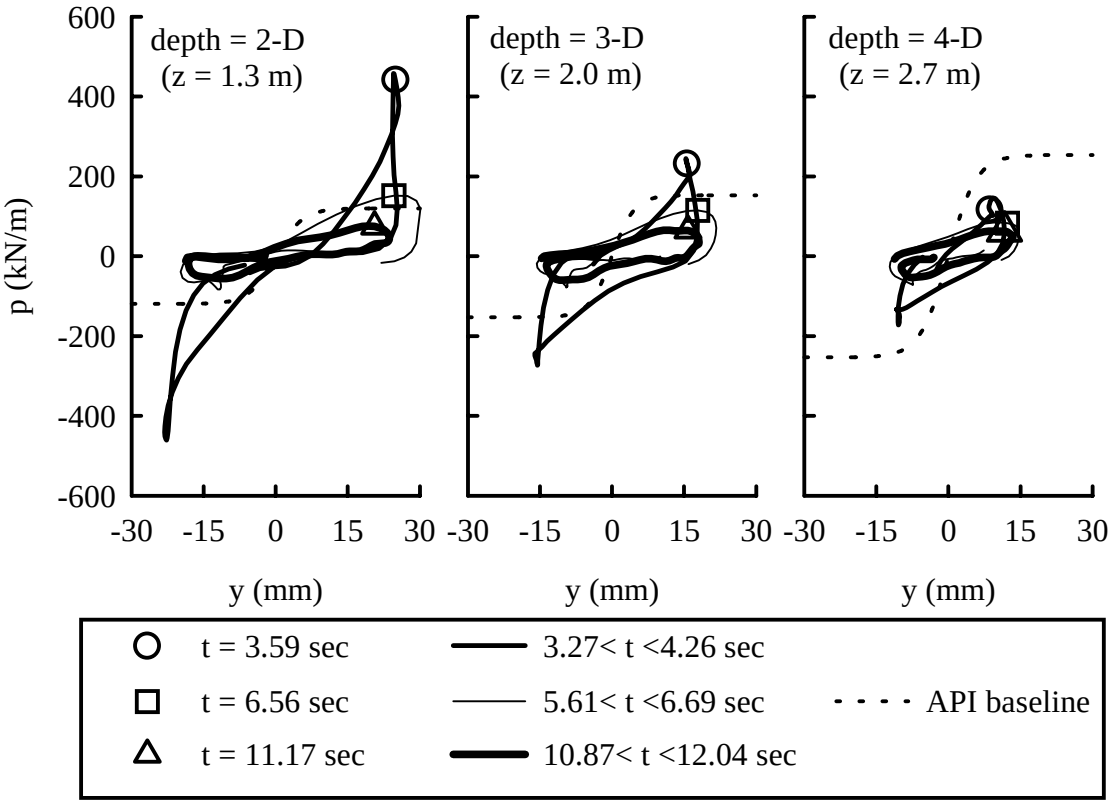

Figure 6.11: Lateral resistance in Csp3 event J
loose sand (Dr ≈ 55%), base motion Kobe, $a_{max,base}$=0.22 g

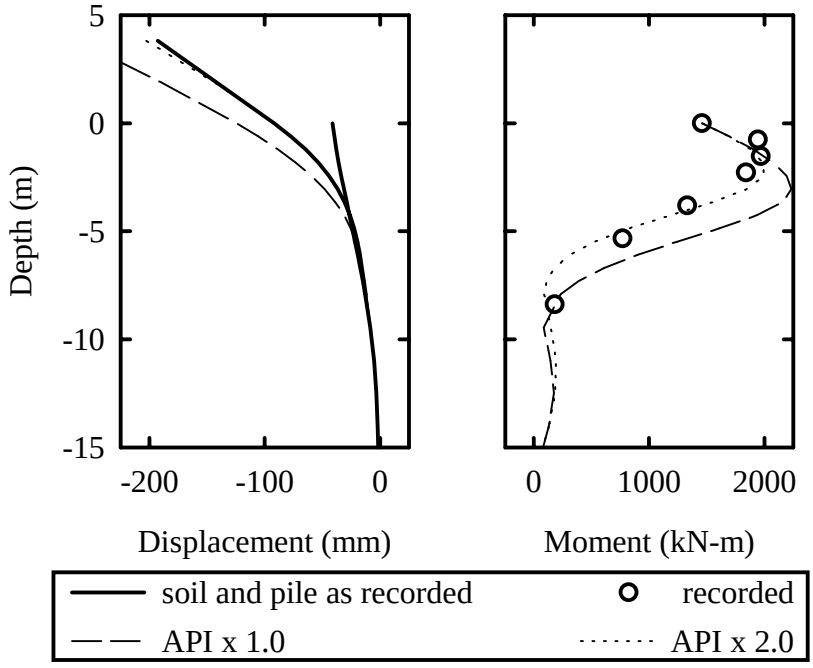

Figure 6.12: Calculated versus measured response for snapshot Csp3 J-a

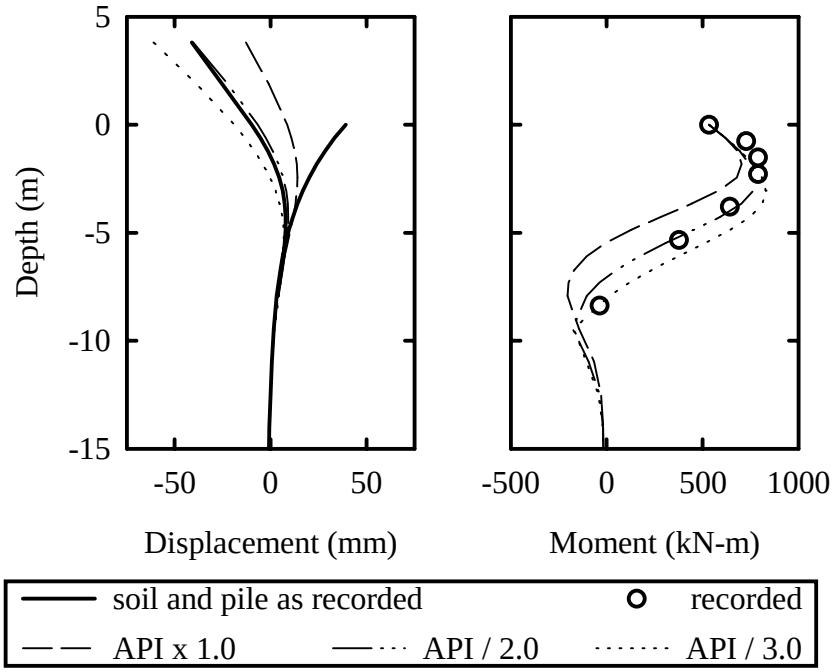

Figure 6.13: Calculated versus measured response for snapshot Csp3 J-b

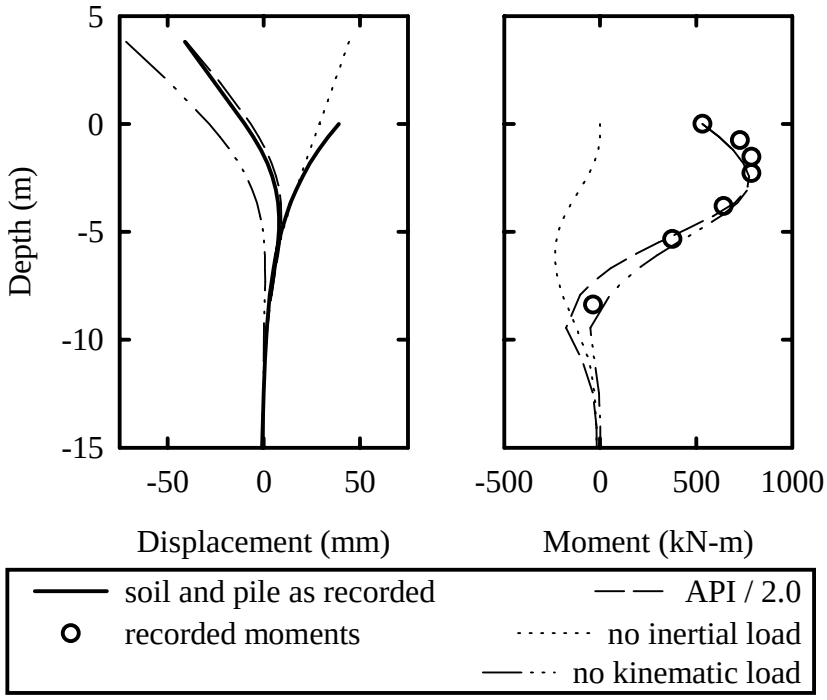

Figure 6.14: Effect of superstructure and kinematic loading on calculated versus measured response for snapshot Csp3 J-b

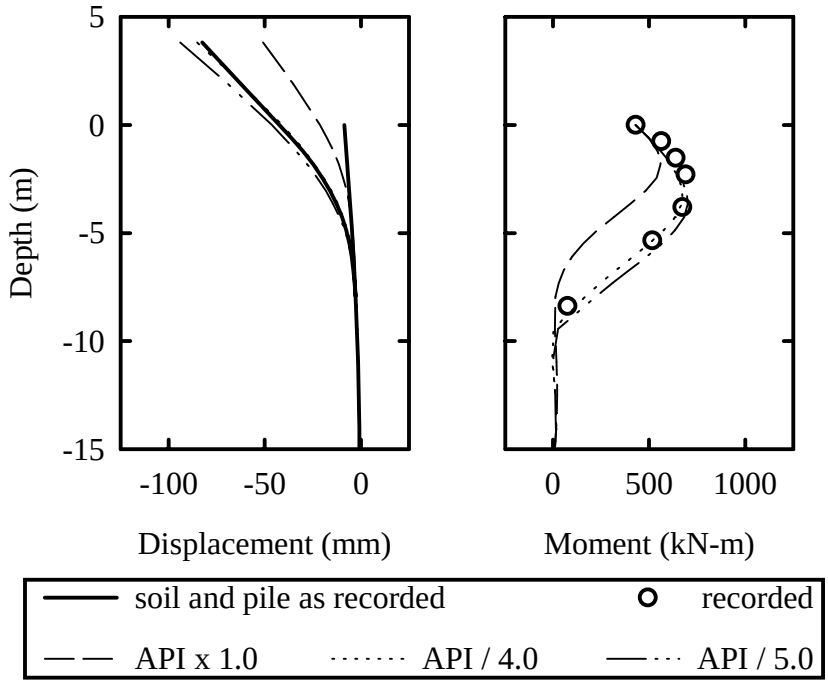

Figure 6.15: Calculated versus measured response for snapshot Csp3 J-c

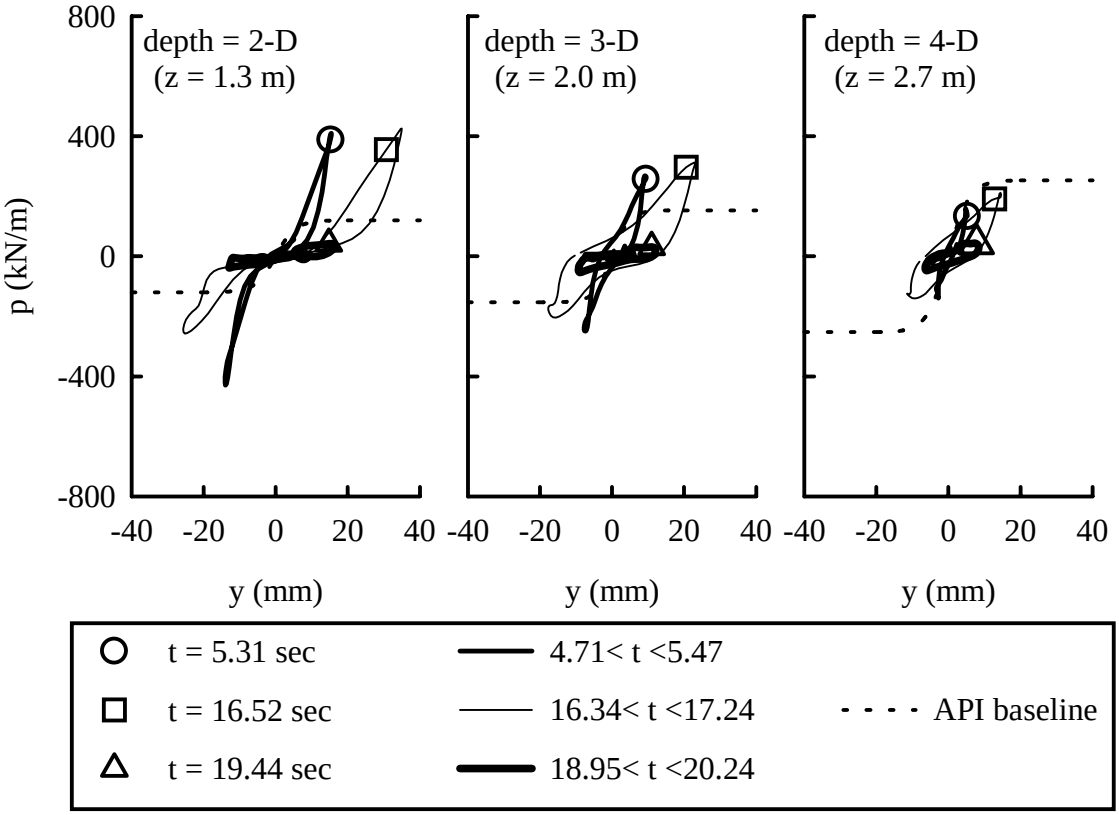

Figure 6.16: Lateral resistance in Csp3 event M
loose sand (Dr ≈ 55%), base motion Kobe, $a_{max,base}$=0.41 g

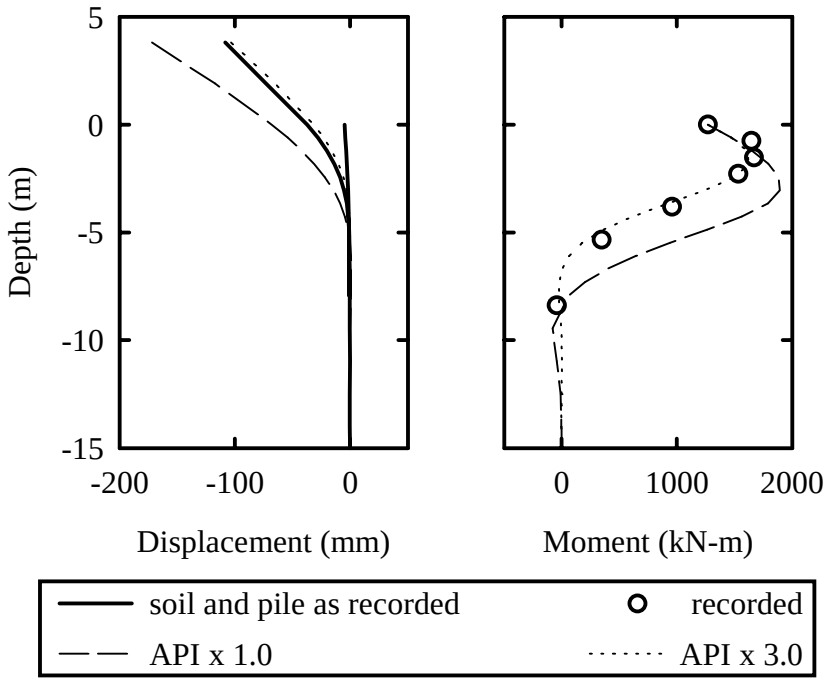

Figure 6.17: Calculated versus measured response for snapshot Csp3 M-a

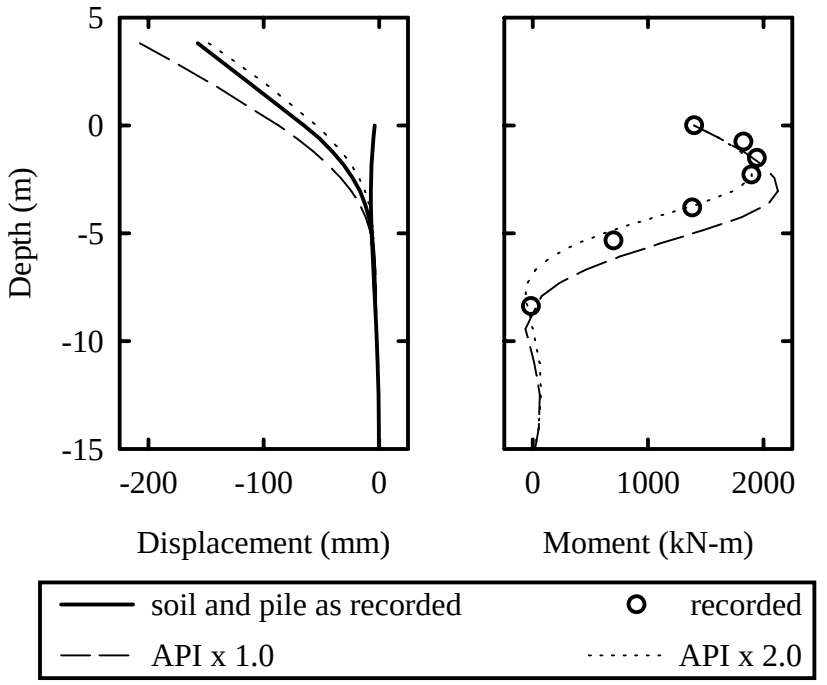

Figure 6.18: Calculated versus measured response for snapshot Csp3 M-b

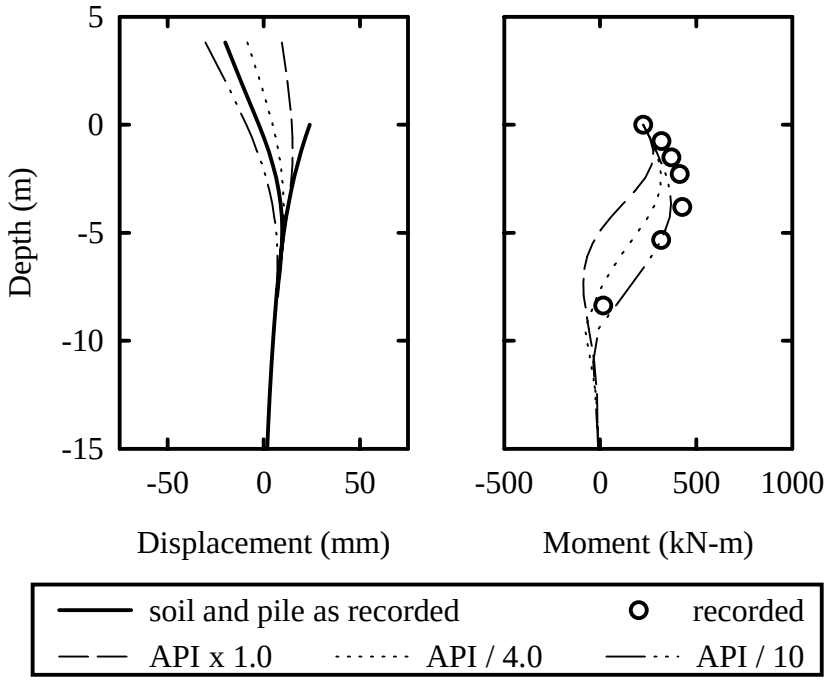

Figure 6.19: Calculated versus measured response for snapshot Csp3 M-c

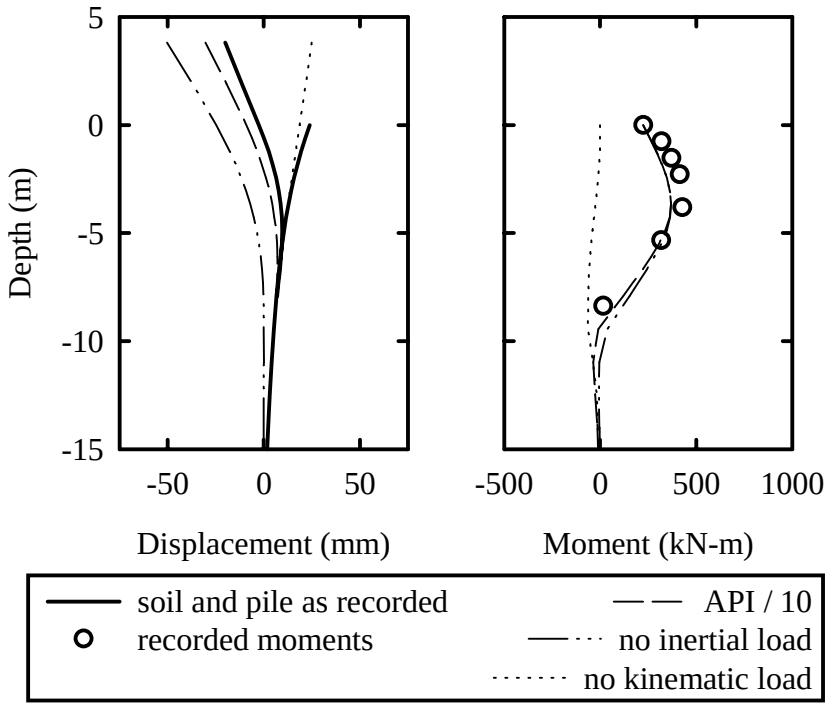

Figure 6.20: Effect of superstructure and kinematic loading on calculated versus measured response for snapshot Csp3 M-c

CHAPTER SEVEN

Summary, Conclusions, and Future Work

7.1 SUMMARY

This dissertation described the results of a study on the dynamic response of pile foundations in soft clay and liquefying sand during strong shaking. The research consisted of four major components: (1) a series of dynamic centrifuge tests of pile supported structures in soft soil and liquefying sand; (2) a critical study of modeling techniques and limitations; (3) back-calculation of p-y behavior; and (4) comparison of pseudo-static "Beam on Nonlinear Winkler Foundation" (BNWF) analyses to the results of the dynamic centrifuge model tests.

7.1.1 Test Documentation

Dynamic centrifuge experiments were performed using several different structural models, different earthquake input motions (varying level of shaking, frequency content, and waveforms), and different soil profiles. Experiments were performed with the upper soil layer being either saturated sand or soft, normally consolidated clay. The results of these experiments have been documented in detail with individual hard-copy data reports and diskettes with raw time histories [Wilson et al. 1997 (a-e)].

7.1.2 Centrifuge Modeling

The results from a series of centrifuge tests on the dynamic response of pile foundations in soft clay and liquefying sand during strong shaking were presented. The tests were performed on the relatively new shaking table on the large geotechnical centrifuge at UC Davis, and thus it was necessary to evaluate the centrifuge modeling system before analyzing the recorded physical data.

The new shaker on the large geotechnical centrifuge was found capable of reproducing nearly the same full spectrum earthquake motions throughout its operational range with minimal yaw between the east and west sides of the table. The new flexible shear beam container FSB1 was found to deform with the soil when the soil was medium dense sand, and in small strain events with softer soils. Noticeable sloshing of the soil occurred when the soil was liquefied loose sand. Vertical motions near the ends of the container were acceptably small in most cases. When the motions were large it was found that they were due to liquefied soil sloshing in the container, rather than due to a loss of complementary shear stress. While not ideal, an appreciation of this behavior is necessary for realistic interpretations of the centrifuge data.

Changing the pore fluid viscosity by a factor of 10 to better simultaneously model dynamic and consolidation processes had apparently little effect on the soil-structure interaction during shaking. Dynamic pore pressures in two similar models with different pore fluids were similar, while consolidation in the sample with the viscous pore fluid was obviously slower. The relatively minor effect of changing pore fluid viscosity seems to imply that the dynamic soil-structure interaction was mostly undrained in all cases presented herein. Note this is not expected to be true in general. Changing pore fluid

viscosity may have a more noticeable effect on other model configurations where partial drainage during dynamic loading may be significant, such as if a more permeable soil or a smaller diameter pile was used.

7.1.3 Back Calculating p-y Curves

Once the characteristics of the centrifuge model were investigated, data processing techniques were developed to quantify the soil-structure interaction directly. This processing consisted of numerical integration of recorded accelerations and numerical differentiation of recorded bending moments. The end results of the data processing were back-calculated p-y curves.

Time histories of bending moments along a single pile system and accelerations of the soil profile and on the single pile were used to back calculate p-y behavior. To calculate y, the soil profile displacements and the pile displacements had to be determined independently. Filtering and integration in the frequency domain was used to calculate displacements from accelerations. While permanent displacements cannot be calculated from the types of accelerometers used in this study, transient displacements could be reliably calculated.

Pile displacements were calculated by double integrating the bending moment distribution at each time step. Global displacements were fixed by assuming the pile moved with the soil at a depth of 9 m, and by using the pilehead accelerometer to calculate pilehead displacements. Superstructure displacements calculated independently were then used as a check on reasonableness of the pile deformed shape. In most cases the agreement was very good. Agreement was unacceptable only in a few cases (i.e. Csp2 event L, where instrumentation limitations corrupted the data).

The lateral resistance was calculated by double differentiating the moment distribution at each time step. Double differentiation of real data has proven difficult in the past. A new differentiation scheme for bending moment data based on the method of weighted residuals was developed. Calculating derivatives with this method produces a derivative that has the same smoothness properties as the original interpolation of the data. Simple cubic splines were also shown to give reasonable second derivatives as long as they were sampled at the spline midpoints. Polynomial interpolation was also used, but was found to give inconsistent results when using integer polynomial powers and forcing the second derivative to be zero at the soil surface. The calculated distribution of lateral resistance was generally consistent independent upon the method of calculation.

The ultimate lateral resistance in loose sand (Csp2, $D_r \approx 35\%$) was usually small when the soil liquefied, even when the displacements were fairly large. It is noted, however, that large lateral resistances and large induced moments were observed in one of the largest shaking events. In fact, for the 0.6 g Kobe event (Csp2 event L), the peak response of the superstructure appeared to be as great as observed in the more dense sand. The motions of this event were severe enough and the strains large enough that the soil became dilatant. It appears that in this event, the dilation of the soil at large strains provided sufficient strength to transmit large accelerations through the ground to the superstructure. This result shows that the effects of liquefaction on structural response depend on the nature of the ground motions and the strains imposed on the soil.

In medium dense sand (Csp3, $D_r \approx 55\%$), the observed p-y behavior was found to be displacement hardening as relative displacements approached or exceeded past values, especially near the surface. Peak values were significantly greater than those

recommended by API (1993) for drained conditions at depths less than about three diameters. This difference may be attributed to the nearly undrained loading conditions and the tendency for the soil to dilate under these loading conditions. The lateral resistance was found to depend strongly on p-y history, and was found to soften with increasing pore pressure and number of cycles. The observed behavior was consistent with the expected behaviors of saturated sands under undrained loading.

The observed p-y behavior in soft NC clay (Csp4) was in good agreement with the recommended static short-term API p-y curves for load cycles that exceeded the maximum strain history of an event. The lateral resistance was again found to be affected by the p-y history, and was much softer when load cycles remained within the envelope of past maximum values.

7.1.4 Pseudo-Static Analyses

Simple pseudo-static analyses at discrete times were then performed to examine the effectiveness of simplified analyses when the input parameters (kinematic and inertial loads) were known, and to quantify the effects of various parameters on the measured lateral resistance of soils.

Pseudo-static analyses were performed using the measured soil profile displacements and superstructure inertial loads and inputs. The moment distribution and displaced shape were found to be fairly insensitive to the selection of p-y curves within a reasonable range. E.g., applying a p-multiplier of 2 to the Csp3 event L-a snapshot decreased the calculated maximum moment by less than 10%. This is consistent with previous findings by many others, e.g. Murchison and O'Neill (1984) and Gazioglu and O'Neill (1984). Note that good agreement between measured moments and displaced

shapes were obtained even though the shapes of the p-y curves used in the analysis did not agree with the shapes of the back-calculated p-y curves.

7.2 RECOMMENDATIONS

7.2.1 Centrifuge Modeling

The geotechnical centrifuge is a useful tool for generating physical data on the dynamic behavior of soils and soil-structure interaction. The series of tests presented in this dissertation alone included some fifty shaking events for fully instrumented soil profiles, each with several fully instrumented structures. This large database has been made available for use by other researchers through request to the Center for Geotechnical Modeling at UC Davis.

As the data becomes more widely used, there is a need for others to better understand where the data comes from, and the inherent limitations in those data. Often when an analysis does not completely match the test data it is attributed to ambiguous "boundary conditions" or "container effects". The VELACS cooperative study demonstrated the importance of characterizing modeling effects from different laboratories (e.g. Scott et. al 1994 and Arulanandan et. al 1994). Modeling constraints such as container effects and instrument interaction effects, and such basic issues as characterizing the data acquisition systems of each facility, need to be examined.

7.2.2 Design of Pile Foundations

The design of pile foundations for seismic lateral loads typically follows one of two distinct paths. The first path is a dynamic analysis of the soil-structure system. The second is the simplified pseudo-static design approach. Recommendations for each method are made below.

7.2.2.1 Dynamic Analyses

The observed dynamic p-y curves in this study cannot be well represented by simple p-multipliers on the API recommended p-y curves for drained loading. Therefore the p-y curves used in a dynamic analysis would ideally account for factors that are known to affect the undrained behavior of soil, such as relative density, p-y history, pore pressure generation, strain rate, partial drainage, as well as other factors including group effects.

7.2.2.2 Pseudo-Static Analyses

The idea of pseudo-static BNWF analyses to determine the design loads and displacement demands on pile foundations seems promising for certain site and pile configurations. However, the use of pseudo-static analyses for dynamic problems does not explicitly account for changes that occur throughout the time history, such as loads before and after the onset of liquefaction. In this study, the peak bending moments and peak superstructure displacements were observed both before and after liquefaction, and thus both conditions need to be considered in design.

Others have suggested that simple p-multipliers based on pore pressure ratio can be applied to static p-y curves to account for the effects of liquefaction. The research presented herein suggests that this multiplier should at least also account for relative

density, is applicable only to virgin undrained loading in liquefied sand, and is not applicable when strains are large enough to cause the sand to become dilatant. For this study, it was found that appropriate p-multipliers for the stronger peak loading cycles after the generation of high excess pore pressures were approximately 0.10-0.20 for liquefying loose soil ($D_r \approx 35\%$), and approximately 0.25-0.35 for liquefying medium dense soil ($D_r \approx 55\%$). Note p-multipliers larger than 1.0 were observed under dilative loading conditions, such as early in shaking for medium dense sand.

Major uncertainties in pseudo-static soil-pile-superstructure analyses for a site with liquefying soils include estimating the free-field site response, estimating the superstructure response, and estimating how the loads from these responses should be combined. In this study the responses of the soil profile and the superstructure were recorded, so the only variable in an analysis was the choice of p-y curve.

It was noted in Chapter 6 that the use of softer springs is not necessarily conservative. Softer p-y springs imply softer soil behavior, which may result in less soil profile motions in the site response analysis. This, in turn, could results in less excitation of the superstructure. Softer p-y springs may also be unconservative in conditions of high kinematic loading, such as occurs with lateral spreading. A sensitivity study should be performed when using the simplified methods to help determine the critical loading conditions.

Finally, this study did not address the problem of soil-structure interaction in laterally spreading ground. For the site and structure geometries chosen in this study, the superstructure inertial loads were typically larger than the kinematic loads from the soil profile displacements. For these loading conditions the use of pseudo-static analyses was

found to give reasonable results for design. However, it is not clear that the analyses will yield reasonable results for cases of large kinematic loading associated with lateral spreading, particularly with an overlying crust of non-liquefied soil. It is anticipated that this problem will be addressed in future centrifuge modeling projects at UC Davis.

7.3 AREAS FOR FUTURE RESEARCH

The interaction between piles and liquefying or soft soil is a poorly understood process, and continued research is needed to improve earthquake risk exposure. This research should include the following items.

- Dynamic analyses of the data presented in this dissertation. These should include both BNWF methods and other techniques, including FEM models of the pile and soil continuum.
- Simple analyses of the pile-group-supported structures recorded in this study. This dissertation focused solely on the behavior of a single-pile-supported structure in five centrifuge tests. Each test included other fully instrumented structures that as yet have not been examined in detail.
- Kinematic loads from liquefaction induced lateral spreading and from layering of soft soils at depth. Damage to piles at depth due to kinematic loading could prove important in many cases.
- Further application of the pseudo-static method used in this dissertation. Combining kinematic loads from site response analyses and inertial loads from response spectra should be examined in more detail.

- Additional back-calculation of p-y curves with a more dense instrumentation array may provide more detailed information on the fundamental mechanisms of soil-pile interaction in soft or liquefied soils. The results in this dissertation illustrated the potential value in such efforts.
- More research needs to be performed studying centrifuge modeling to remove ambiguities in "boundary conditions" or "container effects". Modeling constraints such as container effects and instrument interaction effects, and such basic issues as characterizing the data acquisition systems of the facility, need to be examined.
- There also needs to be more quantification of experimental variability on the centrifuge. Systematic repetitions of select tests would help quantify expected levels of experimental scatter, and provide guidance on whether variations in behavior between two model tests of slightly different designs are due to the design differences and/or experimental scatter.
- Investigating the effects of dilation on site response (e.g. large spikes in acceleration), incorporating the effects of dilation into site response calculations, and investigating the effects of dilation on soil-structure interaction and superstructure response. This phenomenon was observed in Csp2 event L but could not be analyzed due to instrument failure.

BIBLIOGRAPHY

Abdoun, T., Dobry, R., and O'Rourke, T. D. (1997). "Centrifuge and numerical modeling of soil-pile interaction during earthquake induced soil liquefaction and lateral spreading," *Observation and Modeling in Numerical Analysis and Model Tests in Dynamic Soil-Structure Interaction Problems*, T. Nogami, Ed., Geotechnical Special Publication No. 64, ASCE, New York, N.Y., pp. 76-90.

Abghari A. and Chai, J. (1995). "Modeling of soil-pile-superstructure interaction in the design of bridge foundations," *Performance of Deep Foundations under Seismic Loading*, John Turner, Ed., Geotechnical Special Publication No. 51, ASCE, New York, N.Y., pp. 45-59.

AIJ (1988). "Recommendations for design of building foundations," Architectural Institute of Japan. (in Japanese).

Angelides, D.C. and Roesset, J.M. (1980). "Nonlinear dynamic stiffness of piles," Research Report R80-13, Dept. of Civil Engineering, MIT, Cambridge, Massachusetts.

API (1993). "Recommended Practice for Planning, Designing and Constructing Fixed Offshore Platforms," API RP 2A-WSD, 20th ed., American Petroleum Institute.

Arulanandan, K., Dobry, R., Elgamal, A.-W., Ko, H.Y., Kutter, B.L., Prevost, J., Riemer, M.F., Schofield, A.N., Scott, R.F., Seed, R.B., Whitman, R.V., and Zeng, X. (1994). "Interlaboratory studies to evaluate the repeatability of dynamic centrifuge model tests." *Dynamic Geotechnical Testing II*, ASTM STP 1213, R.J. Ebelhar, V.P. Drnevich, and B.L. Kutter, Eds., American Society for Testing and Materials, Philadelphia, pp. 400-422.

Badoni, D. and Makris, N. (1996). "Nonlinear response of single piles under lateral inertial and seismic loads," *Soil Dynamics and Earthquake Engineering*, Vol. 15, pp. 29-43.

Bray, J.D., Espinoza, R.D., Soga, K., and Taylor, R.L. (1995). "GeoFEAP: Geotechnical Finite Element Analysis Program. Version 1.2," Report No. UCBGT/95-05, Department of Civil and Environmental Engineering, University of California, Berkeley.

Boulanger, R.W., Wilson, D.W., Kutter, B.L., and Abghari, A. (1997). "Soil-pile-superstructure interaction in liquefiable sand." *Transportation Research Record No. 1569*, TRB, National Research Council, National Academy Press, Washington, D.C. pp. 55-64.

Boulanger, R.W., Kutter, B.L., and Wilson, D.W. (1998). "The response of piles during earthquakes: dynamic soil-pile-superstructure interaction," Report No. UCD/CGM-98/01, Center for Geotechnical Modeling, Department of Civil and Environmental Engineering, University of California, Davis.

Brown, D.A., Morrison, C. and Reese, L.C. (1988). "Lateral load behavior of pile group in sand," *Journal of Geotechnical Engineering*, Vol. 114, No. 11, pp.1261-1276.

Byrne, P.M., Anderson, D.L., and Janzen, W. (1984). "Response of piles and casings to horizontal free-field soil displacements," *Canadian Geotechnical Journal*, Vol. 21, pp. 720-725.

Café, P.F.M. (1991). "Dynamic response of a pile-supported bridge on soft soil," Masters of Science Thesis, University of California, Davis.

Chang, G.S. and Kutter, B.L. (1989). "Centrifugal modeling of soil-pile-structure interaction, *Engineering Geology and Geotechnical Engineering*, Balkema, pp. 327-334.

Cook, R.D., Malkus, D.S., and Plesha, M.E. (1989). Concepts and Applications of Finite Element Analysis, John Wiley & Sons, Inc., New York

Crouse, C.B., Kramer, S.L., Mitchell, R., and Hushmand, B. (1993). Dynamic tests of pipe pile in saturated peat," *Journal of Geotechnical Engineering*, ASCE, Vol. 119, No. 10, pp. 1551-1566.

Divis, C.J., Kutter, B.L., Idriss, I.M., Goto, Y., and Matsuda, T. (1996). "Uniformity of specimen and response of liquefiable sand model in a large centrifuge shaker." *Proceedings, Sixth Japan-U.S. Workshop on Earthquake Resistant Design of Lifeline Facilities and Countermeasures Against Soil Liquefaction*, Hamada and O'Rourke, Eds., NCEER-96-0012, SUNY, Buffalo, pp. 259-273.

Dou, H., and Byrne, P.M. (1996). "Dynamic response of single piles and soil-pile interaction," *Canadian Geotechnical Journal*, Vol. 33, pp. 80-96.

Dunnavant, T.W. and O'Neill, M.W. (1989). "Experimental p-y model for submerged, stiff clay," *Journal of Geotechnical Engineering*, ASCE, Vol. 115, No. 1, pp. 95-114.

El Sharnouby, B. and Novak, M. (1984). "Dynamic experiments with group of piles," *Journal of Geotechnical Engineering*, ASCE, Vol. 110, No. 6, pp. 719-737.

Faruque, M.O. and Desai, C.S. (1982). "3-D material and geometric nonlinear analysis of piles," *Proceedings of the Second International Conference on Numerical Methods in Offshore Pilling*, University of Texas at Austin, Texas, pp. 553-575.

Fiegel, G.L., Hudson, M., Idriss, I.M., Kutter, B.L., and Zeng, X. (1994). "Effect of model containers on dynamic soil response." *Proceedings, Centrifuge 94*, C.F. Leung, F.H. Lee, and T.S. Tan, Eds., Balkema, Rotterdam, pp. 145-150.

Finn, W.D. and Gohl, W.B. (1987). "Centrifuge model studies of piles under simulated earthquake lateral loading," *Geotechnical Special Publication No. 11*, ASCE, pp. 21-38.

Gazetas, G. (1991). "Foundation Vibrations," Chapter 15 in *Foundation Engineering Handbook*, H.Y. Fang, Ed., Van Nostrand Reinhold, New York.

Gazetas, G., Fan, K., Tazoh, T., and Shimizu, K. (1993). "Seismic response of the pile foundation of Ohba-Ohashi bridge," *Proceedings: Third International Conference on Case Histories in Geotechnical Engineering*, St. Louis, pp. 1803-1809.

Gazioglu, S.M., and O'Neill, M.W. (1984). "Evaluation of p-y relationships in cohesive soils," from *Analysis and Design of Pile Foundations*, proceedings of a symposium sponsored by the ASCE Geotechnical Engineering Division, ASCE National Convention, San Francisco, California, October 1-5, pp. 192-213.

Georgiadis, M., (1983). "Development of p-y curves for layered soils," *Proceedings, Geotechnical Practice in Offshore Engineering*, American Society of Civil Engineers, pp. 536-545.

Honda, M., Ohbo, N., Hayashi, H., Zheng, J., and Scott, R.F. (1994). "Dynamic response of a shaft in dry sands," *Proceedings, Centrifuge 1994*, pp.257-262.

Horikoshi, K., Ohtsu, H., Tanaka, M., and Sueoka, T. (1997). "Centrifuge modeling of a pile subjected to lateral spreading of liquefied soil." *Proceedings of the Third Kansai International Geotechnical Forum on Comparative Geotechnical Engineering*, Kansai Branch of the Japanese Geotechnical Society, Japan, pp. 199-208.

Idriss, I.M. and Ishihara, K. (1998). Proceedings from a US-Japan workshop, in progress.

JRA (1980). Specifications for highway bridges. Japan Road Association. (in Japanese).

Kagawa, T. (1980). "Soil-pile-structure interaction of offshore structures during an earthquake," *12 Annual Offshore Technology Conference*, Houston, Texas, OTC 3820.

Kagawa, T. (1983). "NONSPS: users manual," McClelland Engineers Inc., Houston, Texas.

Kagawa, T., Minowa, C., Mizuno, H., and Abe, A. (1994). "Shaking-table tests on piles in liquefying sand", *Proceedings, Fifth US National Conference on Earthquake Engineering*, Chicago, Illinois, Vol. IV, pp. 107-113.

Kobayashi, K., Nakamura, S., Sato, K., Yoshida, N., and Yao,S. (1991). "Soil-pile interaction in liquefied sand layer," *Fifth International Conference on Soil Dynamics and Earthquake Engineering*, Karlsruhe, Germany, pp. 351-361.

Kuhlemeyer, R.L. (1979). "Vertical vibration of piles," *Journal of Geotechnical Engineering*, ASCE, Vol. 105 No. GT2, pp. 273-288.

Kutter, B.L., Sathialingam, N., and Herrmann, L.R. (1990). "Effects of arching on response time of miniature pore pressure transducer in clay," *ASTM Geotechnical Testing Journal*, Vol. 13, No. 3, pp. 164-178.

Kutter, B.L., Li, X.S., Sluis, W., and Cheney, J.A. (1991). "Performance and instrumentation of the large centrifuge at Davis," *Proceedings, Centrifuge 91*, Ko and McLean, Eds., Balkema, Rotterdam, pp. 19-26.

Kutter, B.L., Idriss, I.M., Kohnke, T., Lakeland, J., Li, X.S., Sluis, W., Zeng, X., Tauscher, R., Goto, Y., and Kubodera, I. (1994). "Design of a large earthquake simulator at UC Davis." *Proceedings, Centrifuge 94*, Leung, Lee, and Tan, Eds., Balkema, Rotterdam, pp. 169-175.

Kutter, B.L. (1992). "Dynamic centrifuge modeling of geotechnical structures." *Transportation Research Record 1336*, TRB, National Research Council, National Academy Press, Washington, D.C., pp. 24-30.

Lam, I.P., and Kapuskar, M.. (under review). "Modeling of pile footings for seismic design", technical report submitted to the National Center for Earthquake Engineering Research.

Liu, L. and Dobry, R. (1995). "Effect of liquefaction on lateral response of piles by centrifuge model tests," *National Center for Earthquake Engineering Research (NCEER) Bulletin*, Vol. 9, No. 1, January, pp. 7-11.

Matlock, H., and Ripperger, E.A. (1956). "Procedures and instrumentation for tests on a laterally loaded pile," *Proceedings, Eighth Texas Conference on Soil Mechanics and Foundation Engineering*, Special Publication No. 29, Bureau of Engineering Research, University of Texas.

Matlock, H. (1970). "Correlations for design of laterally loaded piles in soft clay," *Proceedings, 2nd Annual Offshore Technology Conference*, Houston, Texas, OTC 1204.

Matlock, H., Foo, S.H., and Bryant, L.L. (1978). "Simulation of lateral pile behavior," *Proceedings, Earthquake Engineering and Soil Dynamics*, ASCE, pp. 600-619.

Murchison, J.M., and O'Neill, M.W. (1984). "Evaluation of p-y relationships in cohesionless soils," from *Analysis and Design of Pile Foundations*, proceedings of a symposium sponsored by the ASCE Geotechnical Engineering Division, ASCE National Convention, San Francisco, California, October 1-5, pp. 174-191.

Ochoa, M, and O'Neill, M. (1989). “Lateral pile interaction factors in submerged sand,” *Journal of Geotechnical Engineering*, Vol. 115, No. 3, pp. 359-378.

PMB Engineering Inc. (1988). PAR (Pile Analysis Routine) Manual, 500 Sansome Street, San Francisco, CA 94111.

Prakash, V., Powell, G.H., and Campbell, S., (1993). "DRAIN-2DX base program description and user guide," Version 1.10, Report No., UCB/SEMM-93/17, University of California, Berkeley.

Randolph (1981). “Response of flexible piles to lateral loading,” *Geotechnique*, Vol. 31, No. 2, pp. 247-259.

Rashidi Khozaghi, H. (1994). “Centrifuge and theoretical study of the earthquake soil-pile-structure interaction of structures founded on clays,” Ph.D. dissertation, University of California, Davis.

Sanchez, S.I. (1982). "Static and dynamic stiffnesses of single piles," Research Report GR82-31, Deptartment of Civil Engineering, The University of Texas at Austin, Austin, Texas.

Scott, R.F. (1994). "Review of progress in dynamic geotechnical centrifuge research." *Dynamic Geotechnical Testing II*, ASTM STP 1213, R.J. Ebelhar, V.P. Drnevich, and B.L. Kutter, Eds., American Society for Testing and Materials, Philadelphia, pp. 305-329.

Sen, R., Davis, T.G. and Barnerjee, P.K. (1985). "Dynamic analysis of piles and pile groups embedded in homogeneous soils," *International Journal Earthquake Engineering and Structural Dynamics*, Vol. 13, pp. 53-65.

Stewart, D.P, Chen, Y.R., and Kutter, B.L. (1998). "Experience with the use of methylcellulose as a viscous pore fluid in centrifuge models," *Geotechnical Testing Journal*, GTJODJ, 21 (4), December, 365-369.

Stewart, D.P., Kutter, B.L., Higuchi, S., Robins, P.N., Narayanan, K.R., and Thompson, D.J. (1997). "Centrifuge modeling of the seismic response of LNG production facility structures: Phase I," Report No. UCD/CGM-97/02, Center for Geotechnical Modeling, Department of Civil and Environmental Engineering, University of California, Davis

Tabesh, A. (1997). “Lateral seismic analysis of piles,” Ph.D. thesis, University of Sydney

Ting, J.M. (1987). "Full scale cyclic dynamic lateral pile response," *Journal of Geotechnical Engineering*, ASCE, Vol. 113, No. 1, pp. 30-45

Tokida, K.-I., Matsumoto, H., and Iwasaki, H. (1992). "Experimental study of drag acting of piles in ground flowing by liquefaction." *Proceedings of the Fourth Japan-U.S. Workshop on Earthquake Resistant Design of Lifeline Facilities and Countermeasures for Soil Liquefaction*, Volume 1, Report NCEER 92-0019, National Center for Earthquake Engineering Research, SUNY, Buffalo, N.Y., pp. 511-523.

Tokimatsu, K., Oh-Oka, H., Shamoto, Y., Nakazawa, A., and Asaka, Y. (1997). "Failure and deformation modes of piles caused by liquefaction-induced lateral spreading in 1995 Hyogoken-Nambu earthquake." *Proceedings of the Third Kansai International Geotechnical Forum on Comparative Geotechnical Engineering*, Kansai Branch of the Japanese Geotechnical Society, Japan, pp. 239-248.

Trochanis, A.M., Bielak, J., and Christiano, P. (1991). "Simplified model for analysis of one or two piles," *Journal of Geotechnical Engineering*, ASCE, Vol. 117, No. 3, pp. 448-466.

Van Laak, P.A., Taboada, V.M., Dobry, R., and Elgamal, A.-W. (1994). "Earthquake centrifuge modeling using a laminar box." *Dynamic Geotechnical Testing II*, ASTM STP 1213, R.J. Ebelhar, V.P. Drnevich, and B.L. Kutter, Eds., American Society for Testing and Materials, Philadelphia, pp. 370-384.

Vesic, A.S. (1970). "Expansion of cavities in infinite soil mass," *Journal of Geotechnical Engineering*, ASCE, Vol. 98, No. SM3, pp. 265-290.

Wang, S., Kutter, B.L., Chacko, M.J., Wilson, D.W., Boulanger, R.W., and Abghari, A. (1998). "Nonlinear seismic soil-pile structure interaction." *Earthquake Spectra*, EERI, Vol. 14, No. 2, pp. 377-396.

Wen, Y.-K. (1976). "Method for random vibration of hysteretic systems," *Journal of the Engineering Mechanics Division*, ASCE, Vol. 102, No. EM2, pp. 249-263.

Whitman, R.V., and Lambe, P.C. (1986). "Effect of boundary conditions upon centrifuge experiments using ground motion simulation," *Geotechnical Testing Journal*, ASTM GTJODJ, Vol. 9, No. 2, pp. 61-71.

Wilson, D.W., Boulanger, R.W., Kutter, B.L., and Abghari, A. (1995). "Dynamic centrifuge tests of pile-supported structures in liquefiable sand," *Proceedings, National Seismic Conference on Bridges and Highways*, Sponsored by Federal Highways Administration and Caltrans, San Diego, CA, December 10-13.

Wilson, D.W., Boulanger, R.W., and Kutter, B.L. [1997 (a)]. "Soil-pile-superstructure interaction at soft or liquefiable soil sites - Centrifuge data report for Csp1." Report No. UCD/CGMDR-97/02, Center for Geotechnical Modeling, Department of Civil and Environmental Engineering, University of California, Davis.

Wilson, D.W., Boulanger, R.W., and Kutter, B.L. [1997 (b)]. "Soil-pile-superstructure interaction at soft or liquefiable soil sites - Centrifuge data report for Csp2." Report No. UCD/CGMDR-97/03, Center for Geotechnical Modeling, Department of Civil and Environmental Engineering, University of California, Davis.

Wilson, D.W., Boulanger, R.W., and Kutter, B.L. [1997 (c)]. "Soil-pile-superstructure interaction at soft or liquefiable soil sites - Centrifuge data report for Csp3." Report No. UCD/CGMDR-97/04, Center for Geotechnical Modeling, Department of Civil and Environmental Engineering, University of California, Davis.

Wilson, D.W., Boulanger, R.W., and Kutter, B.L. [1997 (d)]. "Soil-pile-superstructure interaction at soft or liquefiable soil sites - Centrifuge data report for Csp4." Report No. UCD/CGMDR-97/05, Center for Geotechnical Modeling, Department of Civil and Environmental Engineering, University of California, Davis.

Wilson, D.W., Boulanger, R.W., and Kutter, B.L. [1997 (e)]. "Soil-pile-superstructure interaction at soft or liquefiable soil sites - Centrifuge data report for Csp5." Report No. UCD/CGMDR-97/06, Center for Geotechnical Modeling, Department of Civil and Environmental Engineering, University of California, Davis.

Wilson, D.W., Boulanger, R.W., Kutter, B.L., and Abghari, A. [1997 (f)]. "Aspects of dynamic centrifuge testing of soil-pile-superstructure interaction." *Observation and Modeling in Numerical Analysis and Model Tests in Dynamic Soil-Structure Interaction Problems*, T. Nogami, Ed., Geotechnical Special Publication No. 64, ASCE, New York, N.Y., pp. 47-63.

Yan, L., Byrne, P.M., and Dou, H. (1991). “Model studies of dynamic pile response using hydraulic gradient shaking table tests,” *6th Canadian Conference Earthquake Engineering*, Toronto, pp. 335-342.

Youd, T.L. and Bartlett, S.F. (1989). "Case histories of lateral spreads from the 1964 Alaskan earthquake," *Proceedings, Third Japan-U.S. Workshop on Earthquake Resistant Design of Lifeline Facilities and Countermeasures for Soil Liquefaction*, Report NCEER-91-0001, National Center for Earthquake Engineering Research, SUNY, Buffalo, N.Y.

Zeghal, M., and Elgamal, A.-W. (1994). "Analysis of site liquefaction using earthquake records," *Journal of Geotechnical Engineering*, Vol. 120, No. 6, pp.996-1017.

Zeng, X., and Schofield, A.N. (1996). "Design and performance of an equivalent-shear-beam container for earthquake centrifuge modelling," *Geotechnique*, Vol. 46, No. 1, pp. 83-102.